Sorbonne Université

Ecole Doctorale N°158
Cerveau, Cognition, Comportement

Institut du Fer à Moulin
Equipe : Plasticité des réseaux corticaux et épilepsie

Regulation of the Na^+ - K^+ - Cl^- co-transporter NKCC1 by the WNK pathway in neurons through diffusion-capture

Régulation du co-transporteur Na^+ - K^+ - Cl^- NKCC1 par la signalisation WNK dans les neurones via diffusion-capture

Par Etienne Côme

Thèse de doctorat de Neurosciences
Dirigée par Dr. Sabine Lévi

Présentée et soutenue publiquement le 31 mars 2021
devant un jury composé de :

Dr. Claire Wyart	Présidente du jury
Dr. Enrica Petrini	Rapportrice
Dr. Igor Medina	Rapporteur
Dr. Julien Dupuis	Examinateur
Dr. Anna-Maria Hartmann	Examinatrice
Dr. Sabine Lévi	Directrice de thèse

Abstract

Neuronal inhibition is mainly mediated by GABAergic neurotransmission in the mature brain, while in early stages of development GABAA receptor activity is excitatory. Underlying these different responses, intracellular chloride levels are regulated by the activity of the co-transporters KCC2 and NKCC1. While KCC2-mediated chloride extrusion in mature brain has been described in many publications, NKCC1 role as a chloride loading transporter scarcely reported. However under several pathological conditions where synaptic inhibition is impaired, the role of NKCC1 has been highlighted. This is the case in epilepsy, whether from clinical epilepsy or experimental models, and is remarkable given the otherwise elusive functions of NKCC1 in the mature brain. As the regulatory pathways of NKCC1 are mainly unknown in the adult brain, we lack information on the underlying processes leading to its abrupt “awakening”. My PhD project aimed to determine whether and how NKCC1 is regulated by neuronal activity.

I demonstrated using quantum-based single particle tracking, immunofluorescence and STORM imaging approaches that the membrane stability of NKCC1 is rapidly regulated by lateral diffusion in an activity-dependent manner at the surface of mature hippocampal cultured neurons. Basal glutamatergic activity regulates the membrane dynamics of NKCC1 in the axon but not in the somato-dendritic compartment indicating a specific regulatory mechanism depending on the cell compartment. In the somato-dendritic compartment, NKCC1 is tuned by GABAAR-mediated signaling. Blocking or activating GABAA receptors with muscimol or gabazine rapidly slow down and confine transporters in the membrane. Transporter confinement would be consecutive to the recruitment and storage of transporters within endocytic zones. I then identified the underlying molecular mechanism. GABAergic activity would control the diffusion/capture and clustering of NKCC1 via the chloride-sensitive WNK1 kinase and the downstream SPAK and OSR1 kinases that would directly phosphorylate NKCC1 on key threonine T203/T207/T212/T217/T230 phosphorylation sites. The fact that KCC2 is also regulated in mature neurons by the WNK1/SPAK/OSR1 pathway and that this

regulation has an inverse effect on the membrane stability, clustering and function of KCC2 indicates that this pathway could be a target of interest in pathologies associated with an alteration of chloride homeostasis. Inhibition of the pathway would prevent the loss of KCC2 and the increase of NKCC1 at the surface of the neuron, thus preventing the abnormal rise of [Cl-]i in the pathology and the resulting adverse effects. I thus assessed the relevance of inhibiting this kinase pathway in the context of ictogenesis. I used a PTZ-induced seizure assay in SPAK243A/243A mice, who express a non-active form of SPAK. Behavioral indicators (Racine scale) and electrocorticograms (EcoG) showed that the effects of the mutation on these variables were mild, with a reduced death rate and a non-significant decrease in the duration of seizures. The moderate effect could be due to the fact that other effector of the WNK1 pathway such as the OSR1 kinase remains active in these mice.

This work provides the first in-depth characterization of NKCC1 regulation in neurons and emphasize targeting the WNK1/SPAK/OSR1 pathway to regulate neuronal chloride homeostasis and thus neuronal hyperactivity in epilepsy.

Résumé

Dans le cerveau adulte, l'inhibition synaptique passe majoritairement par l'activité des récepteurs GABA de type A (RGABAA). Cette inhibition dépend du gradient électro-chimique du chlorure, qui est principalement régulé par les co-transporteurs du chlore KCC2 et NKCC1. KCC2 transporte le chlore hors du neurone, tandis que NKCC1 est responsable de son influx. Ainsi au cours des premiers stades du développement l'activité de NKCC1 prédomine rendant l'activité des RGABAA excitatrice, cependant KCC2 voit son expression augmenter au cours du développement, résultant en une transmission GABAergique inhibitrice dans le cerveau adulte. Du fait de son importance fonctionnelle dans les neurones matures, les fonctions de KCC2, ainsi que sa régulation transcriptionnelle et post-traductionnelle sont nombreuses. En revanche peu de données existent sur les fonctions de NKCC1 dans le cerveau adulte, et sur sa régulation. Néanmoins dans des cas pathologiques en lien avec une altération de la transmission GABAergique, NKCC1 revêt une importance fonctionnelle certaine qui tranche avec son rôle apparemment discret dans l'homéostasie du chlore. Ceci est notamment le cas dans le contexte de l'épilepsie, expérimentale ou clinique. Résultant du peu de connaissances sur les mécanismes moléculaires et cellulaires de la régulation de NKCC1 dans les neurones, la cause de ce "réveil" du co-transporteur est encore inconnue.

J'ai démontré, à l'aide d'approches de suivi de particules uniques, d'immunofluorescence et d'imagerie STORM, que la stabilité membranaire de NKCC1 est rapidement régulée par diffusion latérale d'une manière dépendante de l'activité à la surface des neurones matures de l'hippocampe. L'activité glutamatergique basale régule la dynamique membranaire de NKCC1 dans l'axone mais pas dans le compartiment somato-dendritique, ce qui indique un mécanisme de régulation compartiment-spécifique. Dans le compartiment somato-dendritique, NKCC1 est réglé par une signalisation médiée par le RGABAA. Le blocage ou l'activation des RGABAA par le muscimol ou la gabazine ralentit et confine les transporteurs dans la membrane. Le confinement des transporteurs serait consécutif à leur recrutement et stockage dans les

zones endocytiques. J'ai ensuite identifié le mécanisme moléculaire sous-jacent. L'activité GABAergique contrôlerait la diffusion/capture et le regroupement de NKCC1 via la kinase WNK1 sensible aux chlorures et les kinases SPAK et OSR1 en aval qui phosphoryleraient directement NKCC1 sur les sites de phosphorylation clés de la thréonine T203/T207/T212/T217/T230. Le fait que KCC2 est également régulé dans les neurones matures par la voie WNK1/SPAK/OSR1 et que cette régulation a un effet inverse sur la stabilité membranaire, l'agrégation et la fonction de KCC2 indique que cette voie pourrait être une cible d'intérêt dans les pathologies associées à une altération de l'homéostasie du chlorure. L'inhibition de cette voie permettrait d'éviter la perte de KCC2 et l'augmentation de NKCC1 à la surface du neurone, empêchant ainsi l'augmentation anormale de [Cl-]i dans la pathologie et les effets néfastes qui en résultent. J'ai donc évalué la pertinence de l'inhibition de cette voie dans le contexte de l'ictogenèse. J'ai utilisé un test d'ictogénese induite par PTZ dans des souris SPAK243A/243A, qui expriment une forme non active de SPAK. Les indicateurs comportementaux (échelle de Racine) et les électrocorticogrammes ont montré que les effets de la mutation sur ces variables étaient légers, avec un taux de mortalité réduit et une diminution non significative de la durée des crises. Cet effet modéré pourrait être dû au fait qu'un autre effecteur de la voie WNK1, comme la kinase OSR1, reste actif chez ces souris.

Ce travail fournit la première caractérisation approfondie de la régulation de NKCC1 dans les neurones et met l'accent sur le ciblage de la voie WNK1/SPAK/OSR1 pour réguler l'homéostasie du chlorure neuronal et donc l'hyperactivité neuronale dans l'épilepsie.

Remerciements

Je remercie en premier lieu ma famille, proche ou lointaine, pour son soutien et son affection sans failles. Je pense en particulier à mes parents, qui ont passé un bon nombre d'années à s'occuper de moi, pour au final me voir écrire un pavé sur la régulation de NKCC1 par la neurotransmission GABAergique. Merci Cécile de m'avoir accompagné et soutenu pendant ces années où ça n'a pas toujours été facile.

Merci à l'équipe Vivant de la Cité des Sciences et de l'Industrie, pour son enthousiasme et sa pédagogie. Je reste disponible à l'avenir si il y a des quiz à faire.

Merci à tous les membres de l'IFM pour leur bienveillance, qui font de cet institut un endroit où il est agréable de travailler.

Je remercie chaleureusement les membres de l'équipe 3, grâce à qui j'ai appris tant de choses. Je pense notamment à Clémence, Éric, Ferran, Jessica, Marianne, Marie et Sana pour leur accueil au sein de l'équipe et leur soutien. Je remercie également Manisha pour son altruisme, et Xavier pour m'avoir aidé avec ce microscope intimidant. Merci à Donovan, Samy, Rémi, Adrianna, Lysa, Marion, Hesni et Simon, que j'ai eu la chance d'encadrer, et qui ont participé à l'obtention de résultats présentés ici. Bonne chance Donovan et Samy pour votre doctorat, et bonne continuation à tous !

Un grand merci à Florian et Marion, pour leur complicité dans la rigolade comme dans les petites déprimes au cours de ces années. Je ne sais pas comment j'aurais fait sans vous ! Bon courage aux nouvelles recrues : Anne-Lise, Claire et Zaha (enfin doctorante dans l'équipe après 3 ans dans le labo). Vous allez gérer, la thèse c'est facile.

Merci à Jean-Christophe pour tes remarques pertinentes sur mes travaux et nos discussions scientifiques. Mais je retiendrai surtout ton humour acéré et ce rire si discret qui va avec.

Enfin, merci Sabine pour m'avoir accompagné avant même que je ne débute ma thèse sous ta direction. Tu m'as beaucoup apporté scientifiquement, mais surtout personnellement, par ton humilité, ta rigueur et ton attention. Je suis fier d'avoir fait ce travail sous ta direction.

Table of Contents

Figures and Tables....4
Index of Tables....5
Abbreviations....6
Introduction....8
1. Chloride and the neuron....10
1. A. A homeostatic state regulated by the chloride co-transporters KCC2 and NKCC1....10
1. A. a. Chloride homeostasis and $GABA_AR$ action....10
1. A. b. Chloride concentration in neurons, a question of diversity....13
1. A. b. i. Chloride concentration measured with electrophysiology....14
1. A. b. ii. Chloride concentration measured with genetically-encoded ratiometric probes in vivo and in vitro....15
1. A. b. iii. Chloride concentration measured with MQAE....17
1. A. b. iv. Chloride concentration distribution and evolution in neurons....18
1. A. c. Alterations of $[Cl^-]_i$ and their consequences....20
1. A. d. KCC2 and NKCC1 function in neuronal chloride homeostasis....23
1. B. KCC2 and NKCC1, Cation-Chloride Co-transporters dynamically expressed throughout the brain....30
1. B. a. The CCC family....30
1. B. b. Expression patterns of NKCC1 and KCC2 in the central nervous system 32
1. B. c. Transcriptional regulation of NKCC1....35
1. B. d. NKCC1 Structure....36
2. NKCC1 is a protein crucial for neuronal chloride homeostasis....38
2. A. A chloride loading transporter....38
2. A. a. NKCC1-mediated chloride loading in the developping CNS....38
2. A. b. A discussed role for NKCC1 in chloride homeostasis under physiological condition in the mature brain....40

2. B. Under several pathological models related with $[Cl^-]_i$ dysregulation, NKCC1 activity is determinant....43
2. B. a. NKCC1 and epilepsy in the immature brain....43
2. B. b. NKCC1 and epilepsy in the mature brain....45
2. B. c. Impaired GABAergic signalling does not only involve NKCC1 or KCC2....47
3. NKCC1 post-translational regulation....49
3. A. A homeostatic regulation by the WNK-SPAK-OSR1 pathway....49
3. A. a. NKCC1 is phosphorylated at its NTD after $[Cl^-]_i$ depletion....49
3. A. b. The WNK-SPAK-OSR1 system....51
3. A. b. i. Involved kinases....51
3. A. b. ii. Activation mechanisms of WNK-SPAK-OSR1....53
3. A. b. iii. Interplay with phosphatases....56
3. A. c. A homeostatic regulation of NKCC1 phosphorylation by the WNK-SPAK-OSR1 pathway....58
3. A. d. Roles of WNK-SPAK-OSR1 in neuronal chloride homeostasis....60
3. A. e. Respective roles of tonicity and phosphorylations on KCC2 and NKCC1 activity....60
3. B. Diffusion-capture regulation of transporters at the membrane of neurons...63
3. B. a. The diffusion model....63
3. B. b. Diffusion-capture regulation of KCC2....68
3. B. b. i. Under control conditions....68
3. B. b. ii. Regulation of KCC2 membrane stability through diffusion-capture...69
3. B. d. Lateral diffusion of NKCC1 in neurons....71
Materials and methods....73
Results....75
Regulation of the NKCC1 chloride importer by the GABAergic inhibition and the WNK-SPAK-OSR1 signalling pathway in mature hippocampal neurons....76
Abstract....76
Introduction....77

Results.....80
Discussion.....94
Materials and Methods.....100
Figures.....109
Tables.....127
References.....128
Discussion.....135
1. NKCC1 regulation by GABAergic activity has a specific diffusion-capture signature 136
1. A. An increased constraint associated with endocytosis.....136
1. B. Factors tuning NKCC1 diffusion and clustering at the membrane.....138
1. C. Does an increased neuronal activity impact NKCC1 membrane stability ?…141
2. Entanglement of KCC2 and NKCC1 phosphorylation by WNK-SPAK-OSR1.....143
2. A. WNK-SPAK-OSR1 regulates KCC2 and NKCC1 in opposite directions.....143
2. B. Changes in NKCC1 lateral diffusion are correlated with its phosphorylation state.....146
2. C. KCC2 dominant transport activity in the mature hippocampus retroactively regulates NKCC1 via changes in $[Cl^-]_i$.....148
3. Can the WNK-SPAK-OSR1 signalling inhibition alleviate ictogenesis symptoms via the regulation of KCC2 and NKCC1 phosphorylation ?.....153
3. A. Targetting a pathway regulating both KCC2 and NKCC1.....153
3. B. Genetic inhibition of SPAK does not have a big impact on ictogenesis severity 153
General conclusions.....157
Bibliography.....158

Table of Figures

Figure 1.....8
Figure 2.....9
Figure 3.....12
Figure 4.....15
Figure 5.....19
Figure 6.....21
Figure 7.....26
Figure 8.....28
Figure 9.....30
Figure 10.....35
Figure 11.....37
Figure 12.....41
Figure 13.....43
Figure 14.....46
Figure 15.....51
Figure 16.....52
Figure 17.....54
Figure 18.....56
Figure 19.....64
Figure 20.....67
Figure 21.....68
Figure 22.....69
Figure 23.....70
Figure 24.....72
Results, Figure 1.....109
Results, Figure 2.....111
Results, Figure 3.....113

Results, Figure 4.....115
Results, Figure 5.....117
Results, Figure 6.....119
Results, Figure 7.....121
Results, Figure 8.....123
Results, Figure 9.....125
Figure 25.....137
Figure 26.....138
Figure 27.....139
Figure 28.....141
Figure 29.....145
Figure 30.....147
Figure 31.....148
Figure 32.....156

Index of Tables

Table 1.....18
Results, Table 1.....127
Results, Table 2.....127
Results, Table 3.....127

Abbreviations

4-AP	4-Aminopyridine
aa	Amino acid
ACSF	Artificial cerebro-spinal fluid
AE	Anion exchangers
AIS	Axon initial segment
AMPA	α-amino-3-hydroxy-5-methyl-4-isoxazolepropionic acid
AMPAR	AMPA receptor
ATP	Adenosine triphosphate
CA	*Cornu ammonis*
cAMP	Cyclic adenosine monophosphate
Cab39	Calcium-binding protein 39
CCC	Cation chloride co-transporter
CFP	Cyan fluorescent protein
CIP1	Cation-chloride co-transporter interacting protein 1
CNS	Central nervous system
CTD	C-terminal domain
DNA	Deoxyribonucleic acid
EPSC	Excitatory postsynaptic current
EPSP	Excitatory postsynaptic potential
ERK	Extracellular signal-regulated kinase
F-actin	Filamentous actin
FLIM	Fluorescence lifetime imaging microscopy
FRAP	Fluorescence recovery after photobleaching
GABA	γ-amino butyric acid
$GABA_AR$	Receptor subtype A for GABA
$GABA_BR$	Receptor subtype B for GABA
GFP	Green fluorescent protein
GlyR	Glycine receptor
HEK-293	Human Embryonic Kidney 293
HIF-1α	hypoxia-inducible factor 1α
HSN2	Hereditary sensory and autonomic neuropathy II
IPSC	Inhibitory postsynaptic current
IPSP	Inhibitory postsynaptic potential
KCC	K^+-Cl^- co-transporter
LEL	Large extracellular loop
LTP	Long-term potentiation
MQAE	*N*-(ethoxycarbonylmethyl)-6-methoxy-quinolinium bromide
mRNA	Messenger ribonucleic acid
NCC	Na^+-Cl^- co-transporter
NKCC	Na^+-K^+-Cl^- co-transporter
NMDA	N-methyl-D-aspartate
NMDAR	NMDA receptor
NRT	*nucleus reticularis thalami*
NTD	N-terminal domain

OSR1	Oxydative stress response 1
PKA	Protein kinase A
PKC	Protein kinase C
PP1	Protein phosphatase 1
PP2A	Protein phosphatase 2A
QD	Quantum dot
RMP	Resting membrane potential
RNA	Ribonucleic acid
SCLM	SuperClomeleon
shRNA	Small hairpin ribonucleic acid
SLC	Solute carrier
SPAK	STE20/SPS1-related, proline alanine-rich kinase
SPT	Single particle tracking
STORM	Stochastic Optical Reconstruction Microscopy
TLE	Temporal lobe epilepsy
TM	Transmembrane segment
WNK	With no lysine
YFP	Yellow fluorescent protein

Introduction

Neuronal network activity relies on the integration of synaptic events conditioning the action potential firing frequency. Release of neurotransmitters at chemical synapses triggers the activation of ionotropic and metabotropic receptors, allowing specific ions to cross the plasma membrane. Depending on the activated receptors, the response can notably be excitatory postsynaptic currents (EPSC) or inhibitory postsynaptic currents (IPSC). These currents will change the postsynaptic potential, leading to either a depolarization (increased membrane potential) in the case of an inward flow of positive charges, or an hyperpolarization in the opposite case.

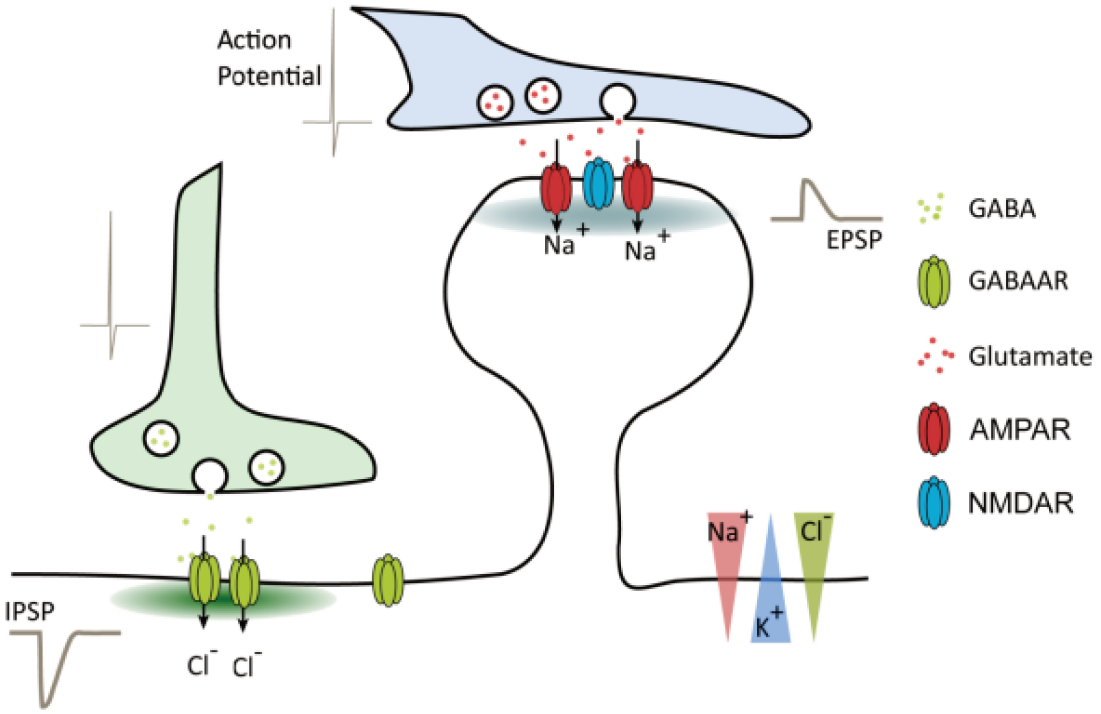

Figure 1, neuronal activity in the mature central nervous system importantly depends on GABAergic and glutamatergic synaptic neurotransmissions. Excitatory synapses are typically localized in dendritic spines, presynaptic glutamate release leads to the activation of receptors such as AMPAR and NMDAR, generating a sodium-dependent excitatory post-synaptic potential (EPSP). On the other hand, GABAergic synapses are mainly found on the dendritic shaft, GABA release triggers $GABA_AR$ and $GABA_BR$ activation. $GABA_AR$ opening leads to rapid inhibition through chloride influx, generating inhibitory PSC.

Like often in the living, there is a remarkable diversity of neuronal responses to a stimulus, may it be an electrical or chemical one. The GABAergic neurotransmission is no exception. The γ-Amino Butyric Acid (GABA) is a neurotransmitter activating the ionotropic subtype A ($GABA_AR$) and the metabotropic subtype B ($GABA_BR$) receptors. In the mature brain $GABA_AR$ activation allows fast inhibition in most brain regions via entrance of chloride anions in neurons through the receptor channel (Fig. 1). However during early development the activity of the same receptor provokes a depolarization, often associated with excitatory outcomes. Hence depending on the maturation of the neuron, its electrical response to GABAergic neurotransmission will radically differ.

The GABAergic shift has been identified as a consequence of the decrease in intracellular chloride during development and correlated with an increase in the K^+-Cl^- co-transporter 2 (KCC2) expression. KCC2 is the major chloride extruder in neurons, using the potassium electrochemical gradient. In immature neurons the higher chloride concentration is notably dependent on the Na^+-K^+-$2Cl^-$ co-transporter 1 (NKCC1) which, oppositely to KCC2, imports chloride following the sodium gradient. As it stands, chloride homeostasis in neurons importantly relies on the active transport of potassium and sodium by those co-transporters, allowing the regulation of chloride electrochemical gradient. It is noteworthy to underline that the electrochemical gradient for these ions is dependent on the Na^+/K^+ ATPase activity (figure 2). Hence chloride homeostasis should be at least considered with the inclusion of those 4 transmembrane proteins (Fig. 2).

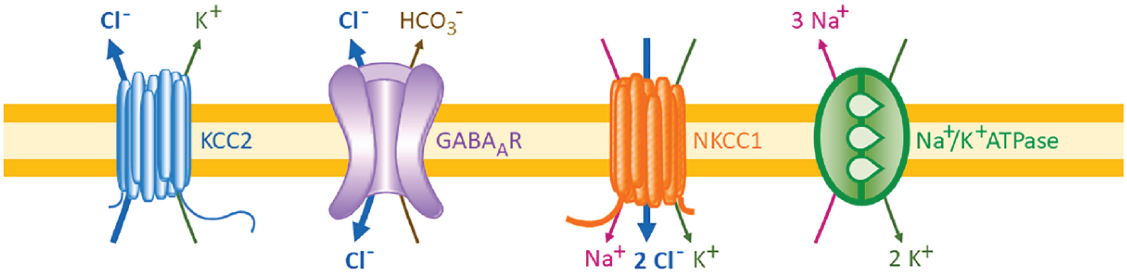

Figure 2, KCC2 and NKCC1 are secondary chloride transporters depending on Na^+/K^+ ATPase to dictate $GABA_AR$ activity polarity. KCC2-mediated chloride extrusion depends on the potassium electrochemical gradient. NKCC1-dependent chloride influx relies on the soduim gradient. The prevalent activity of KCC2 in the majority of mature neurons leads to an inward chloride flow upon $GABA_AR$ opening causing post-synaptic hyperpolarization. Adapted from, *Côme et al. 2019*.

Changes in NKCC1 and KCC2 expression or activity can critically affect neuronal function and especially inhibitory neurotransmission efficiency. Furthermore several pathologies are related to their mis-regulation at the transcriptional or post-translational levels, notably in epilepsy or neuropathic pain. Interestingly KCC2 is regulated by synaptic excitation and inhibition through changes in specific residues phosphorylation state. On the other hand there is still much to decipher on NKCC1 dynamic tuning in neurons and the functional implications in mature neurons.

The research work performed during my PhD is mainly aiming at determining whether neuronal inhibition can directly tune NKCC1 through changes in its plasma membrane distribution in mature hippocampal neurons. The other project adds a focus on the outcomes of inhibiting a pathway regulating KCC2 and NKCC1 under ictogenesis context with an *in vivo* model, and will be presented in the discussion.

1. Chloride and the neuron

1. A. A homeostatic state regulated by the chloride co-transporters KCC2 and NKCC1

1. A. a. Chloride homeostasis and $GABA_AR$ action

In the developped brain, fast inhibitory neurotransmission is mainly driven by GABA A receptors ($GABA_AR$) activation. $GABA_AR$ are composed of 5 subunits, from a pool of 19 possible subunits. Hence when we talk about GABA A receptors the accent should be put on their diversity, as ~50 different subunits combinations are hypothesized to be present in the brain (Smart and Stephenson 2019). The main architecture is suspected to include subunits α:β:γ with a 2:2:1 stoechiometry including identical α and β subunits pairs, although this is not meant to be a general rule. This diversity is notably relevant as different $GABA_ARs$ do not have the same subcellular distribution, notably regarding inhibitory synapses, or sensitivity to GABA (Lu et al. 2014).

Inhibitory neurotransmission mediated by $GABA_AR$ in the central nervous system (CNS) is mainly dependent on intracellular chloride concentration $[Cl^-]_i$ due to their conductance to chloride ions. Another less addressed variable are bicarbonate ions HCO_3^-. $GABA_AR$ being permeant to chloride but also bicarbonate ions, omitting the latter may lead to an under-estimation of the receptor's reversal potential. I will here succintly describe the thermodynamical aspects of chloride homeostasis and their impact on $GABA_AR$ responses.

First, we need some definitions. The reversal potential for an ion is defined as follow :

$E_{ion} = \frac{RT}{zF} \ln\left(\frac{[ion]_o}{[ion]_i}\right)$; where R is the gas constant, T the temperature (in Kelvin), z the valence and F the Faraday constant.

The reversal potential gives a theoretical voltage value where the electrical gradient and the chemical gradient cancel each other, resulting in the absence of net flow of the considered ion. The current flow across the membrane is physically formalized as :

$I_{ion} = g_{ion}(V_m - E_{ion})$; where Iion is the ionic current, gion the membrane conductance to the ion ($g = \frac{1}{R}$, with R being the electrical resistance) and Vm the membrane potential.

The term Vm – Eion is referred as the "driving force" and illustrates the effective electrical gladient : how different is the resting membrane potential (RMP) from the equilibrium potential of the considered ion. It is often seen as a more function-related variable than the raw reversal potential, notably when studying Cl^- flow through the membrane (Doyon et al. 2011; Goutierre et al. 2019; Schmidt et al. 2018). The conductance on the other hand quantifies the membrane permeability to the ion, ant notably depends on membrane proteins allowing its passing through the membrane. Considering the usual timigns to assess the reversal potential, the current is typically attributed to channel receptors. $GABA_AR$ s being permeant to both chloride and bicarbonate, their reversal potential is inferred from both ionic species concentrations and conductances using the Goldman-Hodgkin-Katz equation. For a system where HCO_3^- and Cl^- ions are present we get the following reversal potential :

$$E_{GABA} = \frac{RT}{z} \ln\left(\frac{P_{Cl} \times [Cl]_i + P_{HCO_3} \times [HCO_3]_i}{P_{Cl} \times [Cl]_o + P_{HCO_3} \times [HCO_3]_o} \right)$$; with P_{ion} being the receptor permeability to the considered ion, which can be seen as a relative measure for ionic conductances.

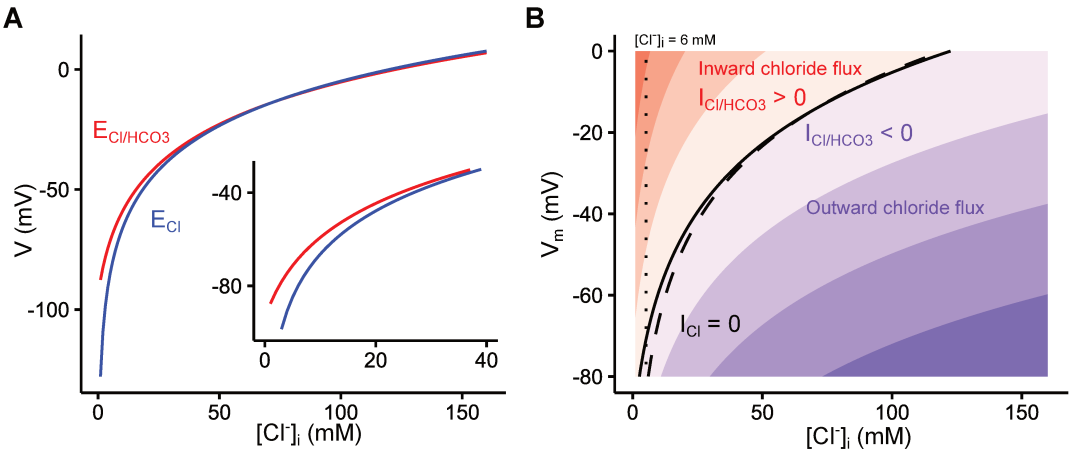

Figure 3, dependence of $GABA_AR$ activation on intracellular chloride. **A**, chloride reversal potential (E_{Cl}) and E_{GABA} depending on $[Cl^-]_i$. The insert displays values for the range generally observed in neurons. **B**, electrical current mediated by $GABA_ARs$ activation whether accounting (plain line) or not (dashed line) on bicarbonate ions. In mature neurons with $[Cl^-]_i$ around 6 mM (dotted line), bicarbonate permeability can have important functionnal consequences on the current polarity. Used parameters : $[Cl^-]_o$ = 120 mM, $[HCO3^-]_o$ = 25 mM, $[HCO3^-]_i$ = 15 mM, $GABA_AR$ permeability to chloride = 4 times $GABA_AR$ permeability to bicarbonate (Doyon et al. 2011).

Because it includes bicarbonate, the GHK-computed reversal potential gives a more precise estimate of E_{GABA}. E_{HCO3} being higher than E_{Cl} due to pH-regulatory mechanisms, this results in $E_{HCO3} > E_{GABA} > E_{Cl}$. On the other hand, E_{GHK} requires more parameters to estimate intracellular concentrations, hence using E_{GABA} as an affine estimation of E_{Cl} is often a decent compromise, for instance when HEPES buffer is used to stabilize extracellular pH. As is can be logically determined from the presented equations, $[Cl^-]_i$ range is determinant for $GABA_AR$ polarity and the resulting post-synaptic current triggered by their activation.

The role of membrane potential and $[Cl^-]_i$ on $GABA_AR$-mediated current, combined with the diversity in the receptor subunit composition influencing the biophysical properties of the channels (open-close-desensitized states, flow rates, distribution at the membrane, etc.), lead to a variety of responses to pre-synaptic GABA release (Lu et al. 2014; Mody 2005; Mody and Pearce 2004). The diversity in GABA release modalities (e.g. spillover) adds yet another layer of complexity. The activity pattern of these receptor activity is either described as “phasic” or

"tonic", the former generating short polarization episodes while the later leads to more persistent changes in membrane polarization through repetitive currents. Phasic activation typically involves the activation of synaptic receptors while tonic activation is due to extrasynaptic receptors activation by ambient GABA levels. As seen previously, the polarity of the response at a given membrane potential is dependent on E_{GABA}. Hyperpolarization is provoked by the entrance of chloride inside the neuron leading to a decrease in local membrane potential, inhibiting neuronal activity. On the other hand, we may straight-forwardly interpret GABAergic depolarizing currents as excitation. Yet it was demonstrated that $GABA_AR$-dependent depolarization can also induce a shunting inhibition, leading to a reduction in neuronal spiking through a decrease in the local input resistance and thus reducing co-occuring excitatory post-synaptic potentials (EPSP) (Vida, Bartos, and Jonas 2006). Shunting inhibition typically occurs when $RMP < E_{SYN} < V_{AP}$. In their work, Vida el al. mention a significant role of bicarbonate ions in the setting of a relatively positive reversal potential for the inhibitory synapse, complementing the biophysical aspects described before. Note that I made a static description of chloride homeostasis. Computational works on intracellular chloride dynamics demonstrated its functional impacts on neurons (Currin et al. 2020; Doyon et al. 2011). Reversal potential is a good tool to assess potential flux of chloride ions through the plasma membrane, however one should be aware of the other components of the system, such as intracellular chloride dynamics, rendering it more complex than a simple electrical conductance.

GABAergic neurotransmission mediated by $GABA_AR$ activation has a wide array of consequences on the post-synaptic neuron, from depolarization to hyperpolarization, with a variety of dynamics due to the diversity of $GABA_AR$ compositions and their distribution on the dendrite. Nevertheless the polarity of the response and its functional consequences on somatic polarization are strongly dictated by $[Cl^-]_i$.

1. A. b. Chloride concentration in neurons, a question of diversity

As a result of the heavy dependency of GABA-mediated inhibition in the mature brain on intraneuronal chloride concentration, it is a parameter of upmost importance. Several techniques were used by neuroscientists to determine intracellular chloride concentration and its dynamics.

1. A. b. i. Chloride concentration measured with electrophysiology

Using patch-clamp techniques on brain slices, researchers were able to access the resting membrane potential (RMP) or E_{GABA} (Achilles et al. 2007; Deisz et al. 2011; Elgueta and Bartos 2019; Otsu et al. 2020; Puskarjov et al. 2012; Vida, Bartos, and Jonas 2006; Witte et al. 2014; Wright et al. 2017; Yamada et al. 2004; Zions et al. 2020). To estimate $[Cl^-]_i$, gramicidin perforated patch combined with local GABA uncaging is performed. Recorded E_{GABA} values usually span over a 10-20 mV interval. For instance, this corresponds to a $[Cl^-]_i$ range of [4.6, 9.8] mM when applying the Nernst equation with $[Cl^-]_o$ = 135 mM and a E_{GABA} of [-90, 70] mV in adult rats dentate gyrus (Goutierre et al. 2019). Yamada et al. reported $[Cl^-]_i$ values inferred from E_{GABA} in a [5, 12] mM interval in P11-P20 neocortical pyramidal neurons. While these intervals are short, note that in the majority of cases the measurements of variables related to GABAergic neurotransmission are performed with a **pharmacological inhibition of neuronal activity** (AMPA receptors, NMDA receptors, $GABA_B$ receptors or Na^+ channel inhibition for example), stabilizing the measurements but also leading to an **underestimation of $[Cl^-]_i$ variance**, and **limitating the diversity of observed states**. Another hurdle is that reversal potential recorded at the soma may depend more on the local subcortical chloride concentration than on the mean value of somatic $[Cl^-]_i$ (Gonzalez-Islas, Chub, and Wenner 2009; Otsu et al. 2020). Hence straight-forward inferrence of neuronal $[Cl^-]_i$ from E_{GABA} values with thermodynamical formulae is not as direct as suggested by the corresponding equations. On the other hand it allows precise quantifications of parameters influencing $GABA_AR$ function. Another patch-clamp technique relevant for E_{GABA} measurement is the cell-attached recording, with the advantage of being non-invasive. It was notably used by Tyzio et al. in 2008 to determine the driving force of single $GABA_AR$ in CA3 pyramidal cellls during early developmental stages (Tyzio et al. 2008).

1. A. b. ii. Chloride concentration measured with genetically-encoded ratiometric probes in vivo and in vitro

Electrophysiological approaches provide precise measurements of biophysical properties for individual neurons. However they are invasive techniques and rely on pharmacological inhibition of excitatory activity combined with theoretical equations to determine $[Cl^-]_i$. Intracellular chloride-sensitive ratiometric probes have been used to overcome these limitations (Arosio and Ratto 2014). Genetically encoded intracellular probes such as Clomeleon or ClopHensor were used *in vitro* to quantify intracellular chloride concentrations (Duebel et al. 2006; J. Glykys et al. 2014a; Joseph Glykys et al. 2009). These studies report an **important variability in intercellular and inter-regional $[Cl^-]_i$ levels when compared with electrophysiology assays**. This likely is a consequence of the **higher throughput** of these assays and of the **wider number of states recorded** (limited pharmacological inhibition, non-invasive approach), but **might also be the consequence of the variance of $[Cl^-]_i$ being higher in the soma than in the subcortical domains**.

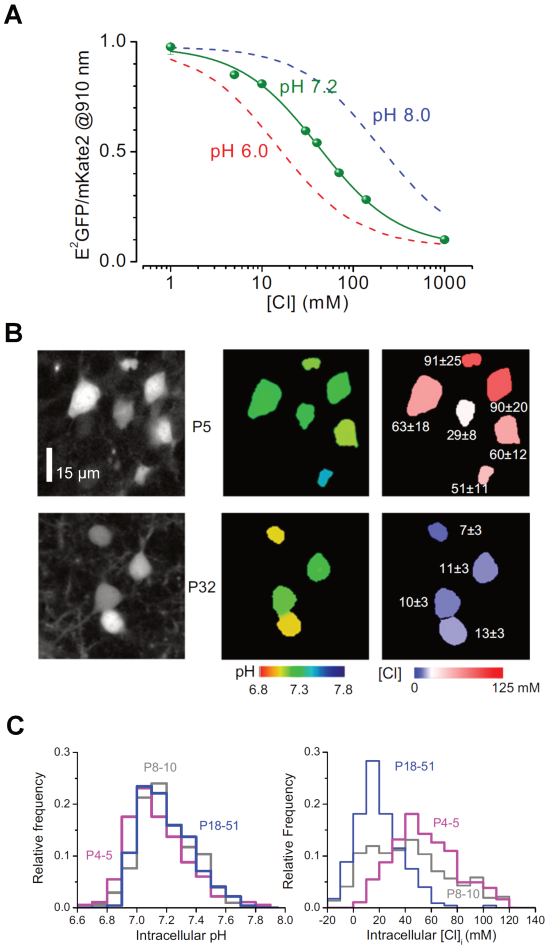

Figure 4, In vivo measurement of intracellular chloride concentration. **A**, sensitivity of LSSmKate2Clo pHensor to $[Cl^-]_i$ and pH_i. **B**, two-photon imaging of ClopHensor in vivo with corresponding pH_i and $[Cl^-]_i$ estimations. **C**, pH_i distribution is highly conserved across different developmental stages, while a decrease in $[Cl^-]_i$ values is observed. Adapted from Sulis-Sato et al. 2017.

Functional aspects of GABAergic activity, such as chloride loading following inhibitory synaptic activity, were described when using Clomeleon mice (K. Berglund et al. 2016; Ken Berglund et al. 2006, 2008; Lillis et al. 2012; Pond 2006). Using ClopHensor on hippocampal slices, Raimondo et al. mentioned an increased $[Cl^-]_i$ in hippocampal pyramidal neurons after GABAergic pathways stimulation (Raimondo 2013). Hence chloride imaging allows the non-invasive study of chloride homeostasis and $GABA_AR$ activity *in vitro*.

Two works used such probes to determine the intracellular chloride concentration of neurons *in vivo* (Boffi et al. 2018; Sulis Sato et al. 2017). Sulis Sato et al. made use of the LSSmClopHensor construction, composed of a Cl^-/pH-sensitive GFP mutant, E^2GFP, and a Cl^-/pH-insensitive red fluorescent protein, LSSmKate2 (Arosio et al. 2010; Paredes et al. 2016). The fluorescent properties of both fluorophores, notably E^2GFP emission depending on the excitation wavelength, allow to untangle pH_i and $[Cl^-]_i$ effects. Combining these properties with corrections for light diffraction caused by the complex optical properties of the brain, the authors could measure somatic pH_i and $[Cl^-]_i$ values *in vivo*. A noteworthy statement from this work is the observed **variability in $[Cl^-]_i$, with values in [-20, 120] mM in P4-P10 mice visual cortex layer 2/3 pyramidal neurons for example.**

Boffi et al. measured intracellular chloride of layer 2/3 pyramidal cells in the motor cortex of adult mouse (Boffi et al. 2018). Instead of using LSSClopHensor, they performed separate measurements of $[Cl^-]_i$ with SuperClomeleon (SCLM) (Grimley et al. 2013), and pH_i with the SE-pHluorin probe (Miesenböck, De Angelis, and Rothman 1998). SCLM being pH-sensitive without allowing pH measurement, the authors used the second probe to measure the pH range observed in these cells to calibrate SCLM. However, the measured chloride concentrations are not directly displayed in their work, but rather the SCLM ratios. This is likely a consequence of the large range of recorded concentrations including abnormal negative values, like observed by Sulis Sato et al. in 2017. From their SCLM measurements and the corresponding calibration curves the range would be around [0, 100] mM, but this is probably a under-estimation as the variability reported when calibrating the probe is not accounted for here.

These recent results display how **difficult the measurement of intracellular chloride level is *in vivo***, with the need for many controls, calibrations and data corrections. Nevertheless, both

studies reported significant changes in $[Cl^-]_i$ between different experimental conditions, proving that **physiological changes in chloride concentrations can be detected using these tools**. Nevertheless, despite their relevance they suffer from several flaws impairing their efficiency. The **complex optical properties of the brain**, **photo-bleaching**, but also **slow binding kinetics**, **high dissociation constant** or their **dependence on other intracellular parameters** (such as the pH) require thorough calibration and offline corrections to obtain good estimates. Sulis Sato et al. 2017 exhaustively describe this aspect in their work (Material and Methods, Supplementary Information).

1. A. b. iii. Chloride concentration measured with MQAE

An alternative to genetically encoded ratiometric probes are **synthetic dyes**, such as the commonly used N-(ethoxycarbonylmethyl)-6-methoxyquinolinium bromide (MQAE). This dye was synthetized and characterized by Verkman et al. who highlighted its **light sensitivity to pH or bicarbonate ions concentration together with a high Cl^- sensitivity and quenching kinetics**, as well as its loading in cells by transmembrane diffusion (Verkman et al. 1989). Engblom and Åkerman measured synaptoneurosome $[Cl^-]_i$ (estimated at 14 ± 4 mM) and observed chloride currents resulting from $GABA_AR$ activation using MQAE (Engblom and Åkerman 1993). Marandi et al. in 2002, using two-photon microscopy on cortical and hippocampal slices, further demonstrated the relevance of MQAE usage for neuronal $[Cl^-]_i$ estimation (Marandi, Konnerth, and Garaschuk 2002). Another advantage of MQAE is the possibility to perform fluorescence lifetime imaging (FLIM) to avoid a number of bias present with direct intensity measurement (Hiroshi Kaneko et al. 2002). MQAE FLIM estimation of $[Cl^-]_i$ has been used in several papers to study neuronal $[Cl^-]_i$, with measured ranges of [40, 80] mM in dendritic knobs of olfactory sensory neurons (H. Kaneko 2004), **[10, 100] mM and [50, 110] mM in dorsal root ganglion neurons respectively in adult and newborn mice** (Gilbert et al. 2007). Such ranges are reminiscent of the ones reported with genetically-encoded probes *in vitro*. This variability may arise from several technical biases, but a more sensible hypothesis is that those ranges actually reflect an actual variability in $[Cl^-]_i$. MQAE still displays some disadvantages over genetically-encoded probes like **non-conditional targetting of cells**, **crossing of the plasma membrane**, and **demonstration of its relevance *in vivo* has been limited** (Kovalchuk and Garaschuk 2012).

Probe	Cl^- K_D (mM)	pKa	Cl^- binding time constant (ms)	References
MQAE	40 (Stern-Volmer constant)	Outside of phys. range	< 1	*Marandi 2002, Verkman et al. 1989*
Clomeleon	167	5.2	100-200	*Kuner and Augustine, 2000*
SuperClomeleon	21.2 ± 2.2	6.4 ± 0.1	n.a.	*Grimley et al. 2013*
ClopHensor	49 ± 5	6.78 ± 0.04	175 ± 4	*Arosio et al. 2010*
LSSmClopHensor	14.27 ± 3.5	0	n.a.	*Paredes et al. 2016*

Table 1 : physico-chemical properties of chloride probes. Chloride K_D values were obtained in cells with pH between 7.1 and 7.4. Adapted from *Arosio et al. 2014* and *Berglund et al. 2015*.

Electrophysiology and imaging techniques allow to access different variables. Electrophysiology permits to precisely measure variables associated with $GABA_AR$ function like the polarity of chloride flux. Chloride imaging with ratiometric probes or MQAE on the other hand is non-invasive, and the estimations of $[Cl^-]_i$ can be dynamically recorded without pharmacological tools to selectively measure chloride conductances. However the sensitivity and kinetics of the probes/dyes limitate their resolution. These techniques are complementary, and allowed the recording of a considerable amount of data regarding chloride homeostasis in neurons.

1. A. b. iv. Chloride concentration distribution and evolution in neurons

The results we presented outline the variability in $[Cl^-]_i$. In addition to intra-population variability, different chloride concentrations among different cell types were reported with electrophysiology. For example Yamada et al. reported a ~ 5 mM higher $[Cl^-]_i$ in neocortical layer 2/3 pyramidal neurons compared with pyramidal neurons from the layer 5/6 in P4 rat (Yamada et al. 2004). In the dentate gyrus, Vida et al. measured a E_{GABA} of -50 mV in basket cells of adult rat while Elgueta et al. reported a E_{GABA} of -60 mV in parvalbumin-expressing interneurons (Elgueta and Bartos 2019; Vida, Bartos, and Jonas 2006). Glykys et al. also reported different $[Cl^-]_i$ distributions in different brain regions using Clomeleon (J. Glykys et al. 2014b; Joseph Glykys et al. 2009). Furthermore, depending on the subcellular region, GABA reversal potential may also substantially differ. Several works highlighted changes in E_{GABA} depending on the localization of $GABA_AR$ activation (Elgueta and Bartos 2019; Khirug et al. 2008; Otsu et al. 2020; Rinetti-Vargas et al. 2017). This subcellular heterogenous distribution of intracellular chloride was also observed with Clomeleon in ON-Type retinal bipolar cells (Duebel et al. 2006). Intracellular dynamics and spatial distribution of chloride regarding $GABA_AR$ activity have been

studied using computational approaches, providing insights on the subcellular differences in E_{GABA} and potential consequences on GABAergic neurotransmission (Currin et al. 2020; Doyon et al. 2011; Jedlicka et al. 2010; Lewin, Aksay, and Clancy 2012). In conclusion chloride intracellular concentration is highly variable between different neuronal types, but also neuronal compartments, and measurements are carried under various experimental conditions with different techniques. It thus appear difficult as of today to give precise physiological ranges of neuronal [Cl-]i, even if focusing on a precise sub-population.

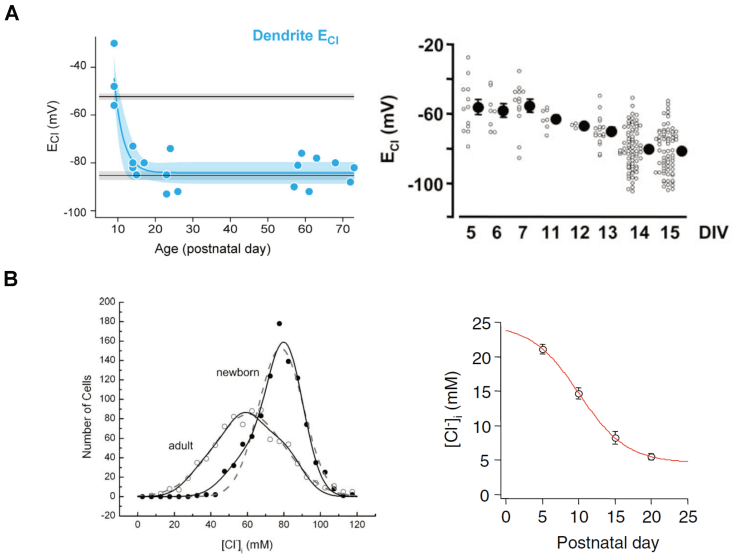

Figure 5, Developmental decrease in intraneuronal chloride and correspondingly decreased $GABA_AR$-mediated excitation. **A**, decrease in E_{GABAAR} during development in slices (left, Rinetti-Vargas et al. 2017) and dissociated cultures (right, Fiumelli et al. 2005). **B**, chloride imaging demonstrated a developmental decrease in $[Cl^-]_i$ (left : DRG neurons, Gilbert et al. 2007 ; right : hippocampal pyramidal neurons, Berglund et al. 2006). **C**, this decrease in $[Cl^-]_i$ is correlated with a decreased frequency of GABAergic excitation in cultures (left, Ganguly et al. 2001) and an inhibitory action of chloride influx (mediated by light-activated stGtACR2 channelrhodopsin) in CA1 pyramidal cells (right, Murata et al. 2020).

A consistently reported factor influencing chloride levels is development. Developmental decrease in $[Cl^-]_i$ estimates was observed with electrophysiology and chloride imaging tools *in vitro* and *in vivo* in several regions (Fiumelli, Cancedda, and Poo 2005; Gilbert et al. 2007; Joseph Glykys et al. 2009; Sulis Sato et al. 2017; Yamada et al. 2004). In fact a shift of GABAergic neurotransmission from excitatory to inhibitory during development has been described in most brain regions and correlated with a decrease in $[Cl^-]_i$, demonstrating the previously described functional importance of the chloride transmembrane gradient on GABAergic neurotransmission function (Ben-Ari 2002; G. Chen, Trombley, and van den Pol 1996; Cherubini et al. 1990;

Luhmann and Prince 1991; Owens et al. 1996). This phenomenon has been extensively reported in tissues such as the hippocampus and the cortex, notably by (Rinetti-Vargas et al. 2017) who reported a **decrease of E_{GABA} from -40 mV to -82 mV between P2 and P60 in neocortical pyramidal cells**. A recent work made a significant breakthrough with an ***in vivo*** **manipulation of neonatal interneurons**, demonstrating the interneurons exerts excitatory actions in the hippocampus at P3, while by P7 their activity became mainly inhibitory (Murata and Colonnese 2020). This developmental dynamic of $GABA_AR$ polarity is however not occuring in all neurons. This is notably the case in the olfactory bulb, where the neurotransmission remains excitatory in correlation with chloride loading (H. Kaneko 2004; Reuter et al. 1998). Interestingly, further differences can be observed when looking in other taxons, for example in birds auditory system (Milenković and Rübsamen 2011) where GABA activity is excitatory at mature stages, illustrating the remarkable diversity of GABAergic neurotransmission in the living (I will refrain from mentioning other roles of GABA in fungi, bacteria or plants). Nevertheless, beyond some notable exceptions, a decrease in $[Cl^-]_i$ and the consequent increase in $GABA_AR$ driving force appears to be the general rule in the mammalian brain. The consequences of the GABAergic shift on post-synaptic neuronal responses differ between cell types : Banke and McBain in 2006 reported a shunting GABAergic transmission in CA3 interneurons throughout development, while pyramidal CA3 cells responses exhibited a switch from depolarizing to hyperpolarizing (Banke and McBain 2006). In both cases, GABA realease causes inhibition in the mature hippocampus.

1. A. c. Alterations of $[Cl^-]_i$ and their consequences

I discussed the importance of chloride homeostasis for neuronal inhibition mediated by GABA, and described how $[Cl^-]_i$ differs among subcellular domains, cell types, brain regions but also evolves during development. Proper regulation of neuronal inhibition and excitation is essential for the network activity, allowing synchrony and precise patterns of activation (Konstantoudaki et al. 2014). GABAergic activity potential to trigger depolarization or hyperpolarization with a great diversity of patterns results in a wide array of responses from individual neurons, influencing in turn the network activity.

A **correlation of chloride homeostasis dysregulation with pathological conditions**, such as ones associated with neuropathic pain (M. Gagnon et al. 2013; Lorenzo et al. 2020), epilepsy

(Huberfeld et al. 2007; Kourdougli et al. 2017; Y. Wang, Wang, and Chen 2018), an experimental model of Parkinson's disease (Lozovaya et al. 2018), or a model of Rett syndrom (Lozovaya et al. 2019), has been established. The pathological and therapeutical aspects of chloride homeostasis have been well covered by several reviews highlighting mechanistic aspects which will be presented in the following sections (Auer et al. 2020; Blaesse et al. 2009; Joseph Glykys et al. 2017; Kaila et al. 2014; Medina et al. 2014). Under those conditions an impairement of GABAergic inhibition can be observed. However one shall not make this observation an equivalence, as excitatory GABAergic neurotransmission can occur without pathological consequences, and conversely changes in GABAergic signalling effects are not observed in all neurons or in all studies focusing on these pathologies.

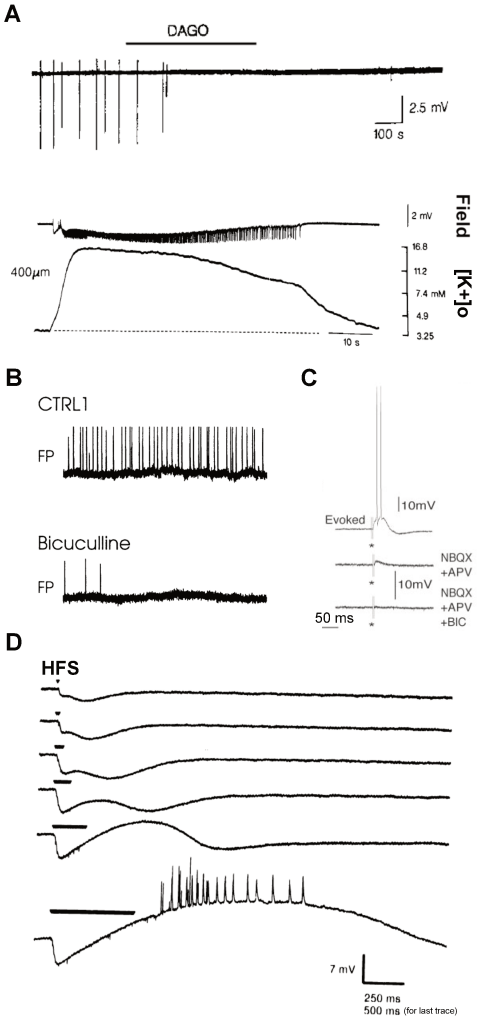

Figure 6, involvement of GABAergic neurotransmission in epileptiform activities. **A**, blockade of presynaptic GABA release in young rat hippocampus prevents 4-AP mediated spontaneous potentials and subsequent ictal discharges (Barbarosie et al. 1994). **B**, 4-AP mediated epileptiform activities are correlated with increased $[K^+]_o$ levels due to $GABA_AR$ activity, potentially causing a generalized depolarization in neurons (Avoli et al. 1996). **C**, $GABA_AR$ blockade abolishes the occurence of depolarizing potentials in epileptic patients' neocortical temporal lobe tissue (Kohling et al. 1998). **D**, GABAergic-mediated pyramidal cell excitation during inter-ictal events (Cohen et al. 2002). E, high frequency stimulation increased duration causes a $GABA_AR$-dependent depolarization (Jackson et al. 1999).

The link between GABAergic interneurons activity and epilepsy was seldom explored. While studying 4 amynopyridine (4-AP, a blocker of Kv1 channels and a potentiator of voltage-gated Ca^{2+} channels (Z.-Z. Wu et al. 2009)) effects in CA1 hippocampal pyramidal slices, Avoli and Perreault observed important **GABA-dependent depolarizations** (Avoli and Perreault 1987). After demonstrating that 4-AP can lead to interictal epileptiform discharges and intracellular long-lasting depolarizations in hippocampus slices, it was suggested that the latter effect was due to **GABAergic interneuron activity** (Perreault and Avoli 1992). Further work demonstrated the implication of these GABAergic conductances in the initiation of ictal-like discharges in the slices (Avoli et al. 1996). The authors' model revolved around a role of GABAergic activity in the increase of $[K^+]_o$ *via* synchronous actitivy of interneurons, allowing the spreading of these activities due to the general depolarization caused by K^+ efflux. These works unravelled a non-synaptic role of GABA in the onset and development of epileptiform events in the enthorinal cortex and the hippocampus. Kaila et al. in 1997 showed that a GABA-dependent mechanism of increased $[K^+]_o$ after high frequency stimulation was dependent on bicarbonate ions, resulting in large and long-lasting GABA-dependent depolarization in hippocampal slices (Kaila et al. 1997). These efforts revealed the **importance of neuronal inhibition in the synchronicity and the spreading of ictal-like discharges, with the hypothesis of a $[K^+]_o$ build-up following intense activity of GABAergic interneuron.**

Other results pointed at **changes in $GABA_AR$ activity under pathological contextes**, with an impaired inhibition mediated by these receptors. Kapur and Coulter observed a decreased (or absent) I_{GABAAR} in a majority of neurons from rats after *status epilepticus* (Kapur and Coulter 1995). Another effort by van den Pol et al. reported a **$GABA_AR$-dependent $[Ca^{2+}]_i$ increase in hypothalamic neurons after neuronal trauma** (e.g : neurite transection or osmotic imbalance), hence confirming a change in $GABA_AR$ driving force (van den Pol, Obrietan, and Chen 1996). When working on tissue from patients with temporal lobe epilepsy Kohling reported hyperpolarizing post-synaptic potentials depending mainly on chloride (Kohling 1998). However blocking several glutamatergic or $GABA_A$ receptors suppressed hyperpolarizing but also depolarizing potentials, suggesting **$GABA_AR$ are heavily involved in the epileptiform activites by providing a synchronicity relying on a "reset mechanism"**, in addition to the identified depolarizing activity of some GABAergic synapses. Cohen in the same context of temporal lobe epilepsy observed spontaneous synchronous activities in the subiculum (Cohen 2002). Like in

Kohling et al., blocking either glutamatergic or $GABA_AR$ neurotransmissions prevented these events. Pyramidal cells discharging during interictal-like events also underwent depolarizing synaptic events, further validating the role of GABA in population events, notably due to a depolarizing action of this neurotransmission. Combined with this proactive role of $GABA_AR$ in excitation Taira et al. demonstrated that $GABA_AR$ could mediate posttetanic excitation in rat CA1 pyramidal neurons, causing a late and prolonged spike firing, following intense activation of GABAergic interneurons (Taira, Lamsa, and Kaila 1997). A similar cause for $GABA_AR$ actions was identified by Jackson and Esplin who reported **$GABA_AR$-dependent depolarizing responses in CA1 pyramidal cells following high-frequency stimulation of interneurons**, suggesting that repetitive stimulation of interneurons can lead to a depolarizing effect of the neurotransmitter on pyramidal neurons (Jackson and Esplin 1999).

Hence $GABA_AR$ activity is related to the occurrence of depolarizing synaptic GABAergic currents, and **the role of GABAergic neurotransmission on the network activity is crucial in the context of epilepsy**. **Similarly to the developmental shift in GABAergic response polarity, chloride homeostasis has a considerable importance under pathological conditions in the mature brain**. Thus understanding the mechanisms at play in chloride homeostasis is pivotal.

1. A. d. KCC2 and NKCC1 function in neuronal chloride homeostasis

I presented how the regulation of $[Cl^-]_i$ directly impacts GABAergic-mediated depolarization and excitation occurences. Two situations illustrating this phenomenon are the GABAergic shift during development, and alterations in GABAergic neurotransmission polarity under several physio-pathological contexts. A key protein in neuronal chloride homeostasis was identified by (Rivera et al. 1999), who presented the **K^+-Cl^- co-transporter 2 (KCC2) as a crucial chloride extruder in hippocampal neurons**, with an expression pattern correlated with the observed decrease in $[Cl^-]_i$ during development. This transporter was previously identified and characterized by Payne et al. who underlined its **remarkable expression pattern, strictly restricted to central nervous system neurons** (Payne, Stevenson, and Donaldson 1996). KCC2 transports chloride ions using the free energy provided by potassium ions gradient in an electroneutral fashion (1 Cl^- and 1 K^+ stoechiometry). Another key chloride transporter, the **Na^+–K^+–Cl^- co-transporter 1 (NKCC1), is expressed in the majority of cell types, including glial cells**,

and is a co-transporter typically involved in cell volume regulation and osmotic response (Delpire et al. 1999; Gamba 2005a; Henneberger et al. 2018; Payne et al. 2003; Schmidt et al. 2018; Stenesen et al. 2019). NKCC1 is an electroneutral transporter (2 Cl^-, 1 Na^+ and 1 K^+ stoechiometry) **mainly associated with chloride loading in the cells**. NKCC1 expression in neurons was demonstrated using *in situ* hybridization and immunofluorescence (Plotkin et al. 1997). NKCC1 function in neuronal $[Cl^-]_i$ regulation was demonstrated by Sung et al. in mature dorsal root ganglion (DRG) neurons using NKCC1$^{-/-}$ mice and bumetanide (a specific inhibitor of NKCC1) (Sung et al. 2000). The functional role of NKCC1 in mature neurons was also reported in the hippocampus, together with a first quantification of the contribution of carbonate ions to E_{GABA} (Tyzio et al. 2008). The functional relevance of these transporters in physio-pathological models has furthermore been reported in a number of publications (Dzhala et al. 2005; Dzhala and Staley 2020; Joseph Glykys et al. 2009; Huberfeld et al. 2007). Thus KCC2 and NKCC1 are important regulators of neuronal chloride homeostasis, and the correlation of their expression with $[Cl^-]_i$ has been demonstrated in neurons by Yamada et al. in 2004 (Yamada et al. 2004).

The thermodynamical aspects of NKCC1 and KCC2 are thoroughly described in (Kaila et al. 2014), notably in the supplementary information. I here succintly present the consequences of those aspects on neuronal homeostasis. The energy available for the transporter's transport is dependent on ions' free energy (FE) :

$$\Delta FE_{ion} = FE_{ion,o} - FE_{ion,i}$$

$\Delta FE_{ion} = RTln\left(\frac{[ion]_o}{[ion]_i}\right) - z_{ion}FVm$; note that when FE > 0 there is an inward flow of the considered ionic specie.

We have :

$$\Delta FE_{KCC2} = \Delta FE_{Cl} + \Delta FE_K$$
$$\Delta FE_{NKCC1} = 2 \times \Delta FE_{Cl} + \Delta FE_K + \Delta FE_{Na}$$

Thermodynamic equilibrium for KCC2 is then reached when :

$$[Cl]_i = [Cl]_o \times \left(\frac{[K]_o}{[K]_i} \right)$$

if $[Cl]_i > [Cl]_o \times \left(\frac{[K]_o}{[K]_i} \right)$, KCC2 mediates chloride efflux ;

if $[Cl]_i < [Cl]_o \times \left(\frac{[K]_o}{[K]_i} \right)$, KCC2 mediates inward transport.

Thermodynamic equilibrium for NKCC1 is reached when :

$$[Cl]_i = [Cl]_o \times \sqrt{\left(\frac{[Na]_o \times [K]_o}{[Na]_i \times [K]_i} \right)}$$

if $[Cl]_i > [Cl]_o \times \sqrt{\left(\frac{[Na]_o \times [K]_o}{[Na]_i \times [K]_i} \right)}$, NKCC1 mediates chloride efflux ;

if $[Cl]_i < [Cl]_o \times \sqrt{\left(\frac{[Na]_o \times [K]_o}{[Na]_i \times [K]_i} \right)}$,NKCC1 mediates inward transport.

With ionic concentrations set as follow : $[Cl^-]_o$ = 120 mM, $[K^+]_o$ = 4mM, $[Na^+]_o$ = 145 mM ; $[K^+]_i$ = 155 mM, $[Na^+]_i$ = 12 mM, we have the following equilibrium values :

$[Cl^-]_i$(KCC2) = 3.1 mM

$[Cl^-]_i$(NKCC1) = 67 mM

Consequently, **given physiological concentration ranges, KCC2 usually mediates chloride efflux and NKCC1 chloride influx**. Nevertheless inversion of the co-transporter's polarity have been reported and even associated with pathological conditions. Interestingly, while most electrophysiology publications disclose the reversal potential for chloride or $GABA_AR$ activity, it is rarely complemented with measurements of the corresponding driving force. Hence non-canonical effects of those transporters on the resting membrane potential may be ignored (Goutierre et al. 2019), and the functional consequence of their expression not fully assessed.

Although the functional importance of KCC2 and NKCC1 chloride transport activity in neurons has been widely reported and reviewed (Ben-Ari 2002; Boffi et al. 2018; Kristopher T. Kahle et al. 2013; Otsu et al. 2020; Schulte, Wierenga, and Bruining 2018; Sulis Sato et al. 2017), inhibition with pharmacological or genetic means of either KCC2 or NKCC1 reveals the presence of other $[Cl^-]_i$ regulatory mechanisms. A first statement is that the inhibition of NKCC1 or KCC2 with respectively bumetanide or VU0240551 does not lead to a monotonous response in neuronal $[Cl^-]_i$ (J. Glykys et al. 2014a; Sulis Sato et al. 2017). The study of NKCC1$^{-/-}$ mice underlined the **importance of compensatory mechanisms in several cell subtypes, among which anion exchangers (AE) play a significant role** (Gonzalez-Islas, Chub, and Wenner 2009; Nickell et al. 2006; Nickell, Kleene, and Kleene 2007; Pfeffer et al. 2009; Taylor-Burds, Cheng, and Wray 2015). A notable category of anion exchangers involved in chloride homeostasis are the Cl^-/HCO_3^- exchangers, which expression and function are reviewed in (Bonar and Casey 2008). Among these exchangers, expression in the nervous system has been reported for AE2, AE3, NDCBE,

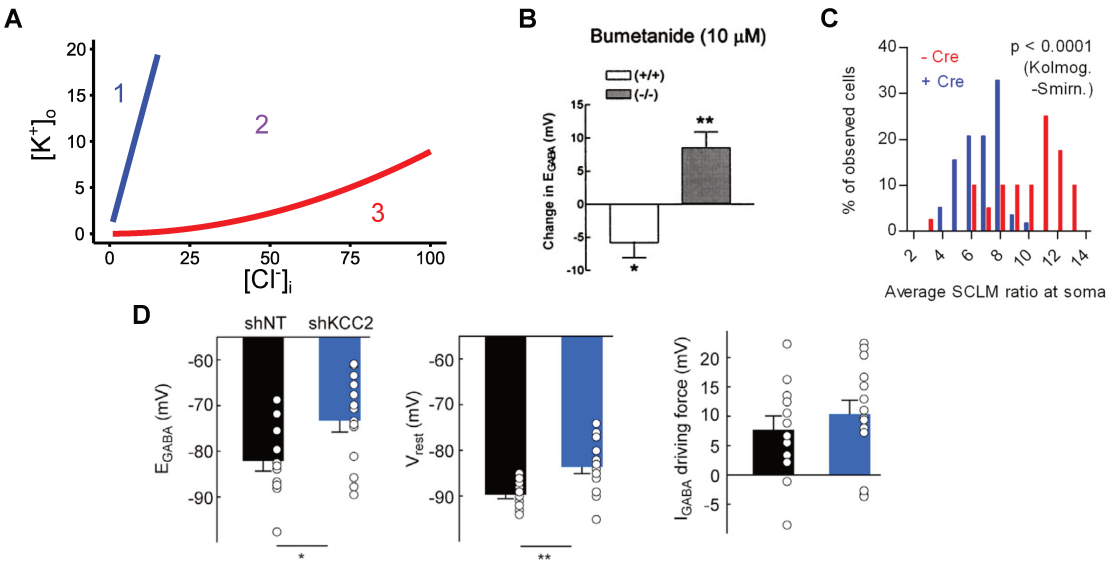

Figure 7, Contribution of KCC2 and NKCC1 function in neuronal chloride homeostasis. **A**, theoretical driving force equilibrium of KCC2 (blue) and NKCC1 (red) depending on $[Cl^-]_i$ and $[K^+]_o$. State 1 : KCC2 and NKCC1 exert inward transport (notably includes high potassium context) ; state 2 : KCC2 exerts outward transport while NKCC1 mediates inward transport (assumed to be the most common state) ; state 3 : KCC2 and NKCC1 mediate outward transport. Note that NKCC1 thermodynamical equilibrium also depends on sodium ions. **B**, NKCC1 activity increases Cl^--dependent E_{GABAAR}. In NKCC1(-/-) mice, NKCC1 blockade had an opposite effect, suggesting compensatory mechanisms of chloride intrusion in DRG neurons (Sung et al. 2000). **C**, KCC2 activity is crucial to maintain low levels of intracellular chloride in the mature brain (+ Cre condition is a conditionnal KCC2 KO) (Boffi et al. 2018). **D**, KCC2 interacts with a K^+ channel, allowing its expression at the membrane of neurons. Consequently, knock-down of KCC2 in the dentate gyrus did not alter $GABA_AR$ driving force, but rather increased the RMP due to the potassium channel not being expressed at the membrane. This result highlights the importance of non-canonical roles of KCC2 and NKCC1 beyond chloride transport (Goutierre et al. 2019).

NCBE and SLC26A7 (olfactory epithelium and retina). Their function has been associated with pH_i regulation due to the transport of bicarbonate ions with the implication of the Carbonic anhydrases catalysis. Hence there is a tight coupling between pH and $[Cl^-]_i$ in neurons in addition to the functional importance of HCO_3^- in GABAergic neurotransmission.

The voltage-sensitive chloride channel 2 (CLC-2) is another protein involved in neuronal chloride homeostasis. Its role in $[Cl^-]_i$ modulation was hypothesized in dopaminergic neurons in the absence of KCC2 expression (Gulácsi et al. 2003). However further evidence regarding its functional importance in chloride homeostasis is lacking, which is likely a consequence of KCC2-mediated chloride flux being more important (Yelhekar, Druzin, and Johansson 2017). Yelhekar et al. furthermore reported the intervention of $GABA_AR$ activity in chloride resting conductance and recovery. It is noteworthy that, although KCC2 and NKCC1 are presented as the sole CCC expressed in CNS neurons, KCC3 has also been presented as a potential actor in neuronal intracellular chloride modulator (Lucas et al. 2012, 20). However, akin to NKCC1, its wide expression pattern complicates its study, combined with its homology with KCC2. In the end its expression and function in neurons are supposed to be limited (Payne et al. 2003).

Another proposed mechanism intervening in the regulation of $[Cl^-]_i$ was presented by Glykys et al. in 2014, where the authors advance the hypothesis that intracellular and extracellular organic anion distributions play a role on $[Cl^-]_i$ (J. Glykys et al. 2014a). The authors established a negative correlation between the cytoplasmic nucleic acids (intracellular anions) or extracellular matrix staining (extracellular anions) concentrations and $[Cl^-]_i$. These results led to the idea that the **negative charges of these impermeant anions influence chloride electrochemical gradients**. Although this papers was vividly discussed in the scientific community (J. Glykys et al. 2014b; Luhmann, Kirischuk, and Kilb 2014; Voipio et al. 2014), notably due to its bold conclusions regarding the role of KCC2 and NKCC1 in transmembrane chloride transport, it has the merit to explore other mechanisms of chloride homeostasis. Nevertheless this **role of impermeant anions has actually not been linked with functional aspects regarding $GABA_AR$ driving force** (Doyon et al. 2016; Düsterwald et al. 2018; Klein et al. 2018), and the co-transporters are still regarded as the main actors of chloride concentration regulation (Boffi et al. 2018; Doyon et al. 2011; Otsu et al. 2020; Rinetti-Vargas et al. 2017).

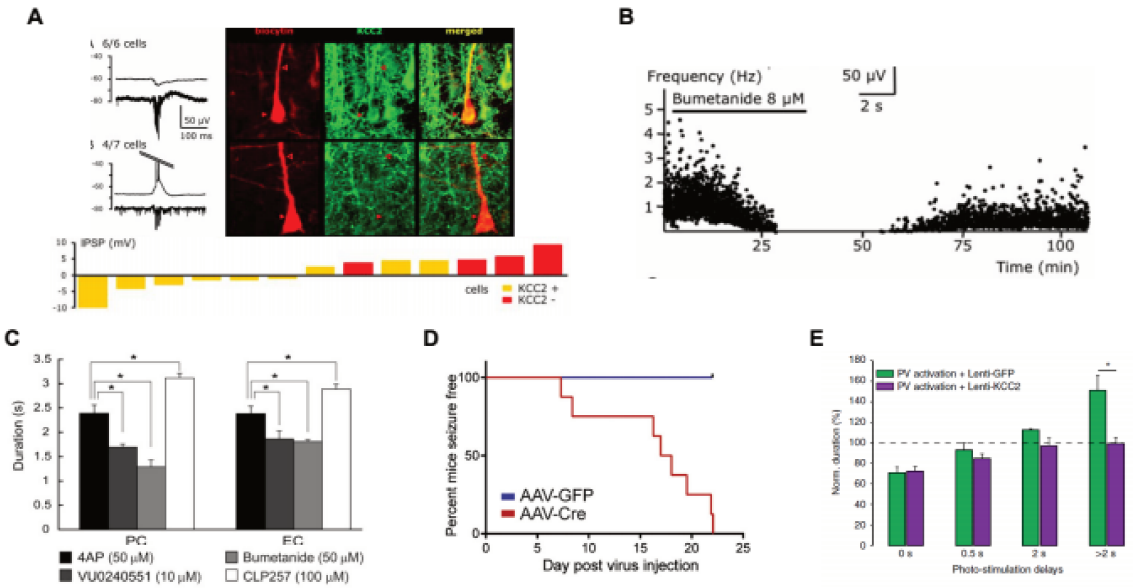

Figure 8, Impaired GABAergic inhibition is associated with KCC2 and NKCC1 activities and/or expression. **A**, depolarizing current mediated by $GABA_AR$ in subiculum pyramidal cells was correlated with an absence of KCC2 staining. **B**, interictal-like activities were blocked after bumetanide bath application (Huberfeld et al. 2007). **C**, duration of epileptiform events in 4-AP triggered epileptiform activity was decreased by KCC2 (VU0240551) and NKCC1 inhibition, while KCC2 stimulation (CLP257, although the drug's effect is debated) increases their duration (Hamidi et al. 2015). EC : enthorinal cortex, PC : piriform cortex. **D**, following conditionnal inactivation of KCC2 in mice hippocampus principal neurons (AAV-Cre condition), spontaneous seizures were observed in the following days (Kelley et al. 2018). **E**, over-expression of KCC2 in visual cortex L5 pyramidal neurons prevents PV interneuron activity-mediated seizure extension when stimulation delay was > 2s (Magloire et al. 2019).

Looking back at early works suggesting the role of a $[K^+]_o$ build up in synchronous interictal-like spikes due to GABAergic activity, it is worth noting that, as KCC2 chloride extruding activity relies on potassium gradient, it was found to have a part in this build-up (DeFazio et al. 2000; Di Cristo et al. 2018; Viitanen et al. 2010). A following work aimed at modelizing the functional importance of a KCC2-dependent increase of $[K^+]_o$ in in a context of epileptiform events induction by 4-AP in the enthorinal cortex (González et al. 2018). The authors reported that after **preventing KCC2-dependent $[K^+]_o$ augmentation through inhibition of its activity the interneurons stimulation does not induce epileptiform ictal events**. Hence, in addition to an intracellular chloride depletion role, **KCC2 also acts as an extracellular potassium accumulating transporter**. KCC2 would thus be a Dr. Jekyll (Kelley et al. 2018; Moore et al. 2018; Silayeva et al. 2015; S. Sivakumaran et al. 2015) and Mr. Hyde (González et al. 2018; Hamidi and Avoli 2015;

Taylor-Burds, Cheng, and Wray 2015; Viitanen et al. 2010) case regarding the excitation/inhibition balance in the hippocampus. Observed divergences may derive from the use of different pharmacological tools or protocols. **Recent works tend to favorize the hypothesis of a beneficial role of KCC2 in the context of inhibitory neurotransmission**, which was observed in a variety of models while its detrimental effects were essentially recorded in 4-AP treated hippocampal slices.

The timing aspect of KCC2 role in GABAergic neurotransmission was recently studied in (L.-Y. Chen, Lévesque, and Avoli 2020) and (Magloire et al. 2019). The first publication reports an increased firing of enthorinal cortex interneurons at the onset of interictal-like spikes with KCC2 pharmacological inhibition, and a disrupted recruitment in the falling phase of those spikes. Magloire et al. used a pilocarpine model of epilepsy, with more straight-forward conclusions. They observed that stimulation of parvalbumin interneurons at the seizure onset reduced the seizure length by around 40%, while stimulation 2 seconds or more after the onset led to an increase in their duration by around 40%. When the interneurons over-expressed KCC2, a decrease in seizure duration was observed (<0.5s after onset) but no significant change was reported for stimulations occuring later. Hence there is indeed an **importance in the interneurons firing timing, which can be either "protective" or "aggravating"**. Combined with the complex dynamics of epileptic neuronal networks, it appears that KCC2 and linked GABAergic inhibition effects can importantly differ depending on recruitment timings for example.

1. B. KCC2 and NKCC1, Cation-Chloride Co-transporters dynamically expressed throughout the brain

Having presented the functional importance of KCC2 and NKCC1 in GABAergic neurotransmission via their chloride transport activities, I will here present these proteins with more details regarding their expression pattern and structure.

1. B. a. The CCC family

KCC2 and NKCC1 belong tho the cation chloride co-transporters (CCC) family, which comprises nine electro-neutral transporters. They are expressed from the solute carrier 12 (SLC12) A 1-9 genes. This family includes two “orphan” members, co-transporter interacting protein 1 (CIP1) and CCC9, which have ~ 20% of identity with the rest of the family and mostly unknown function (Gamba 2005a; Hartmann and Nothwang 2015). We will focus on the seven other members of the family : the K^+-Cl^- co-transporters KCC1, KCC2, KCC3, KCC4, the Na^+-K^+-Cl^- co-transporters NKCC1, NKCC2, and the Na^+-Cl^- co-transporter NCC.

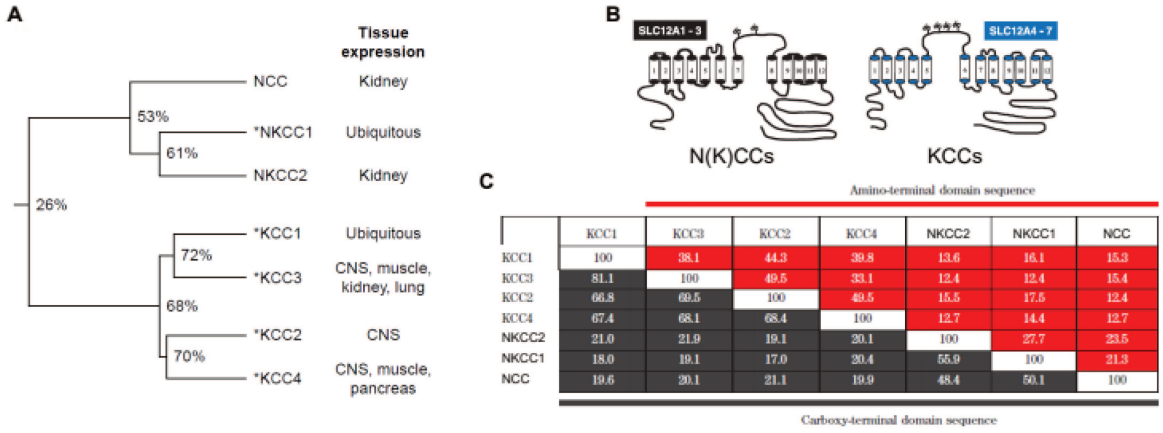

Figure 9, cation-chloride co-transporter family. **A**, phylogenetic tree of CCCs based on identity between aligned human sequences (Payne et al. 2003). Note that the main divergences are between N(K)CCs and KCCs, and between NKCCs and NCC. **B**, schematic structure of N(K)CCs and KCCs, at the time derived from hydropathy indexes and sequences homology. **C**, identity among the different members of the CCC family, regarding the NTD (red) and the CTD (black) domains. Full sequences and central hydrophobic sequences share ~60% to 70% identity among KCCs or N(K)CCs, while CCCs NTD appears to be quite divergent, as well as N(K)CCs CTD (Gamba 2005).

CCC proteins are expressed at the plasma membrane, and have an apparent molecular weight of 120-200 kDa. Their structural features were inferred from hydrophobicity profiles (Gerelsaikhan and Turner 2000; Payne et al. 1997; Payne, Stevenson, and Donaldson 1996, 199; Race et al. 1999; J. C. Xu et al. 1994). These analysis suggested a 12 transmembrane domains structure with intracellular termini. Structural insights of CCC from X-rays experiments were reported. (Warmuth, Zimmermann, and Dutzler 2009) obtained the 3D structure of a procaryotic (*Methanosarcina acetivorans*) CCC (MaCCC) C-terminal domain (CTD). The co-transporter only displays a 24% identity with human NKCC2, with higher identity in the transmembrane (TM) region (31%). These differences with mammalian CCC and other features such as no long N-terminal domain (NTD) in MaCCC's structure indeed impair the possibility to generalize the presented data to human N(K)CC. Nevertheless it provided valuable information, with a **confirmation and further insights of the homodimerization of N(K)CC** (Moore-Hoon and Turner 2000; Parvin, Gerelsaikhan, and Turner 2007). Agez et al., using electron microscopy, identified **monomers and homo-dimers of KCC2** (Agez et al. 2017). Their work suggests that KCC2 CTD is crucial for the transporter dimerization and function, providing the first 3D structure of KCC2. Highly resolutives structures of KCC1 (S. Liu et al. 2019), KCC4 (Reid, Kern, and Brohawn 2020), KCC2, KCC3 (Chi et al. 2020, 3) and NKCC1 (Chew et al. 2019; X. Yang, Wang, and Cao 2020) have been recently obtained with cryo-electron microscopy, providing important insights for their transport function and oligomerization. A key difference between KCC and N(K)CC is the localization of their large extracellular loop : between TM5-6 in KCC (S. Liu et al. 2019; Reid, Kern, and Brohawn 2020) with apparently different functions in KCC4 and KCC1, and between TM7-8 in N(K)CC (Chew et al. 2019; Gamba 2005a; X. Yang, Wang, and Cao 2020), although this loop appears to be one of the most divergent regions among NKCC1 homologs. In conclusion, recent publications allow a better understanding of the CCC structure and function in mammals but also in other taxa (Chew et al. 2019; Zimanyi et al. 2020).

These transporters have been associated with ionic transport, but also water flux, making them key players in cell volume regulation, notably in case of change in environmental osmolarity (Gamba 2005a). This convergence in function and structure is combined with important differences in terms of tissue expression and in terms of response to tonicity (Garneau et al. 2020; Mercado et al. 2006; Murillo-de-Ozores et al. 2020; Payne et al. 2003). The greatest difference lies in the distinction between KCC and N(K)CC transport polarity, with **KCC being**

associated to the extrusion of potassium and chloride, and N(K)CC with intrusion of sodium, (potassium) and chloride with corresponding water flow. Hence CCC play crucial roles in tissues such as the kidney or epithelia where ionic transport and translocation are of upmost importance. To illustrate this versatility we will take the example of NKCC1. Its functional relevance was demonstrated in a wide variety of processes, with an impact on cellular processes such as mitochondrial respiration (Omer, Koumangoye, and Delpire 2020), regulation of cell proliferation via cell volume tuning (Demian et al. 2019), a role in cerebrospinal fluid formation (Steffensen et al. 2018), or in hearing (Delpire et al. 1999). For a comprehensive review on NKCC1 roles and regulations, see (Delpire and Gagnon 2018). Hence when we discuss CCC functions in an organism, one must look out for more actions than chloride transport or cell volume, not mentionning splicing variants or post-translational regulations which bring further diversity.

In the following sections I will mainly focus on KCC2 and NKCC1 expression and function in the brain, and especially in neuronal cells.

1. B. b. Expression patterns of NKCC1 and KCC2 in the central nervous system

NKCC1 is an broadly expressed co-transporter (Delpire et al. 1994), encoded by the SLC12A2 gene located on chromosom 5 in humans. NKCC1 was found to be expressed in neurons but no evidence for NKCC1 expression in glial cells was reported in the same work (Plotkin et al. 1997). Another effort later suggested the opposite (C. Wang et al. 2002) with the confirmation of its expression in neural cells. A similar discrepancy was initially reported in the dorsal horn (Galan and Cervero 2005; Morales-Aza et al. 2004). However, likewise, several publications reported NKCC1 expression in glial cells (Peng et al. 2013). These discrepancies are mainly due to the **difficulty to study NKCC1 expression via immunofluorescence approaches** (Blaesse et al. 2009), and in situ hybridization efficiency can be limited in astrocytes (Peng et al. 2013). Hence scientists have resorted in using **functional inhibition of NKCC1 to determine its expression**. It is now generally accepted that **NKCC1 is expressed in glial cells, and notably astrocytes, where its function is crucial** (Henneberger et al. 2018; C. S. Wilson and Mongin 2019).

The regional expression of the co-transporter in the brain, as well as the regulation of this

expression during development has been subject to debates. These interrogations were thouroughly described in a recent review from which I here present the most relevant features regarding my work (Virtanen et al. 2020). These debates notably arise from the existence of **two different isoforms : NKCC1a and NKCC1b**. These isoforms differ by the splicing of exon 21 for NKCC1b, coding for an amino-acid sequence in the CTD and containing a putative PKA phosphorylation site as well as a dileucine motif which likely have functional relevance (Randall, Thorne, and Delpire 1997, 7). Two studies specifically focusing on their respective expression in the brain had different conclusions regarding the prevalence of one on another (Gregoriades et al. 2019 ; Vibat et al. 2001). The evolution of NKCC1 expression in neurons is also debated. **Published work on this matter do not agree with reports of an upregulation, a downregulation or a stable expression during development**. An alternative option is to measure NKCC1 mRNA levels using either PCR or in situ hybridization, at the cost of a more indirect estimation of the transporter protein levels. Nevertheless, the results obtained using this approach were divergent as well. Hence technical difficulties in targetting NKCC1, together with the apparent variability in the transporter expression depending on cell types, limits the conclusions on NKCC1 expression level in neurons (Blaesse et al. 2009). Recent single-cell transcriptomics databases allowed quantitative and reproductible evaluation of NKCC1 transcription in the brain, suggesting that NKCC1 is much more expressed in glial cells than in neurons. They should thus prove essetial in the future to answer these interrogations.

On the other hand, the **study of KCC2 expression has been more straightforward**, notably due to its expression restrained to neurons (Payne, Stevenson, and Donaldson 1996). Consequently immunohistochemistry, mRNA and biochemistry assays to determine regional, cellular and developmental patterns of KCC2 expression in neurons are easier to interpret. **The co-transporter expression has been observed in most of the brain** (Watanabe and Fukuda 2015), including regions such as the hippocampus (Rivera et al. 1999). In the same fashion, aforementioned **KCC2 up-regulation during development has been described in numerous papers** (Dzhala et al. 2005; Fiumelli, Cancedda, and Poo 2005; H. Li et al. 2002; Rivera et al. 1999; Sedmak et al. 2016; Stein et al. 2004; C. Wang et al. 2002). Similarly to NKCC1, **two main isoforms compose KCC2 population : KCC2a and KCC2b**. Unlike NKCC1 isoforms which differ by alternative splicing, KCC2a and KCC2b differ in an alternative first exon under the regulation of different promoters (Uvarov et al. 2007). It was demonstrated that the predominant isoform in

terms of protein expression in the mature brain is KCC2b, undergoing a developmental up-regulation relatively to KCC2a, while having similar regional expression (Uvarov et al. 2009). The study of the subcellular distribution of KCC2a and KCC2b suggested a mainly intracellular expression of the first isoform (Markkanen et al. 2014). However a following work by the same authors showed that both isoforms are in fact expressed at the membrane and functional (Markkanen et al. 2017). The different staining was due to the interaction of a regulatory protein with the antibody-targetted epitope in KCC2a. The results obtained in KCC2a/b levels with immuno-staining were confirmed using mRNA quantifications, so the developmental up-regulation of KCC2b is still valid (Markkanen et al. 2017). Yet the respective roles of KCC2a and KCC2b in neurons are yet to be deciphered.

Regarding their subcellular distribution, NKCC1 is expressed in the somato-dendritic, but also in the axonal compartments (Khirug et al. 2008; Plotkin et al. 1997). Due to the aforementioned technical difficulties to look at the co-transporter expression in neurons, our knowledge is rather limited beyond these insights. KCC2 on the other hand is expressed at the membrane in the somato-dendritic compartment, with a strong presence at the vicinity and the periphery of inhibitory and excitatory synapses in CA3 pyramidal cells (Chamma et al. 2013; Gauvain et al. 2011; Gulyás et al. 2001). Interestingly **KCC2 is not expressed in the axon, including the axon initial segment (AIS)** (Chamma et al. 2013; Hübner, Lorke, and Hermans-Borgmeyer 2001), however a study on the chloride homeostasis in the AIS suggests a role of KCC2 in this region following bath application of a KCC2 inhibitor in adult stages (Rinetti-Vargas et al. 2017). This effect is likely due to KCC2 function in the somato-dendritic compartment influencing the AIS chloride reversal potential. KCC2 expression pattern in the brain has been extensively characterized, helped by its restriction to neurons. Conversely studying NKCC1 expression has been much more challenging, further hindering our ability to understand its function and regulation in the mature brain. As my work was centered on NKCC1, I will focus on this transporter in the following parts.

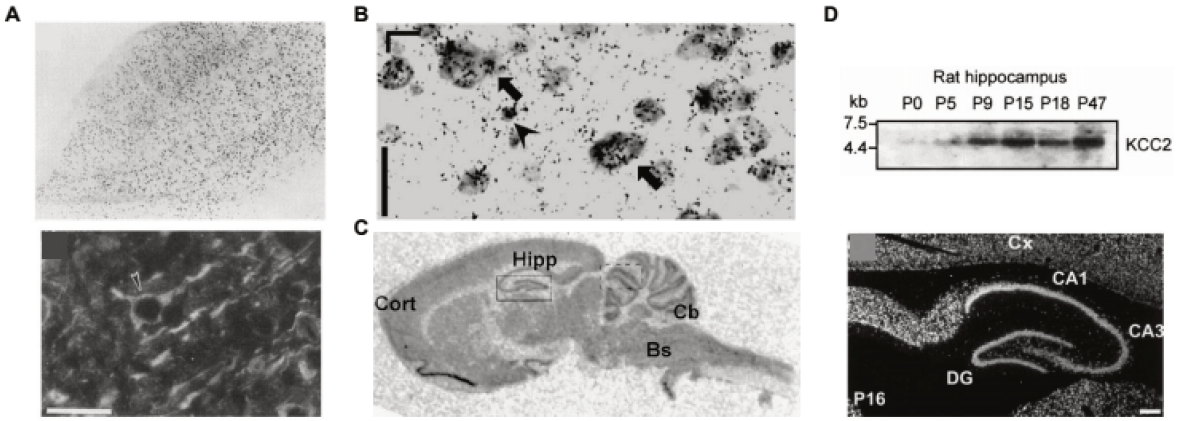

Figure 10, KCC2 and NKCC1 are expressed in the brain. **A**, in situ hybridization with NKCC1 probes showing NKCC1 mRNA in neurons of the cerebral cortex (*up*, in dark), where the co-transporter is expressed in the soma and the dendrites (*bottom*, in light), however no staining was reported in glial cells (Plotkin et al. 1997). **B**, in situ hybridization of NKCC1 mRNA, confirming an expression in neurons, but also suggesting its expression in glial cells. Arrow : neurons, arrowhead : glial cells (Wang et al. 2002). **C**, KCC2 mRNA is broadly expressed in the brain, with an enrichment in the hippocampus or the cerebellum. KCC2's expression, conversely to NKCC1, is restricted to neurons (Payne et al. 1996). **D**, Northern blot of KCC2 over development, demonstrating its developmental up-regulation in rat (*up*). KCC2 expression is up-regulated in the hippocampus, with a substantial increase at P16 (*bottom*) (Rivera 1999).

1. B. c. Transcriptional regulation of NKCC1

NKCC1 mRNA transcription regulation was studied in different tissues, including experimental models of pathologies such as hypertension of cerebral edema. Lee et al. demonstrated *in vitro* and *in vivo* that **methylation of NKCC1 promoter region decreases the transporter mRNA expression**, notably in the rat cerebral cortex (H.-A. Lee, Baek, et al. 2010; H.-A. Lee, Hong, et al. 2010). Ibla et al. in 2006 reported that hypoxia-inducible factor 1α (HIF-1α) down-regulates NKCC1 mRNA expression in epithelial cells while on the other hand Yang et al. in 2019 suggested that NKCC1 mRNA expression in hippocampal neurons is positively regulated by HIF-1α and negatively regulated by nuclear factor of activated T cells 5 in a context of hypoxic-ischemic encephalopathy (Ibla et al. 2006; X.-L. Yang et al. 2019). Cho et al. in 2013 reported that methylation of NKCC1 promoter in a spontaneous hypertensive rat model involves specificity protein 1 (Sp1) in the heart and the aorta (Cho et al. 2013). Huang et al. in 2014 observed an up-regulation of NKCC1 transcription by tumor necrosis factor alpha and interleukin-1 β in astrocytes after cerebral edema (L.-Q. Huang et al. 2014). A **higher methylation of KCC2 DNA, together with a lower methylation of NKCC1 DNA was reported in patients with juvenile myoclonic epilepsy** (Genç et al. 2019). Hence there seems to be a variety of regulators of NKCC1 transcription in different tissues, but these were mainly observed in pathological contextes. So

far only the methylation appears as a consistent regulation of NKCC1 transcription .

Another factor of prime importance (but frequently forgotten) is the sex-specific regulation of mRNA levels. (Perrot-Sinal et al. 2007) analyzed NKCC1 levels between E20 and P5 in rat hypothalamus depending on the sex. The **protein levels of NKCC1 was higher in males at E20 and P0, while females exhibited higher KCC2 levels at P5**. The authors mention the complexity of KCC2 and NKCC1 expression differences between males and females, indicating that the role of estradiol is not obvious. A higher expression of KCC2 was also observed in P15-P30 females by Galanopoulo et al. in 2003 (A. Galanopoulou 2003). Galanopoulo and Moshé in 2003 observed a downregulation of KCC2 mRNA levels in the substantia nigra by estradiol in P15 male rats, but no effect was seen with females (A. S. Galanopoulou and Moshé 2003). This is especially relevant as the need for sex-specific studies has been demonstrated, notably in health-related fields.

1. B. d. NKCC1 Structure

High-resolution structures of zebra fish NKCC1 (Chew et al. 2019) **and human NKCC1** (X. Yang, Wang, and Cao 2020) **were solved in the last two years**, along with several KCC structures, allowing a greater understanding of the CCC family (Delpire and Guo 2019). Unfortunately both efforts did not manage to resolve NKCC1 NTD, which Chew et al. described as a consequence of a disordered structure or conformational flexibility. An important flexibility was also reported for NKCC1 CTD by the same authors, likely preventing Yang et al. to resolve human NKCC1 CTD. Yang et al. remarked that human NKCC1 structure is highly similar to that of *Danio rerio* NKCC1, with the main differences located in their extracellular domains and in loops connecting transmembrane helices. **Both papers identified NKCC1 in homodimers**. An interesting mention from Yang et al. is that **NKCC1, NKCC2 and NCC exhibit only modest sequence identity within their TM11–TM12 helices, which could be a cause for the absence of hetero-dimerization of N(K)CC**. The authors also looked for potential transport mechanisms of NKCC1, suggesting ionic binding sites and pockets. Chew et al. mention the plausible role of a cooperative ion binding involving Cl^-, K^+ and Na^+, while Yang et al. identified several “entryways” for the ionic species. A feature of interest mentioned by Yang et al. is the **curvature of the detergent micells around the transporter**. They make the hypothesis that an important density of NKCC1 would cause the lipid membrane to be deformed locally, and that **membrane fluidity may regulate NKCC1**

transport activity.

Although this kind of output is quite technical, the publication of high-resolution structures of subdomains of NKCC1, KCC1, KCC2, KCC3 and KCC4 is a major step in understanding the CCC.

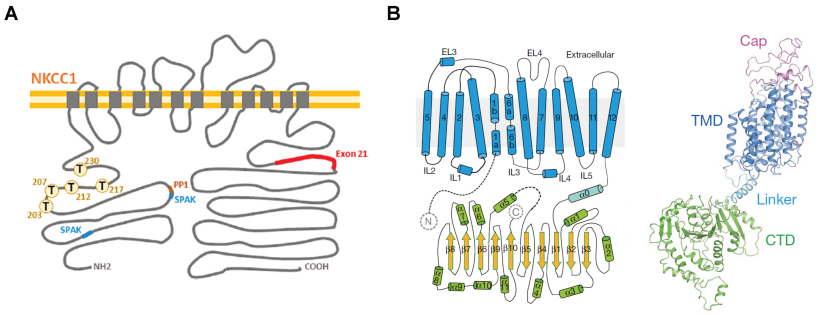

Figure 11, NKCC1 forms homodimers and is regulated by phosphorylation-dephosphoryation. **A**, NKCC1 contains several kinase and phosphatase binding sites, and is phosphorylated at 5 threonine residues. NKCC1a includes the exon 21, lacking in NKCC1b, an exon containing a putative PKA phosphorylation (Côme et al. 2019). **B**, 2D and 3D structure of NKCC1. Note that the NTD could not be resolved. **C**, NKCC1 forms homodimers (Chew et al. 2019). **D**, NKCC1 dimerization may cause a local deformation of the plasma membrane, potentially affecting its structure in regions where NKCC1 is in high density (Yang 2020).

2. NKCC1 is a protein crucial for neuronal chloride homeostasis

Due to their crucial role in regulating chloride homeostasis and GABAergic neurotransmission, KCC2 and NKCC1 have been associated with several conditions of impaired inhibition. In early developmental stages NKCC1 mediates chloride loading in the neurons while in later stages KCC2 activity ends up predominating, resulting in a low $[Cl^-]_i$. The **discrete role of NKCC1 in mature neurons and the challenging evaluation of its protein and mRNA levels result in a low level of understanding and interest in this protein in the mature brain compared with KCC2**.

2. A. A chloride loading transporter

2. A. a. NKCC1-mediated chloride loading in the developping CNS

I have mentioned the roles of KCC2 and NKCC1 in chloride transport. There is a general concensus on the important effect of on KCC2 transport activity on $[Cl^-]_i$ and GABAergic inhibition. However, regarding NKCC1 data are more difficult to interpret in a straight-forward fashion due to the evolution of its prominence in chloride homeostasis throughout development.

Neuronal GABA responses are mainly depolarizing and excitatory in early developmental stages. In 1999, Sun et al. reported bumetanide-sensitive potassium influx in immature cortical neurons. They also demonstrated the regulation of NKCC1 activity in neurons by chloride, sodium and potassium ions (D. Sun and Murali 1999). Yamada et al. in 2004 reported the **decrease of E_{GABA} in neocortical rat pyramidal neurons during development, a change correlated with a decrease in NKCC1 mRNA levels and an increase in KCC2 mRNA levels**. They also observed this correlation when looking at regional differences in E_{GABA}. The involvement of NKCC1 in neuronal chloride loading was observed comparing NKCC1-negative neurons and bumetanide applications, leading to $[Ca^{2+}]_i$ elevations due to GABAergic-dependent depolarizations (Yamada et al. 2004). A similar **decrease of E_{GABA} upon bumetanide application** has been reported by Friedel et al. in immature cultured hippocampal neurons (Friedel et al. 2015), in addition to its impact on immature neurons $[Cl^-]_i$ *in vivo* (Sulis Sato et al. 2017). These results confirm the functional importance of NKCC1 activity on GABAergic neurotransmission at early stages of development. The transport

mediated by NKCC1 affects the activity of the neuronal network in the immature brain, and notably in the hippocampus (Pfeffer et al. 2009; Sipilä et al. 2006).

Further analysis were performed on **NKCC1-mediated chloride transport in immature neurons**, providing data on its kinetics and thermodynamics. Achilles et al. studied $GABA_AR$-mediated chloride current dynamics in Cajal-Retzius cells using gramicidin-perforated patch-clamp (Achilles et al. 2007). After $GABA_AR$ activation, leading to a decrease in $[Cl^-]_i$, **exponential $[Cl^-]_i$ recovery is dependent on NKCC1 activity**, allowing a more depolarized value at steady-state, although the time constant does not significantly change. Interestingly the authors reported no effect of an incubation with 0 mM extracellular chloride concentration on E_{GABA}, while Sun and Murali described an increased activity of the co-transporter under similar conditions. The difference in readouts used (E_{GABA} and Rb^+ transport rate) is a plausible explanation for this divergence. A recent publication by Kolbaev et al. on CA3 pyramidal cells of immature rats describes the consequences of NKCC1 blockade on baseline $[Cl^-]_i$ inferred from E_{GABA} (Kolbaev et al. 2020). **Chloride concentration hence dropped from ~ 20 mM to ~10 mM whithin ~ 10 minutes after bumetanide application, demonstrating that NKCC1 is involved in baseline $[Cl^-]_i$ maintenance**. A more formal study on the contribution of passive diffusion or NKCC1 on chloride transport in P5 rat CA1 neurons was accomplished by Brumback and Staley (Brumback and Staley 2008). They studied the intracellular chloride levels restoration after chloride loading or depletion, and its reliance on the activity of NKCC1. Note that “passive” chloride transport referred in these studies encompasses all non-NKCC1-dependent chloride transport ($GABA_AR$ activity, AE, etc.). They reported the **importance of Na^+/K^+ ATPase activity for NKCC1-mediated chloride loading**, with the pump activation (by action potentials for example) stimulating the co-transporter driving force. This latter result is reminiscent of the report by Sun et al. (1999) of a stimulation of NKCC1's transport after NMDA application, concurrent with increased Na^+/K^+ ATPase activity (D. Sun and Murali 1999). Interestingly Sun and Murali also observed that GABA or muscimol application increased NKCC1 transport activity, an effect correlated with a decrease in $[Cl^-]_i$, confirming the importance of thermodynamical aspects in NKCC1's transport function.

NKCC1 function in maintaining high intracellular levels of chloride has been extensively studied and characterized in early developmental stages, when the co-transporter activity is important for the maturation of the neuronal networks (Ben-Ari 2002; Cancedda et al. 2007; Pfeffer et al.

2009; D. D. Wang and Kriegstein 2011). It is important to keep this positive aspect in mind, as NKCC1 is often associated with non-physiological contextes.

2. A. b. A discussed role for NKCC1 in chloride homeostasis under physiological condition in the mature brain

Increased KCC2 expression, enhancing neuronal chloride extrusion, lowers intracellular chloride, making GABAergic neurotransmission inhibitory. This developmental maturation process occurs in the brain, but also in cultured cells which is quite remarkable. With some notable exceptions like in the olfatory bulb, KCC2 activity appears to be the main driver of chloride homeostasis in mature neurons (Banke and McBain 2006; Ben-Ari 2002; Rivera et al. 1999; Stein et al. 2004). Despite being expressed in mature neurons, as seen from protein and mRNA labelling, or functional characterization with either bumetanide or NKCC1 KO mice, **NKCC1 contribution is often described as minor regarding chloride homeostasis in the developped brain**.

Several papers raised this question. Using chloride imaging, (J. Glykys et al. 2014a) reported that bumetanide application did not yield significant effects on intracellular chloride levels of adult rat neocortical neurons, although their data representations are not the most adequate to support these conclusions. In addition the authors did not provide the confirmation of a strict chloride-dependent modulation of the recorded ratio, which is concerning given the sensitivity of Clomeleon to other factors such as pH and the absence of buffers such as Hepes. On the other hand they observed an effect of NKCC1 inhibition on cellular volume, demonstrating that **NKCC1 is functional but does not significantly impact $[Cl^-]_i$**. Schmidt et al. in 2018 studied mature *nucleus reticularis thalami* (NRT) neurons where NKCC1-mediated chloride loading has been suggested (Schmidt et al. 2018). They report minor effects of NKCC1 inhibition using bumetanide on E_{GABA}, concluding that the **absence of KCC2 expression is the main cause for a higher $[Cl^-]_i$ in NRT neurons**. Furthermore other not well identified chloride loading mechanisms (like AE) could be involved like suggested in gonadotropin-releasing hormone-1 neurons or in the olfactory epithelium whith NKCC1$^{-/-}$ mice (Nickell et al. 2006; Taylor-Burds, Cheng, and Wray 2015). These results seem to confirm the light impact of NKCC1 on chloride levels in mature neurons, whereas KCC2 activity predominates. The respective effects of KCC2 and NKCC1 inhibition were also studied electrophysiologically in principal cells and interneurons from adult

rat hippocampus (Otsu et al. 2020). Even after blocking KCC2-mediated transport, application of bumetanide did not change somatic GABA reversal potential in interneurons, although a slight E_{GABA} decrease was observed in principal cells. As a result, NKCC1 transport function is often described as minimal in the somato-dendritic compartment, and **mostly detectable after KCC2 is inhibited**.

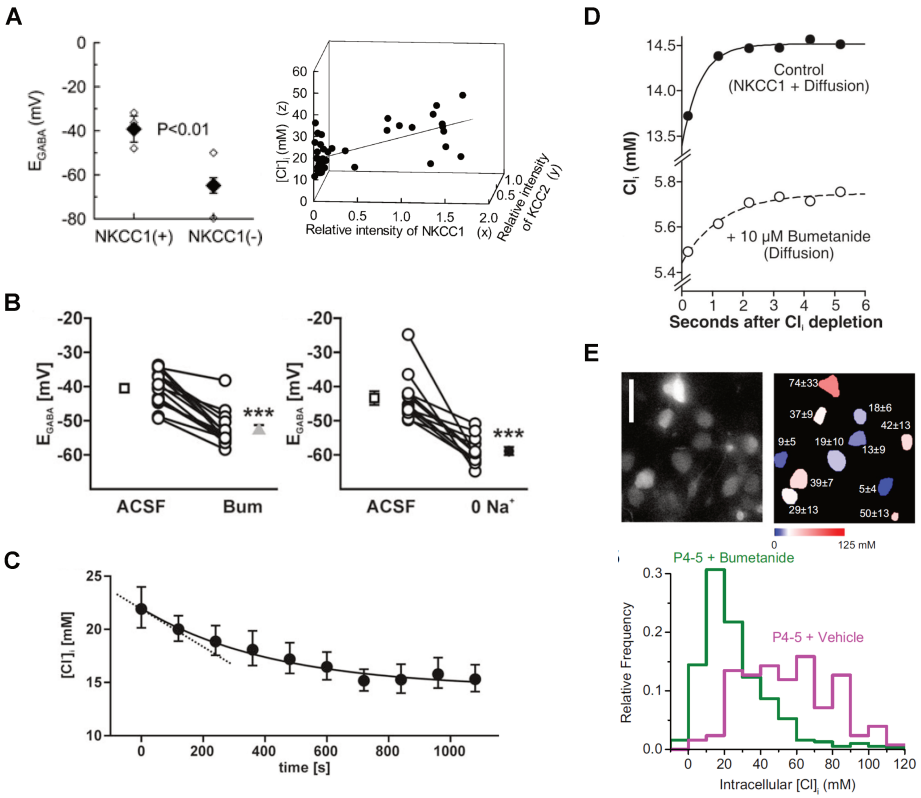

Figure 12, NKCC1 is pivotal for chloride homeostasis in immature neurons. **A**, NKCC1 KO neurons exhibit a higher E_{GABAAR} (*left*), correlated with NKCC1 expression levels (*right*) (Yamada 2004). **B**, pharmacological inhibition of NKCC1 also leads to a decreased E_{GABAAR} (*left*). The role of NKCC1 in $GABA_AR$ response is heavily dependent on sodium ions (*right*), although the cumulative effect of bumetanide and ouabain were not explored. **C**, theoretical evolution of $[Cl^-]_i$ after NKCC1 inhibition with bumetanide, inferred from E_{GABAAR} and Nernst equation (Achilles 2007). **D**, NKCC1 allows $[Cl^-]_i$ recovery after either chloride loading or chloride depletion (shown here). Note the effect of NKCC1 inhibition on both $[Cl^-]_i$ at t=0 and on the recovery kinetics (Brumback 2008). E, NKCC1 loads chloride in neurons *in vivo*(Sato 2017).

A specific role of the co-transporter with functional relevance regarding neuronal activity has been suggested in the axon initial segment. When studying differences in E_{GABA} across different neuronal compartments, Khirug et al. observed that **NKCC1 maintained a more depolarized E_{GABA} in the axon initial segment** (Khirug et al. 2008). The work of Rinetti-Vargas et al. mentioned earlier described a **developmental shift in the AIS chloride levels**, in addition to the well known

GABAergic shift in the somato-dendritic compartment. According to the authors this more depolarizing E_{GABA} is due to NKCC1 activity until ~ P30, then a developmental decrease in the AIS chloride concentrations occurs in later stages, increasingly involving KCC2 activity (Rinetti-Vargas et al. 2017). KCC2 expression was never observed in the axon, consequently this effect could be due to somatic KCC2 inhibition influencing AIS E_{GABA}, explaining a later maturation (Doyon et al. 2011). A recent paper explored proteasomes positions in the AIS in developping neurons (M. Lee et al. 2020). Disrupting these proteasomes in Ecm29 KO mice leads to higher NKCC1 expression in the AIS, an accumulation resulting in a **delayed GABAergic shift due to NKCC1 activity**. It has to be noted that NKCC1 activity could still be significant in the distal axon (e.g. at presynaptic sites), as KCC2 transport in the soma would not lead to changes through chloride diffusion.

Hence in most neurons after early development, chloride homeostasis is heavily driven by KCC2, as the effects of NKCC1 are light and only detected in absence of KCC2 activity. On the other hand the activity of NKCC1 is crucial in the AIS, maintaining a depolarizing GABAergic action. This has consequences on local excitability and action potential generation, $GABA_AR$s being the only known ligand-gated ion channels mediating neurotransmission at the AIS (Leterrier 2018). In neocortical interneurons of P18-24 mice activation of $GABA_AR$ in the AIS leads to an inhibition of neuronal excitability (Jiang 2018). On the other hand Pan-Vazquez et al. in a recent publication showed that Chandelier cells interneurons exert a depolarizing response on principal cells AIS in P12-P18 mice, and become inhibitory by P40-P46 (Pan-Vazquez 2020). Thus, in agreement with Rinetti-Vargas et al., a delayed shift in AIS chloride homeostasis occurs, suggesting a decrease in NKCC1 activity prevalence. As a side note, the majority of studies use bath bumetanide application to inhibit NKCC1 activity, likely triggering effects in cells such as astrocytes leading to off-target effects. An alternative is to perform intracellular incubation of cells with bumetanide through whole-cell clamp (Henneberger et al. 2018). This however comes at the cost of altering intracellular ionic concentrations.

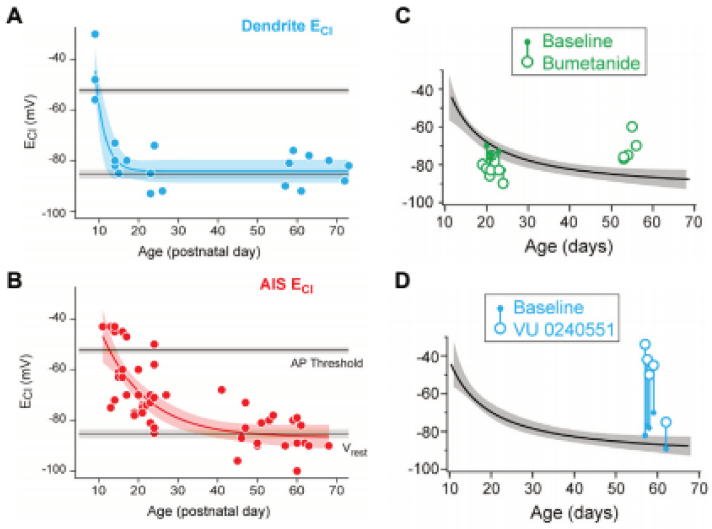

Figure 13, KCC2 activity becomes predominant over NKCC1 in the later stages of development. **A**, in the dendrite chloride reversal potential sharply decreases during the first postnatal days, due to an up-regulation of KCC2 expression. **B**, On the other hand, the axon initial segment (AIS) undergoes such a shift later in development. **C**, this slower decrease in AIS E_{Cl} is due to the activity of NKCC1, keeping the reversal potential at more depolarized values. **D**, at later stages, KCC2 activity strongly affect AIS E_{Cl} while NKCC1 inhibition only has little effect, akin to the dendritic situation (Rinetti-Vargas et al. 2017).

2. B. Under several pathological models related with $[Cl^-]_i$ dysregulation, NKCC1 activity is determinant

NKCC1 transport activity is crucial in the immature brain, leading to depolarizing GABAergic responses and intracellular Ca^{2+} transients. However its prevalence decreases over development in most neurons, due to enhanced KCC2 expression and function. In consequence NKCC1 influence in somato-dendritic and AIS chloride levels appear to be minimal passed certain stages under physiological context. However **an interesting aspect of NKCC1 is its involvement in pathological conditions such as epilepsy**.

2. B. a. NKCC1 and epilepsy in the immature brain

NKCC1's transport activity role in neonatal seizures and epilepsy models was mainly observed *via* the use of bumetanide. In a model of ictal-like activities induced in CA3 by high extracellular

potassium concentration, the drug prevented the occurrence of synchronous network activities and caused a decrease in the recorded signal power (~ mean amplitude) over time (Dzhala et al. 2005). This last effect of bumetanide was not visible in slices from rats older than P21 and NKCC1$^{-/-}$ mice also seemed to experience milder symptoms. **The involvement of NKCC1 in epilepsy was correlated with chloride homeostasis** (Joseph Glykys et al. 2009). NKCC1-mediated chloride loading leads to depolarizing responses to GABA in the neocortex of P7 rats prevented phenobarbital – an allosteric modulator of $GABA_AR$ – from having beneficial effects on kainic acid-induced epileptiform activities. On the other hand in the thalamus, where GABA is hyperpolarizing at this stage, phenobarbital decreased event power. Hence baseline chloride homeostasis regulation by NKCC1 seriously impacts these events, a point further proven by the effect of phenobarbital + bumetanide application which decreased the power of epileptiform activities in both the neocortex and the thalamus

Several works analyzed the morphological consequences of epilepsy, and the related role of NKCC1 activity. Neonatal hypoxic ischemia seizures is a common model, leading to the development of epilepsy. Several papers showed that NKCC1 inhibition with bumetanide can prevent or reduce several effects of hypoxic ischemia such as EEG seizure length and frequency or cells proliferation and migration in the dentate gyrus following the initial trauma (Hu et al. 2017; Luo et al. 2018; S. Wang et al. 2015). During complex febrile seizures (events thought to possibly cause TLE later in life), studied in P5 rats, NKCC1 knock-down with small interfering RNA was reported to prevent abnormal dentate gyrus granule cells migration (Koyama et al. 2012). The authors also observed preventive effects of bumetanide on this migration, as well as a decrease in the severity of later symptoms of the following epilepsy at P60, and a reduced frequency of limbic seizures after bumetanide-mediated NKCC1 inhibition. These effects were associated with $GABA_AR$ signalling, demonstrating a **functional role of NKCC1 in pathologies where GABAergic neurotransmission is impaired *via* cellular migration mechanisms**.

Note that biochemistry expreiments to quantify NKCC1 levels are performed in several of the cited works (Dzhala et al. 2005; Hu et al. 2017; Luo et al. 2018). Biases mentioned earlier prevent a precise analysis of these data due to the wide expression pattern of NKCC1 (Virtanen et al. 2020). The same goes for the actions of bumetanide, which can indeed target neurons to decrease NKCC1-mediated chloride loading, but also astrocytes or other glial cells for example.

2. B. b. NKCC1 and epilepsy in the mature brain

Functional relevance of NKCC1 in immature brain pathological conditions involving GABAergic pathway dysregulation is consistent with its function in immature neurons. However, as introduced previously, **several pathological models with mature neurons, such as Parkinson's disease or neuropathic pain, are associated with a NKCC1-mediated GABAergic signalling alteration**. In the context of epilepsy in the mature brain, several papers also demonstrated a regulation of NKCC1.

A coincident reduction in KCC2 mRNA expression and increase in NKCC1 mRNA levels have been reported along with a higher E_{GABA} in the subiculum of Temporal Lobe Epilepsy (TLE) patients (Palma et al. 2006). However no direct functional impact of NKCC1 was presented in this work. A more explicit link between NKCC1 function and epileptiform activities was described in another work using TLE patients tissues (Huberfeld et al. 2007). The authors described a **correlation between the absence of KCC2 expression and depolarizing inhibitory post-synaptic potential (IPSP) occurences in subiculum pyramidal cells**, observed in a minority of neurons. Thus a KCC2 down-regulation seems to be the important factor. However the application of bumetanide led to a transient prevention of interictal-like activities. **The proactive role of NKCC1 in these events was dependent on $GABA_AR$ activity, demonstrating that NKCC1-mediated chloride loading alters GABAergic neurotransmission responses**. "Protective" effects of bumetanide have also been reported in experimental models. In an *in vivo* kainic acid-induced *status epilepticus* model, intrahippocampal bumetanide application treatment reduced the duration of ictal activities, together with an increased latency until first events (Sudhir Sivakumaran and Maguire 2016). Inhibition of NKCC1 activity by administration of bumetanide was also studied in a pilocarpine model of epilepsy (Kourdougli et al. 2017). The authors reported an increase in NKCC1 expression and a down-regulation of KCC2 expression, which is a most prominent feature shared by studies on the co-transporters role in epilepsy, under both immature and mature contexts, although this point can be discussed (R. Liu et al. 2020). Interestingly, reminiscent of the presented works in the neonatal brain which described cellular proliferation and migration, **chronic bumetanide administration also prevented ectopic mossy fibers sprouting in the mature dentate gyrus**. These effects could be related to the transporter's function in cellular migration (Mejia-Gervacio, Murray, and Lledo 2011; Schiapparelli et al. 2017), or the alteration

of glial-neuronal interactions (Henneberger et al. 2018). The treatment also led to decreased seizure frequency and prevented the effects of pilocarpine treatment on KCC2 and NKCC1 expression levels.

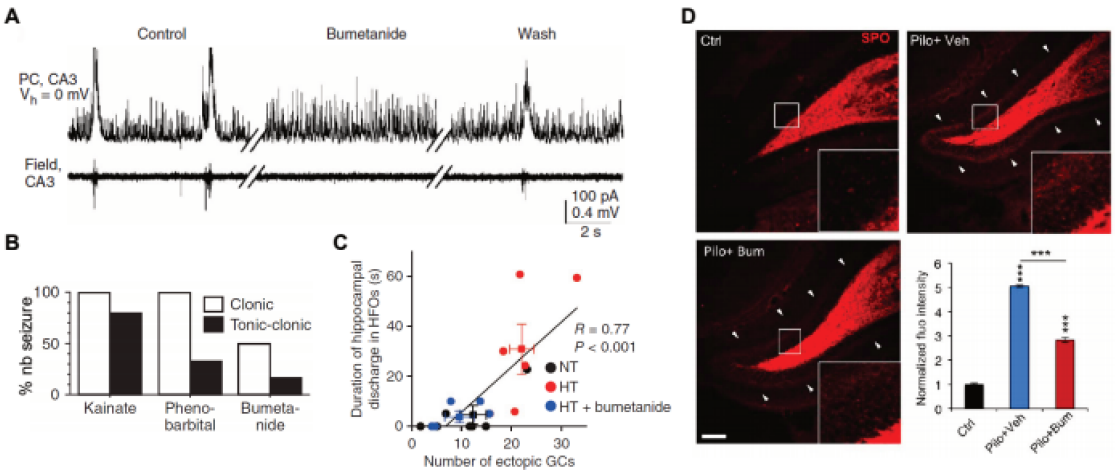

Figure 14, NKCC1 transport activity is involved in epilepsy at neonatal stages but also in adulthood. **A**, Effects of bumetanide on CA3 pyramidal cells and spontaneous network activities in hippocampus slices from P4 rats. Synchronous network activities mediated by $GABA_AR$ activation are suppressed upon bumetanide application. **B**, effect of bumetanide on a neonatal seizure model. NKCC1 inhibition with intra-peritoneal bumetanide administration before kainate-induced seizure led to a decrease in clonic and tonic-clonic seizures occurence (Dzhala et al. 2005). **C**, febrile seizure-induced ectopy of granule cells is prevented by bumetanide application, correlated with a decrease or hippocampal discharges duration in high frequency oscillation (Koyama et al. 2012). **D**, chronic intracerebral infusion of bumetanide reduces ectopic mossy fibers sprouting at 5 days after pilocarpine-induced status epilepticus of adult rat males (Kourdougli et al. 2017).

The effects of NKCC1 inhibition are significant both in terms of morphology (proliferation, morphology, expression) and seizures / epileptiform activities. These results are indeed interesting in the perspective of a potential treatment, and bumetanide uses beyond its “classical” scope have been analysed in the nervous system (Gharaylou et al. 2019; Goubert et al. 2019; W. Xu et al. 2017; Zarepour 2020). Furthermore, a review on bumetanide potential uses in brain disorders has been recently published, proving the interest in this well-known compound andits off-target uses (Kharod, Kang, and Kadam 2019). On the minus side, the authors notably raised the question of bumetanide avaibility in the brain, discussed in a previous study (S. Wang et al. 2015). There is another interrogation on bumetanide : due to NKCC1 expression in virtually all cells in the organism, a **bumetanide treatment may target many pathways, which is a strength but also a weakness**. This lack of specificity does not only concern systemic administrations as bumetanide can indeed impact other brain cells than

neurons. This limitation is analogous to the reported difficulties in studying NKCC1 expression patterns in the brain. On the other hand, KCC2 is exclusively expressed in neurons, making it easier to characterize the pathways involved in the pathologies. Unsurprisingly KCC2 expression and activity have been extensively studied in epilepsy but also other pathologies, together with associated signalling pathways (Andrews, Josiah, and Zhang 2020; Duy et al. 2020; Tang 2020).

Despite the reported limited role of NKCC1 in mature neurons chloride homeostasis, several works demonstrated a significant effect of its transport activity in epilepsy, where GABA-mediated inhibition is impaired.

2. B. c. Impaired GABAergic signalling does not only involve NKCC1 or KCC2

I presented the relevance of chloride co-transporters in experimental and clinical epilepsy, associated with GABAergic neurotransmission alterations. Epilepsy is indeed a complex phenomenon, with inhibition impairement being only a part of it. Furthermore even when this neurotransmission is affected, KCC2 and NKCC1 are not the only relevant players. I will here present several works focusing on GABAergic transmission and epilepsy to give a slight glimpse of how complex these phenomenons are beyond the regulation of CCC. Note that this research field is considerable, and the interplay between GABAergic activity and epilepsy has been extensively studied outside of CCCs before their identification (as presented in 1. A. c). The following paragraphs aim at introducing some works on these subjects, and are by no means meant to be exhaustive. For a broader presentation of the field, and other aspects, one can refer to (Akyuz 2021; Mele, Costa, and Duarte 2019; Righes Marafiga, Vendramin Pasquetti, and Calcagnotto 2020; Treiman 2001).

The timing of interneuron and excitatory cell recruitment at the onset of epilepsy is crucial. I rapidly presented this element when discussing KCC2 activity in epilepsy (L.-Y. Chen, Lévesque, and Avoli 2020; Magloire et al. 2019). In a model of optogenetic seizure induction in the mouse primary motor cortex, Khoshkoo et al. studied the contribution of different interneuron sub-types (Khoshkhoo, Vogt, and Sohal 2017). They reported a rapid recruitment of interneurons at the onset of seizures, followed by excitatory neurons. Optogenetically inhibiting sub-types of interneurons, they demonstrated that the inhibition of vasoactive intestinal peptide-expressing

interneurons led to reduced seizure durations and increased seizure threshold. Similarly looking at the impact of a specific neuronal population on the network activity, Botteril et al. demonstrated mossy cell-mediated excitation of granule cells in the dentate gyrus is enhanced in a pilocarpine model of epilepsy (Botterill et al. 2019), and report that mossy cells contribute to excitotoxicity and epileptogenesis.

Focusing on molecular aspects, Hines et al. reported a role of $GABA_AR$ alpha2 subunit on developmental seizures and related mortality (Hines et al. 2018). When impairing the subunit interaction with collybistin, inhibitory post-synaptic currents (IPSC) amplitude were decreased together with an increased mortality and more severe symptoms from kainic acid-induced seizures. Another demonstrated that TLE patients had a different expression of $GABA_AR$ subunits when compared with autopsy controls (Stefanits et al. 2019), with prospective consequences on the receptor sensitivity and tonic inhibition. This is notably interesting considering the interaction between $GABA_AR$ subunit expression and $[Cl^-]_i$ levels, involving an indirect role of KCC2 (Succol et al. 2012). Thus CCC activity have additional non-canonical effects on other actors of the GABAergic neurotransmission.

In conclusion NKCC1 importance in intracellular chloride regulation decreases over the development, with KCC2 becoming the pivotal actor. However NKCC1-mediated chloride transport has been reported in some papers on mature neurons, and more strikingly its inhibition in several models of epilepsy and TLE can lead to a strong alleviation of related symptoms. The combination of this “awakening” under pathological conditions with the uncertainties on the transporter’s expression and regulation underlines the importance of deciphering pathways regulating it.

3. NKCC1 post-translational regulation

While KCC2 expression is restrained to neurons, NKCC1 is expressed in various cell types in different organs. Hence NKCC1's transport has traditionaly been associated with the kidney or epithelium, where ionic fluxes and cell volume regulation are crucial (J. C. Xu et al. 1994). Hence the first studies on its post-translational regulations were carried in the context of osmotic stress.

3. A. A homeostatic regulation by the WNK-SPAK-OSR1 pathway

The first observation of a phosphorylation of NKCC1 was correlated with the presence of cAMP or osmotic stress causing cell shrinkage (Lytle et al. 1992). This phosphorylation was parallelled with an increase in the co-transporter's activity. cAMP signalling-dependent phosphorylation of NKCC1 was thus the first regulatory mechanism supposed for NKCC1. However the involved kinases were not yet identified, and the observation of NKCC1 phosphorylation at its NTD following cAMP generation stimulation was described as "unexpected" by Kurihara et al., who expected it to be at the CTD where a putative PKA phosphorylation site was identified (Kurihara et al. 1999).

3. A. a. NKCC1 is phosphorylated at its NTD after $[Cl^-]_i$ depletion

The chloride transport function of NKCC1 led scientists to study its regulation in secretory epithelia, such as the rectal gland from where it was first cloned (J. C. Xu et al. 1994). Osmotic stress leading to cell shrinkage in the shark rectal gland led to direct and reversible phosphorylation of NKCC1, at serine and threonine (including T189, T217 in the human sequence) residues (Lytle et al. 1992). In a following work, **a decrease in intracellular chloride concentration without cell shrinkage was reported to cause an increase in NKCC1 transport activity and phosphorylation** (M. Haas, McBrayer, and Lytle 1995). Beyond homeostasis aspects, these early works draw a clear correlation between NKCC1 activity and phosphorylation in a variety of tissues (Kurihara et al. 1999 ; Tanimura et al. 1995). For a review on the state of the art at the time, one can read (Mark Haas and Forbush III 2000) and (Russell 2000) for a comprehensive review on the subject. As evidence suggested that **PKA is not involved in $[Cl^-]_i$-**

mediated NKCC1 phosphorylation (Tanimura et al. 1995) and that cAMP effects were variable (Russell 2000), molecular pathways regulating NKCC1 were still elusive. Note that PKA consensus site of phosphorylation is located in exon 21, specifically spliced resulting in NKCC1b isoform expression. As a result the effects obtained with shark NKCC1 (not including this exon) were not explainable by the phosphorylation of this residue by PKA. This could partly explain the various and unclear effects of PKA on the co-transporter (Russell 2000). At this stage, the most obvious causes for NKCC1 phosphorylation were osmosis and $[Cl^-]_i$ levels. Further characterizing NKCC1 phosphorylation, researchers reported a **phosphorylation stoechiometry of 3 +/- 0.4 residues on NKCC1 : T184, T189, T202 (T212, T217, T230 in human NKCC1)** (Darman and Forbush 2002; Flemmer et al. 2002). These residues are conserved between NKCC1 and NKCC2 and their phosphorylation was indeed correlated with enhanced transport activity from the transporter. The identification of P**rotein Phosphatase 1 (PP1) interaction with NKCC1 via a RvxF motif on its NTD**, with the statement that this interaction actually **inhibits the co-transporter's transport function** (Darman, Flemmer, and Forbush 2001), confirmed **NKCC1's NTD as a crucial regulatory domain**.

Regarding K^+-Cl^- co-transport, the concept of a regulation by phosphorylation was presented in (Jennings et al. 1990), where they suggested that dephosphorylation is necessary for swelling-induced transport. They further suggest that cell swelling would lead to kinases inhibition rather than phosphatases inhibition. PP1 and PP2A were reported as a regulators of K^+-Cl^- co-transport, complementing the swelling-dependent serines and threonines dephosphorylation observation (Bize et al. 1999 ; Starke and Jennings 1993). Tyrosine phosphorylation of KCC2 was also demonstrated to inhibit its transport activity in oocytes (Strange et al. 2000) although another work, using cultured hippocampal neurons, suggested an opposite effect of tyrosine phosphorylation (Kelsch et al. 2001). Hence by the early 2000's the relationship between (N)KCC activity and their phosphorylation was clearly established, with opposite consequences on their activities.

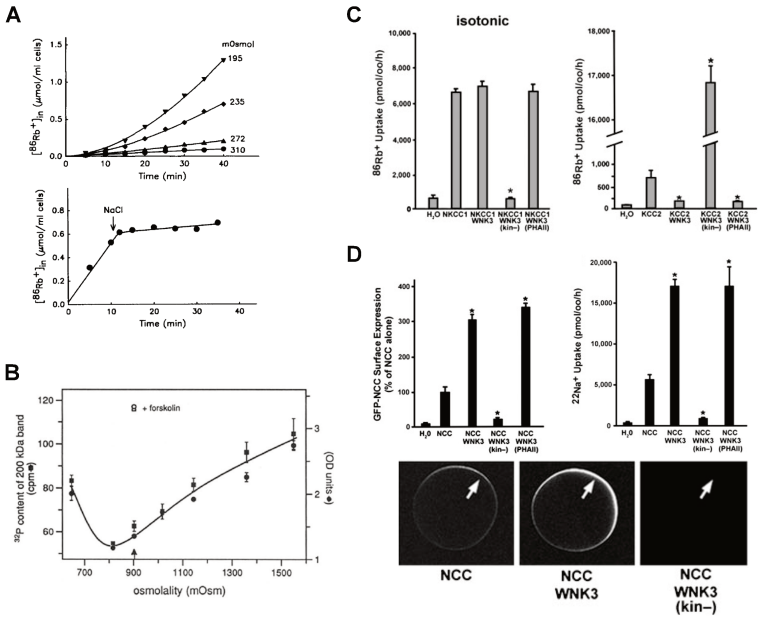

Figure 15, CCC activity is tuned by osmolarity and phosphorylation in a synergetic fashion. **A**, ouabain-insensitive potassium currents are dependent on the environment osmolarity (*up*) and on the presence of sodium and / or chloride (*bottom*) (Jennings and Al-Rohil 1990). **B**, NKCCs are phosphorylated in an osomolarity-dependent fashion, stimulating a homeostatic response (Lytle and Forbush 1992). **C**, WNK kinases stimulates or inhibits NKCC1 and KCC2 transport respectively independently from extracellular tonicity (Kahle et al. 2005). **D**, NCC transport rate is correlated with its membrane expression, suggesting a role of WNK in CCC expression at the membrane (Rinehart et al. 2005).

3. A. b. The WNK-SPAK-OSR1 system

3. A. b. i. Involved kinases

With No lysine Kinases (WNK) are serine/threonine kinases expressed in four isoforms, WNK1-4, expressed in diverse organ systems. They lack a well conserved lysine in ß-strand 3 of the kinase subdomain II. The catalytic activation loop of WNK kinases is changed such that a lysine in ß-strand 2 can assure ATP-binding and catalysis of phosphoryl transfer (Min et al. 2004; B. Xu et al. 2000). They are specifically enriched in tissues with a generally high expression of WNK1 while expression levels of WNK2-4 are more diverse. **In the human brain the isoforms 1 and 3 are highly expressed with a developmental downregulation of WNK3 expression**, while WNK2 is expressed moderately throughout development and WNK4 expression remains at low levels (Kristopher T. Kahle et al. 2013). WNK kinases vary in size from 1243 amino acids for WNK4 to 2382 amino acids for WNK1 (human). **The kinase domain shows high conservation across the**

different isoforms, with a minimum of 84% sequence identity between them. Although sharing high identity of amino acids in the kinase domain, WNK kinases display differential substrate specificity.

Additionaly to the diversity among the different isoforms, which have slightly different properties, these isoforms also have isoforms of their own (e.g. a truncated isoform of WNK1 lacking the kinase domain) (Vidal-Petiot et al. 2013). A pathologically relevant isoform of WNK1 is WNK1-HSN2, related to Hereditary Sensory and Autonomic Neuropathy II (Rahmani et al. 2018; Rivière et al. 2004). This variant is preferentially expressed in neuronal tissue (Shekarabi et al. 2008; Vidal-Petiot et al. 2013). Thus **tissue-specific splicing events, occuring to WNK1 in the**

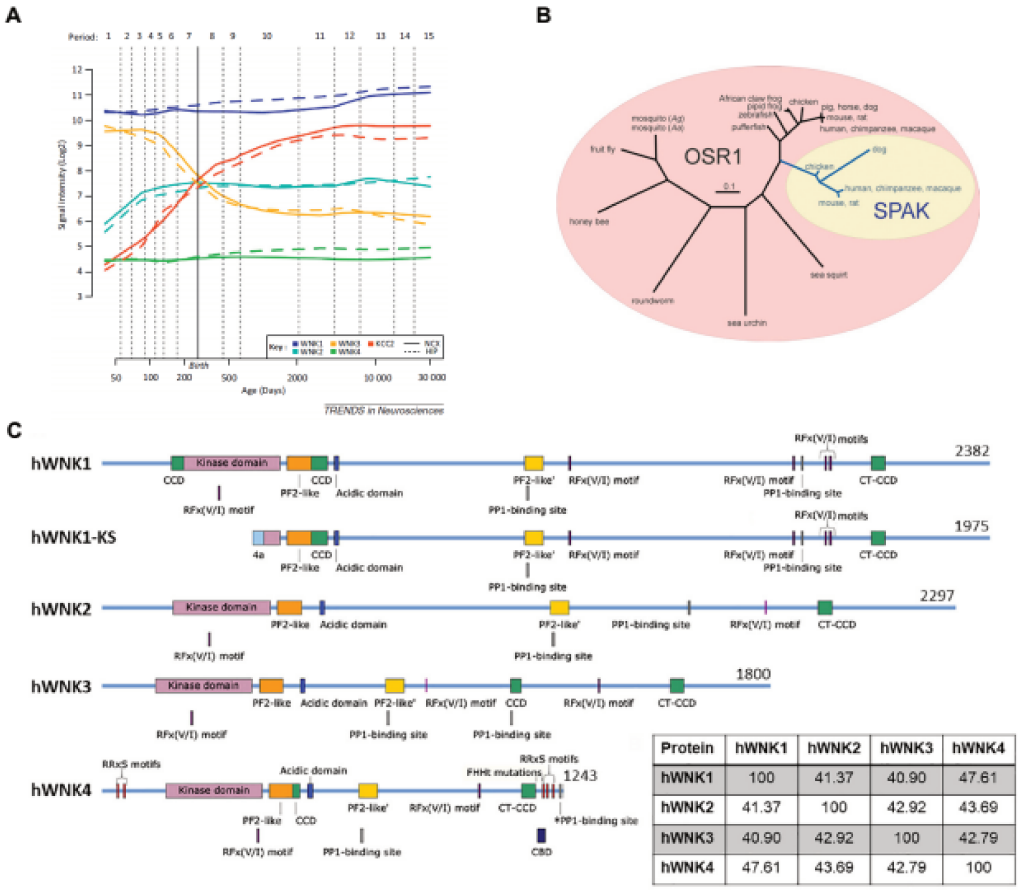

Protein	hWNK1	hWNK2	hWNK3	hWNK4
hWNK1	100	41.37	40.90	47.61
hWNK2	41.37	100	42.92	43.69
hWNK3	40.90	42.92	100	42.79
hWNK4	47.61	43.69	42.79	100

Figure 16, the WNK-SPAK-OSR1 kinases. **A**, mRNA levels of WNK isoforms and KCC2 in the brain throughout development. While WNK1 remains the most expressed isoform, WNK3 expression has an opposite evolution to KCC2 (Kahle et al. 2013). **B**, cluster dendrogram based on aligned proteins sequences of OSR1 and SPAK (Delpire and Gagnon 2008). **C**, WNK isoforms have numerous common features included in their sequences, notably including PP1-binding sites and SPAK/OSR1-binding sites (RFx(V/I) motifs). The table indicates the percentage of identity between aligned full-length sequences. On the other hand kinase domains display a remarkable conservation among isoforms with 80% to 95% identity (Murillo de Ozores et al. 2020).

kidney for example, must be taken into account when interpreting data on WNK expression or activity as overexpressed isoforms haven't always been adapted to the studied organ (Vidal-Petiot et al. 2013). Hence as a majority of the presented results were obtained in oocytes, a critical look is necessary for their functional interpretation and extrapolation to other cell types such as neurons.

STE20/SPS1-related proline-alanine-rich kinase (SPAK) and oxidative stress response kinase (OSR1) are part of a kinase family sharing homology with yeast Ste20/Sts1 kinases (Dan, Watanabe, and Kusumi 2001). These kinases have **66% amino acid identity and evolved probably as a result of gene duplication during vertebrate evolution** (Delpire and Gagnon 2008). Given their high homology and equal expression levels in the studied tissues (Ushiro et al. 1998), no study was able until now to show any functional difference between both kinases so far.

3. A. b. ii. Activation mechanisms of WNK-SPAK-OSR1

WNK are considered as the "engaging" kinases : they act upstream of SPAK and OSR1 by activating them *via* a **phosphorylation** in their catalytic T-loop (Vitari et al. 2005). The activation of SPAK and OSR1 requires another protein, the mouse protein 25 (**Mo25**). Li et al. proposed a **"double-lock" activation mechanism for SPAK and OSR1** (C. Li et al. 2014). They suggest a removal of the kinases autoinhibition by WNK binding on the CCT (Villa et al. 2007) and phosphorylation of SPAK/OSR1 in their T-loop. Then MO25 can interact with the "unlocked" kinases to maintain them in an activated state (Filippi et al. 2011). This would in turn lead to SPAK/OSR1-mediated phosphorylation of transport proteins. The 4 WNK kinases phosphorylate SPAK and OSR1 at a threonine residue in the activation loop of the catalytic domain (233 for SPAK, 185 for OSR1) and at a serine residue situated within the C-terminus (373 for SPAK, and 325 for OSR1) (Moriguchi et al. 2005; Vitari et al. 2005). This model where MO25 would enhance WNK activity via maintained activation of SPAK/OSR1 effects is consistent with more recent publications (Q. Sun et al. 2018).

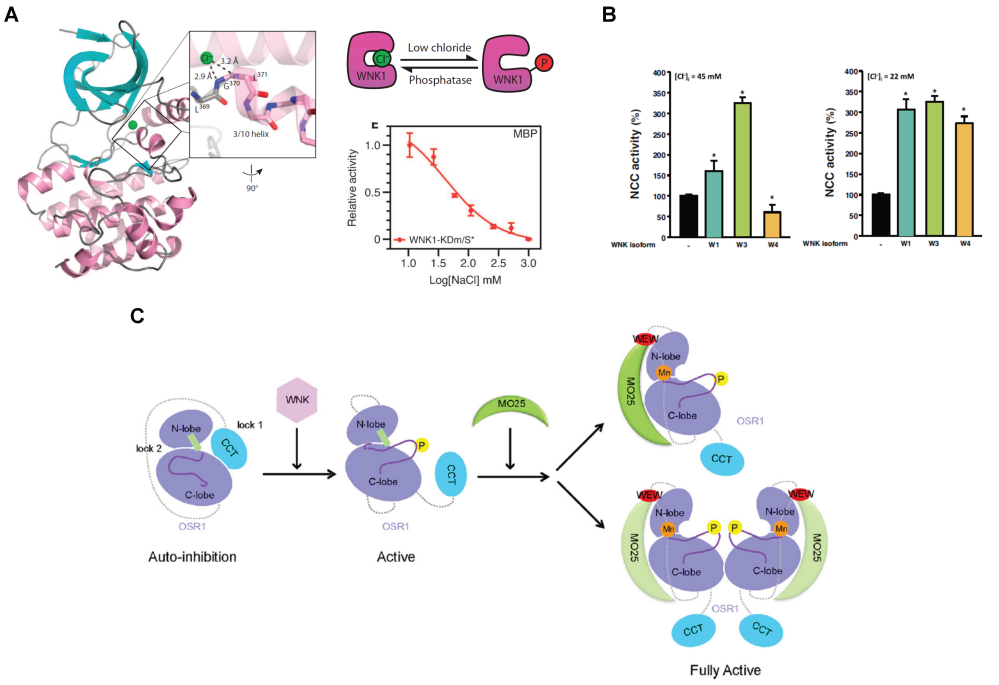

Figure 17, activation of the WNK-SPAK-OSR1 signalling depends on chloride concentrations and several molecular actors. **A**, chloride inhibits WNK1 activation by preventing the autophosphorylation of the kinase by binding to its catalytic site (Piala et al. 2014). **B**, chloride sensitivity differs among the different WNK isoforms, allowing a differential tuning of CCC activity. Note the high sensitivity of WNK4 to $[Cl^-]_i$ while on the other hand WNK3 effect was barely affected by the change in $[Cl^-]_i$ (Bazùa-Valenti et al. 2015). **C**, prooposed model for SPAK/OSR1 activation downstream of WNK activation. Protein-protein interactions (such as WNK-SPAK/OSR1 or MO25-SPAK/OSR1), as well as protein subdomain interactions, are crucial for the control of the pathway activation (Li et al. 2014).

In addition to WNK and MO25-dependent SPAK/OSR1 activation, **WNK autophosphorylation is a crucial step for the signalling activation**. The autophosphorylation of WNK1 was observed by Xu et al. in 2002, after a work where they identified the new kinase in 2000 (B. Xu et al. 2000, 2002). The autophosphorylation of S382 is crucial for the kinase activity, and is a conserved feature across different species and WNK isoforms (Zagórska et al. 2007). The authors further suggested a trans-autophosphorylation, as catalytically inactive WNK1 is phosphorylated at this residue after stimulation of WNK1, likely via endogeneous WNK activity. Interestingly WNK1 also has an autoinhibitory domain, which solution structure was reported (Moon et al. 2013). The authors noticed that this autoinhibitory domain binds peptides containing a RfxV motif, similarly to the subdomain of SPAK/OSR1 interacting with WNK1 which shares a remarkable homology. Thastrup et al. demonstrated that WNK can interact via their C-terminal coiled-doil domain (CCD), but also suggest that this interaction is not mandatory for this autophosphorylation

(Thastrup et al. 2012). Interestingly they observed that WNK1-3 can mediate this phosphorylation on WNK1, but not WNK4.

A recent paper looked at potential molecular dynamics of WNK1 depending on its phosphorylation state (Jonniya, Sk, and Kar 2019). According to their results, S382 phosphorylation stabilizes the activation loop of WNK1. Reconciling the chloride-sensing feature of the WNK kinases with their activation, Piala et al. reported the **binding of a Cl^- ion in WNK1 catalytic site, inhibiting the kinase autophosphorylation** (Piala et al. 2014). Moreover, S382 is apparently not involved in this interaction, it is rather the chloride binding which prevents its phosphorylation, providing another molecular mechanism regulating the pathway. **Differences in sensitivity between WNK isoforms to chloride hence likely depend on this interaction** (Bazúa-Valenti et al. 2015). Interestingly, low chloride hypotonic stress used by Bazua-Valenti et al. did not trigger any change in WNK3 phosphorylation. Pacheco-Alvarez et al. suggested that WNK3, likely via a differing CTD from WNK4, may not be regulated by a chloride-sensitive mechanism, but rather by cellular volume changes (Pacheco-Alvarez et al. 2020). However the data provided has low numbers of replicates and will require further confirmations. Akella et al. looked at the effect of soaking of phosphorylated WNK1 and WNK3 crystals with osmolyte sucrose (Akella et al. 2020). They mentioned changes in the activation loop and in another kinase activation locus, hence reported volume changes effects on WNK3 activity could depend on the increased concentration of intracellular molecules such as sucrose. Hence subtle differences between the different WNK kinases allow the WNK-SPAK-OSR1 pathway to be finely tuned by ionic homeostasis-related factors.

The WNK-SPAK-OSR1 signalling is a finely tuned kinases cascade regulated through phosphorylation. I have described their sensitivity to chloride, inhibiting WNK auto-phosphorylation capacity. Another system regulating WNK is the CUL3-KLHL3 complex (Alessi et al. 2014). This complex acts by ubiquitylating WNK proteins, leading to their degradation. The pathway activity is also tuned by manganese ions, proposed to be effective cofactors for the pathway-mediated phosphorylations on NKCC1 (K. B. E. Gagnon, England, and Delpire 2006a). However **a most prominent regulator of WNK-SPAK-OSR1 is PP1**.

3. A. b. iii. Interplay with phosphatases

The phosphatase involvement in CCC activity tuning was suspected for a long time (Jennings et al. 1990) and was later demonstrated (Darman, Flemmer, and Forbush 2001). However the molecular mechanisms were still unclear. The two major phosphatases associated with CCC activity regulation through changes in their phosphorylation state are PP1 and PP2A (Bize et al. 1999 ; Darman, Flemmer, and Forbush 2001). PP1 was shown to interact with NKCC1, an interaction enhancing the inhibitory effect of PP1 activity on NKCC1-mediated transport (K. B. Gagnon and Delpire 2010b). In this work, the authors formulated an interesting model, where **NKCC1 assists PP1-mediated SPAK/OSR1 dephosphorylation by scaffolding both proteins**. This would have for consequence a potent, 2-stages (SPAK and NKCC1) regulation of NKCC1 phosphorylation by PP1 allowing a rapid modulation of the co-transporter activity in response to diverse stimuli (in particular changes in $[Cl^-]_i$ or in tonicity).

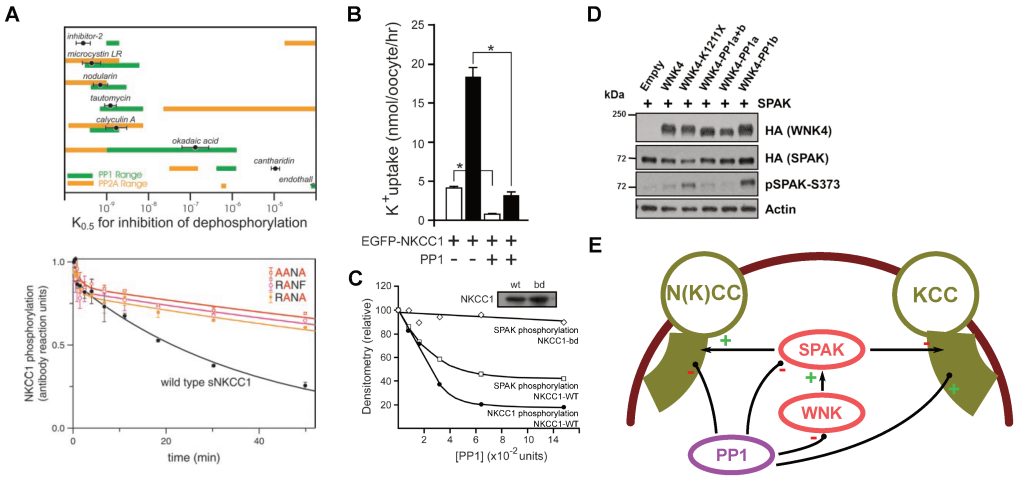

Figure 18, phosphatases are multi-stage regulators of WNK-SPAK-OSR1 pathway. **A**, NKCC1 undergoes a PP1-dependent dephosphorylation, as shown by the sensitivity of its dephosphorylation to different drugs (*up*). This dephosphorylation is impaired when NKCC1 PP1-binding site is mutated (*bottom*) (Darman et al. 2001). **B**, NKCC1 dephosphorylation leads to a decrease in its transport activity under isosmotic (*white*) or hyperosmotic (*black*) conditions. **C**, NKCC1-SPAK interaction allows PP1-mediated SPAK dephosphorylation through scaffolding of PP1 and SPAK. NKCC1-bd : SPAK-binding deficient, cells expressing NKCC1 and SPAK (Gagnon et al. 2010). **D**, mutation of WNK4 PP1-binding site alters impacts SPAK phosphorylation downstream of WNK4. Mutation of a PP1 interaction sequence (PP1b) increases WNK4-mediated SPAK phosphorylation (Murillo de Ozores et al. 2018). **E**, PP1 regulates all actors of the WNK signalling, allowing the monitoring of CCCs activity in response to osmotic stress and $[Cl^-]_i$ changes. Arrows : effect mediated through phosphorylation ; endpoints : effect mediated through dephosphorylation.

Unlike NKCC1, KCC2 sequence does not include a consensus PP1 interaction domain. **Pathways regulating KCC2 have been well studied, and several signallings have been described beyond the WNK kinases** (Kristopher T. Kahle et al. 2013; Kaila et al. 2014; Lévi 2019). PP1-dependent regulation of KCC2 may also dephosphorylate KCC2 **S940 (PKC-dependent)** (H. H. C. Lee et al. 2007), **Y903/Y1087 (Src-dependent)** (Watanabe et al. 2009), or **T906/T1007 (SPAK/OSR1-dependent)** (Friedel et al. 2015; Jesse Rinehart et al. 2009). These phosphorylations have different effects on KCC2 cellular distribution, and different consequences on KCC2 function, with S940 phosphorylation stimulating KCC2 membrane expression via a reduced internalization rate, correlating with increased KCC2-mediated transport (H. H. C. Lee et al. 2007). On the other hand T906/T1007 phosphorylation leads to a decrease in the transporter's membrane pool fraction and transport activity (Friedel et al. 2015). Serine 940 dephosphorylation by PP1 was described in neurons, leading to a reduced KCC2 activity following NMDAR activation (H. H. C. Lee et al. 2011). **Rinehart et al. in 2009 reported the dephosphorylation of KCC3 at residues analogous to KCC2's T906/T1007 by PP1 and PP2A in HEK293 cells, which would result in the up-regulation of KCC2 membrane levels and transport activity** (Jesse Rinehart et al. 2009). Thus PP1 and PP2A have different effects depending on the dephosphorylated residue. Hence KCC2 regulation by phosphorylation relies on a diversity of pathways, and assessing the dominance of one on another is not an easy task, as these different pathways do not have the same characteristics in terms of activation and effects. A work by Titz et al. in 2015 looked at KCC2 transport-mediated changes in pH_i and E_{GABA} after NH4+ incubation with different mutations (Titz, Sammler, and Hormuzdi 2015). Their results suggest that **S940 or Y1087 phosphorylation override T906/T1007 phosphorylation effects on KCC2 activity**. Still the **relevance of KCC2 phosphorylation at these residues has been well documented, and their functional implications are not to dismiss**, especially given the small amount of publication on this specific subject (Friedel et al. 2015; Pisella et al. 2019; Watanabe et al. 2019; Zhang et al. 2020).

PP1 also interacts with WNK proteins. In a work where they identified several variants of WNK4 in the kidney, Murillo-de-Ozores et al. in 2018 demonstrated that this interaction was functionaly important, as WNK4 variants not including a PP1 interaction site (Murillo-de-Ozores et al. 2018). A reciprocal action of WNK3 on phosphatases activity, allowing for a more effective modulation of CCC phosphorylation, was suggested in an earlier work (de los Heros et al. 2006). As a result **PP1 mediates dephosphorylation, and thus inhibition of the WNK-SPAK-OSR1**

pathway at the three stages of its activation process, and by this way is a potent regulator of NKCC1. For a comprehensive and up-to-date review on this signalling and its interaction with CCC, see (Murillo-de-Ozores et al. 2020).

3. A. c. A homeostatic regulation of NKCC1 phosphorylation by the WNK-SPAK-OSR1 pathway

SPAK and OSR1 interact with NKCC1, and colocalize in the brain (Piechotta, Lu, and Delpire 2002). The function of this interaction was however discussed, as mechanistic aspects were still unclear (Dowd and Forbush 2003; Piechotta et al. 2003). Piechotta et al. suggested a scaffolding role of SPAK with the gathering other stress-related proteins, while Dowd et al. reported a direct effect of SPAK on the transporter's transport activity and phosphorylation. The identification of WNK mutations correlated with hypertension led scientists to study their potential role in CCC regulation, notably because both WNK and several CCC are expressed in the kidney (F. H. Wilson 2001). **WNK1 was reported to phosphorylate SPAK and OSR1, a phosphorylation associated with hypotonic stress and activation of those two downstream kinases** (Moriguchi et al. 2005). They also highlighted a **direct phosphorylation of NKCC1, NKCC2 and NCC by SPAK and OSR1**, confirming the role of those kinases in osmotic stress-mediated regulation of NKCC1 downstream of WNK activation. These works provided first evidences for the WNK-SPAK-OSR1 pathway-mediated regulation of CCC activity through phosphorylation

A corpus of publications focused on the WNK role in chloride co-transport by N(K)CC and KCC (de los Heros et al. 2006; K. T. Kahle et al. 2005; J. Rinehart et al. 2005). Using Rb^+ transport in oocytes injected with CCC and WNK3 they demonstrated that **WNK3 stimulates N(K)CC while inhibiting KCC**. They observed a correlation between NCC activity and their expression at the membrane, suggesting that **WNK3-dependent phosphorylation of CCC regulates the transporter expression at the membrane** (J. Rinehart et al. 2005). These works provided further demonstration of a tonicity-dependent regulation of this pathway, with increased transporter phosphorylation under hypertonic conditions, and also confirmed its dependence on chloride ions as observed by Lytle et al. in 1992.

Threonine residues phosphorylated by SPAK and OSR1 (T203/207/212 in human) were identified

by Vitari et al. in 2006 (Vitari et al. 2006). Note that NKCC1 residues undergoing a phosphorylation were supposed to be T212/217/230 in a previous study, suggesting the pathway targets the 5 residues (Darman and Forbush 2002). Vitari et al. moreover reported thaa SPAK and OSR1 have a conserved C-terminal (CCT) domain interacting with RFxV motif, a **sequence located on NKCC1 and WNK1 and WNK4**, providing molecular insights on the WNK-SPAK-OSR1-NKCC1 pathway function. A following work demonstrated the implication of the phosphorylation of those threonines in chloride- or tonic-mediated changes in NKCC2 activity, providing a **molecular sensor of $[Cl^-]_i$ in the WNK pathway for the long-time known regulation of NKCC by intracellular chloride** (Lytle et al. 1992) (J. Ponce-Coria et al. 2008). Furthermore they demonstrated that the interaction between WNK3 and SPAK was necessary for this homeostatic response of the system.

WNK2-dependent regulation of CCC was reported later (Jesse Rinehart et al. 2011), with the interesting statement that WNK2 would be a neuronal-enriched isoform and not expressed in the kidney. This statement was however later put into perspective, as WNK1 and WNK3 were recently identified as the main brain isoforms (Heubl et al. 2017; Kristopher T. Kahle et al. 2013). WNK4 and SPAK-mediated regulation of KCC2 and NKCC1 was also reported, with the noted importance of WNK4-SPAK interaction to observe a functional effect on NKCC1 transport (K. B. E. Gagnon, England, and Delpire 2006b). On the other hand, a prior work stated an inhibitory effect of WNK4 on NCC, and another reported the same effect on the renal K^+ channel ROMK (Kristopher T Kahle et al. 2003; F. H. Wilson et al. 2003). Despite this result, most data on WNK isoforms, including WNK4, support the hypothesis of a WNK-dependent activation of SPAK/OSR1, with a subsequent stimulation of N(K)CC (Anselmo et al. 2006; C.-L. Huang and Cheng 2015; Richardson et al. 2008). A possible cause for these contradictions would be chloride affinity, as suggested by (Bazúa-Valenti et al. 2015). They confirmed a regulation of WNK by intracellular chloride, and reported that the **chloride affinity of WNK4 is higher to that of WNK1 or WNK3**. Thus depending on the experimental conditions, the activity of these isoforms would be different, and inactive WNK4 could act as a dominant negative WNK. A recent work by Chen et al. demonstrated with the modulation of $[Cl^-]_i$ in an *in vivo* model of mouse expressing a chloride-insensitive WNK4 knock-in, demonstrating that this chloride-sensing of WNK4 is physiologically relevant (J.-C. Chen et al. 2019, 4).

The WNK-SPAK-OSR1 pathways appears as a **central regulator of $[Cl^-]_i$ through regulation of chloride co-transporters**, with a retro-effect of $[Cl^-]$ on the pathway activity. This signalling is relevant in a context of neuronal inhibition dependent on intracellular chloride levels.

3. A. d. Roles of WNK-SPAK-OSR1 in neuronal chloride homeostasis

The importance of cell volume control and ionic homeostasis makes the WNK-SPAK-OSR1 a crucial actor in the kidney for example. Its functional importance in this organ has been extensively characterized (Alessi et al. 2014; Furusho, Uchida, and Sohara 2020; Gamba 2005b; Shekarabi et al. 2017). In addition to its important role in renal function, the pathway was also studied in the brain.

In the majority of cases, the pathway importance is mentioned in the light of the final regulation of KCC2. This is explained by the fact that, in the mature brain, KCC2 is considered as the main actor of chloride homeostasis. Several review adress the topic, with more or less emphasis on the WNK-SPAK-OSR1 pathway (H. Huang et al. 2019; Kristopher T. Kahle and Delpire 2016; Kaila et al. 2014; Lévi 2019). Although several works focused on a pathological background, like ischemia (Bhuiyan et al. 2017; Zhang et al. 2020), pain (Gao et al. 2019), epilepsy (Jeong et al. 2018; Moore et al. 2018) or intracerebral hemorrhage (D. Wu et al. 2020), **the functional importance of WNK signalling has also been demonstrated in physiological processes such as development** (Friedel et al. 2015; Pisella et al. 2019; Watanabe et al. 2019) **or neuronal inhibition** (Friedel et al. 2015; Heubl et al. 2017). The effects of WNK-SPAK-OSR1-mediated phosphorylation of NKCC1 and KCC2 can admittedly have an impact on $[Cl^-]_i$ and E_{GABA}, however other morphologic effects such as dendritic volume and spines organization are also depending on it.

3. A. e. Respective roles of tonicity and phosphorylations on KCC2 and NKCC1 activity

I previously described the thermodynamical aspects of chloride co-transport, notably focusing on NKCC1. Usually the metric used to determine the co-transporter transport activity polarity is the free energy difference of ions across the membrane. The thermodynamical equilibrium is the point where the transporter-mediated net ionic flux equals 0. Thus free energy does not

directly describe a kinetic aspect of CCC-mediated transport but rather the energy of a system, determining the polarity of KCC2 and NKCC1's transport.

The kinetics of ionic transport can be described by the ionic current for each transported ionic specie (which in total results in an electroneutral transport). A proposed modelling is (Doyon et al. 2011) :

$I_{Cl,KCC2} = \frac{I_{Cl,KCC2,max} \times \Delta FE_{KCC2}}{\Delta FE_{KCC2} + \Delta FE_{KCC2}(I_{Cl,1/2})}$; as $I = g \times U$, here $I_{Cl,max}$ is a quantification of KCC2 transport kinetics, while the second term is a relative measure of the potential difference (we could replace the free energy terms by the driving force, and the Faraday constant terms would simplify each other). This way of formalizing transport in analogy to Ohm's law is broadly used (Brumback and Staley 2008; Yelhekar, Druzin, and Johansson 2017). Brumback et al. however use a slightly different approach to modelize the transport velocity (here written with previously used terms for clarity), however with a similar idea.

These models, relying on rather simple electrochemical equations, do however not capture some aspects of CCC transport activity. For example, N(K)CC activity is increased by temperature, when KCC activity is actually decreased upon pre-incubation at a higher temperature, challenging simple thermodynamical modelling (Hannemann and Flatman 2011; Hartmann and Nothwang 2011). Moreover **KCC2 is active under isotonic conditions, while other KCC are only active under hypotonic conditions** (Mercado et al. 2006). Mercado et al. deciphered the molecular tenants of KCC2 isotonic transport, with the use of KCC2-KCC4 chimeras. Their work suggest that a CTD region, called ISO domain (1022-1307 residues) allows KCC2 isotonic transport activity independently of changes in the co-transporter surface expression. Acton et al. in 2012 provided further insights on the importance of this domain in KCC2 transport activity in neurons, altering chloride reversal potential (Acton et al. 2012). Consistently with other KCC, KCC2ΔISO transport activity was recovered upon hypotonic stress, while KCC4-ISO was able to perform isotonic transport in neurons. In consequence KCC2 isotonic transport and swelling-induced transport involve different molecular components of KCC2. **Interestingly WNK3, WNK4 and SPAK/OSR1 were suggested to tune the co-transporter activity under both tonicity conditions** (K. B. E. Gagnon, England, and Delpire 2006b; de los Heros et al.

2006).

In a similar fashion, NKCC1 was reported to be more stimulated by hypertonicity when compared to NKCC2 (K. B. Gagnon and Delpire 2010a). With the use of various NKCC1-NKCC2 chimeras the authors were able to find the 1st intracellular loop and the 2nd extracellular loop of NKCC1 to be the keys for the transporter's higher stimulation by hyperosmosis. It was demonstrated that **PP1 dephosphorylation affecting WNK-SPAK-OSR1-targetted residues, inhibited NKCC1's transport under both iso- and hyper-tonic conditions**, confirming the importance of NKCC1 phosphorylation on its transport activity independently of the tonicity (K. B. Gagnon and Delpire 2010b). Hence other factors than the co-transporter driving force shall be integrated when modelling their transport activity, such as specific responses to tonicity and modulation of transport activity by phosphorylations.

The ability of CCC to transport ions across the membrane is governed by thermodynamical constraints, determining their polarity and efficacy. However several differences among KCC and N(K)CC modulate their sensitivity to the environment. These subtle differences allow a finely modulated transport of chloride and cations across the membrane. In addition to the role of tonicity on CCC transport, post-translational modifications, notably including WNK-SPAK-OSR1-mediated phosphorylations and PP1/PP2A dephosphorylation, change the transporters net transport activity. Their effects being apparently independent from the tonicity, we can hypothethize a **direct effect of threonine phosphorylations of KCC2 and NKCC1 on their transport rate**. Another hypothesis is that these changes in transport activity can be due to **modifications in their localization at the membrane** (Friedel et al. 2015; J. Rinehart et al. 2005; Jesse Rinehart et al. 2009). In both cases, this pathway is amplifying the homeostatic response of the cell. As 3D structures of CCC did not provide much insights on the possible effects of phosphorylations on NKCC1 or KCC2 structures, disentangling both expected effects (e.g. on transport rate and membrane stability) of the WNK pathway on NKCC1 or KCC2 transport activity requires other complementary approaches.

3. B. Diffusion-capture regulation of transporters at the membrane of neurons

The study of membrane proteins expression and distribution requires biochemistry and imaging approaches. As phosphorylation/dephosphorylation can be rapidly triggered and lead to subtle changes in the membrane distribution of receptors or transporters for instance, the **diffusion-capture model is a popular model to describe swift changes in their dynamics at the membrane**. This model proposes that the lateral diffusion of membrane proteins reflects their **interaction and trapping in regions (clusters, endocytic zones) by changing their exploration and motion speed at the plasma membrane**. Thus it relies on the modelling of the protein diffusion, and the study of its distribution at the membrane, notably clustering. I will first present the technical and theoretical background of the lateral diffusion of membrane proteins, and specifically discuss lateral diffusion of KCC2 and how it is related to changes in its stability at the membrane.

3. B. a. The diffusion model

The diffusion-capture model aims at describing particles, and more specifically membrane proteins, behaviour. The movement (diffusion) of such particles can then be analyzed to infer potential **obstacles (molecular crowding) or interactions with other molecular actors (scaffolding proteins, other membrane proteins) leading to their confinement (capture)**, or highlight **different particle populations** based on their different behaviours. **Single particle tracking (SPT) live imaging** has made the analysis of individual trajectories possible, and the potential of such tools in the study of membrane proteins and in cellular neurosciences was demonstrated, notably thanks to its spatial resolution (Bannai et al. 2006; Triller and Choquet 2008). Using the high photostability and signal-to-noise ratio of quantum dots (QD), the molecule localization can be estimated with a resolution of 5 to 20 nm, and tracked over long periods of time. In addition to accessing individual molecules diffusion while Fluorescence Recovery After Photobleaching (FRAP) only allows to study a population, SPT analysis relies on a **well-defined diffusion model** allowing to uncouple diferent parameters. Eventually, trajectory analysis can give access to various biophysical properties (interactions, diffusion kinetics, etc.)

thanks to the very flexible raw data generated. In the following parts I will focus on the analysis of particles in 2D, as we are interested in the use of SPT and the diffusion-capture model in the context of membrane transporters regulation.

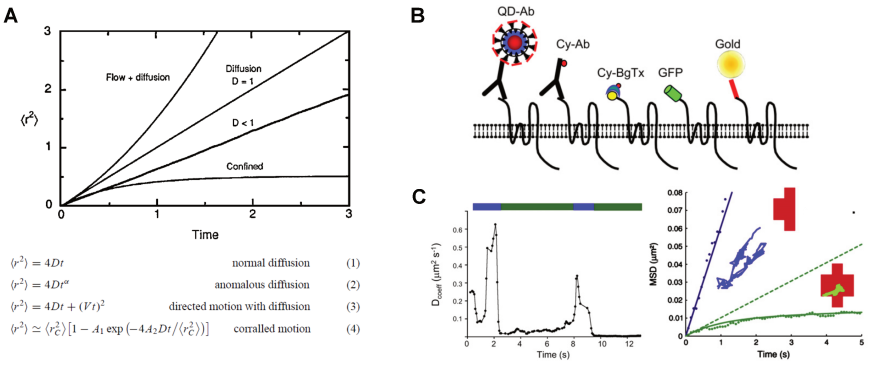

Figure 19, MSD-derived description of the lateral diffusion of membrane protein. **A**, different motion modalities and MSD theoretical description. In the context of membrane proteins diffusing on dendrites, motion can be directed by the geometry of the dendrite (Saxton and Jacobson 1997). **B**, experimental tracking of individual membrane proteins can be performed thanks to several tools, a common one being the quantum dot (QD). **C**, using quantum-dot single particle tracking combined with MSD analysis, we can notice different behaviours depending on the region the protein explores. Here glycine receptors are noticeably slower and more confined when being at inhibitory synapses (extrasynaptic : *blue* ; inhibitory synapse : *green*) (Triller and Choquet 2008).

To quantify and characterize the movement of particles, a commonly used metric is the **mean-square displacement** :

$$MSD(n\tau)=\frac{1}{N-n}\sum_{i=1}^{N-n}\left[(x_{i+n}-x_i)^2+(y_{i+n}-y_i)^2\right]$$; with n being the jump size.

The interest of the MSD is the inferrence of physical variables, and notably the apparent diffusion coefficient D. Under the hypothesis of a brownian motion we have :

$$C(r,t)=\frac{1}{4\pi Dt}\exp\left(\frac{-r^2}{4Dt}\right)$$; the concentration of a particle at a time t and distance r from the starting point for a 2D brownian diffusion along an axis.

$P(r,t)dr=2\pi r\,dr\,C(r,t)$; the probability density or r, the first term expressing the integration of the concentration of the particle in a circle with dr width. After integration, the mean-square displacement in a brownian 2D diffusion is :

MSD(t) = 4Dt

This is the basic model from which a particle (for example KCC2 or NKCC1) diffusion coefficient is computed. However the hypothesis of a free, obstacle-free diffusion in a neuron's plasma membrane is usually not validated. The presence of membrane proteins, lipid rafts, but also scaffolding proteins have a strong influence on the membrane protein lateral diffusion. In addition a maybe more obvious (and thus easier to forget) parameter is the diffusion substrate shape : membrane proteins diffusing on a dendrite or an axon have their diffusion directed by the width of the explorable area. This effect can be compared to the diffusion of a molecule combined with flow (or drift). The effects of passive diffusion and flow on a single molecule diffusion as well as broader theoretical aspects of SPT analysis are described in (Michalet 2010; Qian, Sheetz, and Elson 1991; Michael J. Saxton and Jacobson 1997; M.J. Saxton 1993).

To deal with these limitations regarding the hypothesis of a brownian diffusion of membrane protein at the membrane of cells, several strategies for the determination of D can be followed. The first is to limit the linear regression on the first steps of the MSD, typically from step 2 to 5 (Chamma et al. 2013; Heubl et al. 2017; M. Renner et al. 2017). This theoretically prevents constraints to the brownian movement which are more likely to occur whithin a greater time of integration. Another possibility to insure a proper estimation of D is the filtering of the trajectories based on the quality of the MSD ~ D regression, for example keeping only D values where $R^2 > 0.8$. MSD-derived D measurement have been discussed by Hansen et al. in the 1st Appendix of their publication. However the evaluation context differs (3D SPT), hence the conclusions might differ when considering 2D diffusion of membrane proteins (Hansen et al. 2018). Another possibility is to discriminate the particles based on qualitative differences in the MSD function or the covariance matrix of coordinates, indicative of a corralled or directed movement, adding another information on the different displacement trends among a population (M.J. Saxton 1993; Toulme and Khakh 2012). **In the majority of cases direct estimation of the diffusion coefficient from the first MSD time steps is performed**. In addition to the diffusion coefficient, MSD allows the estimation of the **confinement area of a particle**, with the limit value of MSD as an estimation of the domain's size (M.J. Saxton 1993). Its **simple implementation and the possibility to get D and confinement area (or explored area, EA) has made the MSD a common tool for the quantitative description of trajectories.**

An alternative to the MSD was proposed by Persson et al. in 2013 : the **variational Bayes for SPT**

(vbSPT) (Hansen et al. 2018; Persson et al. 2013). This algorithm combines Hidden-Markov Modelling and Bayesian inference, with the segmentation of the trajectories in different "states", while keeping the same diffusion model. Hence it adds statistical formalism to the estimation of diffusion coefficient from **different diffusion states** (along with other variables, such as the probability of transitionning from state i to state j at each iteration). On the other hand localization error is not covered by vbSPT algorithm, which may limit the estimation of low diffusion coefficients (akin to MSD). MSD has been more used traditionaly as it was formalized earlier than vbSPT, together with more accessible theoretical basis.

However **a major limitation of MSD-derived measurements compared with vbSPT is the study of different sub-populations with different diffusion properties** (as it is a mean-square displacement). The most common approach is to perform a fit on D values histograms or cumulative frequency to detect different different groups (Hansen et al. 2018). Hence no actual statistical model is used when determining the diffusion coefficient of different sub-populations. Another limitation mentioned by the authors is the poor handling of localization error by this method, mainly hindering the measurement of low values of D.

In the context of my work, the analysis were mainly performed using a custom program (SPTrack_v5, (Bonneau, Dahan, and Cohen 2005; M. Renner et al. 2017)) featuring a reconnection system and MSD-mediated estimations (without R^2 threshold). It allows the tracking of relatively long trajectories (spanning over at least 15 time windows = 450 ms) and bijective attribution of diffusion coefficients (D) and explored areas (EA) to trajectories. This is especially important as the experiments were performed on several cultures, enabling **inter-culture and intra-culture variability checking**. Another key feature is the possibility to use binary masks, separating different trajectories based on their **localization** on the neuron (like synaptic regions with Gephyrin and Homer masks in the context of my work). Regarding vbSPT, the software does not implement the reconnection of trajectories or localization features. In addition, as it requires sufficient data for the estimators' convergence (Persson et al. 2013), separating trajectories from each culture may come at the cost of a less effective convergence. A last point is that vbSPT only provides estimations on D meta-parameters (mean, standard deviation) and not D values distribution. On the other hands vbSPT allows the detection of **multiple diffusion states whithin single trajectories**, and provides **other variables** regarding the

transitions between those states, while having a **better resolution than MSD-dependent procedure** (Weimann et al. 2013). Thus these analysis algorithms are quite complementary. SPTrack_v5 was mainly used due to its transparence in variables distribution and its easier implementation, and vbSPT was performed to get additional information on the different subpopulations in different experimental conditions (see in the discussion).

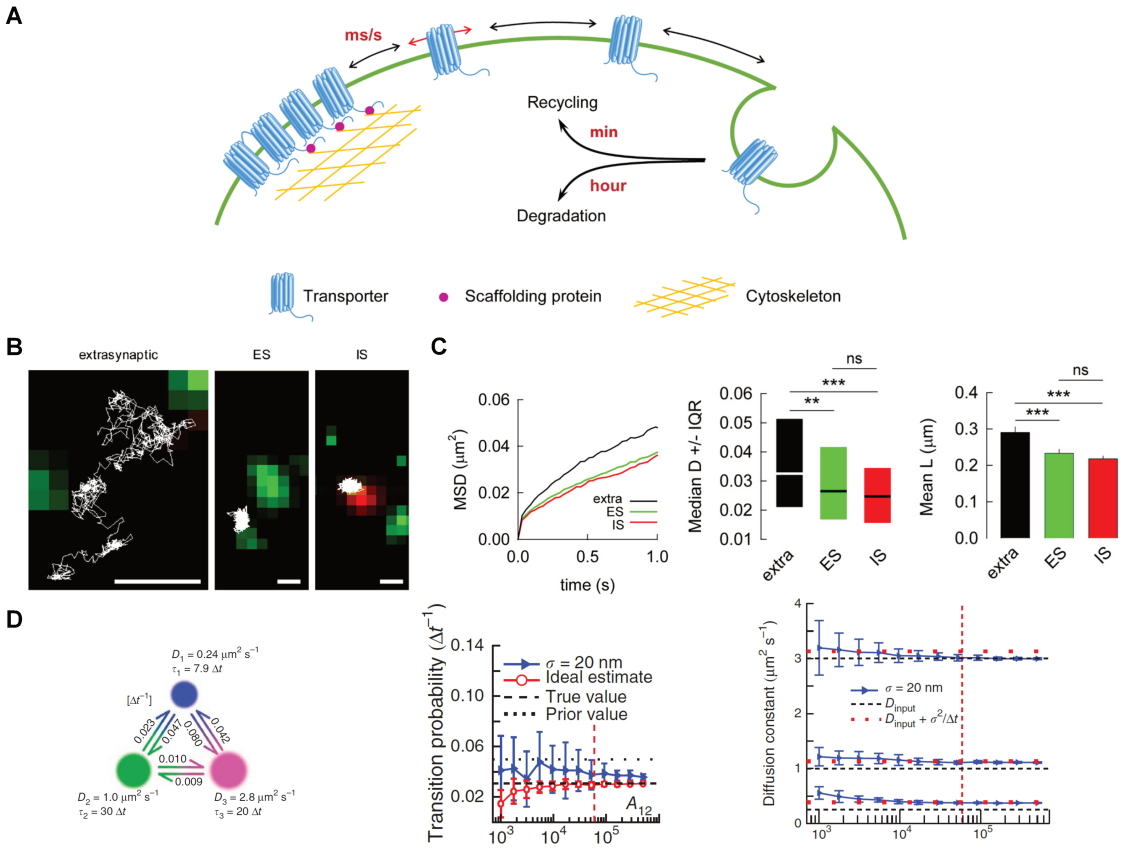

Figure 20, diffusion-capture regulation of membrane proteins. **A**, illustration of the diffusion-capture model. The aggregation of a membrane protein in clusters prevents its trapping in endocytic zones (Côme et al. 2019). **B**, MSD-derived analysis of KCC2 lateral diffusion at the membrane of hippocampal neurons. Re-constructed trajectories from QD-labelled KCC2 (ES : excitatory synapses ; IS : inhibitory synapses). **C**, MSD traces depending on KCC2 localization towards synapses, with corresponding diffusion coefficient (D) and confinement area (L), computed from MSD values. These results demonstrate a slower and more restrained diffusion of trajectories at the proximity of synapses (Chamma et al. 2013). **D**, vbSPT allows to study intra-trajectorie different diffusive states, while MSD approach is limited to the analysis of trajectories as a whole. *Left* : vbSPT-estimated diffusion characteristics of a particle, including the diffusion coefficient (D_i) and the dwell time (tau_i). The dwell time here describes the amount of time a particle remains in the i-th state. *Middle and right* : Bayesian updating performed whithin vbSPT to estimate the diffusion parameters. *Middle* : probability for the particle to transition from state 1 to state 2 ; *right* : diffusion coefficients of the 3 states. The x-axis represents the number of trajectories inputed (Persson et al. 2013).

I will describe several examples of SPT uses focusing on KCC2 and NKCC1, with applications of the diffusion-capture model to characterize their dynamics at the plasma membrane and their link with membrane stability (i.e. the probability that a protein is not internalized). Although I will focus on KCC2 and NKCC1 in the following paragraphs, note that SPT provided insights for other neuronal proteins, such as AMPA (Choquet 2018; Gauvain et al. 2011), NMDA (Lesept et al. 2016; Michaluk et al. 2009), glycine (Dahan 2003) or $GABA_A$ receptors (Barberis 2020; Lévi et al. 2015; de Luca et al. 2017; Petrini and Barberis 2014).

3. B. b. Diffusion-capture regulation of KCC2

3. B. b. i. Under control conditions

KCC2 role at excitatory synapses had been explored in several papers (Fiumelli, Cancedda, and Poo 2005; Gauvain et al. 2011; Gulyás et al. 2001; H. Li et al. 2007) leading Chamma et al. to study the co-transporter localization at the membrane (and notably its colocalization with synaptic regions) (Chamma et al. 2013). **Correlated with its accumulation at synapses, smaller confinement domains and lower diffusion coefficient values were reported at synapses when compared with extra-synaptic transporters**. As KCC2 forms clusters on the neuron's dendrites membrane, the decreased diffusion area and speed at excitatory synapses was shown to derive from the co-transporter trapping through **interaction with F-actin** (H. Li et al. 2007). **KCC2-actin interaction was also demonstrated to enhance the co-transporter's clustering (capture) at the proximity of excitatory synapses**. KCC2 undergoes diffusion-capture at excitatory synapses, with its its confinement and stabilization in peri-synaptic clusters.

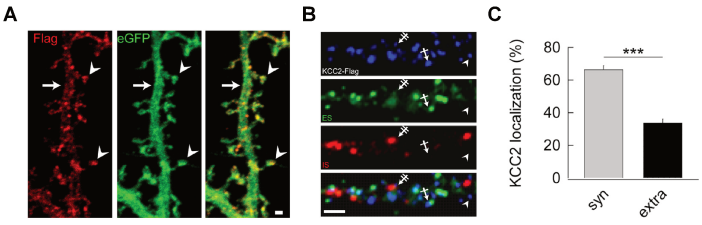

Figure 21. KCC2 forms peri-synaptic clusters at the membrane. A, membrane stainging of KCC2 (red) displays its clustered distribution, bar : 1 µm. B, KCC2 clusters are localized at the periphery of excitatory and inhibitory synapses (arrows). This is consistent with its decreased lateral in synaptic regions, due to its clustering. Bar : 2 µm. C, KCC2 is enriched at the periphery of synapses due to its stabilization in clusters. Adapted from Chamma et al. 2013.

3. B. b. ii. Regulation of KCC2 membrane stability through diffusion-capture

As mentioned previously, KCC2 is subject to several post-translational modifications. These modifications notably include its phosphorylation by several pathways (Kristopher T. Kahle et al. 2013; Kaila et al. 2014; Lévi 2019). **Serine 940 is a major KCC2 phosphorylation site and its phosphorylation enhances KCC2 membrane stability through reduced endocytosis** (H. H. C. Lee et al. 2007). The phosphatase PP1 mediating S940 dephosphorylation being calcium-dependent, another work reported that NMDAR activity-dependent increase in $[Ca^{2+}]_i$ leads to a rapid decrease (visible after ~ 10 minutes) in KCC2 activity in neurons due to its internalization and subsequent degradation (H. H. C. Lee et al. 2011; Puskarjov et al. 2012). It thus appears that KCC2 undergoes a rapid, activity-dependent regulation of its membrane pool through S940 dephosphorylation. This process was further studied by Chamma et al. in 2013, with the report of **decreased membrane KCC2 clustering correlated with greater diffusion kinetics under increased neuronal activity** (Chamma et al. 2013). These effects were associated with a S940 dephosphorylation, hence demonstrating that **KCC2 membrane pool is quickly regulated through the transporter's lateral diffusion at the membrane**. When confined in clusters, KCC2 would be less likely to cross an endocytic region, eventually resulting in an increased membrane stability (Côme et al. 2020).

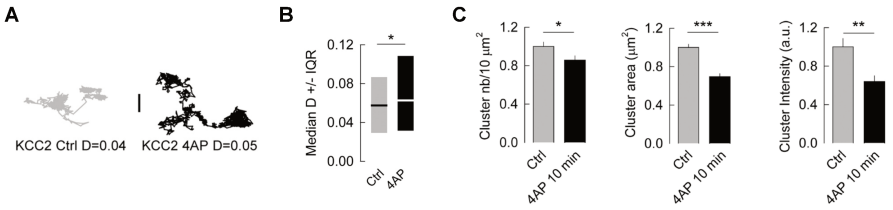

Figure 22, KCC2 membrane pool is regulated by neuronal activity through diffusion-capture. **A**, KCC2 trajectories at the membrane of hippocampal neurons, obtained by QD-SPT, under control and 4-AP conditions. **B**, 4-AP treatment increases KCC2 diffusion and explored area. **C**, along with an enhanced lateral diffusion, the clustering of KCC2 at the membrane is decreased after 4-AP application, both in terms of number of clusters and amount of KCC2 in those clusters. The reduced confinement of KCC2 following S940 dephosphoryation leads to its un-clustering, allowing its trapping in endocytic zones. Adapted from Chamma et al. 2013

In the same way, **KCC2 phosphorylation by the WNK-SPAK-OSR1 signalling was reported to decrease the transporter stability at the membrane** (Friedel et al. 2015). As KCC2 phosphorylation at S940, but also at Y903/Y1087, are regulated by glutamatergic and acetylcholinergic neuronal neurotransmissions (H. H. C. Lee et al. 2011; H. H. C. Lee, Jurd, and

Moss 2010), the question of its membrane distribution and internalization regulation by GABAergic activity was discussed. Heubl et al. in 2017 demonstrated an **increase in KCC2 diffusion coefficient (D) and explored area (EA, cf. 3. B. a) upon $GABA_AR$ blockade, an effect observed on the whole dendritic KCC2 population** (Heubl et al. 2017). This regulation of KCC2 diffusion was independent of the pathway regulating its phosphorylation at S940, but is rather caused by its **phosphorylation at T906/T1007 by SPAK/OSR1**. The authors proposed an homeostatic model on the regulation of neuronal $[Cl^-]_i$ by this regulation, with **changes in $[Cl^-]_i$ resulting in WNK autophosphorylation up- or down-regulation resulting in a regulation of $[Cl^-]_i$ via the tuning of KCC2 lateral diffusion**. Hence KCC2 activity has been linked with its membrane expression and stability, which are dependent on the transporter's diffusion-capture modulating its endocytosis but also its spatial distribution at the neuron's membrane (Côme et al. 2020). Thus the study of NKCC1 lateral diffusion and clustering at the membrane of neurons could yield interesting results regarding its baseline distribution but also its rapid regulation *via* WNK-SPAK-OSR1 phosphorylations.

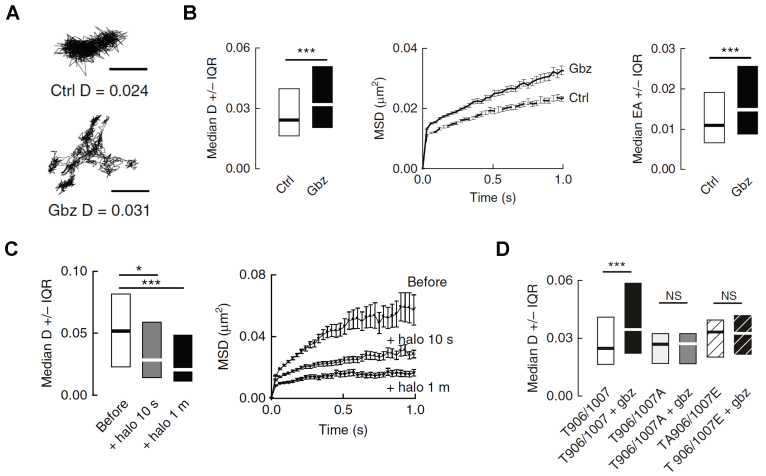

Figure 23, $GABA_AR$ activity regulates KCC2 via diffusion-capture through the chloride-sensitive WNK-SPAK-OSR1 signalling. **A**, QD-SPT trajectories of KCC2 are affected by $GABA_AR$ blockade with gabazine (excitatory neurotransmission blocked). **B**, *left* : KCC2 diffusion coefficient is higher after gabazine application. *Middle* and *right* : MSD and explored area of KCC2 are similarly higher after gabazine application. **C**, gabazine effects on KCC2 lateral diffusion are caused by the receptor-mediated chloride influx blockade, here demonstrated by halorhodopsin stimulation. **D**, chloride acts as a second messenger by inhibiting WNK-SPAK-OSR1-dependent KCC2 phosphorylation. Adapted from Heubl et al. 2017

3. B. d. Lateral diffusion of NKCC1 in neurons

In a recent publication, we presented NKCC1 subcellular expression and lateral diffusion in 21

DIV cultured hippocampal neurons (Côme et al. 2020). To our knowledge this is the **first characterization of the transporter's distribution and dynamics at the membrane of neurons**. **NKCC1 forms clusters at the membrane in the dendrites**. These clusters seem quite evenly distributed at the membrane, with a slight accumulation near inhibitory and excitatory synapses, however a statistical analysis of these observations will be necessary. In addition to its clustering, we studied its lateral diffusion depending on the compartment, and observed that **extra-synaptic NKCC1 is characterized by greater diffusion coefficient and explored area values than synaptic NKCC1** (especially regarding excitatory synapses). This observation suggests that the transporter could undergo diffusion-capture at the synapses, limitating its diffusion and increasing its clustering. In addition to dendritic NKCC1, we also looked at axonal NKCC1 lateral diffusion. Interestingly **the transporters in the axon are much more mobile and less restricted than in the dendrite, suggesting a different regulation than in the dendrite**.

These results illustrate the relevance of SPT to study the regulation of NKCC1 at the membrane. Being a highly resolutive tool with several readouts, it may help deciphering molecular pathways and mechanisms regulating its stability at the membrane, as they are yet poorly understood. We suggested that NKCC1 is regulated by diffusion-capture, a regulation which may be involved in its regulation by phosphorylation (like observed for KCC2). Furthermore an interesting insight was that axonal NKCC1 seems to be differently regulated through diffusion-capture, as suggested by different diffusion kinetics and area.

NKCC1 role in chloride homeostasis is decisive in the immature brain, and its involvement in epilepsy has been highlighted. But the physiological functions of this broadly expressed, major actor of stress response in many cell types and tissues, remain elusive in the adult brain. Due to the lack of data on its regulation in mature neurons, an important aspect of chloride homeostasis, and hence of GABAergic inhibition, has yet to be explored.

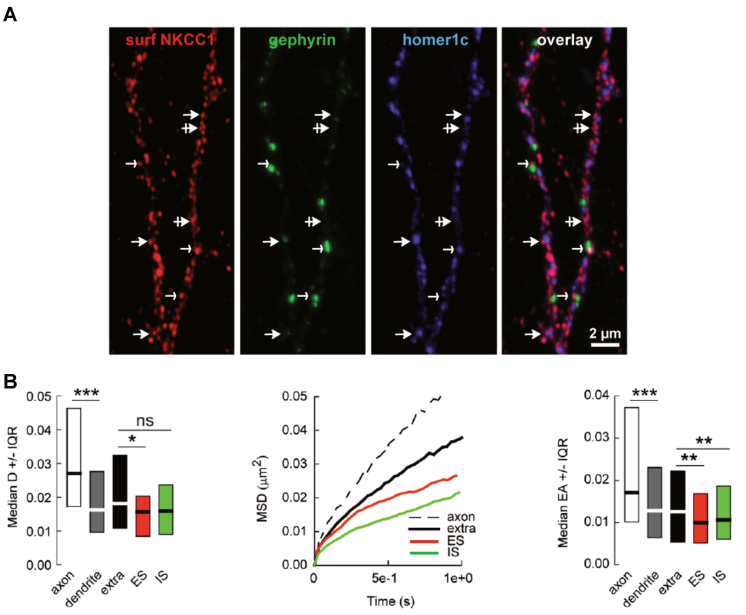

Figure 24, NKCC1 forms clusters at the membrane of mature hippocampal neurons, and has a compartment-specific diffusion. **A**, membrane NKCC1 forms clusters near inhibitory and excitatory synapses, but does not colocalize with them. **B**, quantification of NKCC1 lateral diffusion based on MSD analysis of QD-SPT trajectories. The transporter is more constrained nearby synapses compared with extrasynaptic NKCC1, alike KCC2. Interestingly axonal NKCC1 is more mobile and less restrained than dendritic NKCC1. Adapted from Côme et al. 2019.

Materials and methods

The following methods were developped and / or used in data presented in the Results part. For a thourough description of those please refer to the Materials and Methods section of the Results part.

Neuronal culture (15)

DNA constructs (15, 25, 29, 31)

Transfection and transduction

Peptide treatment and pharmacology

Live cell staining for single-particle imaging

Single-particle tracking and analysis (15, 19, 48, 49, 50)

Chloride imaging

Immunocytochemistry

Fluorescence image acquisition and analysis

***STORM microscopy* (51)**

Statistics

Here are presented the protocols and methods used for experiments and analysis not included in the Results part, but presented in the discussion :

Animal breeding. The C57BL6 mice carrying the SPAK 243A mutation were breeded with food and water *ad libitum* (Rafiqi et al. 2010). Heterozygous $SPAK^{243A/+}$ were used for mating, while we used the homozygous ones were used for experiments. Samples were sent to Charles River for PCR analysis of the mutations as described in (Rafiqi et al. 2010).

In vivo pentylenetatrazole injection. Adult (12-14 weeks) C57BL6 from our breeding were injected subcutaneously with pentylenetatrazole (PTZ, 75 mg/kg, dissolved in saline), and

recorded right after injection using video recordings. The procedure was made in accordance with the guidelines of the French Agriculture and Forestry Ministry for handling animals and with the agreement of the Comité National de Réflexion Ethique sur l'Expérimentation Animale (#4018). The sampling of animals, as well as the experimental procedure and analysis of the data were determined based on previous published work. Animals used for the experiments were $SPAK^{243A/243A}$ and $SPAK^{+/+}$, both males and females. After 60 min of observation, animals were killed by cervical dislocation, brains were rapidly extracted on ice and the cortex and the hippocampus were dissected, frozen in liquid nitrogen and stored at –80 °C until use for biochemistry. The first seizures were observed after 6–7 min of injection and a second sequence of seizures and/or abnormal gait were sometimes detected after 14–15 min. Only four out of thirty animals injected with 75 mg/kg of PTZ did not have tonic-clonic seizures, and only two had tonic-clonic seizures with rigid paw extension followed by death (as defined using Racine's scale). Mouse behaviour was scored according to the following modified Racine's scale: stage 0 : no symptoms, stage 1 : immobility and prostration; stage 2 : neck and body clonus, stage 3 : forelimb clonus and rearing, stage 4 : tonico-clonic seizure, stage 5 : death.

Electrocorticogram (EcoG) electrode implantation. 9 weeks old C57BL/6J mice were anesthetized by intraperitoneal injection of ketamine / xylazine (75/10 mg/kg) and subcutaneous injection of buprenorphine (0.05 mg/kg) for analgesia. Animals were then head-fixed in a stereotaxic apparatus. Two electrodes were placed above each hippocampus, at the following coordinates : AP -2.0 mm, ML ± 1.5 mm. A third screw was placed above the cerebellum and used as reference.

EcoG recordings. EcoG data were acquired at 20 kHz using Epoch Wireless recording system (Ripple) and Clampex software (Molecular Devices). Both video and EcoG data were acquired for one hour following PTZ injection. Animals were then sacrificed and brain were recovered and processed for biochemistry.

Analysis of EcoG signals and behaviour. EcoG signal analysis were performed offline using MATLAB built-in functions and custom-written scripts as well as Chronux (http://chronux.org/) and the FMAToolbox (http://fmatoolbox.sourceforge.net/). Prior to spectral analysis and events detection the traces were cleaned from disconnection events using a custom script. Power

spectra and spectrograms were computed using multitapers estimates on the raw LFP, and were used for seizure and recovery detection. A custom Racine's scale was used to characterize the severity of symptoms experienced by injected mice : 0 no symptoms, 1 prostration, 2 partial clonies, 3 generalized clonies, 4 tonico-clonic seizure, 5 death.

Results

Regulation of the NKCC1 chloride importer by the GABAergic inhibition and the WNK-SPAK-OSR1 signalling pathway in mature hippocampal neurons

The function and regulation of the Na^+-K^+-Cl^- co-transporter NKCC1 in mature hippocampal neurons are yet to decipher. Despite its relatively low contribution to chloride transport, NKCC1 appears to be up-regulated, both in terms of activity and expression, in epilepsy-related conditions. The objective of our work was to determine the molecular tenants of NKCC1 regulation in mature hippocampal neurons. Combining several complementary imaging approaches, I was able to analyse the consequences of $GABA_AR$ activity on NKCC1 distribution at the membrane. The following results demonstrate that :

- NKCC1 undergoes diffusion-capture at the membrane of mature hippocampal neurons, with a decreased diffusion speed and exploration at the periphery of synapses.
- NKCC1 lateral diffusion is likely regulated by axonal activity in the distal axon, while baseline glutamatergic activity does not change its diffusion in dendrites.
- $GABA_AR$ activity activity increases NKCC1 trapping in endocytic regions, regulating the co-transporter in a homeostatic fashion.
- This regulation involves the chloride-sensitive WNK-SPAK-OSR1 pathway, which activity is modulated by $GABA_AR$-mediated chloride flow into the cell. NKCC1 and KCC2 are regulated by the same signalling involving chloride as a second messenger.

In the light of its documented up-regulation in conditions of excitation/inhibition imbalance in the mature brain, these results describe a rapid homeostatic modulation of NKCC1 by GABAergic neurotransmission following the diffusion-capture model. A default in WNK-SPAK-OSR1 regulation is a promising lead to explain KCC2 and NKCC1 regulation in pathological contextes.

Regulation of the NKCC1 chloride importer by the GABAergic inhibition and the WNK-SPAK-OSR1 signalling pathway in mature hippocampal neurons

Etienne Côme[1], Marion Russeau[1], Imane Moutkine[1], Simon Blachier[1], Marion Mallet[1], Samy Hamadache[1], and Sabine Lévi[1]

1 INSERM UMR-S 1270, Sorbonne Université, Institut du Fer à Moulin, 75005, Paris, France

Abstract

In epilepsy, upregulation of the Na^+ - K^+ - $2Cl^-$ co-transporter NKCC1, the main importer of chloride into neurons, may lead to a depolarizing/excitatory GABAergic response in neurons and thus to hyperactivity of the neuronal network which would be at the origin of epileptic seizures. Understanding the regulatory mechanisms of NKCC1 would allow at term the identification of new therapeutic tools to cope with the intra-neuronal chloride buildup that occurs in the pathology and thus limit the onset or extent of epileptic seizures. However, these mechanisms are poorly understood. Here, we demonstrate that the membrane stability of NKCC1 is rapidly regulated by lateral diffusion in an activity-dependent manner at the surface of mature hippocampal neurons. The membrane dynamics and clustering of NKCC1 is tuned by $GABA_AR$-mediated signalling and chloride-sensing WNK1 kinases and downstream SPAK/OSR1 effector kinases though the phosphorylation of NKCC1 T203/T207/T212/T217/T230 residues. The fact that KCC2 is also regulated in mature neurons by the WNK1/SPAK/OSR1 pathway and that this regulation has an inverse effect on the membrane stability, clustering and function of KCC2 indicates that this pathway is a target of interest in the pathology. Inhibition of the pathway

would prevent the loss of KCC2 and the increase of NKCC1 at the surface of the neuron, thus preventing the abnormal rise of $[Cl^-]_i$ in the pathology and the resulting adverse effects.

Introduction

Upon activation by GABA, GABA type A receptors ($GABA_ARs$) open a selective chloride/bicarbonate conductance. The direction of chloride (Cl^-) flux through the channel depends on transmembrane Cl^- gradients. Therefore, Cl^- homeostasis critically determines the polarity and efficacy of GABAergic transmission in the brain. Pharmaco-resistant epilepsies are often associated with altered Cl^- homeostasis (1, 2). It is therefore crucial to discover novel mechanisms regulating neuronal Cl^- homeostasis that may help develop new and efficient treatment for these forms of epilepsy and other diseases associated with impaired inhibition, such as neuropathies and neuropsychiatric disorders (3).

The increase in $[Cl^-]_i$ and subsequent depolarized shift in the reversal potential of GABA (EGABA) observed in adult epilepsy models are often attributed to reduced expression/function of the neuronal K^+-Cl^- cotransporter KCC2, responsible for Cl^- export (4). Furthermore, up-regulation of the Na^+-K^+-Cl^- cotransporter NKCC1, which imports chloride into neurons, also contributes to the increase in $[Cl^-]_i$ and depolarization of E_{GABA}. This has been observed in the subiculum of patients with Temporal Lobe Epilepsy (TLE) (5, 6) as well as in several in vivo and in vitro animal models of epilepsy such as the glioma-induced (7), the traumatic brain injury-induced (8) models of epilepsy in rodents, and the kainic acid and pilocarpine epilepsy models in tissue slices (9–11). Targeting NKCC1 in epilepsy with the inhibitor bumetanide is protective: it abolished glioma-induced seizures in rats (7), it reduced the frequency of interictal-like activities(6), the duration

of ictal activities (9), and the sprouting of mossy fibers (10).

Key cellular and molecular mechanisms regulate the membrane turnover of KCC2. They involve activity-dependent regulation of the transporter membrane turnover and endocytosis (12, 13). KCC2 is rapidly down-regulated by enhanced neuronal activity and glutamatergic neurotransmission in mature neurons (14–16). NMDA receptor-induced Ca^{2+}-influx leads to PP1-dependent KCC2 Serine S940 (S940) dephosphorylation and C-terminal domain cleavage by Ca2+-activated protease calpain (14, 17, 18). This in turn leads to increased endocytosis of KCC2 and transporter degradation (14). GABAergic signalling can also tune KCC2 at the neuronal membrane through $GABA_AR$ activity and Cl^--dependent phosphorylation of KCC2 Thr906/1007 residues (19). Cl^- acts as a second messenger in this regulation by tuning the activity of the Cl^- sensing With No lysine (K) serine-threonine kinase WNK1 and its downstream effectors Ste20 Proline Asparagine Rich Kinase (SPAK) and Oxydative Stress Response kinase 1 (OSR1) (20). Interestingly, this signalling not only promote KCC2 T906/T1007 but also NKCC1 T203/T207/T212 phosphorylation (21). This results in a powerful modulation of Cl^- transport by inhibiting KCC2 and activating NKCC1; both regulations leading to elevation in intracellular Cl^- level in non-neuronal cells (22). Therefore, inhibiting KCC2 and NKCC1 phosphorylation mediated by the WNK signalling might normalize the membrane expression/function of transporters, thereby preventing the intracellular Cl^- buildup in epilepsy and the intensity or emergence of epileptic seizures. Our team has shown the contribution of lateral diffusion in the rapid control of KCC2 membrane stability and Cl^- neuronal homeostasis in response to changes in neuronal activity (15, 19). The transporter alternates between periods of confinement within clusters near synapses and periods of free movement outside the clusters. The free transporter can then be

targeted to the endocytic wells where it is internalized and then degraded or recycled to the plasma membrane. These two pools of transporters are in dynamic equilibrium, allowing fine-tuning of synapses in response to local fluctuations in synaptic activity (13). Since changes in KCC2 mobility occur within tens of seconds (19), lateral diffusion is probably the primary cellular mechanism modulating KCC2 membrane stability. Recently, we showed with confocal microscopy that NKCC1 is targeted to the axonal and somato-dendritic plasma membrane and that it forms clusters at the periphery of synapses of hippocampal neurons (12). Quantum Dot-based Single Particle Tracking (QD-SPT) in living cultured hippocampal neurons indicated that NKCC1 explore large areas of the somato-dendritic extrasynaptic membrane while others are confined near excitatory and inhibitory synapses (12). Transitions between NKCC1 confinement at/near synapses and less constrained diffusion in extrasynaptic areas is reminiscent of KCC2 diffusion (15, 19). Therefore, similar to KCC2, NKCC1 responds to the diffusion-trapping mechanism (12). A rapid activity-dependent regulation of NKCC1 diffusion/clustering, may thus locally affect its function, and in turn GABA signalling.

Here, we show that GABAergic neuronal activity rapidly regulates the diffusion/trapping and thereby the clustering of NKCC1 at the surface of hippocampal neurons. Blocking or activating GABAA receptors with muscimol or gabazine rapidly slow down and confine transporters in the membrane. Transporter confinement would be consecutive to the recruitment of transporters within endocytic zones. We then identified the underlying molecular mechanism. GABAergic activity would control the diffusion/capture and clustering of NKCC1 via the chloride-sensitive WNK1 kinase and the downstream SPAK and OSR1 kinases that would directly phosphorylate NKCC1 on key threonine T203/T207/T212/T217/T230 phosphorylation sites. These results

emphasize targeting the WNK1/SPAK/OSR1 pathway to regulate neuronal chloride homeostasis and thus neuronal hyperactivity in epilepsy.

Results

The lateral diffusion of NKCC1 is regulated by basal glutamatergic activity in the axon but not in the dendrite

There are two splicing variants of NKCC1: NKCC1a and NKCC1b (Randall, J. et al., Am. J. Physiol. 1997, 273, C1267–C1277). NKCC1b differs from NKCC1a by the absence of an exon 21-encoded region that contains a putative consensus sequence for PKA phosphorylation (23) and a dileucine motif essential for the basolateral sorting of NKCC1 in polarized epithelial cells (24). In the absence of antibodies labeling NKCC1a and NKCC1b on the surface of neurons, we expressed recombinant human NKCC1a or NKCC1b transporters bearing a 2xHA tag at position Histidine 398 in their second extracellular loop (i.e. the NT931 construct in (25)). The recombinant transporters also carry a 3xFlag tag and a monomeric Venus tag inserted at the N-terminus after the initiation codon (25). The insertion of these tags does not alter the membrane expression and transport function of the NKCC1 proteins as checked by HA surface labeling and 86Rb influx studies in HEK 293 cells (25). In agreement with these results, we showed using surface labeling that the recombinant NKCC1a (12) and NKCC1b transporters (data not shown) are targeted to the axonal and somato-dendritic plasma membranes. The fact that NKCC1b was detected in the somato-dendritic compartment in the same way as NKCC1a suggests that the dileucine motif is not sufficient for targeting the transporter there. Since NKCC1a predominates in the brain (26), we focused our study on this isoform. We have previously shown that, in basal activity

conditions, NKCC1a forms numerous clusters on the surface of dendrites of mature pyramidal neurons of the hippocampus (12). The clusters are found in the extrasynaptic membrane but also near the glutamatergic excitatory and GABAergic inhibitory synapses (12). In addition, the transporter responds to the “diffusion-trap” mechanism (12). This is reminiscent of the regulation of KCC2 at the plasma membrane (15, 19). Our initial characterization of NKCC1 membrane dynamics and clustering was done in basal activity conditions (12). Since we demonstrated that the regulation of the diffusion of KCC2 by excitatory and inhibitory activity rapidly tunes the membrane stability of KCC2 and thus chloride homeostasis and GABAergic signalling (15, 19), we wanted to examine whether NKCC1a membrane dynamics and clustering could be modulated by neuronal activity. We studied the regulation of the membrane dynamics of NKCC1a (named NKCC1 from there on) by neuronal activity using Quantum Dot-based Single Particle Tracking (QD-SPT) technique in cultures of mature hippocampal neurons (DIV 21–24). To this end, neurons were transfected at DIV14 with NKCC1-HA construct (modified from NT931 construct, see Methods), and stained live the day of the experiment with QD-coupled anti-HA antibody and imaged (see Methods).

We first checked whether the diffusion of NKCC1 is regulated by basal glutamatergic activity. To this end, NKCC1 diffusion was explored in the presence of the Na+ channel blocker tetrodotoxin TTX (1µM), the ionotropic glutamate receptor antagonist kynurenic acid (KYN, 1 mM), and the group I/group II mGluR antagonist R,SMCPG (500 µM). Cells were exposed to the cocktail "TTX + KYN + MCPG" 10 minutes before the recordings and were imaged up to one hour in the presence of the drugs. We observed that, when exposed to TTX + KYN + MCPG, exploration of individual QDs was limited to smaller areas in the axon, compared to QDs on dendrite (Fig. 1A).

Statistical analysis of hundreds of trajectories showed that the slope of the mean square displacement function (MSD) as a function of time was reduced for trajectories recorded in the axon compared to those recorded in the dendrite (Fig. 1B), indicating increased confinement of NKCC1 in the axon. Consistent with this observation, the median values of the diffusion coefficient (D) (Fig. 1 C-D) and the size of the area explored (EA) (Fig. 1 E-F), which are calculated from the MSD versus time curves, are also significantly decreased in the axons compared to the dendrites (Table 1). The cumulative graphs of log(D) and log(EA) describe an overall trend with no apparent sub-populations of QDs when looking at the cumulative distributions (Fig. 1 D, F). These results show that NKCC1 is slower and more confined in the axon than in the dendrite under conditions of blockade of basal glutamatergic transmission. These results, unlike those obtained in the absence of activity blockers (12), suggest that the mobility and exploration of NKCC1 in the axon but not in the dendrite is regulated by glutamatergic activity.

We then analyzed the diffusion properties of NKCC1 in relation to synapses in conditions of glutamatergic activity blockade. We studied the diffusive behavior of NKCC1 on the dendrites of neurons co-transfected with NKCC1-HA and the inhibitory and excitatory synaptic markers Gephyrin-Finger-YFP and Homer1c-DsRed, respectively (Fig. 1G). For receptors enriched in the postsynaptic membrane (e.g. $GABA_AR$, glycine receptor or AMPAR...), trajectories are usually considered synaptic when they overlap the synaptic mask or extrasynaptic for spots located two pixels (380 nm) apart (15, 19). The application of this parameter did not detect enough synaptic trajectories of NKCC1. This means that NKCC1 is at distance from the synapse. Assuming that QDs are slowed down and confined to the synapse, we increased the size of the area around the synaptic mask until we identified a distance that allows to separate confined trajectories from

free trajectories. Thus, a threshold of 4 pixels (760 nm) was determined. Using this parameter, we found that individual QDs explored restricted surface area of the membrane near both GABAergic and glutamatergic synapses compared to extrasynaptic ones (Fig. 1G). This was associated with a reduced slope of the MSD vs. time function for synaptic trajectories as compared with extrasynaptic ones (Fig. 1H), indicative of increased confinement at the periphery of the synapse. Consistently, the median D and EA values were also significantly decreased (Fig. 1I-J). Thus, NKCC1 is confined at the periphery of synapses, regardless of whether (this work) or not glutamatergic transmission is blocked (12). Although the diffusion coefficient and the size of the explored zone of NKCC1 were similar near both excitatory and inhibitory synapses, NKCC1 spent 2.3 fold more time near glutamatergic synapses than GABAergic synapses (Fig. 1K, Table 1). This resulted in a 1.89 fold increase in NKCC1 residency time near glutamatergic synapses compared to inhibitory synapses (Fig. 1L, Table 1). Thus, NKCC1 is more confined at the periphery of glutamatergic synapses than near GABAergic synapses under conditions of glutamatergic activity blockade. These results do not differ from those obtained in the absence of activity blockade (12), consistent with the fact that the mobility of NKCC1 at the surface of dendrites is apparently not dependent on basal glutamatergic activity.

<u>$GABA_AR$ activity regulates NKCC1 diffusion-capture and clustering</u>

We then questioned whether inhibitory GABAergic transmission influences NKCC1 lateral diffusion. Since basal glutamatergic activity affects NKCC1 diffusion in the axon (Fig. 1), and that this may in turn influence the neuronal or network activity, the impact of a pharmacological activation or blockade of $GABA_ARs$ was explored in the presence of TTX + KYN + MCPG and

compared to the TTX + KYN + MCPG “control” condition. Neurons were acutely exposed to the $GABA_AR$ agonist muscimol (10 µM) or competitive antagonist gabazine (10 µM), two drugs that were shown using electrophysiological recordings to increase or block $GABA_AR$-mediated inhibition in mature (DIV21-23) hippocampal cultured neurons (19). QDs explored smaller areas of the dendritic membrane following exposure to gabazine or muscimol, compared to the control condition (Fig. 2A). Analysis performed on the bulk population (extrasynaptic + synaptic) of dendritic trajectories revealed that the MSD function displayed a less steep slope for trajectories recorded in the presence of muscimol or gabazine as compared with control (Fig. 2B), indicative of increased confinement upon $GABA_AR$ activation or blockade. Consistent with this observation, the median diffusion coefficient and explored area were also significantly decreased upon muscimol and gabazine application (Fig. 2 C-D, Table 2). These data indicate that the lateral diffusion of NKCC1 on the dendrite is regulated by inhibitory GABAergic transmission: the transporter being slowed down and confined in response to an increase or decrease in GABAeric activity.

We then analyzed the effects of gabazine and muscimol on the diffusive behavior of NKCC1 in extrasynaptic and synaptic domains of neurons co-transfected with NKCC1-HA and the excitatory and inhibitory synaptic markers Homer1c-DsRed and Gephyrin-Finger-YFP, respectively. Muscimol and gabazine reduced the transporter mobility and surface exploration of individual QDs (Fig. 2E). Quantitative analysis on populations of QDs revealed an impact of the treatments on diffusion coefficient and explored area both in the extrasynaptic membrane and at excitatory and inhibitory synapses (Fig. 2 F-G, Table 2). The effect was greater on the diffusion coefficient than on the explored area for NKCC1 trajectories at excitatory synapses and vice versa for

trajectories near inhibitory synapses (Fig. 2F-G, Table 2). Thus, NKCC1 exhibits increased diffusion constraints at extrasynaptic sites and in the vicinity of synapses upon $GABA_AR$ activation or blockade.

Increased protein confinement may result in i) increased clustering of the protein at the membrane or ii) targeting of the protein to endocytic zones where it is either stored to form a reserve pool that can be re-mobilized by lateral diffusion in response to activity changes or internalized to be recycled to the membrane or degraded. To determine whether the regulation of NKCC1 diffusion by GABAergic activity is related to an endocytic process, we investigated the effects of activating or inhibiting $GABA_AR$ activity in conditions of blockade of endocytosis. We observed that blocking clathrin-mediated endocytosis with an inhibitory peptide prevented the reduction in the surface explored by individual NKCC1 transporters (Fig. 2H). In these conditions, neither gabazine nor muscimol decreased the diffusion coefficient (Fig. 2I) and the area explored (Fig. 2J), in comparison with the conditions where the agonist and antagonist were added alone (Fig. 2C-D). We therefore concluded that treatment of neurons with muscimol or gabazine target the transporters to endocytic wells.

We then wanted to know if the increased confinement of the transporter in endocytic zones following activation or blockade of the GABAergic activity was accompanied by an increase in its internalization. We measured in hippocampal neurons the mean fluorescence intensity per pixel of the surface and total (surface + intracellular) pools of transporters (Fig. 3A) and made the ratio (see Methods). The fluorescence ratio remained unchanged (Fig. 3B) after exposure to muscimol or gabazine for 30 minutes. These data indicate that changes in $GABA_AR$ activity do

not affect the membrane turnover of the transporter. We previously demonstrated that the regulation of KCC2 lateral diffusion by excitation or inhibition allows for a rapid regulation of the transporter clustering (15, 19). We therefore examined whether changes in $GABA_AR$-dependent inhibition resulted in altered NKCC1 clustering in hippocampal neurons. In control conditions, NKCC1 formed small size clusters at the surface of dendrites (Fig. 3A). Muscimol application reduced membrane-associated NKCC1-HA immunoreactivity (Fig. 3A). Quantifications indicated that muscimol significantly reduced by 1.28-fold the density of NKCC1 clusters at the surface of transfected neurons (Fig. 3C). Furthermore, a 30 min exposure to muscimol reduced by 1.1-fold the mean size of NKCC1 clusters (Fig. 3D), as compared with untreated cells. In contrast, muscimol did not affect the mean fluorescence intensity of the clusters (Fig. 3E). Overall, these results indicate that the increased confinement of NKCC1 in endocytic zones induced by muscimol is accompanied by a rapid reduction in the number of clusters in the plasma membrane. Unlike muscimol, gabazine did not noticeably alter the density of NKCC1 clusters (Fig. 3A). Indeed, acute gabazine treatment of neurons did not affect the number of NKCC1 clusters (Fig. 3C). However, it significantly reduced the size (Fig. 3D) and intensity (Fig. 3E) of the clusters. Since the NKCC1 aggregates are small and that their size is at the limit of the resolution of a standard epifluorescence microscope, it is difficult to conclude that gabazine has not much effect on NKCC1 clustering.

We therefore studied NKCC1 clustering using super-resolution STORM microscopy. Under control condition, NKCC1 clusters were evenly distributed along the dendritic shaft (Fig. 4Aa) and in dendritic spines (Fig. 4Ab). NKCC1 clusters displayed round or elongated shapes (Fig. 4A). The average surface area of NKCC1 clusters was 51.1 ± 57.3 nm2 (MEAN +/- SD, n=1315, 5 cultures,

Fig. 4B). On average, 76.8 ± 95.3 single molecules were detected per cluster (Fig. 4C). Both the surface area and the molecular density of clusters displayed a uniform distribution (Fig. 4 C-D) showing that the clusters were homogeneous. Neuronal exposure to gabazine or muscimol altered the nanoscopic organization of NKCC1 (Fig. 4E). The muscimol treatment significantly decreased by 1.16 fold the average size of NKCC1 clusters (Fig. 4F). This effect was not accompanied by a decrease in the number of molecules detected per cluster (Fig. 4G). In fact, the density of particles detected per cluster was significantly increased by 1.43 fold after muscimol exposure (Fig. 4H), indicating molecule compaction. This effect coupled with the loss of NKCC1 clusters observed with standard epifluorescence and the increased confinement of the transporter in endocytic zones is consistent with a muscimol-induced escape of transporters from clusters followed by their recruitment and storage in endocytic zones. STORM microscopy revealed that gabazine treatment induced a significant decrease in the size of NKCC1 clusters (by 0.62-fold on the median, Fig. 4F), accompanied by a 1.5-fold reduction in the number of molecules per cluster (Fig. 4G), in agreement with the notion that transporters escaped clusters. This effect was not associated with a change in the density of molecules per cluster (Fig. 4H), reporting no change in the compaction of molecules within the cluster. Although the effects of muscimol and gabazine differ slightly on the nanoscale organization of NKCC1, both treatments result in the escape of transporters from clusters, which are, then rapidly captured in the endocytic zones where they are stored.

Intracellular chloride regulates NKCC1 diffusion and clustering

We then investigated whether changes in $[Cl^-]_i$ could explain the effects of manipulations of $GABA_AR$ activity on the diffusion of NKCC1, as shown for KCC2 (19). We lowered $[Cl^-]_i$ by

substituting extracellular Cl− with methane sulfonate in the imaging medium and tested its effect on NKCC1 diffusion. The decrease in $[Cl^-]_i$ increased NKCC1 surface exploration for individual trajectories (Fig. 5A). Quantification performed on population of QDs revealed that this treatment had no significant effect on the diffusion coefficient of NKCC1 on dendrites either for extrasynaptic or synaptic trajectories (Fig. 5B). On the other hand, lowering $[Cl^-]_i$ increased the surface explored by extrasynaptic transporters (Fig. 5C), while the one explored by the transporters at the synapse was unchanged (Fig. 5C) (Table 2). These results provide evidence that lowering intracellular chloride levels reduces the confinement of NKCC1 in the extrasynaptic membrane.

Next, we determined whether a decreased confinement of the transporter was associated with a redistribution of the transporter in the membrane. Quantification of the ratio of the surface pool of NKCC1 over the total pool of NKCC1 revealed that lowering $[Cl^-]_i$ by extracellular Cl− substitution increased NKCC1 immunoreactivity on the dendrites (Fig. 5D). This was accompanied by a 1.25 fold increase in the amount of NKCC1 detected at the cell surface (Fig. 5E). This increase in the membrane stability of NKCC1 was accompanied by an increase in its clustering. The treatment did not alter the number of clusters detected at the cell surface (Fig. 5F). However, lowering $[Cl^-]_i$ level led to a 1.12 fold increase in the median size of NKCC1 clusters (Fig. 5G) and a 1.4 fold increase in their median fluorescence intensity (Fig. 5H).These results indicate a chloride-dependent regulation of NKCC1 diffusion-capture, consistent with a homeostatic regulation of the cotransporter.

The WNK signalling pathway regulates NKCC1 diffusion and clustering

The chloride-sensitive WNK signalling pathway regulates NKCC1 activity (for review see (27)). We assessed the role of this pathway in NKCC1 clustering using overexpression of constitutively active (WNK-CA) or kinase-dead (WNK-KD) WNK1 and using WNK1 (WNK463) inhibitor. Under basal conditions, overexpression of WNK-CA had no effect on NKCC1 surface exploration and mobility for individual trajectories (Fig. 6A) and population of QDs (Fig. 6B-C, Table 3). Similarly, overexpressing WNK-CA did not alter the surface expression level of NKCC1 (Fig. 6D-E) nor the number of NKCC1 clusters (Fig. 6F) nor the size and intensity of these clusters (Fig. 6G-H). Based on these results, we concluded that activation of the WNK1 pathway does not affect the diffusion, expression and distribution of NKCC1 at the dendritic surface.

Conversely, we studied the effects of an inhibition of the WNK1 signalling pathway on NKCC1 surface expression and clustering following overexpression of WNK-KD or after addition of the inhibitor WNK463. An acute blockade for 30 min of WNK1 with WNK463 had no effect on the membrane stability of NKCC1 (Fig. 6I-J) while blocking WNK1 activity for 7 DIV by overexpressing WNK-KD significantly reduced the membrane stability of NKCC1 (Fig. 6I-J). On the other hand, WNK inhibition using genetic or pharmacological approaches significantly altered the clustering of NKCC1 by decreasing respectively to 2 fold and 1.6 fold the number of NKCC1 clusters (Fig. 6K). This was not accompanied by a reduction in the size of the clusters upon WNK463 treatment or WNK-KD overexpression (Fig. 6L). However, WNK-KD overexpression decreased to 2 fold NKCC1 cluster intensity (Fig. 6M). Therefore, inhibiting the WNK1 signalling pathway reduces NKCC1 membrane stability and clustering.

We then studied the contribution of the WNK1 effectors SPAK and OSR1 in the regulation of NKCC1 membrane diffusion, stability and clustering using the SPAK/OSR1 inhibitor closantel (28). An acute exposure of neurons to closantel rapidly reduced the surface explored by individual QDs (Fig. 7A). This was accompanied by a 1.14-fold reduction in NKCC1 diffusion coefficients (Fig. 7B, Table 3) and by a 1.28-fold decrease in its explored area (Fig. 7C, Table 3), revealing increased NKCC1 diffusion constraints as compared with control. This effect on diffusion was however not accompanied by a change in the surface expression of NKCC1 (Fig. 7D-E), nor by a change in its clustering as determined by standard epifluorescence on the number of NKCC1 clusters (Fig. 7F), as well as on the size and intensity of the clusters (Fig. 7G-H). However, the analysis of NKCC1 clusters using super-resolution imaging (Fig. 7I) revealed that a 30 min exposure to closantel reduced by 1.3-fold the cluster size (Fig. 7J). This effect was not accompanied by a significant change in the number of particles detected per cluster (Fig. 7K). However, closantel increased by 1.75-fold the density of molecules per cluster (Fig. 7L) as compared with untreated cells, indicative of molecular compaction. Therefore, the closantel-induced confinement of NKCC1 is accompanied by a rapid alteration in the nanoscale organization of the transporter. Taken together these results show that the WNK1/SPAK/OSR1 pathway regulates the membrane dynamics, stability and clustering of NKCC1 in mature neurons under basal activity conditions. The fact that an activation of the WNK1 pathway (by overexpressing WNK-CA) has no effect on NKCC1 membrane dynamics, expression and clustering suggests that this pathway is constitutively active in mature neurons.

WNK kinases promote NKCC1T203/T207/T212 phosphorylation (29), which in turn results in NKCC1 activation (22). In order to test the involvement of NKCC1 T203/207/212/217/230

phosphorylation in the regulation of NKCC1 diffusion, we expressed NKCC1 constructs harboring mutations of T203/T207/T212 or T203/T207/T212/T217/T230 to alanine (TA3 and TA5, respectively) that mimic dephosphorylated states. The mobility and exploration of individual NKCC1 T203/207/212/217/230A was decreased relative to WT especially for extrasynaptic QDs (Fig. 8A). This was reflected by a 1.2 fold slowdown (Fig. 8B) and a 1.48 fold increase in the confinement (Fig. 8C) of QDs in the extrasynaptic membrane without changing the diffusion coefficient or the surface area explored at the inhibitory and excitatory synapses (Fig. 8B-C, Table 3). Therefore, the dephosphorylation of NKCC1 on key threonine residues confines the transporter in the extrasynaptic membrane. In agreement with a basal regulation of NKCC1 by the WNK1 signalling pathway, these results indicate that a proportion of NKCC1 is phosphorylated on T203/207/212/217/230 in mature neurons at rest. This differs from the KCC2 transporter for which regulation by the WNK1 signalling was only observed when $GABA_AR$ activity was challenged (19).

We have previously shown in similar experimental preparations that an acute application of muscimol induces an increase in $[Cl^-]_i$ (19). This is corroborated by the inhibition of WNK1 and dephosphorylation of NKCC1 (19). Knowing that the phosphorylation of NKCC1 by WNK1 regulates its activity in non-neuronal cells (30), we wanted to know if the membrane stability and clustering of the mutated transporter was altered compared to that of WT. Our results show that the surface pool of NKCC1-T203/T207/T212A is decreased (by 1.1 fold) compared to that of the WT transporter (Fig. 8D-E). This decrease in the membrane stability of the transporter was accompanied by a 1.6 fold and a 1.7 fold decrease in the cluster density of NKCC1-T203/T207/T212A and NKCC1-T203/T207/T212/T217/T230A (Fig. 8F), compared to the

WT. The remaining NKCC1-T203/T207/T212A and NKCC1-T203/T207/T212/T217/T230A clusters were not changed in size or fluorescence intensity compared to WT (Fig. 8G-H). This effect is reminiscent of that observed upon muscimol treatment (Fig. 3) or WNK1 inhibition (Fig. 6). Importantly, NKCC1-T203/T207/T212/T217/T230A prevented the muscimol-induced decrease in NKCC1 clustering (Fig. 8I). We conclude that $GABA_AR$-dependent regulation of NKCC1 membrane stability, diffusion and clustering involves phosphorylation of its T203/T207/T212/T217/T230 residues.

Functional relevance of NKCC1 regulation by the WNK signalling pathway in mature hippocampal neurons

Our work describes a regulation of NKCC1 membrane stability and clustering through GABAergic activity. This regulation involves the phosphorylation of the transporter by the WNK/SPAK/OSR1 signalling pathway. To assess the functional relevance of this regulation, we looked at the impact of NKCC1 phosphorylation on $[Cl^-]_i$. We used SuperClomeleon (31) to quantify potential changes in intracellular chloride concentration. Changes of concentration were inferred from changes in YFP/CFP ratios (Fig. 9A). As a control condition, we compared the YFP/CFP ratio of cells transfected with KCC2-WT vs KCC2-T906/T1007E i.e. a construction mimicking the phosphorylated state of the transporter with a reduced capacity to extrude chloride ions, notably by modifying its membrane stability and clustering (19, 29). An important decrease in the ratio was observed in cells transfected with KCC2-TE as compared to KCC2-WT, reflecting a higher $[Cl^-]_i$ (Fig. 9B). Thus, this approach allows the measurement of $[Cl^-]_i$ elevation resulting from manipulations of chloride co-transporter membrane expression and therefore function. We then tested whether the expression of endogenous or recombinant NKCC1 significantly

impacted $[Cl^-]_i$ in our neuronam preparation. First, we determined the impact of an acute blockade of NKCC1 activity with the selective NKCC1 inhibitor bumetanide (5 µM) on the YFP/CFP ratio in neurons transfected with SuperClomeleon alone. The YFP/CFP ratio was comparable in both bumetanide-exposed and non-bumetanide-exposed neurons (Fig. 9C). These results are in agreement with data suggesting that at rest, endogenous NKCC1 do not significantly influence $[Cl^-]_i$ in mature hippocampal neurons (32, 33). Similarly, expression of the recombinant NKCC1-WT in mature neurons did not increase $[Cl^-]_i$ compared to neurons expressing the chloride probe alone, nor did it increase their sensitivity to bumetanide (Fig. 9C). This suggests that the neuron tightly regulates the level of recombinant NKCC1 present at the cell membrane.

If the expression of NKCC1-WT does not influence $[Cl^-]_i$, then it is not surprising that a loss of function of the transporter cannot be detected. Indeed, we found that NKCC1-T203/T207/T212/T217/T230A, which shows a defect in membrane clustering compared to WT, has no effect on either the YFP/CFP ratio or the response to bumetanide (Fig. 9C). However, since NKCC1 plays an important role on $[Cl^-]_i$ under conditions where KCC2 is down-regulated (6, 10, 33), we performed additional analyses on mature neurons co-transfected with the mutant transporter KCC2-TE, which has a reduced chloride extrusion capacity ((29) andFig. 9A). Over-expression of KCC2-TE was preferred to the expression of a shRNA against KCC2 because this strategy killed neurons when NKCC1-HA was expressed in concert. Neuronal death was not observed when the shRNA against KCC2 was expressed alone but only when its expression was combined with that of NKCC1-HA (data not shown). This suggests that the recombinant NKCC1-HA transporter is functional in neurons and that the influx of chloride through NKCC1 into neurons in the absence

of chloride ion extrusion capacity is toxic to the neuron. In agreement with previous work (32, 33), this result also means that in mature neurons KCC2 is the major regulator of $[Cl^-]_i$. However, no effect of the endogenous NKCC1 or of the recombinant NKCC1-WT or NKCC1-T203/T207/T212/T217/T230A was observed on the YFP/CFP ratio, nor on bumetanide sensitivity in conditions of low KCC2 activity (Fig. 9D). We concluded that at rest, in conditions of normal or low KCC2 expression/function, endogenous or exogenous NKCC1 transporters are not significantly contributing to $[Cl^-]_i$ in mature neurons.

Discussion

We have studied, in mature hippocampal neurons, the cellular and molecular mechanisms of the regulation of the co-transporter NKCC1, which transports chloride ions inside neurons. We show here that the transporter displays a heterogeneous distribution at the plasma membrane: it is either diffusely distributed and freely mobile in the membrane, it is organized in membrane clusters where it is slowed down and confined, or it is stored in endocytic zones from which it can be released according e.g. to changes in activity. The transporter can alternate between clustered or confined states in endocytic zones by lateral diffusion. This exchange is rapidly tuned by activity changes. In particular, acute $GABA_AR$ activation or inhibition with muscimol or gabazine respectively causes the escape of transporters from membrane clusters and its translocation to endocytic zones where it is confined. $GABA_AR$-mediated regulation of NKCC1 membrane distribution uses chloride as a secondary messenger and the $^{Cl-}$-sensitive WNK/SPAK pathway, which in turn affects the phosphorylation of a series of threonine residues on NKCC1. At rest, these modifications have little effect on $[Cl^-]_i$ but they could participate to the accumulation of Cl^- in neurons in pathological conditions associated with an up-regulation of

NKCC1.

An increase in clustering generally correlates with a slowing down and confinement of the molecule in a sub-cellular compartment e.g. synapses for neurotransmitter receptors. Conversely, a dispersion of molecules from clusters implies a lifting of the diffusion brakes. Usually, the molecule is confined thanks to its binding to scaffolding proteins that anchors it to the cytoskeleton. However, the molecule can escape from this confined region by lateral diffusion. This is the case of glutamate receptors and $GABA_A$Rs (34–36), and of ion transporters such as the chloride co-transporter KCC2 (15, 19). However, NKCC1 has a different diffusion behavior. The transporter was restricted in its movement when its membrane clustering was decreased (gabazine and muscimol conditions) while its diffusion was not significantly changed when its clustering increased (low chloride condition). This could be explained by the fact that a low proportion of NKCC1 transporters is clustered in the membrane while a more significant proportion of them is targeted to endocytic zones where they are confined and stored (in particular upon $GABA_A$R activity changes).

Acute blockade of basal glutamatergic activity by TTX+KYN+MCPG showed that only lateral diffusion of NKCC1 in the axon was rapidly modified by the treatment while the mobility and confinement of the dendritic transporter was not changed. This shows that the regulation of the membrane dynamics of NKCC1 is different in the axonal vs dendritic compartments and may involve separate regulatory mechanisms. Further studies will be needed to identify the axonal regulatory mechanisms of NKCC1 diffusion and the role of an increased confinement of NKCC1 in the axon upon reduced basal glutamatergic activity. This could be important in the regulation of

action potential firing (32).

Then, we showed a regulation of NKCC1 diffusion and clustering by GABAergic inhibition. We observed a similar effect of $GABA_AR$ activation or inhibition on the diffusion and clustering of NKCC1. In both cases, the transporter was sent to endocytic zones and confined there. The fact that there was no change in the global pool (surface + intracellular) of the transporter indicates that it is stored in the endocytic zones without being further internalized and degraded. These endocytic zones have been shown to constitute reserve pools of neurotransmitter receptors, which can, depending on the synaptic demand, be released and reintegrated into the diffusing pool of receptors (37). In the case of NKCC1, this reserve pool would allow a rapid increase in the transporter availability in the plasma membrane, for example in pathological situations in which an up-regulation of NKCC1 has been observed (10, 19).

Muscimol by activating the $GABA_AR$ raises $[Cl^-]_i$ (19). An increase in $[Cl^-]_i$ inhibits the activity of WNK1 and SPAK, OSR1 kinases (38–40), leading to the dephosphorylation of NKCC1 T203/207/212/217/230 (41–43), and reduced transporter activity (44, 45). We have shown that following exposure to muscimol, NKCC1 escaped from membrane clusters and was confined in endocytic zones. Thus, transition of the transporter between membrane clusters and endocytic zones by lateral diffusion would allow modulating rapidly its availability in the membrane and its activity. The effects of muscimol are compatible with NKCC1 T203/207/212/217/230 dephosphorylation. Pharmacological (WNK463 or closantel) or genetic (WNK-KD) blockade of the WNK/SPAK pathway or the expression of NKCC1-TA3 or NKCC1-TA5 mutants that mimic NKCC1 dephosphorylation have the same effects as muscimol: they restrict NKCC1 in their

movement and reduced the membrane clustering of the transporter. The demonstration that the effect of muscimol directly involve dephosphorylation of NKCC1 T203/207/212/217/230 was provided by the fact that the effect of muscimol on NKCC1 clustering can be prevented when the mutant NKCC1-TA5 was exposed to the drug, compared to WT. In contrast, treatment of neurons with gabazine, by blocking the activity of $GABA_A$Rs, decreases $[Cl^-]_i$. In non-neuronal cells, low chloride activates WNK1/SPAK (38, 39) by auto-phosphorylation of S382 from WNK1 which phosphorylates in cascade S373 from SPAK and S325 OSR1 (46), then phosphorylating NKCC1 on T203/207/212/217/230 and increasing its expression and activity (44, 47). We have shown that this signalling cascade is operant in mature hippocampal neurons: gabazine activates the WNK1/SPAK/OSR1 pathway by phosphorylation thus inducing the phosphorylation of KCC2 T906/1007 as well as NKCC1 T203/207/212/217/230 (19). If muscimol decreases NKCC1 clustering and confines it to endocytic zones, gabazine treatment should conversely induce the escape of the transporter from endocytic zones thereby increasing its clustering and function in the membrane. Although we observed that a decrease in $[Cl^-]_i$ by substituting chloride with methane sulfonate decreases the confinement of NKCC1 and increases its membrane stability and clustering, treatment of neurons with gabazine did not reproduce this effect. On the contrary, gabazine confined the transporter and induced the loss of its clustering just as muscimol did. However, we have shown that antagonizing inhibition with gabazine reduces surface expression of KCC2 by increasing lateral diffusion and endocytosis of the transporter (19). This results in reduced intracellular chloride extrusion capacity of the neuron leading to a significant increase in $[Cl^-]_i$ as monitored by SuperClomeleon imaging (19). We therefore hypothesize that the regulation of NKCC1 by gabazine is not due to a decrease in $[Cl^-]_i$ but instead to an increase in $[Cl^-]_i$ following the regulation of KCC2 by the WNK1/SPAK/OSR1

pathway. Thus, changes in the membrane expression of KCC2 (under control of the WNK1/SPAK/OSR1 pathway) would condition that of NKCC1, thus allowing $[Cl^-]_i$ to be maintained at a low level in mature neurons. This would explain why expressing recombinant NKCC1-WT in mature neurons does not significantly increase its expression at the membrane nor does it increase $[Cl^-]_i$ (Fig. 9). This suggests that the level of expression of NKCC1 at the plasma membrane is under the control of KCC2 and its tuning of $[Cl^-]_i$.

To study the direct effect of the WNK1 pathway on NKCC1, we wanted to isolate NKCC1 in mature neurons by removing KCC2 using a shRNA approach. However, neurons died rapidly after co-transfection of KCC2 shRNA and NKCC1 while the isolated expression of these two plasmids had no toxic effect (data not shown). This suggests that in the absence of KCC2 (shRNA condition), NKCC1 expressed at the membrane would induce a significant influx of chloride into the neuron leading to depolarization and thus death of the transfected cells. One function of KCC2 would therefore be to control neuronal survival by maintaining NKCC1 at a low level at the membrane.

Nevertheless, we show that the membrane stability and clustering of NKCC1 can be rapidly regulated by lateral diffusion and that this mechanism is rapidly controlled by GABAergic inhibition and the WN1K/SPAK/OSR1 pathway on the dendrites of mature neurons. Although this pathway has little influence on the amount/function of NKCC1 at the neuronal surface under basal activity conditions, we propose that it may play a role in pathological situations associated with increased expression levels of NKCC1. Interestingly, in the pathology, upregulation of NKCC1 is often accompanied by a down-regulation of KCC2 at the neuronal

surface (4, 18). KCC2 is also regulated by diffusion-capture. We have shown that a short exposure of neurons to the convulsive agent 4AP increases the lateral diffusion of KCC2, which escapes from the clusters, is internalized and degraded (15). Thus, lateral diffusion would be a general mechanism to control the membrane stability of chloride co-transporters. Moreover, the fact that KCC2 is also regulated in mature neurons by the WNK1/SPAK/OSR1 pathway (19) and that this regulation has an inverse effect on membrane stability, clustering and function of KCC2 indicates that this pathway is a target of interest in the pathology. Inhibition of the pathway would prevent the loss of KCC2 and the increase of NKCC1 at the surface of the neuron, thus preventing the abnormal rise of $[Cl^-]_i$ in the pathology and the resulting adverse effects.

Acknowledgments: We thank J. Nabekura for kindly providing the original pEGFP–IRES–KCC2 full-length construct, D. Choquet for the homer1c–GFP construct, and P. Bregestovski for the chloride sensor CFP–YFP construct. We are grateful to the Cell and Tissue Imaging Facility of Institut du Fer a` Moulin (IFM).

Funding: This work was supported by Institut National de la Santé et de la Recherche Médicale, the Fondation Française pour la Recherche sur l'Épilepsie (SL), the Fondation pour la Recherche sur le Cerveau (SL), and ANR WATT (SL). EC is the recipient of a doctoral fellowship from the Sorbonne Université and of a grant from the Fondation pour la Recherche Médicale. STORM/PALM equipment at the IFM was supported by DIM NeRF from Région Ile-de-France and by the FRC/Rotary 'Espoir en tête.' The Lévi lab is affiliated with the Paris School of Neuroscience (ENP) and the Bio-Psy Laboratory of Excellence.

Author contributions: SL conceptualized the project, designed the experiments and supervised the experimental work. MR prepared primary hippocampal neurons. EC, SB, and MM performed immunofluorescence and SPT experiments and analyzed the data. EC performed the super-resolution and chloride imaging experiments, and analyzed the data. SL and EC wrote the manuscript.

Competing interests: The authors declare no competing financial interests.

Materials and Methods

Neuronal culture. All animal procedures were carried out according to the European Community Council directive of 24 november 1986 (86/609/EEC), the guidelines of the French Ministry of Agriculture and the Direction Départementale de la Protection des Populations de Paris (Institut du Fer à Moulin, Animalerie des Rongeurs, license C 72-05-22). All efforts were made to minimize animal suffering and to reduce the number of animals used. Primary cultures of hippocampal neurons were prepared as previously described (15) with some modifications in the protocol. Briefly, hippocampi were dissected from embryonic day 18 or 19 Sprague-Dawley rats of either sex. Tissue was then trypsinized (0.25% v/v), and mechanically dissociated in 1× HBSS (Invitrogen, Cergy Pontoise, France) containing 10mM HEPES (Invitrogen). Neurons were plated at a density of 120 × 103 cells/ml onto 18-mm diameter glass coverslips (Assistent, Winigor, Germany) pre-coated with 50 µg/ml poly-D,Lornithine (Sigma-Aldrich, Lyon, France) in plating medium composed of Minimum Essential Medium (MEM, Sigma) supplemented with horse serum (10% v/v, Invitrogen), L-glutamine (2 mM) and Na+ pyruvate (1 mM) (Invitrogen). After attachment for 3–4 h, cells were incubated in culture medium that consists of Neurobasal

medium supplemented with B27 (1X), L-glutamine (2 mM), and antibiotics (penicillin 200 units/ml, streptomycin, 200 µg/ml) (Invitrogen) for up to 4 weeks at 37 °C in a 5% CO2 humidified incubator. Each week, one fifth of the culture medium volume was renewed.

DNA constructs. The pcDNA3.1 Flag YFP hNKCC1 HA-ECL2 (NT931) was a gift from Biff Forbush (Addgene plasmid # 49063 ; http://n2t.net/addgene:49063 ; RRID:Addgene_49063; (25). From this NKCC1-HA-Flag-mVenus plasmid, the following constructs were raised : NKCC1-HA-Δflag-ΔmVenus by truncation of the tags located on NKCC1 NTD, NKCC1-TA3-Flag-mVenus and NKCC1-TA3-ΔFlag-ΔmVenus with mutation of T203/207/212 to alanines, and NKCC1-TA5-Flag-mVenus and NKCC1-TA5-ΔFlag-ΔmVenus with mutation of T203/207/212/217/230 to alanines. Threonine nucleotide sequence was changed to GCA for alanine substitution. The following constructs were also used: pCAG_ratKCC2-3Flag-ECL2 (15), pCAG_KCC2-3Flag-ECL2 T906/1007E (Heubl et al. 2017), eGFP (Clontech), pCAG_GPHN.FingR-eGFP-CCR5TC (Gross et al. 2013) (gift from Don Arnold, Addgene plasmid # 46296 ; http://n2t.net/addgene:46296 ; RRID:Addgene_46296), homer1c-DsRed (kindly provided by D. Choquet, IIN, Bordeaux, France), WNK1 with “kinase-dead, dominant-negative domain” (WNK1-KD, D368A), “constitutively active” WNK1 (WNK1-CA, S382E) (29) (kindly provided by I. Medina, INMED, Marseille), and SuperClomeleon (31) (kindly provided by G.J. Augustine, NTU, Singapore). All constructs were sequenced by Beckman Coulter Genomics (Hope End, Takeley, U.K).

Transfection and transduction. Neuronal transfections were carried out at DIV 13–14 using Transfectin (BioRad, Hercules, USA), according to the manufacturers’ instructions (DNA:transfectin ratio 1 µg:3 µl), with 1–2 µg of plasmid DNA per 20 mm well. Simple

transfections of NKCC1-HA-Flag-mVenus plasmid concentration : 1 µg. The following ratios of plasmid DNA were used in co-transfection experiments : 1:0.4:0.4 µg for NKCC1 constructs together with GPHN.FingR-eGFP and homer1c-DsRed ; 1:0.2 µg for NKCC1 constructs with eGFP ; 0.7:0.7 µg for NKCC1 constructs with WNK1-KD or WNK1-CA, NKCC1 constructs with SuperClomeleon ; 0.7:0.7 µg KCC2 constructs with SuperClomeleon ; 0.5:0.5:0.5 µg SCLM + KCC2 + NKCC1. Experiments were performed 7–10 days post-transfection. SPT, STORM and chloride imaging experiments were performed with Δflag-ΔmVenus NKCC1 constructs. Standard epifluorescence microscopy with Flag-mVenus NKCC1 constructs.

Peptide treatment and pharmacology. The following peptides and drugs were used: myristoylated dynamin inhibitory peptide (50 µM; Tocris Bioscience), TTX (1 µM; Latoxan, Valence, France), R,S-MCPG (500 µM; Abcam, Cambridge, UK), S-MCPG (250 µM; HelloBio), Kynurenic acid (1 mM; Abcam), gabazine (10 µM; Abcam), muscimol (10 µM; Abcam), WNK463 (10 µM, MedChemTronica), closantel (10 µM; Sigma), bumetanide (5 µM, Abcam). R,S-MCPG and S-MCPG were prepared in equimolar concentrations of NaOH; TTX in 2% citric acid (v/v); closantel in DMSO (Sigma). Equimolar DMSO concentrations were used for control experiments in these conditions. For SPT experiments, neurons were transferred to a recording chamber, pre-incubated in presence of drugs and/or peptide at 31 °C for 10 min in imaging medium (see below for composition) and used within 45 min in presence of the appropriate drug for imaging. For immunofluorescence experiments, drugs were added directly to the culture medium for 30 min in a CO2 incubator set at 37 °C. The imaging medium consisted of phenol red-free minimal essential medium supplemented with glucose (33 mM; Sigma) and HEPES (20 mM), glutamine (2 mM), Na+-pyruvate (1 mM), and B27 (1×) from Invitrogen. The 138mM [Cl^-] extracellular

solution was composed of 2 mM CaCl2, 2 mM KCl, 3 mM $MgCl_2$, 10 mM HEPES, 20 mM glucose, 126 mM NaCl, 15 mM Na_+ methane sulfonate; the 0 mM [Cl^-] extracellular solution was made of 1 mM $CaSO_4$, 2 mM K+ - methane sulfonate, 2 mM $MgSO_4$, 10 mM HEPES, 20 mM glucose, 144 mM Na^+ - methane sulfonate.

Live cell staining for single-particle imaging. Neurons were labelled as described previously. Briefly, cells were incubated for 8 min at 37 °C with primary antibodies against HA (rabbit, 1:250, Cell signalling Technology, cat #C29F4). After washes, cells were incubated for 1 min with F(ab')2-Goat anti-Rabbit IgG (H+L) Secondary Antibody Qdot emitting at 655 nm (1 nM; Invitrogen) in PBS (1 M; Invitrogen) supplemented with 10% Casein (v/v) (Sigma).

Single-particle tracking and analysis. Cells were imaged as previously described using an Olympus IX71 inverted microscope equipped with a 60X objective (NA 1.42; Olympus) and a 120W Mercury lamp (X-Cite 120Q, Lumen Dynamics). Individual images of gephyrin-YFP and homer1c-DsRed, and QD real time recordings (integration time of 30 ms over 1200 consecutive frames) were acquired with an ImagEM EMCCD camera and MetaView software (Meta Imaging 7.7). Cells were imaged within 45 min following appropriate drugs pre-incubation. QD tracking and trajectory reconstruction were performed with homemade software (Matlab; The Mathworks, Natick, MA) as described in refs (15, 48). One to two sub-regions of dendrites were quantified per cell. In cases of QD crossing, the trajectories were discarded from analysis. Trajectories were considered synaptic when overlapping with the synaptic mask of gephyrin-mRFP or homer1c-GFP clusters, or extrasynaptic for spots four pixels (760 nm) away54. The inclusion area was increased relatively to previous studies on KCC2 (15, 19) due to the low

numbers of NKCC1 trajectories recorded with a 380 nm distance. Expanding the radius did actually not change results for perisynaptic NKCC1 lateral diffusion, suggesting its clusters are located further away from synapses than KCC2 ones. Values of the mean square displacement (MSD) plot vs. time were calculated for each trajectory by applying the relation:

$$MSD(n\tau)=\frac{1}{N-n}\sum_{i=1}^{N-n}[(x_{i+n}-x_i)^2+(y_{i+n}-y_i)^2]$$

where τ is the acquisition time, N is the total number of frames, n and i are positive integers with n determining the time increment. Diffusion coefficients (D) were calculated by fitting the first four points without origin of the MSD vs. time curves with the equation: MSD(nτ) = 4Dnτ + σ ; where σ is the spot localization accuracy. Depending on the type of lamp used for imaging, the QD pointing accuracy is ~20–30 nm, a value well below the measured explored areas (at least 1 log difference). The explored area reflects the area in which the moving particle is confined (49). Synaptic dwell time was defined as the duration of detection of QDs at synapses on a recording divided by the number of exits as detailed previously (48). The explored area of each trajectory was defined as the MSD value of the trajectory at two different time intervals of at 0.42 and 0.45 s as explained previously (50). The number of QD vary from one cell to another and from one condition to another in a given experiment.

Chloride imaging. Neurons were imaged at 33 °C in a temperature-controlled open chamber (BadController V; Luigs & Neumann) mounted onto an Olympus IX71 inverted microscope equipped with a 60X objective (1.42 numerical aperture (NA); Olympus). CFP and YFP were detected using Lambda DG-4 monochromator (Sutter Instruments) coupled to the microscope through an optic fiber with appropriate filters (excitation, D436/10X and HQ485/15X; dichroic, 505DCXR; emission, HQ510lp; CFP and YFP filters from Chroma Technology). Images were

acquired with an ImagEM EMCCD camera (Hamamatsu Photonics) and MetaFluor software (Roper Scientific). Mean background fluorescence (measured from a nonfluorescent area) was subtracted and the ratio F480/F440 was determined. Z-stack images (16-bit; 512 × 512) were typically acquired every 30 s for 5 minutes, with an integration time of 30 ms. Regions of interest (ROIs) were selected for measurement if they could only be measured over the whole experiment.

Immunocytochemistry. NKCC1-HA-Flag-mVenus membrane expression and clustering was assessed with staining performed after a short fixation at room temperature (RT) in paraformaldehyde (PFA; 4% w/v; Sigma) and sucrose (20% w/v; Sigma) solution in 1× PBS. The cells were then washed in PBS and incubated for 30 min at RT in goat serum (GS; 3% v/v; Invitrogen) in PBS to block non-specific staining. Neurons were then incubated for 60-180 min at RT with HA antibody (rabbit, 1:250, Cell signalling Technology, cat #C29F4) in PBS–GS blocking solution. After washing, neurons were incubated with Cy™3 AffiniPure Donkey Anti-Rabbit IgG (H+L) (1.9 µg/ml; Jackson ImmunoResearch, cat #111-165-003) for standard epifluorescence assays, or Alexa Fluor® 647 AffiniPure Donkey Anti-Rabbit IgG (H+L) (2 µg/ml, Jackson ImmunoResearch, cat #711-605-152) for super-resolution experiments, in PBS-GS solution. The coverslips were then washed, and mounted on slides. Coverslips were mounted on slides with mowiol 844 (48 mg/ml; Sigma). Sets of neurons compared for quantification were labeled and imaged simultaneously.

Fluorescence image acquisition and analysis. Image acquisition was performed using a ×100 objective (NA 1.40) on a Leica (Nussloch, Germany) DM6000 upright epifluorescence microscope

with a 12-bit cooled CCD camera (Micromax, Roper Scientific) run by MetaMorph software (Roper Scientific, Evry, France). Quantification was performed using MetaMorph software (Roper Scientific). To assess NKCC1-HA clusters, exposure time was fixed at a non-saturating level and kept unchanged between cells and conditions. For the dendritic intensity and clustering analysis, the ROI was precisely traced around focused dendrites, and global ROI pixel intensity was measured. For the clustering images were flatten background filtered (kernel size, 3 × 3 × 2) to enhance cluster outlines, and a user defined intensity threshold was applied to select clusters and avoid their coalescence. Clusters were outlined and the corresponding regions were transferred onto raw images to determine the mean NKCC1-HA cluster number, area and fluorescence intensity. For whole-dendrite intensity measurements to estimate the membrane pool fraction of NKCC1, mean pixel intensity of Venus emission and mean pixel intensity of Cy3-tagged membrane NKCC1 were computed, and then the ratio was calculated before the background flattening. The dendritic surface area of the region of interest was measured to determine the number of clusters per pixel. For each culture, we analyzed ~10 cells per experimental condition.

STORM microscopy. Stochastic Optical Reconstruction Microscopy (STORM) imaging on fixed samples was conducted on an inverted N-STORM Nikon Eclipse Ti microscope with a 100× oil immersion objective (NA 1.49) and an Andor iXon Ultra EMCCD camera (image pixel size, 160 nm), using specific lasers for STORM imaging of Alexa 647 (640 nm). Videos of 30,000 frames were acquired at frame rates of 50 ms. The z position was maintained during acquisition by a Nikon perfect focus system. Single-molecule localization and 2D image reconstruction was conducted as described in Specht et al. (2013) (51) by fitting the PSF of spatially separated

fluorophores to a 2D Gaussian distribution. The position of fluorophore were corrected by the relative movement of the synaptic cluster by calculating the center of mass of the cluster throughout the acquisition using a partial reconstruction of 2000 frames with a sliding window (51). STORM images were rendered by superimposing the coordinates of singlemolecule detections, which were represented with 2D Gaussian curves of unitary intensity. To correct multiple detections coming from the same Alexa 647 molecule (51), we identified detections occurring in the vicinity of space (2σ) and time (15 s) as belonging to the same molecule. The surface of NKCC1 clusters and the densities of NKCC1 molecules per square nanometer were measured in reconstructed 2D images through cluster segmentation based on detection densities. The minimal thresholds to determine clusters were 1% intensity, 0.1 per nm^2 minimum detection density and 10 detections. The resulting binary image was analyzed with the function "regionprops" of Matlab to extract the surface area of each cluster identified by this function. Density was calculated as the total number of detections in the pixels (STORM pixel size = 20 nm) belonging to a given cluster, divided by the area of the cluster.

Statistics. Sampling corresponds to the number of quantum dots for SPT, number of cultures or animals for biochemistry, cells for ICC and chloride imaging. Sample size selection for experiments was based on published experiments, pilot studies, as well as in-house expertise. All results were used for analysis except in few cases. For imaging experiments (chloride and calcium imaging, SPT, immunofluorescence), cells with signs of suffering (apparition of blobs, fragmented neurites) were discarded from the analysis. Data representation was usually done with boxplots or cumulative frequency plots. The statistical test to compare two groups was either Welch t-test when normality assumption was met (Q-Q plots and cumulative frequency

fit), otherwise Mann-Whitney test was performed to assess the presence of a dominance or no between the two distributions. For variables following a log-normal distribution, such as variables obtained from SPT and STORM assays, we applied the log(.) function after division by the control group's median. For super-resolution experiments, as an important variability could be observed between different cells in a same coverslip, a balanced random selection of clusters across neurons, conditions and cultures was performed, then variables from each culture were divided by the median of the control group. Results from different cultures were pooled and log(.) was applied, then the Mann-Whitney U value was computed. The process was repeated 1000 times and the p-value was determined from U distribution using the basic definition of the p-value. For SPT analysis, note that each QD is associated with 3 EA values, thus the sample size is 3 times greater. Statistical analysis were performed with R version 3.6.1 (R Core Team (2019). R: A language and environment for statistical computing. R Foundation for Statistical Computing, Vienna, Austria. Package used : ggplot2, matrixStats). Statistical tests were performed between a condition and its control only using cultures where both conditions were tested. Differences were considered significant for p-values less than 5% (*p ? 0.05; **p < 0.01; ***p < 0.001; NS, not significant).

Figures

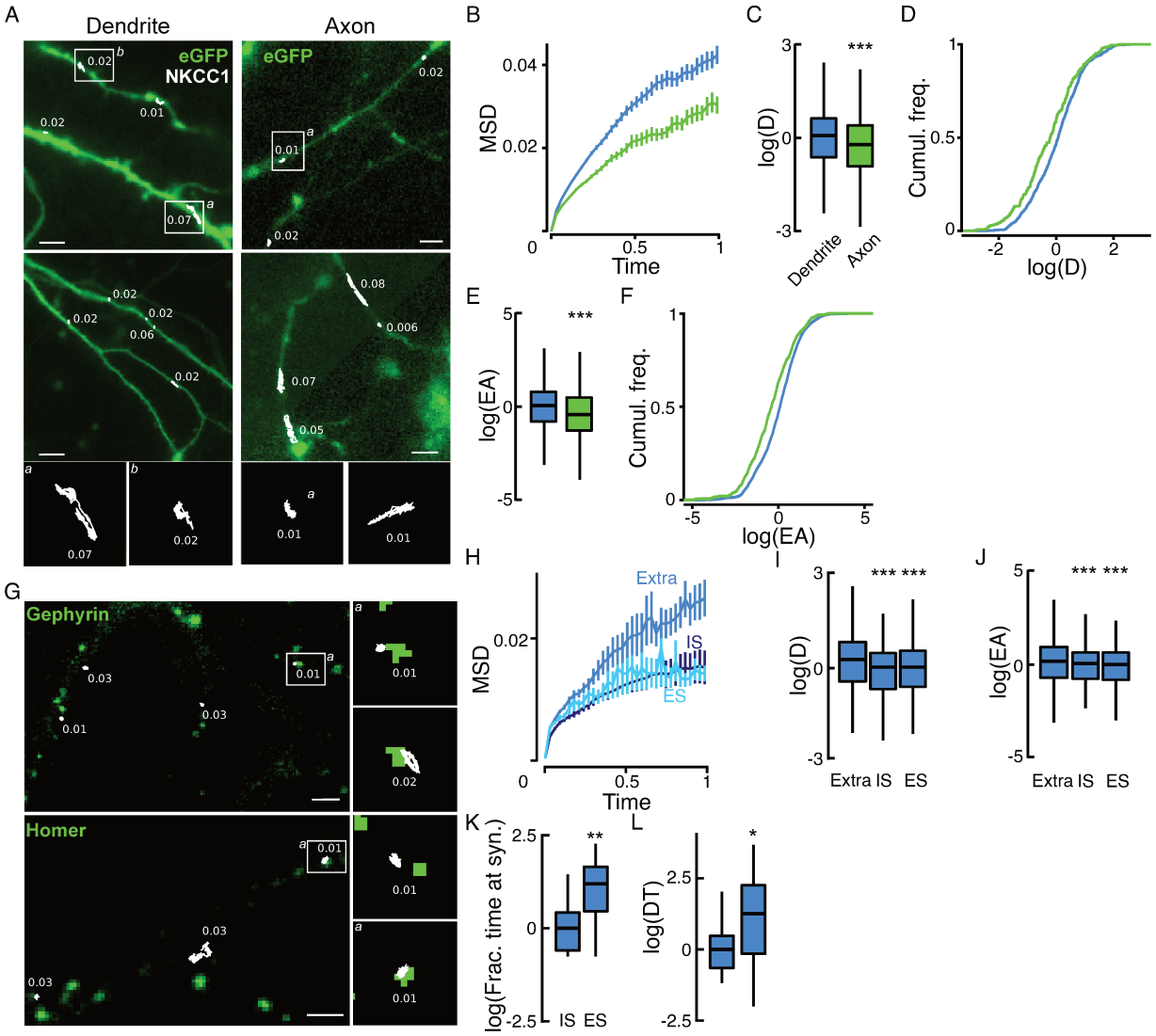

Figure 1. Membrane dynamics of the NKCC1 transporter studied with QD-based SPT in conditions of basal glutamatergic activity blockade. A, Representative trajectories (white) of QD-bound HA-tagged recombinant NKCC1 on dendritic membranes (left), and along the axons (right). QD trajectories (white) were overlaid with fluorescent labeling of cytoplasmic eGFP to label neurites (green). Mean diffusion coefficient values ($\mu m^2.s^{-1}$) are displayed for each trajectory. Scale bars, 4 µm. **B**, Time-averaged MSD functions of dendritic QDs (blue) and axonal

QDs (green). The MSD versus time relationship for dendritic trajectories shows a steeper initial slope, suggesting that trajectories were less confined. $N_{dendrite}$ = 707 QDs, N_{axon} = 305 QDs, 37 cells from 4 cultures. **C-D**, Box plots (C) and cumulative probabilities (D) of QD diffusion coefficients D in dendritic (blue) or axonal (green) compartments. Note the reduced diffusion in the axon. Welch t-test, p = 6.3 10^{-4}. **E-F**, Box plots (E) and cumulative probabilities (F) of explored area EA in dendritic (blue) or axonal (green) compartments. Note the reduced exploration in the axon. Welch t-test test p = 2.3 10^{-8}. **G**, Representative trajectories (white) of QD-bound HA-tagged recombinant NKCC1 at inhibitory synapses (left), at the surface of gephyrin-Finger-YFP (up) or homer1c-DsRed (bottom) transfected neurons. QD trajectories (white) were overlaid with fluorescent clusters of Gephyrin-Finger-YFP (green), or Homer1c-DsRed (green) to identify inhibitory (IS) and excitatory (ES) synapses, respectively. Scale bars, 4 µm. **H**, Time-averaged MSD functions of extrasynaptic QDs (blue), QDs at excitatory synapses (light blue), and QDs at inhibitory synapses (deep blue). The MSD versus time relationship for extrasynaptic trajectories shows a steeper initial slope, suggesting that trajectories were less confined. Extra, n = 747 QDs, IS, n = 209 QDs, ES, n = 369 QDs, 27 cells from 5 cultures. **I-J**, Boxplots of log(D) (I) and log(EA) (J) showing a reduced mobility and an increased confinement of NKCC1 at IS and ES compared to extrasynaptic QDs. Diffusion coefficient (D): IS, Welch t-test, p = 1.58 10^{-14}; ES, Welch t-test, p = 8.4 10^{-13}. Explored area (EA): IS, Welch t-test, p = 5.6 10^{-11}; ES, Welch t-test, p = 7.2 10^{-10}. **K**, Boxplots of log(Time) spent by NKCC1 at inhibitory (IS) and excitatory (ES) synapses showing increased time at ES as compared with IS. Mann Whitney test, p = 0.0012, 18 cells from 5 cultures. **L**, Boxplots of log(dwell time, DT) of NKCC1 at inhibitory (IS) and excitatory (ES) synapses showing increased DT at ES as compared with IS. Mann Whitney test, p = 0.029. C, E, I: D in $\mu m^2.s^{-1}$; E, J: EA in μm^2; D, H: MSD in μm^2 vs time (s); K: Frac. Time in s; L : DT in s.

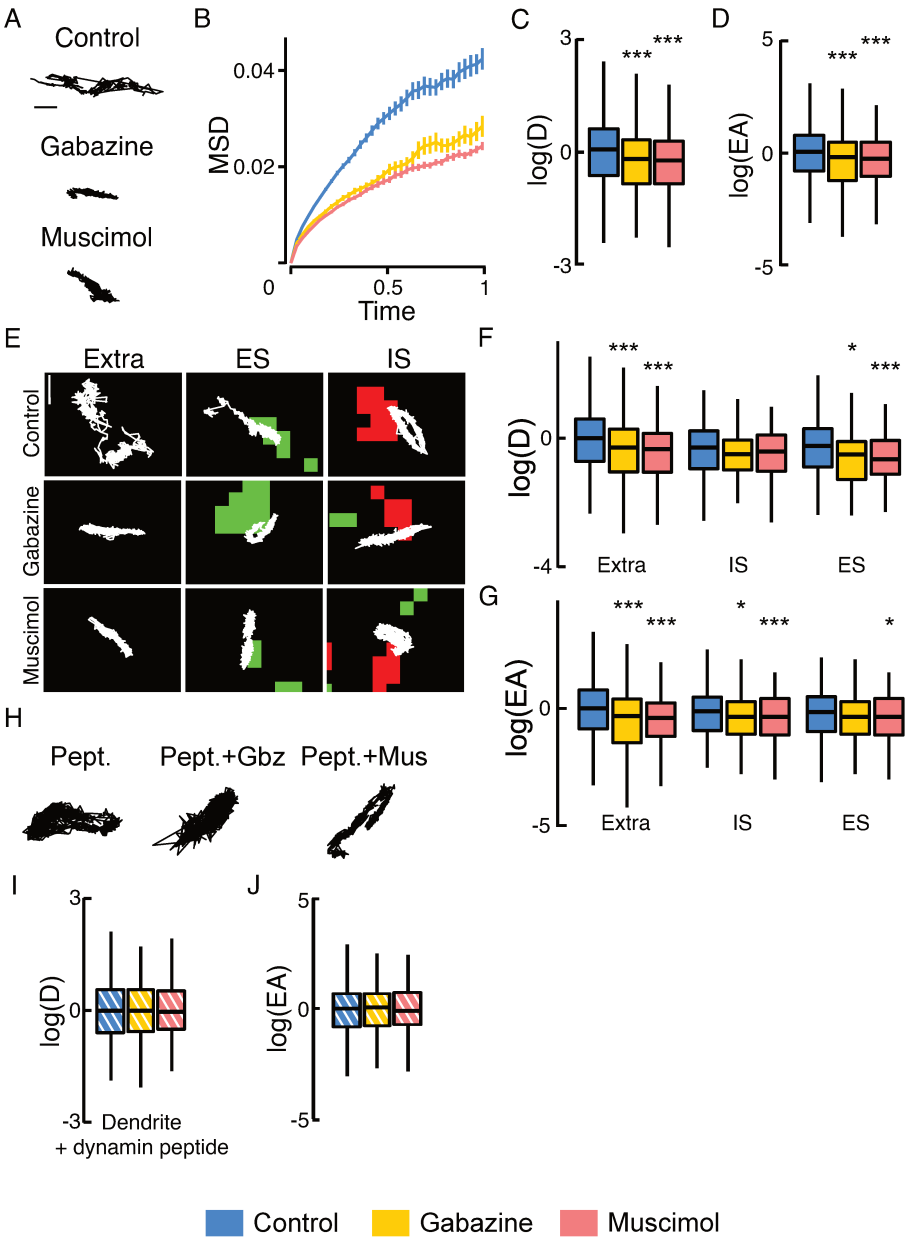

Figure 2. GABA$_A$R activity regulates NKCC1 membrane dynamics. A, Examples of NKCC1 trajectories showing reduced surface exploration in the presence of gabazine or muscimol. Scale bar, 0.5 µm. **B**, Time averaged MSD functions in control (blue) vs. gabazine (yellow) or muscimol (orange) conditions show increased confinement upon gabazine or muscimol application. **C-D**,

Boxplots of log(D) of NKCC1 in control condition (blue) or upon application of gabazine (yellow) or muscimol (orange) showing reduced diffusion upon gabazine or muscimol application. N n = 1558 QDs (control, 41 cells), n = 387 QDs (gabazine, 18 cells), Welch t-test, p = 1.3 10^{-6}, n = 545 QDs (muscimol, 27 cells), Welch t-test, p = 2.1 10^{-12}, 5 cultures. **D**, Median explored area EA in control vs. gabazine or muscimol conditions show increased confinement upon gabazine (Welch t-test, p = 2 10^{-8}) or muscimol (Welch t-test, p = 4.2 10^{-11}) application. **E**, Trajectories (white) overlaid with fluorescent clusters of recombinant homer1c-DsRed (green) or gephyrin-Finger-YFP (red) to identify extrasynaptic trajectories (extra), trajectories at excitatory (ES) and inhibitory synapses (IS). Scale bar, 0.4 µm. **F-G**, Log(D) (**F**) and EA (**G**) of NKCC1 are decreased upon gabazine or muscimol application as compared with control condition. Note that the effect is more pronounced for extrasynaptic trajectories than for ES or IS trajectories. Diffusion coefficient (test : Welch t-test) (D): Extra, n = 899 QD (control), 227 QD (gabazine), p = 2.9 10^{-5}, n = 268 Qds (muscimol) p = 2.2 10^{-9}; IS, n = 244 QD (control), 79 Qds (gabazine) p = 0.16; n = 142 (muscimol) p = 0.19; ES, n = 415 Qds (control), n = 81 QD (gabazine) p = 0.021, n = 135 QD (muscimol) p = 0.00046 . Explored area (EA): Extra, gabazine p = 2.9 10^{-5}, muscimol p = 2.2 10^{-9}; IS, gabazine p = 0.16, muscimol p = 0.19; ES, n = 415 QD (control), n = 81 QD (gabazine) p = 0.021, n = 135 QD (muscimol) p = 0.00046 . **H**, NKCC1 trajectories in control vs. Gbz or Musc conditions in the presence of an endocytosis blocking peptide. Scale bar, 0.5 µm. **I-J**, No effect of Gbz or Musc on log(D) (**I**) and EA (**J**) of NKCC1 in conditions of blockade of endocytosis. Diffusion coefficient (D): Bulk Ctrl n = 491 QD (31 cells), Gbz n = 238 QD (10 cells), p = 0.6 and Musc n = 243 QD (26 cells), p = 0.61, 5 cultures. Explored area (EA): Gbz QD, p = 0.84 and Musc, p = 0.81, 5 cultures. B, F, I: D in $\mu m^2.s^{-1}$; C: MSD in μm^2 vs time (s); D, G, J: EA in μm^2.

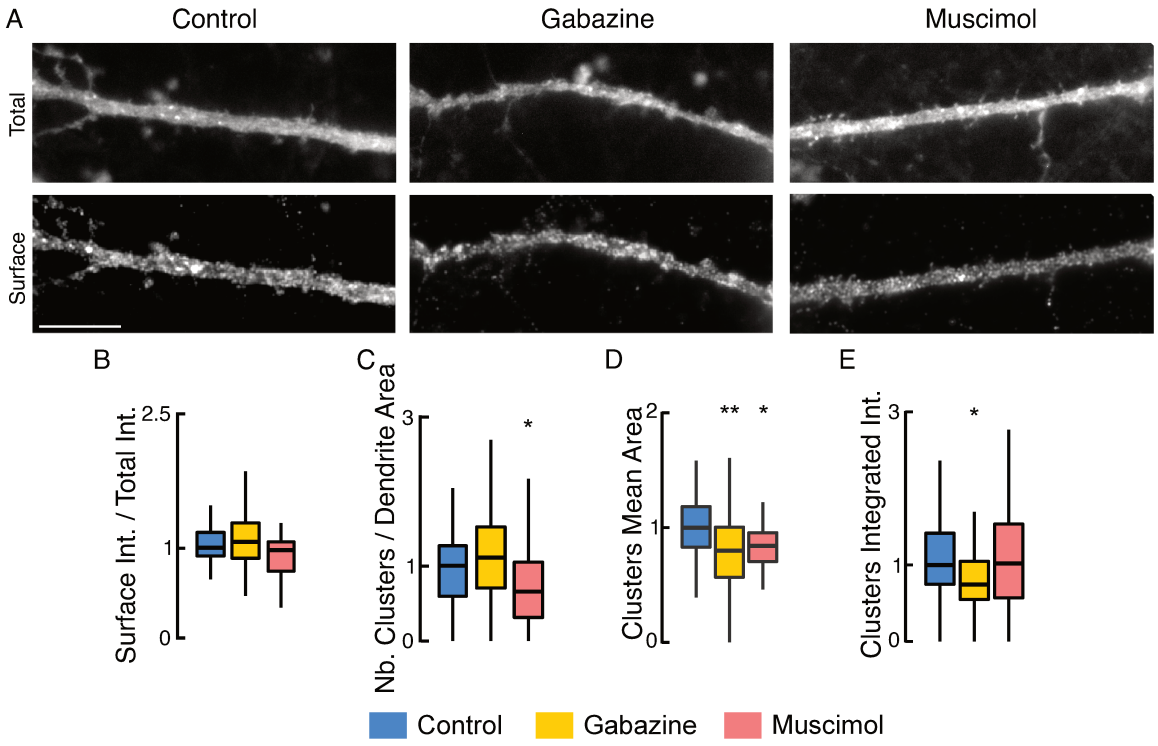

Figure 3. Regulation of NKCC1 membrane clustering by $GABA_AR$-mediated inhibition. A, HA surface staining in hippocampal neurons (DIV 21) expressing recombinant NKCC1-HA in absence (Ctrl) or presence of gabazine (Gbz), or muscimol (Musc) for 30 min. Scale bar, 10 µm. **B**, Quantification of the ratio of the surface pool of NKCC1 over the total pool of NKCC1 in control (blue), gabazine (yellow), and muscimol (orange) conditions showing no significant changes of surface NKCC1 after gabazine or muscimol treatment. Ctrl n = 30 cells, Gbz, n = 41 cells, MW test p = 0.87, Musc n = 38 cells, p = 0.17, 8 cultures. **C-E**, Quantification of NKCC1-HA cluster number (**C**), area (**D**), and intensity (**E**) shows reduced density and size of NKCC1 clusters upon muscimol treatment while gabazine treatment reduced the size and intensity of NKCC1 clusters.. Values were normalized to the corresponding control values. The MW test was used for data

comparison. Gabazine : cluster number (nb) p = 0.49, area p = 0.003, intensity p = 0.017. Muscimol : cluster nb p = 0.027 , area p = 0.029, intensity p = 0.92. C : μm^{-1}, D : μm^2.

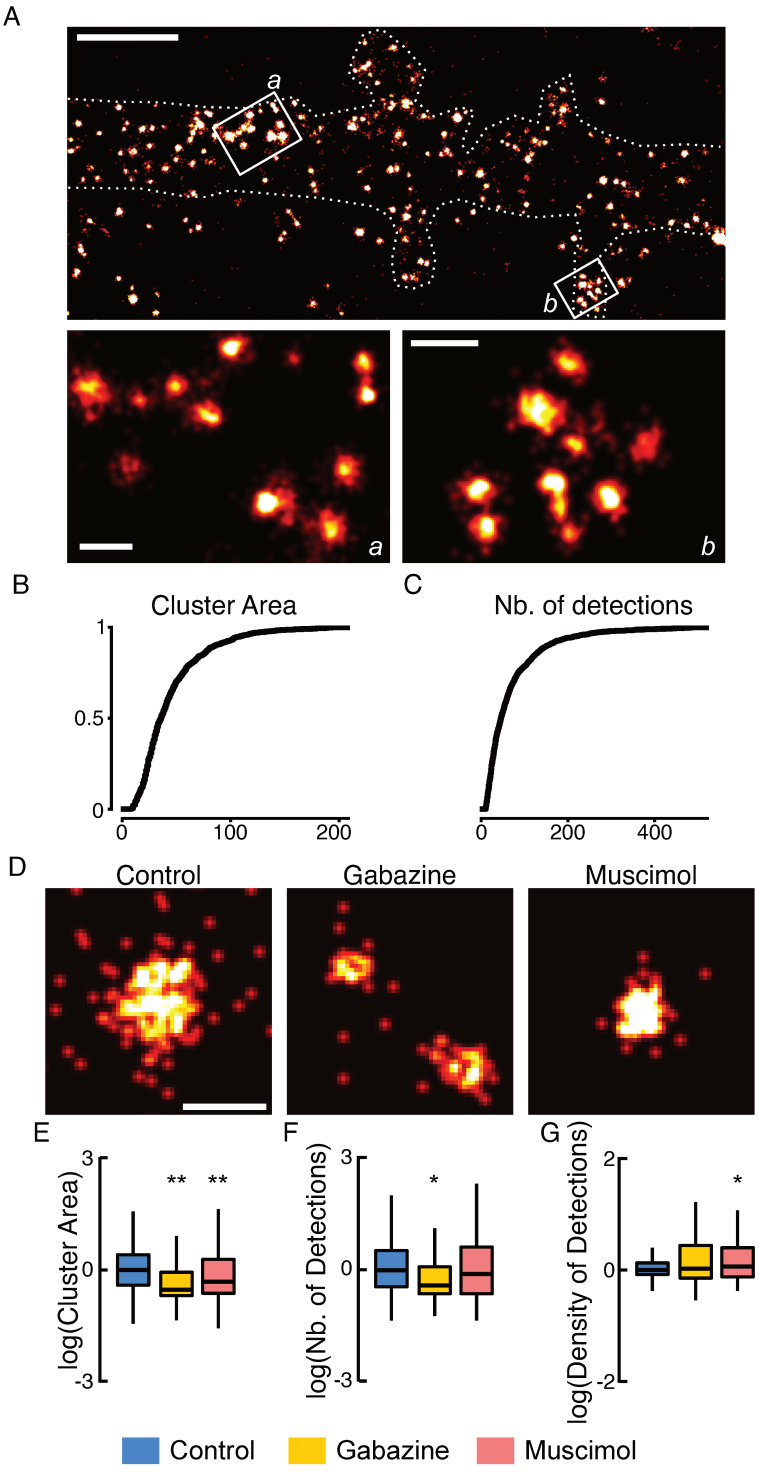

Figure 4. STORM imaging showing that gabazine and muscimol treatments alter NKCC1

clustering at the surface of hippocampal neurons. A, Super-resolution image reconstruction of membrane-associated NKCC1-HA in neurons maintained in control condition. Up, NKCC1 shows a punctate distribution on dendritic shaft and spines. Scale bar, 2 µm. Bottom, magnification of the inserts delineated on the dendrite shown above. Scale bar, 0.2 µm. **B**, Cumulative distribution of the size of NKCC1 clusters showing that clusters typically have a size between 10 and 100 nm^2. The mean size of NKCC1 cluster is 51.1 ± 57.3 nm^2. **C**, Cumulative distribution of the number of single particles detected per cluster. The mean number of detections is 60.8 ± 49.4. **D**, Representative images of NKCC1 at the surface of neurons exposed 30 min to gabazine or muscimol. Scale bar, 0.1 µm. **E**, Quantification of NKCC1 cluster area using STORM shows reduction in cluster size upon gabazine and muscimol treatment. Ctrl n = 550 clusters, Gbz n = 192 clusters, Monte-Carlo simulations of the MW test p = 0.002 , Musc n = 410 clusters, p = 0.004, 4 cultures. **F**, Quantification of the number of particles detected per cluster showing reduced number of detection upon gabazine (Monte-Carlo simulations of MW test, p = 0.012) but not muscimol (p = 0.3) exposure. **G**, Quantification of density of NKCC1 molecules per square micrometer highlighting denser NKCC1 packing upon neuronal exposure to muscimol (Monte-Carlo simulations of MW test, p = 0.016) but not gabazine (p = 0.97). E : nm^2, G : μm^{-1}.

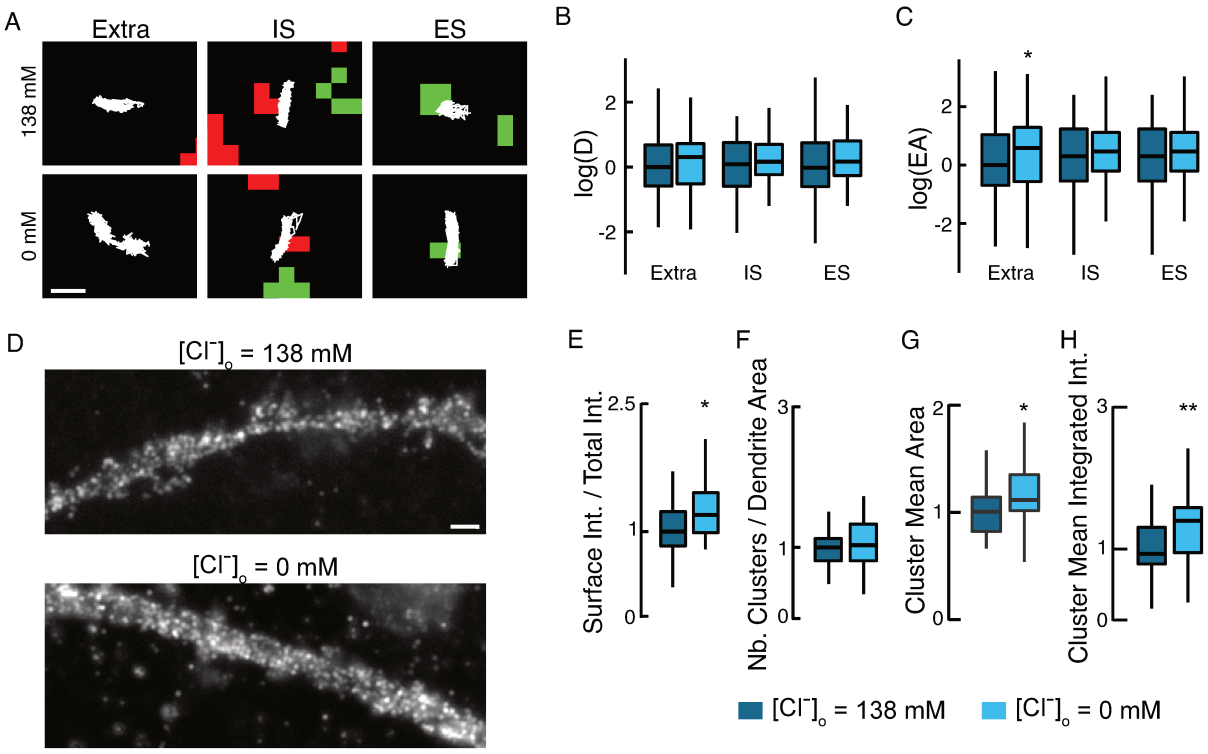

Figure 5. Lowering intracellular chloride concentration increases the membrane stability and clustering of NKCC1. A, NKCC1 trajectories in high vs. low extracellular Cl^- concentration in the extrasynaptic area (extra), and at inhibitory (IS) or at excitatory (ES) synapses. Scale bar, 0.4 µm. **B-C**, No major effect of a reduction of Cl^- concentration on log(D) (**B**) and log(EA) (**C**) of NKCC1. Diffusion coefficient (D): extra, low Cl^- n = 128 QDs, high Cl^- n = 93 QDs, Welch t-test p = 0.89; IS, low Cl^- n = 64 QDs, high Cl^- n = 56 QDs, Welch t-test p = 0.74; ES, low Cl^- n = 62 QDs, high Cl^- n = 68 QDs, Welch t-test p = 0.36, 2 cultures. Explored area (EA): extra, low Cl^- Welch t-test p = 0.01; IS, Welch t-test p = 0.6; ES, Welch t-test p = 0.6. **D-H**, Lowering intracellular chloride increases surface detection and clustering of NKCC1. **D**, HA surface staining in neurons expressing recombinant NKCC1-HA in in high vs. low extracellular Cl^- concentration for 30 min. Scale bar, 1

µm. **E**, Quantification of the ratio of the surface pool of NKCC1 over the total pool of NKCC1 in high (dark blue), and low (light blue) Cl^- concentration showing increase of NKCC1 surface staining upon reduction of Cl^- concentration. Low Cl^- n = 35 cells, high Cl^- n = 40 cells, Welch t-test p = 0.01, 3 cultures. **F-H**, Quantification of NKCC1-HA cluster number (**F**), area (**G**), and intensity (**H**) shows increased size and intensity of NKCC1 clusters upon reduction of Cl^- concentration. Values were normalized to the corresponding control values. Cluster Number (Nb) MW test p = 0.2, area MW test p = 0.018, intensity MW test p = 0.0056. B: D in $\mu m^2.s^{-1}$; C: EA in μm^2 ; F : μm^{-1}; G : μm^2.

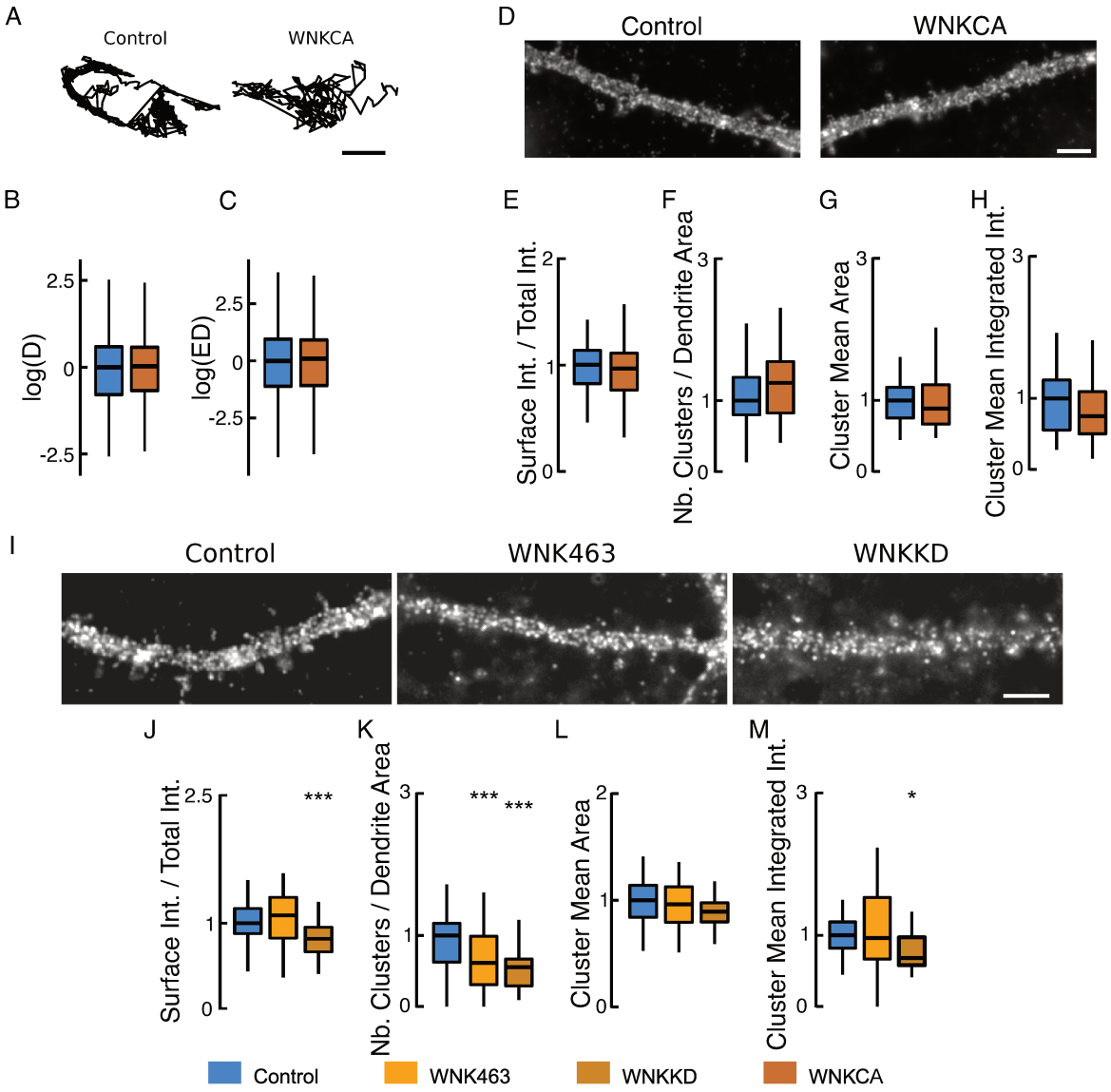

Figure 6. Inhibiting WNK1 reduces the clustering of NKCC1 at the neuronal surface. A, Representative trajectories of NKCC1 in neurons expressing constitutively-active WNK1 (WNK-CA, blue) vs. control (gray). Bar : 0.4 µm. **B-C**, WNK-CA over-expression does not change NKCC1 diffusion at the plasma membrane, with no effect on D (**B**) and EA (**C**). Diffusion coefficient (D): Bulk, Ctrl n = 305 QD, WNK-CA n = 358 QD, Welch t-test P = 0.81, 3 cultures; Explored area (EA):

Welch t-test P = 0.49. **D**, HA surface staining in hippocampal neurons expressing recombinant NKCC1-HA together with WNK1-CA or a control plasmid. Scale bar, 4 µm. **E**, Overexpressing WNK-CA does not modify the level of NKCC1 expressed at the cell surface. Ctrl n = 45 cells, WNK-CA : n = 43 cells, Welch t-test P = 0.26, 3 cultures. **F-H**, No effect of WNK-CA expression on NKCC1 cluster number (**F**), area (**G**), and intensity (**H**). Values were normalized to the corresponding control values. Cluster Number (Nb) MW test p = 0.14, area MW test p = 0.32, intensity MW test p = 0.25. **I**, Impact of an inhibition of WNK1 on HA surface staining of neurons transfected with NKCC1-HA. WNK1 was inhibited either by incubating the neurons for 30 min with a specific inhibitor WNK-463 or by co-expressing kinase-dead WNK1 (WNK1-KD). Scale bar, 4 µm. **J**, Incubating the neurons with WNK-463 (orange) does not modify the surface level of NKCC1 compared to controls (blue), however over-expression of WNK-KD (brown) sharply reduced NKCC1 surface levels. WNK-463 experiment: Ctrl n = 24 cells, WNK-463 n = 25 cells, Welch t-test P = 0.58. WNK-KD experiment: Ctrl n = 34 cells, WNK-KD n = 24 cells, Welch t-test P = 0.0096, 4 cultures. **K-M**, Loss of NKCC1 clusters (**K**) and reduced cluster size (**L**) but not cluster intensity (**M**) upon WNK1 activity suppression with either WNK-KD or WNK-463, as compared to control conditions. Values were normalized to the corresponding control values. The MW test was used for data comparison. WNK-KD experiment: Cluster Number (Nb) p = 0.45 10^{-6}, area p = 0.012, intensity p = 0.0031. WNK-463 experiment: Cluster Number (Nb) p = 0.0008, area p = 0.86, intensity p = 0.83. F, K : μm^{-1}, G, L : μm^2.

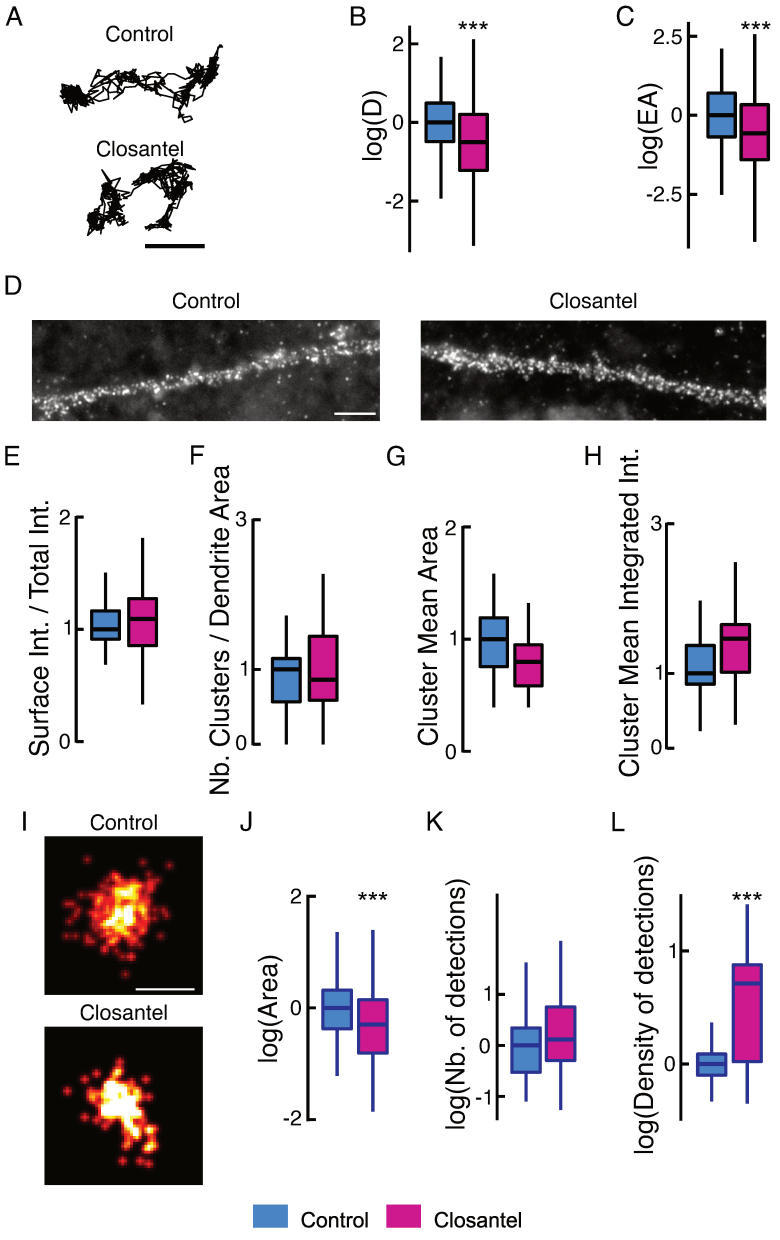

Figure 7. Inhibiting SPAK-OSR1 activity tunes NKCC1 membrane diffusion and clustering. **A**, NKCC1 trajectories showing reduced surface exploration in the presence of closantel. Scale bar, 0.5 µm. **B-C**, Log (D) (**B**) and EA (**C**) of NKCC1 are decreased upon closantel application (pink) as compared with control condition (blue), indicating reduced mobility and increased confinement.

Diffusion coefficient (D): Bulk, Ctrl n = 433 QD (25 cells), closantel n = 371 QD (31 cells), Welch t-test p = 5.5 10^{-5}, 2 cultures. Explored area (EA): Welch t-test p = 4.8 10^{-11}. **D-H**, Standard epifluorescence microscopy showing no significant effect of closantel on NKCC1 membrane immunoreactivity. **D**, HA surface staining in hippocampal neurons expressing recombinant NKCC1-HA treated or not with closantel. Scale bar, 4 µm. **E**, Closantel treatment does not alter the surface expression level of NKCC1. Ctrl n = 51 cells, closantel n = 61 cells, Welch t-test p = 0.49, 7 cultures. **F-H**, Closantel has no impact on NKCC1 cluster number (**F**), area (**G**), and intensity (**H**). Cluster Number (Nb) MW test p = 0.6, area MW test p = 0.09, intensity MW test p = 0.81. **I-L**, STORM imaging showing that closantel affects NKCC1 organization at the nanoscale. **I**, Representative images of NKCC1 at the surface of neurons exposed 30 min to closantel vs control condition. Scale bar, 0.1 µm. Quantification of NKCC1 cluster area (**J**), number of particles per cluster (**K**) and density of detections in the clusters (**L**) reveal reduction in cluster size upon closantel treatment. Ctrl n = 218 clusters, closantel n = 147 clusters, 2 cultures. Cluster area: Monte-Carlo simulations of the MW test p < 0.001 ; Nb detection: MW test p = 0.058, density : MW test p < 0.001. F : μm^{-1}, G : μm^2.

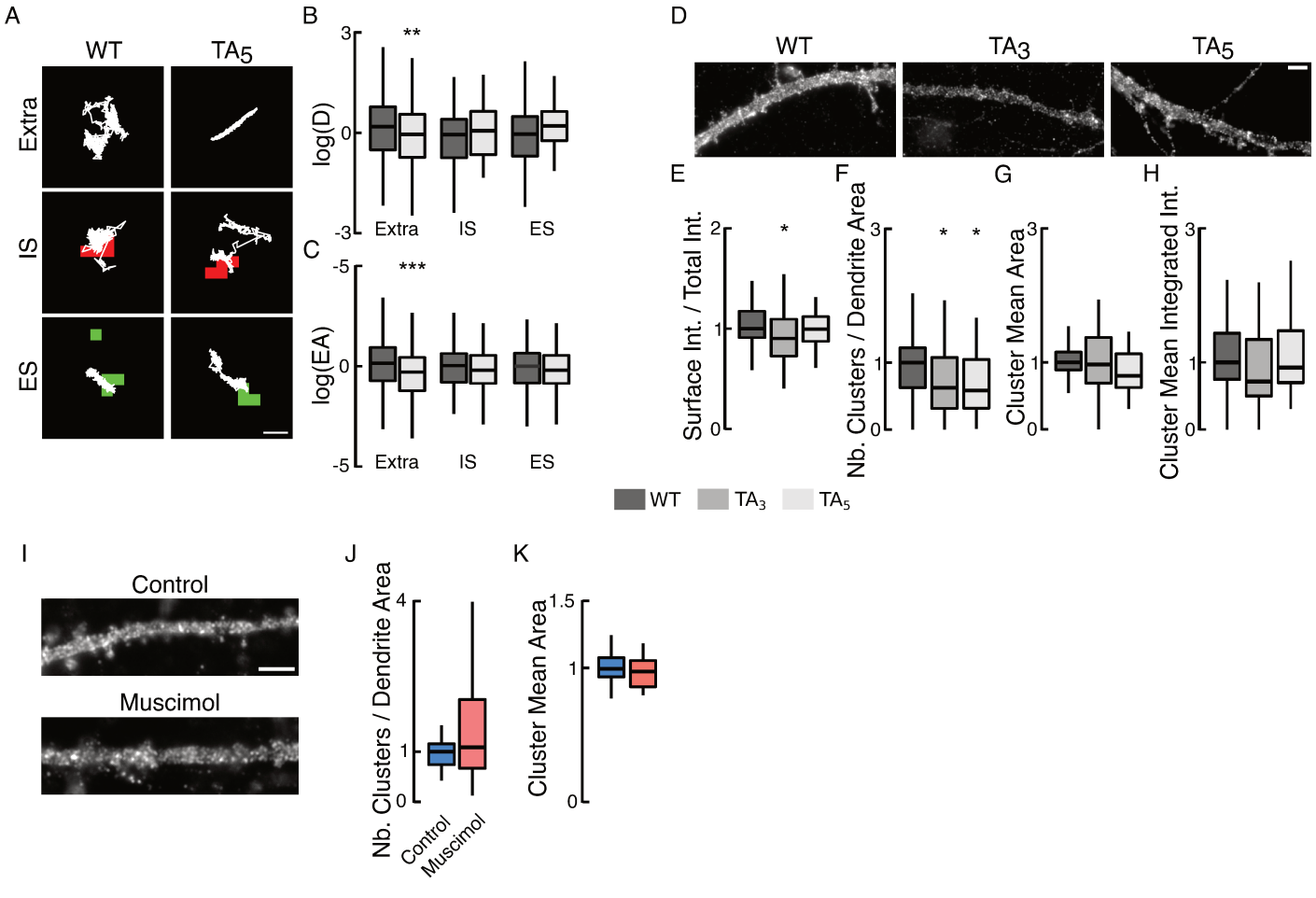

Figure 8. NKCC1 membrane dynamics, stability and clustering is dependent on NKCC1 phosphorylation of T203/207/212/217/230. A, Examples of NKCC1-T203/207/212/217/230 (WT) and NKCC1-T203/207/212/217/230A (TA_5) trajectories in resting condition at extrasynaptic site (extra), at inhibitory (IS) and excitatory glutamatergic (ES) synapses. Scale bar, 0.5 µm. **B-C**, Log(D) (**B**) and EA (**C**) show that the dephospho-mimetic NKCC1-TA_5 (light gray) was slower and more confined than NKCC1-WT (gray) at extrasynaptic sites but not near synapses. Diffusion coefficient (D) : WT : extra, n = 189 QDs, IS, n = 42 QDS, ES n = 30 QDs; TA_5 : extra, n = 166 QDs, IS, n = 33 QDS, ES n = 34 QDs; from 67 cells and 2 cultures. Welch t-test : extra p = 0.0088, IS p =

0.28, ES p = 0.73. Explored area (EA): extra p = 4.5 10^{-4}, IS p = 0.71, ES p = 0.45. **D**, HA surface staining in hippocampal neurons expressing recombinant NKCC1-WT vs NKCC1-TA_3 or NKCC1-TA_5 in resting conditions. Scale bar, 4 µm. **E**, Expression of NKCC1-TA3 is slightly reduced at the plasma membrane as compared to NKCC1-WT. WT (dark gray) n = 68 cells, TA_3 (gray) n = 43 cells, TA_5 (light gray) n = 36 cells (9 cultures) ; WT vs TA_3 Welch t-test p = 0.041, WT vs TA_5 p = 0.87, 9 cultures. **F-H**, Quantification of cluster number (**F**), area (**G**) and intensity (**H**) for NKCC1-TA_3, NKCC1-TA_5 vs NKCC1-WT. Note the reduced density of cluster (**F**) for NKCC1-TA_3 and NKCC1-TA_5 as compared to NKCC1-WT. Cluster Number (Nb) WT vs TA3 MW test p = 0.042, WT vs TA_5 MW test p = 0.014; area: WT vs TA_3 MW test p = 0.46, WT vs TA_5 MW test p = 0.22; intensity WT vs TA_3 MW test p = 0.3, WT vs TA_5 MW test p = 0.86. **I**, HA surface staining in hippocampal neurons expressing recombinant NKCC1-TA_5 exposed or not to muscimol. Scale bar, 4 µm. **J-K**, Muscimol application has no effect on NKCC1-TA_5 cluster number : MW test, P = 0.45 (**J**) and area : MW test, P = 0.38 (**K**). Control : 26 cells, muscimol : 22 cells, 3 cultures. F, J : μm^{-1}, G, K : μm^2.

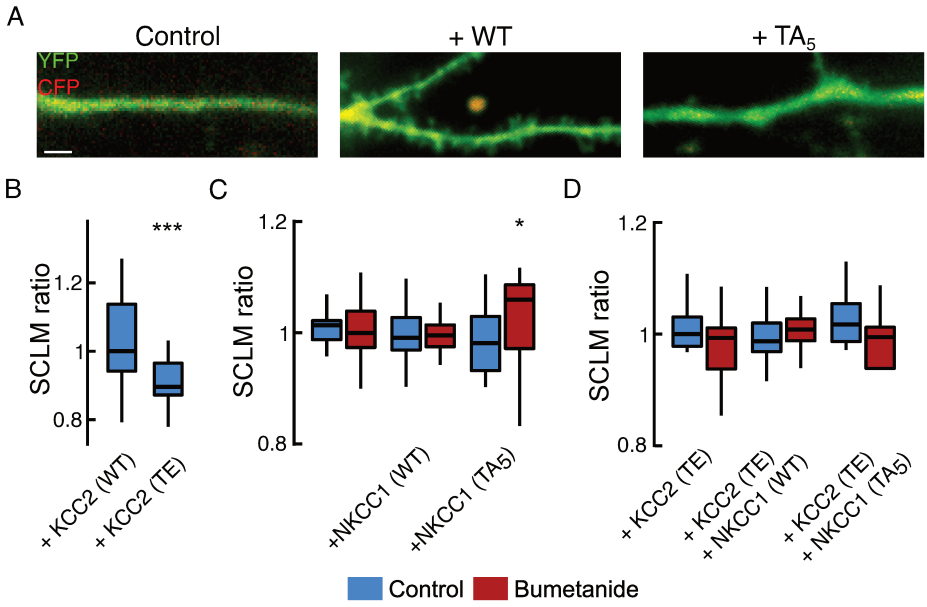

Figure 9. Expression of recombinant WT or dephospho-mimetic NKCC1 have no major impact on $[Cl^-]_i$ in mature hippocampal neurons. A, composite images of CFP (red) and YFP (green). in neurons expressing SuperClomeleon (SCLM) alone (Control) or in combination with NKCC1-T203/207/212/217/230 (WT) or NKCC1-T203/207/212/217/230A (TA_5) in resting conditions. Scale bar, 2 µm. **B**, CFP/YFP fluorescence ratio in hippocampal neurons expressing SCLM together with KCC2-T906/T1007 (WT) or phospho-mimetic KCC2-T906/T1007E (TE). KCC2-WT n = 36 cells, KCC2-TE n = 39 cells, MW test p = 7.1 10^{-6}, 3 cultures. **C**, CFP/YFP fluorescence ratio in neurons expressing SCLM alone or in combination with NKCC1-WT or NKCC1-TA_5 before (blue) and after (red) 10-30 min application of bumetanide. SCLM Ctrl n = 20 cells, Bumet n = 17 cells; SCLM + NKCC1-WT Ctrl n = 18 cells, Bumet n = 20 cells; SCLM + NKCC1-TA_5 Ctrl n = 21 cells, Bumet n = 16 cells; 3 cultures. Ctrl vs Bumet: SCLM MW test p = 0.96, SCLM + NKCC1-WT MW test p = 0.53, SCLM + NKCC1-TA_5 MW test p = 0.029. SCLM vs SCLM + NKCC1-WT, MW test p = 0.71, SCLM vs SCLM + NKCC1-TA_5, MW test p = 0.69; SCLM + NKCC1-WT vs SCLM + NKCC1-TA5,

MW test p = 0.89. **D**, CFP/YFP fluorescence ratio in neurons expressing the same recombinant proteins than in B but in the presence of KCC2-TE before (blue) and after (red) bumetanide treatment. SCLM + KCC2-TE Ctrl n = 15 cells, Bumet n = 15 cells, MW test p = 0.15; SCLM + KCC2-TE + NKCC1-WT Ctrl n = 13 cells, Bumet n = 16 cells, MW test p = 0.56 ; SCLM + KCC2-TE + NKCC1-TA_5 Ctrl n = 21 cells, Bumet n = 8 cells, MW test p = 0.092; SCLM + KCC2-TE vs SCLM + KCC2-TE + NKCC1-WT, MW test p = 0.65, SCLM vs SCLM + KCC2-TE + NKCC1-TA_5, MW test p = 0.2, SCLM + KCC2-TE + NKCC1-WT vs SuperClomeleon + KCC2-TE + NKCC1-TA_5, MW test p = 0.12. 2 cultures.

Tables

Experimental conditions	Fig. Nb.	25% , 50% , 75% quantiles, D (10^{-2} $\mu m^2 s^{-1}$)	Fig. Nb.	25% , 50% , 75% quantiles, EA (10^{-2} μm^2)	Fig. Nb.	25% , 50% , 75% quantiles, DT (s)
Bulk Dendrite	1 C, D	[0.9 ; 1.8 ; 3.3]	1 E, F	[0.5 ; 1.1 ; 2.2]	NA	NA
Axon	1 C, D	[0.7 ; 1.4 ; 2.6]	1 E, F	[0.3 ; 0.7 ; 1.7]	NA	NA
Extra Dendrite	1, I	[1 ; 2 ; 3.7]	1, J	[0.5 ; 1.1 ; 2.5]	NA	NA
IS Dendrite	1, I	[0.8 ; 1.6 ; 2.6]	1, J	[0.5 ; 1.1 ; 2]	1, L	[0.5 ; 0.9 ; 3.2]
ES Dendrite	1, I	[0.9 ; 1.7 ; 2.8]	1, J	[0.5 ; 1 ; 2]	1, L	[1.7 ; 3.8 ; 15.7]

Table 1 : compartment-specific NKCC1 lateral diffusion.

Experimental conditions	Fig. Nb.	25% , 50% , 75% quantiles, D (10^{-2} $\mu m^2 s^{-1}$)	Fig. Nb.	25% , 50% , 75% quantiles, EA (10^{-2} μm^2)
Bulk Control	2 C	[0.9 ; 1.9 ; 3.6]	2, D	[0.5 ; 1.2 ; 2.3]
Bulk Gabazine	2 C	[0.7 ; 1.4 ; 2.4]	2, D	[0.3 ; 0.9 ; 1.8]
Bulk Muscimol	2, C	[0.7 ; 1.3 ; 2.3]	2, D	[0.4 ; 0.8 ; 1.7]
Bulk $[Cl^-]$ = 138 mM	1 B	[0.6 ; 1.1 ; 2.1]	1 C	[0.3 ; 0.6 ; 1.5]
Bulk $[Cl^-]$ = 0 mM	1, B	[0.7 ; 1.2 ; 2.1]	1, C	[0.3 ; 0.8 ; 1.7]

Table 2 : regulation of NKCC1 diffusion-capture by $GABA_AR$ activity through changes in $[Cl^-]_i$

Experimental conditions	Fig. Nb.	25% , 50% , 75% quantiles, D (10^{-2} $\mu m^2 s^{-1}$)	Fig. Nb.	25% , 50% , 75% quantiles, EA (10^{-2} μm^2)
Bulk Control	1 C, D	[0.7 ; 1.4 ; 2.5]	1 E, F	[0.4 ; 1 ; 2.1]
Bulk WNK-CA	1 C, D	[0.6 ; 1.1 ; 2.1]	1 E, F	[0.4 ; 0.9 ; 2]
Bulk Closantel	1, I	[0.6 ; 1.1 ; 2.2]	1, J	[0.3 ; 0.7 ; 1.8]
Bulk TA_5	1 C, D	[0.8 ; 1.6 ; 3]	1 E, F	[0.4 ; 0.9 ; 1.8]

Table 3 : regulation of NKCC1 diffusion-capture by WNK-SPAK-OSR1 phosphorylation

References

1. P. Kwan, M. J. Brodie, Definition of refractory epilepsy: defining the indefinable? The Lancet Neurology. 9, 27–29 (2010).

2. G. L. Krauss, M. R. Sperling, Treating patients with medically resistant epilepsy. Neurology: Clinical Practice. 1, 14–23 (2011).

3. K. Kaila, T. J. Price, J. A. Payne, M. Puskarjov, J. Voipio, Cation-chloride cotransporters in neuronal development, plasticity and disease. Nat Rev Neurosci. 15, 637–654 (2014).

4. R. Liu, J. Wang, S. Liang, G. Zhang, X. Yang, Role of NKCC1 and KCC2 in Epilepsy: From Expression to Function. Front. Neurol. 10, 1407 (2020).

5. E. Palma, M. Amici, F. Sobrero, G. Spinelli, S. Di Angelantonio, D. Ragozzino, A. Mascia, C. Scoppetta, V. Esposito, R. Miledi, F. Eusebi, Anomalous levels of Cl- transporters in the hippocampal subiculum from temporal lobe epilepsy patients make GABA excitatory. Proceedings of the National Academy of Sciences. 103, 8465–8468 (2006).

6. G. Huberfeld, L. Wittner, S. Clemenceau, M. Baulac, K. Kaila, R. Miles, C. Rivera, Perturbed Chloride Homeostasis and GABAergic Signaling in Human Temporal Lobe Epilepsy. Journal of Neuroscience. 27, 9866–9873 (2007).

7. S. Robel, X. S. C. Buckingham, X. J. L. Boni, S. L. Campbell, N. C. Danbolt, T. Riedemann, B. Sutor, H. Sontheimer, Reactive Astrogliosis Causes the Development of Spontaneous Seizures, 16.

8. F. Wang, X. Wang, L. A. Shapiro, M. L. Cotrina, W. Liu, E. W. Wang, S. Gu, W. Wang, X. He, M. Nedergaard, J. H. Huang, NKCC1 up-regulation contributes to early post-traumatic seizures and increased post-traumatic seizure susceptibility. Brain Struct Funct. 222, 1543–1556 (2017).

9. S. Sivakumaran, J. Maguire, Bumetanide reduces seizure progression and the

development of pharmacoresistant status epilepticus. Epilepsia. 57, 222–232 (2016).

10. N. Kourdougli, C. Pellegrino, J.-M. Renko, S. Khirug, G. Chazal, T.-K. Kukko-Lukjanov, S. E. Lauri, J.-L. Gaiarsa, L. Zhou, A. Peret, E. Castrén, R. K. Tuominen, V. Crépel, C. Rivera, Depolarizing γ-aminobutyric acid contributes to glutamatergic network rewiring in epilepsy: GABA and Glu-ergic Rewiring. Ann Neurol. 81, 251–265 (2017).

11. G. Barmashenko, S. Hefft, A. Aertsen, T. Kirschstein, R. Köhling, Positive shifts of the GABAA receptor reversal potential due to altered chloride homeostasis is widespread after status epilepticus: Positive Shifts of the GABAA Receptor Reversal Potential. Epilepsia. 52, 1570–1578 (2011).

12. E. Côme, X. Marques, J. C. Poncer, S. Lévi, KCC2 membrane diffusion tunes neuronal chloride homeostasis. Neuropharmacology. 169, 107571 (2020).

13. S. Lévi, Reciprocal Regulation of KCC2 Trafficking and Synaptic Activity. Frontiers in Cellular Neuroscience. 13, 16 (2019).

14. H. H. C. Lee, T. Z. Deeb, J. A. Walker, P. A. Davies, S. J. Moss, NMDA receptor activity downregulates KCC2 resulting in depolarizing GABAA receptor–mediated currents. Nat Neurosci. 14, 736–743 (2011).

15. I. Chamma, M. Heubl, Q. Chevy, M. Renner, I. Moutkine, E. Eugène, J. C. Poncer, S. Lévi, Activity-Dependent Regulation of the K/Cl Transporter KCC2 Membrane Diffusion, Clustering, and Function in Hippocampal Neurons. J. Neurosci. 33, 15488–15503 (2013).

16. W. Wang, N. Gong, T.-L. Xu, Downregulation of KCC2 following LTP contributes to EPSP–spike potentiation in rat hippocampus. Biochemical and Biophysical Research Communications. 343, 1209–1215 (2006).

17. H.-Y. Zhou, S.-R. Chen, H.-S. Byun, H. Chen, L. Li, H.-D. Han, G. Lopez-Berestein, A. K.

Sood, H.-L. Pan, N-Methyl-D-aspartate Receptor- and Calpain-mediated Proteolytic Cleavage of K ⁒-Cl⁒ Cotransporter-2 Impairs Spinal Chloride Homeostasis in Neuropathic Pain*□S. 287, 12 (2012).

18. M. Puskarjov, F. Ahmad, K. Kaila, P. Blaesse, Activity-Dependent Cleavage of the K-Cl Cotransporter KCC2 Mediated by Calcium-Activated Protease Calpain. Journal of Neuroscience. 32, 11356–11364 (2012).

19. M. Heubl, J. Zhang, J. C. Pressey, S. Al Awabdh, M. Renner, F. Gomez-Castro, I. Moutkine, E. Eugène, M. Russeau, K. T. Kahle, J. C. Poncer, S. Lévi, GABAA receptor dependent synaptic inhibition rapidly tunes KCC2 activity via the Cl−-sensitive WNK1 kinase. Nat Commun. 8, 1776 (2017).

20. M. Shekarabi, J. Zhang, A. R. Khanna, D. H. Ellison, E. Delpire, K. T. Kahle, WNK Kinase Signaling in Ion Homeostasis and Human Disease. Cell Metabolism. 25, 285–299 (2017).

21. K. T. Kahle, E. Delpire, Kinase-KCC2 coupling: Cl − rheostasis, disease susceptibility, therapeutic target. Journal of Neurophysiology. 115, 8–18 (2016).

22. J. A. McCormick, D. H. Ellison, The WNKs: Atypical Protein Kinases With Pleiotropic Actions. Physiological Reviews. 91, 177–219 (2011).

23. J. Randall, T. Thorne, E. Delpire, Partial cloning and characterization of Slc12a2 : the gene encoding the secretory Na + -K + -2Cl − cotransporter. American Journal of Physiology-Cell Physiology. 273, C1267–C1277 (1997).

24. M. Carmosino, I. Giménez, M. Caplan, B. Forbush, Exon Loss Accounts for Differential Sorting of Na-K-Cl Cotransporters in Polarized Epithelial Cells. MBoC. 19, 4341–4351 (2008).

25. S. Somasekharan, M. Y. Monette, B. Forbush, Functional Expression of Human NKCC1 from a Synthetic Cassette-Based cDNA: Introduction of Extracellular Epitope Tags and Removal

of Cysteines. PLoS ONE. 8, e82060 (2013).

26. J. M. C. Gregoriades, A. Madaris, F. J. Alvarez, F. J. Alvarez-Leefmans, Genetic and pharmacologic inactivation of apical NKCC1 in choroid plexus epithelial cells reveals the physiological function of the cotransporter, 73.

27. E. Delpire, K. B. Gagnon, in Comprehensive Physiology, R. Terjung, Ed. (John Wiley & Sons, Inc., Hoboken, NJ, USA, 2018; http://doi.wiley.com/10.1002/cphy.c170018), pp. 871–901.

28. E. Kikuchi, T. Mori, M. Zeniya, K. Isobe, M. Ishigami-Yuasa, S. Fujii, H. Kagechika, T. Ishihara, T. Mizushima, S. Sasaki, E. Sohara, T. Rai, S. Uchida, Discovery of Novel SPAK Inhibitors That Block WNK Kinase Signaling to Cation Chloride Transporters. JASN. 26, 1525–1536 (2015).

29. P. Friedel, K. T. Kahle, J. Zhang, N. Hertz, L. I. Pisella, E. Buhler, F. Schaller, J. Duan, A. R. Khanna, P. N. Bishop, K. M. Shokat, I. Medina, WNK1-regulated inhibitory phosphorylation of the KCC2 cotransporter maintains the depolarizing action of GABA in immature neurons. Sci. Signal. 8, ra65–ra65 (2015).

30. K. B. Gagnon, E. Delpire, Multiple Pathways for Protein Phosphatase 1 (PP1) Regulation of Na-K-2Cl Cotransporter (NKCC1) Function: THE N-TERMINAL TAIL OF THE Na-K-2Cl COTRANSPORTER SERVES AS A REGULATORY SCAFFOLD FOR Ste20-RELATED PROLINE/ALANINE-RICH KINASE (SPAK) AND PP1. J. Biol. Chem. 285, 14115–14121 (2010).

31. J. S. Grimley, L. Li, W. Wang, L. Wen, L. S. Beese, H. W. Hellinga, G. J. Augustine, Visualization of Synaptic Inhibition with an Optogenetic Sensor Developed by Cell-Free Protein Engineering Automation. Journal of Neuroscience. 33, 16297–16309 (2013).

32. S. Khirug, J. Yamada, R. Afzalov, J. Voipio, L. Khiroug, K. Kaila, GABAergic Depolarization of the Axon Initial Segment in Cortical Principal Neurons Is Caused by the Na-K-2Cl Cotransporter NKCC1. Journal of Neuroscience. 28, 4635–4639 (2008).

33. Y. Otsu, F. Donneger, E. J. Schwartz, J. C. Poncer, Cation–chloride cotransporters and the polarity of GABA signalling in mouse hippocampal parvalbumin interneurons. J Physiol. 598, 1865–1880 (2020).

34. D. Choquet, Linking Nanoscale Dynamics of AMPA Receptor Organization to Plasticity of Excitatory Synapses and Learning. J. Neurosci. 38, 9318–9329 (2018).

35. G. Gouzer, C. G. Specht, L. Allain, T. Shinoe, A. Triller, Benzodiazepine-dependent stabilization of GABAA receptors at synapses. Molecular and Cellular Neuroscience. 63, 101–113 (2014).

36. A. Triller, D. Choquet, New Concepts in Synaptic Biology Derived from Single-Molecule Imaging. Neuron. 59, 359–374 (2008).

37. E. M. Petrini, J. Lu, L. Cognet, B. Lounis, M. D. Ehlers, D. Choquet, Endocytic Trafficking and Recycling Maintain a Pool of Mobile Surface AMPA Receptors Required for Synaptic Potentiation. Neuron. 63, 92–105 (2009).

38. S. Bazúa-Valenti, G. Gamba, Revisiting the NaCl cotransporter regulation by with-no-lysine kinases. American Journal of Physiology-Cell Physiology. 308, C779–C791 (2015).

39. A. T. Piala, T. M. Moon, R. Akella, H. He, M. H. Cobb, E. J. Goldsmith, Chloride Sensing by WNK1 Involves Inhibition of Autophosphorylation. Science Signaling. 7, ra41–ra41 (2014).

40. J. Rinehart, N. Vázquez, K. T. Kahle, C. A. Hodson, A. M. Ring, E. E. Gulcicek, A. Louvi, N. A. Bobadilla, G. Gamba, R. P. Lifton, WNK2 Kinase Is a Novel Regulator of Essential Neuronal Cation-Chloride Cotransporters. J. Biol. Chem. 286, 30171–30180 (2011).

41. J. Ponce-Coria, P. San-Cristobal, K. T. Kahle, N. Vazquez, D. Pacheco-Alvarez, P. de los Heros, P. Juarez, E. Munoz, G. Michel, N. A. Bobadilla, I. Gimenez, R. P. Lifton, S. C. Hebert, G. Gamba, Regulation of NKCC2 by a chloride-sensing mechanism involving the WNK3 and SPAK

kinases. Proceedings of the National Academy of Sciences. 105, 8458–8463 (2008).

42. J. Rinehart, K. T. Kahle, P. de los Heros, N. Vazquez, P. Meade, F. H. Wilson, S. C. Hebert, I. Gimenez, G. Gamba, R. P. Lifton, WNK3 kinase is a positive regulator of NKCC2 and NCC, renal cation-Cl- cotransporters required for normal blood pressure homeostasis. Proceedings of the National Academy of Sciences. 102, 16777–16782 (2005).

43. K. T. Kahle, J. Rinehart, P. de los Heros, A. Louvi, P. Meade, N. Vazquez, S. C. Hebert, G. Gamba, I. Gimenez, R. P. Lifton, WNK3 modulates transport of Cl- in and out of cells: Implications for control of cell volume and neuronal excitability. Proceedings of the National Academy of Sciences. 102, 16783–16788 (2005).

44. R. B. Darman, B. Forbush, A Regulatory Locus of Phosphorylation in the N Terminus of the Na-K-Cl Cotransporter, NKCC1. J. Biol. Chem. 277, 37542–37550 (2002).

45. R. B. Darman, A. Flemmer, B. Forbush, Modulation of Ion Transport by Direct Targeting of Protein Phosphatase Type 1 to the Na-K-Cl Cotransporter. J. Biol. Chem. 276, 34359–34362 (2001).

46. P. de los Heros, D. R. Alessi, R. Gourlay, D. G. Campbell, M. Deak, T. J. Macartney, K. T. Kahle, J. Zhang, The WNK-regulated SPAK/OSR1 kinases directly phosphorylate and inhibit the K+–Cl– co-transporters. Biochemical Journal. 458, 559–573 (2014).

47. A. C. Vitari, J. Thastrup, F. H. Rafiqi, M. Deak, N. A. Morrice, H. K. R. Karlsson, D. R. Alessi, Functional interactions of the SPAK/OSR1 kinases with their upstream activator WNK1 and downstream substrate NKCC1. Biochemical Journal. 397, 223–231 (2006).

48. H. Bannai, S. Lévi, C. Schweizer, M. Dahan, A. Triller, Imaging the lateral diffusion of membrane molecules with quantum dots. Nat Protoc. 1, 2628–2634 (2006).

49. M. J. Saxton, Lateral diffusion in an archipelago. Single-particle diffusion. Biophysical

Journal. 64, 1766–1780 (1993).

50. S. Battaglia, M. Renner, M. Russeau, E. Côme, S. K. Tyagarajan, S. Lévi, eNeuro, in press, doi:10.1523/ENEURO.0203-17.2017.

51. C. G. Specht, I. Izeddin, P. C. Rodriguez, M. El Beheiry, P. Rostaing, X. Darzacq, M. Dahan, A. Triller, Quantitative Nanoscopy of Inhibitory Synapses: Counting Gephyrin Molecules and Receptor Binding Sites. Neuron. 79, 308–321 (2013).

Discussion

My PhD project aimed at determining whether NKCC1 is regulation by neuronal activity, in a fashion analogous to KCC2. I studied the involvement of the WNK-SPAK-OSR1 signalling in the regulation of NKCC1 mediated by $GABA_AR$ activity. This effort was organized in two axis.

NKCC1 distribution at the membrane had never been characterized in mature hippocampal neurons, as well as how this distribution is regulated by synaptic neurotransmission. I observed a highly clustered distribution in the somato-dendritic compartment. Reminiscent of the distribution of other membrane proteins such as KCC2 or post-synaptic repectors, this clustering is associated with a notable lateral diffusion feature, exhibiting a decreased diffusion speed and area when NKCC1 is at the proximity of synapses (Côme et al. 2020). Interestingly, NKCC1 diffusion in the axon was considerably more important when compared with dendritic NKCC1, suggesting that other mechanisms regulating the transporter's distribution at the plasma membrane are at play. In consequence, the diffusion-capture model appeared as an appropriate model for the study of NKCC1 regulation at the membrane. I then looked for a potential role of neuronal activity on NKCC1 expression, and whether the regulation of NKCC1 membrane pool follows the diffusion-capture model. I demonstrated that the WNK-SPAK-OSR1 pathway involved in KCC2 regulation via neuronal inhibition was also responsible of changes in NKCC1 distribution, consistently with a homeostatic response. Another interesting result is the apparent absence of baseline glutamatergic transmission effects on dendritic NKCC1 diffusion, while the axonal co-transporters were considerably slowed down in comparison with dendritic ones.

The second axis of my research project was to explore the potential of inhibiting SPAK kinase activity in a mouse model of ictogenesis (Rafiqi et al. 2010). Using a mutant strain expressing inactive SPAK, I performed behavioural and in vivo electrophysiology assays to quantify the effects of this genetic inhibition on the symptoms of a pentylenetetrazole (PTZ) model of seizure. As SPAK targets both KCC2 and NKCC1, the inhibition of its activity appears as a promising option (Friedel et al. 2015; Moore et al. 2018). Although the effects on the analyzed symptoms were moderate, this work provided additional information on the genetic inhibition of SPAK activity in the context of ictogenesis.

1. NKCC1 regulation by GABAergic activity has a specific diffusion-capture signature

1. A. An increased constraint associated with endocytosis

As presented in the introduction (section 3. B. b.), KCC2 clustering has been correlated with a decreased lateral diffusion, reflecting its stabilization in clusters. My results point towards another link between lateral diffusion and clustering for NKCC1. Upon conditions leading to a decrease in NKCC1 clustering at the membrane, reduced diffusion coefficient and explored area were observed. An important statement is that the inhibition of dynamin interaction with amphyphysn prevents the decrease in NKCC1 lateral diffusion, suggesting that its **increased confinement involves interaction with clathrin endocytosis-related molecular actors and a denser packing in endocytic clusters**. I suggest that upon dephosphorylation at SPAK/OSR1-targeted threonine residues, dendritic NKCC1 clusters (at least some of them) disaggregate, with the transporters diffusing and subsequently being trapped at endocytic regions in less numerous, denser clusters. Such a regulation may have different outcomes on chloride homeostasis depending on NKCC1 activity in those clusters, which could the be seen as a local chloride concentration regulation process. Given the fact that 30 minutes after application those dense clusters are still detectable could also suggest that a fraction of the trapped co-transporters are not undergoing recycling of degradation, but serve as a reserve pool. This higher fraction of NKCC1 located in such clusters is a possible explanation for the differences observed in lateral diffusion when compared with KCC2. The consequences of such a process are however hard to evaluate, given the low contribution of NKCC1 to chloride homeostasis. Keeping a NKCC1 reserve may serve for local chloride influx, or mediate other unknown functions, with a rapidly recruitable pool (by phosphorylation for instance). This assumption of a trapping of membrane proteins in endocytic wells is reminiscent of the concept of a reserve pool of AMPAR or $GABA_AR$ (Kneussel and Hausrat 2016; Petrini et al. 2009). These pools include two main categories : receptors in recycling vesicles, allowing to replenish the pool of mobile receptors at the membrane. The other form of reserve consists in the extrasynaptic receptors. The functional relevance of such reservoirs of has been demonstrated for long-term potentiation of excitatory and inhibitory synapses via the regulation of synaptic receptor

accumulation (Kneussel and Hausrat 2016). Hence this model may be relevant to interpret our data on NKCC1 lateral diffusion, although the functional outcome is still up for suggestions.

Under chloride depletion only a slight increase in the extrasynaptic transporter confinement area was observed, and membrane pool fraction and size of clusters were increased. Thus, phosphorylation of NKCC1 after WNK activation by low chloride could enhance its clustering in non-endocytic regions, increasing in turn its stability at the plasma membrane. These results are consistent with the presented model for NKCC1 regulation by diffusion-capture depending on WNK-SPAK-OSR1 activity.

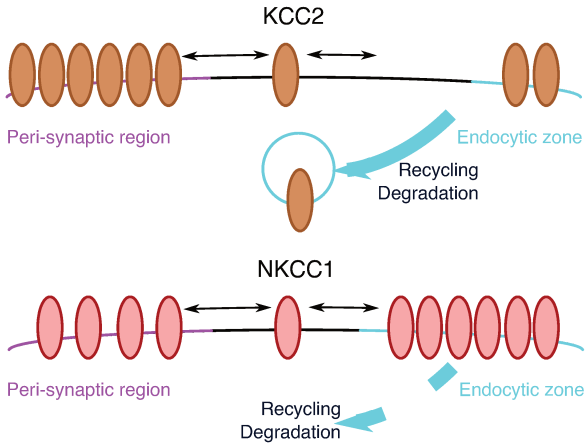

Figure 25, diffusion-capture of KCC2 and NKCC1. KCC2 endocytosis is correlated with increased lateral diffusion, as less KCC2 is located in clusters, transitioning to endocytic regions where it is rapidly endocytosed. Endocytosis-related regulation of NKCC1 is associated with NKCC1 confinement, likely due to its fast trapping in denser endocytic clusters, and a lower endocytosis rate than KCC2 relatively to the amount of trapped molecules.

I have succintly presented **NKCC1 mobility in the axon**, mentioning its potential dependence on action potential firing. Conversely to the observed decrease in dendritic NKCC1 lateral diffusion following $GABA_AR$ stimulation or inihibition, axonal NKCC1 underwent a striking increase in their lateral diffusion after $GABA_AR$ blockade. The explored area inflation was prevented by dynamin peptide pre-incubation, while the increased velocity was not. Due to differences in clathrin-coated vesicles in the dendrite and in the axon the differences in the cytoskeleton organization, it is likely that axonal NKCC1 trapping requires different molecular players (Tao-Cheng 2020). This result further reinforces the idea that axonal NKCC1 diffusion-capture regulation by GABAergic activity differs from the one occuring in the dendrite. As NKCC1 function is highly

relevant in the AIS, the study of NKCC1 regulation in the axon can be instructive about neuronal and network activity.

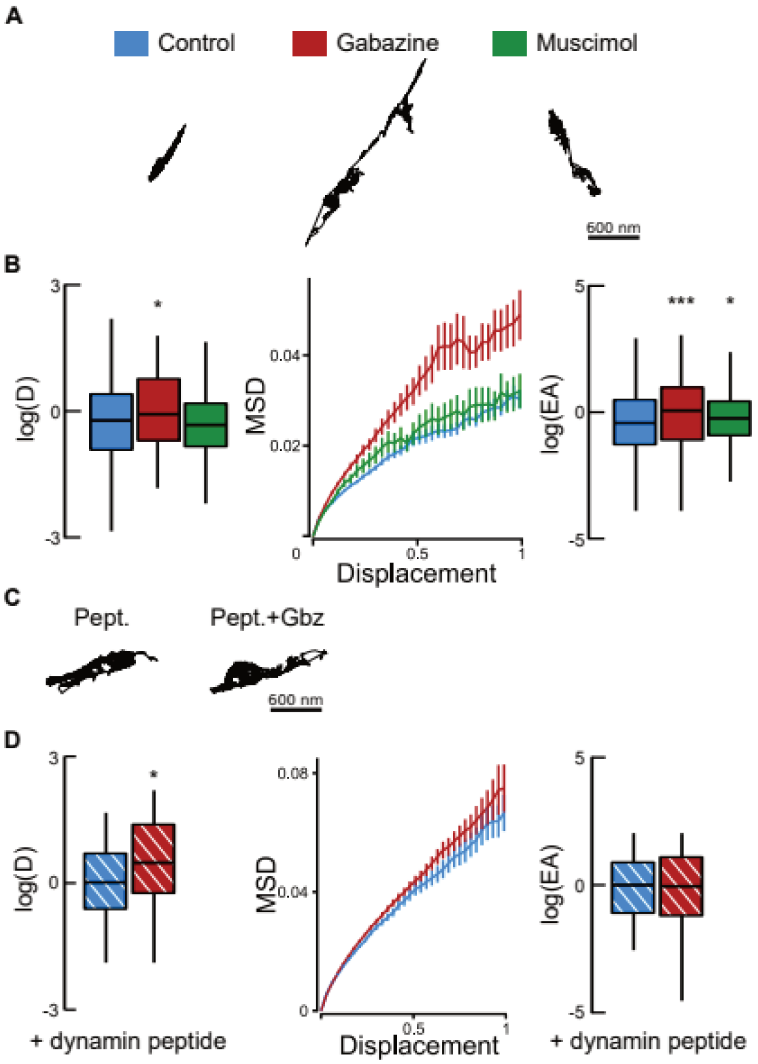

Figure 26. NKCC1 lateral diffusion in the axon is increased upon $GABA_AR$ blockade. **A**, reconstructed trajectories of membrane NKCC1 in the axon depicting the increased surface explored after gabazine treatment. **B**, the diffusion coefficient (left) of axonal NKCC1 increases after gabazine administration, correlated with an increase in MSD (middle) and EA (right) as well. Muscimol application only leads to a slight increase in EA. **C**, example of traces from axonal NKCC1 under peptide and peptide + gabazine conditions. **D**, conversely to dendritic NKCC1, dynamin peptide application did not entirely block gabazine effect on NKCC1 diffusion speed (left). However the EA and MSD increase was prevented (middle and right), suggesting this regulation is clathrin-dependent, but with a different mechanism than in dendrite.

At least 2 cultures per condition, 3 neurons or more per culture and condition. Welch t-test.
* : p-value $\in$]0.05 , 0.01], *** : p-value < 0.001

1. B. Factors tuning NKCC1 diffusion and clustering at the membrane

Lateral diffusion of a membrane protein can be influenced by a multitude of factors. From the membrane fluidity (e.g. lipid composition, cholesterol) or the presence of other components, forming either obstacles (molecular crowding) or interacting with the tracked protein. **Molecular**

crowding at the synapses is a consequence of the important density of receptors, interaction proteins, among others. This congestion can directly lead to a limitation in the membrane protein diffusion, and this effect can be hard to discriminate from the action of molecules interacting with the tracked protein (M. L. Renner et al. 2009). Both KCC2 and NKCC1 form clusters at the periphery of synapses, however the fact that they are both more retained at **glutamatergic synapses** (higher dwell time) than inhibitory ones indicates that more active regulatory systems are at play in their constrainment at the synapses (Chamma et al. 2013). If one knows several specific interactors, the use of pharmacological or genetic approaches can allow to highlight the impact of this interaction on the protein diffusion. For example, **KCC2 interaction with actin through 4.1N was demonstrated to considerably impact the transporter diffusion** at the membrane (Chamma et al. 2013; H. Li et al. 2007). KCC2 interactomes have highlighted its linkage with numerous anchoring or recycling proteins, highlighting the interplay of KCC2 diffusion with its membrane pool regulation (Mahadevan et al. 2017; Smalley et al. 2020).

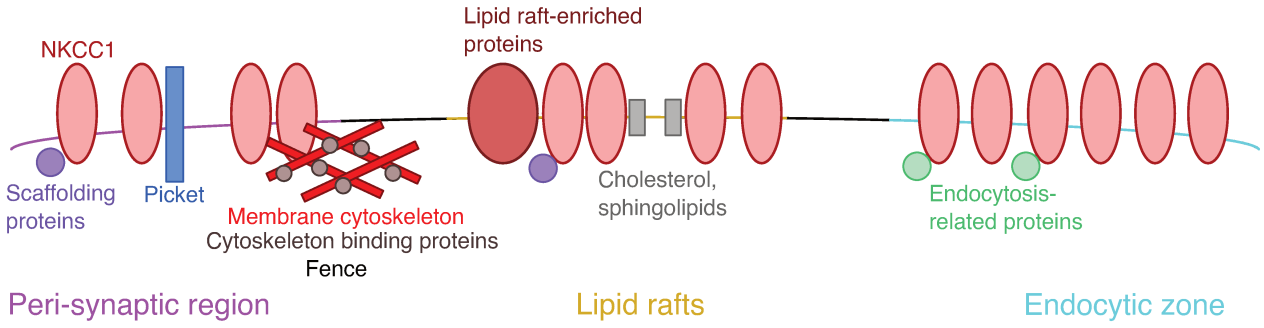

Figure 27, NKCC1 may be localized in several dendritic domains, mainly in the form of clusters. Membrane proteins or lipids, as well as intracellular scaffolding proteins affect its diffusion-capture, either due to sterical limitation (picket and fence model, Kusumi et al. 2011) or molecular interaction. Interaction with the cytoskeleton could be mediated by actin-binding anchoring proteins, dynamically retro-regulated by NKCC1 interaction with cofilin.

The similar clustering pattern of KCC2 and NKCC1, forming numerous, small clusters at the membrane suggests a regulation of NKCC1 distribution by the **cytoskeleton or anchor proteins**. To explore this possibility, the use of pharmacology to disrupt the cytoskeleton (such as latrunculin) or NKCC1 constructs lacking CTD or NTD would be crude, yet simple assays to start. NKCC1 interaction with cofilin was reported in glioblastoma, providing a migration mechanism through actin dynamics changes (Schiapparelli et al. 2017). This interaction was later studied in the context of LTP in the astrocyte, with a **NKCC1-dependent regulation of astrocytic processes**

via combined actions on the actin network and water influx (Henneberger et al. 2020). To this day, no study was performed on the NKCC1-cofilin interaction in neurons, which appears as an interesting starting point to assess transversal functions of NKCC1, including its diffusion-capture regulation. A consistently identified interactor of NKCC1 at the membrane is actually NKCC1 itself, which has been reported to form **homodimers** (Chew et al. 2019; Moore-Hoon and Turner 2000; X. Yang, Wang, and Cao 2020). I presented the latest reported structural data in the introduction (section 1. B. d), which notably stated the importance of the co-transporter's transmembrane domains for its dimerization. Although this does apparently not give determinant insights on the molecular basis of NKCC1 regulation by at the membrane, it is an important result regarding our diffusion-capture model, supporting the idea of an NKCC1 clustering and its likk with its activity. Another factor influencing membrane proteins are lipid rafts. KCC2 was demonstrated to localize in membrane rafts and non-raft regions, while NKCC1 is mainly localized in rafts where it would be the most active (Hartmann et al. 2009). This is especially interesting given the finding by Yang et al. in 2020 that **NKCC1 dimers create a local lipid membrane distortion** which could suggest a pivotal role of the transporter in lipid rafts organization (X. Yang, Wang, and Cao 2020). KCC2 localization in lipid rafts was shown to notably depend on phosphorylation at Y903/1087, an observation correlated with decreased E_{GABA} suggesting an enhancement of its transport activity (Watanabe et al. 2009), while Hartmann et al. reported a negative effect of lipid rafts on KCC2 activity (Hartmann et al. 2009). This apparent discrepancy can arise from the use of different cell models (HEK293 in Hartmann et al., ~ 30 DIV hippocampal neurons in Watanabe et al.) and readouts (Rb^+ transport and E_{GABA}). It can also happen that phosphorylation of KCC2 at these tyrosine residues change its structure and / or interaction with lipid rafts. **NKCC1 localization at the membrane hence appears to be heavily dependent on the distribution of lipid rafts and endocytic regions.**

The clustering of KCC2 and NKCC1 is quite striking and seems to majorly depend on their **phosphorylation**. Additionally to the correlation between KCC2 clustering and transport activity (Watanabe et al. 2009), heterogenous spatial distribution of the co-transporters could have a determinant functional impact on GABAergic inhibition. The question of **local $[Cl^-]_i$ domains** has been adressed in several papers, hence the action of NKCC1 and KCC2 in both immature and mature stages is likely depending on their **spatial distribution** (Arosio and Ratto 2014; Doyon et

al. 2016; Doyon et al. 2011).

1. C. Does an increased neuronal activity impact NKCC1 membrane stability ?

Beyond the surprising characteristics of NKCC1 diffusion-capture upon WNK inhibition after $GABA_AR$ activation, the fact that **GABAergic neurotransmission directly regulates NKCC1** at the membrane is not especially surprising given the existing litterature on NKCC1 regulation by this signalling (Kristopher T. Kahle and Delpire 2016; Murillo-de-Ozores et al. 2018). In addition to that NKCC1 phosphorylation was shown to be modulated by $GABA_AR$ activity in (although it includes glial cells) (Heubl et al. 2017). I have presented the involvement of GABAergic activity and NKCC1 in epilepsy contextes (section 2. B.), highlighting the importance of my results. However the used pharmacology is indeed far from eplileptic-like conditions, and does not mimic an increased network excitability due to excitatory neurotransmission occurence prevention.

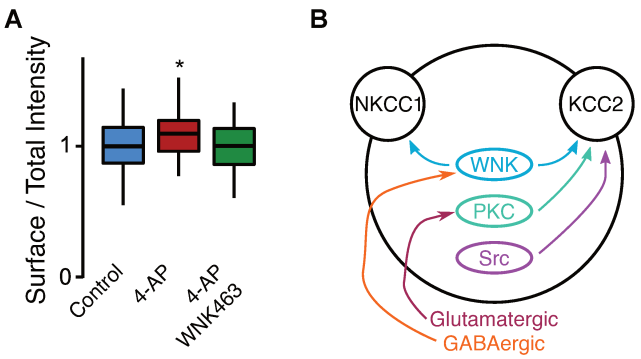

Figure 28. Neurotransmission-dependent regulation of NKCC1 seems to mainly depend on WNK-SPAK-OSR1. **A**, NKCC1 membrane stability is increased in a paradigm of increased neuronal activity. This effect is prevented by a prior inhibition of WNK activity. **B**, while KCC2 is tuned by several kinase pathways, the WNK signalling appears as the main regulator of NKCC1 expression at the plasma membrane of neurons. This prevalence is also present in the context ofactivity-dependent regulation of the transporter.

3 cultures, > 10 cells per culture per condition

Welch t-test, p-value :
Control, 4-AP : 0.004
Control, 4-AP+WNK463 : 0.5

4-AP is a commonly used drug to stimulate neuronal activity, extensively used to obtain synchronous activities in hippocampus slices (section 1. A. c). Hence it makes for a relevant model to start our study of NKCC1 regulation by enhanced glutamatergic activity, and was actually used in the same context for KCC2 (Chamma et al. 2013). Using standard epifluorescence we were able to detect an **increase in NKCC1**

membrane fraction after 30 minutes of 4-AP application. This result demonstrates the quick regulation of NKCC1 expression at the membrane in a model of intense neuronal activity. But the most interesting result is that **WNK activity inhibition by WNK463 pre-incubation abolished the effect of 4-AP**. Although these data are preliminary, they suggest that the WNK-SPAK-OSR1 pathway may be involved in NKCC1 enhanced activity under epilepsy-related contextes. This result would confirm the important prevalence of these kinases on NKCC1 regulation, while KCC2 down-regulation after-AP application seems to depend on S940 dephosphorylation (Chamma et al. 2013; H. H. C. Lee et al. 2007, 2011). This apparent up-regulation of NKCC1 also suggests WNK are more active under a intense neuronal activity. A stimulation of PP1 mediated by increased $[Ca^{2+}]_i$, akin to the PP1-mediated dephosphorylation of KCC2 at Serine 940 following NMDAR activity, would be expected to decrease NKCC1 membrane stability. Hence another pathway might be involved.

Interestingly, another protein is involved in WNK-SPAK-OSR1 activity regulation : the calcium-binding protein 39 (Cab39) (Jose Ponce-Coria et al. 2014). In oocytes injected with WNK4 cRNA, Cab39 was shown to activate the chloride-sensitive kinase in a SPAK-independent fashion. WNK4 isoform being the most sensitive to $[Cl^-]_i$ (Bazúa-Valenti et al. 2015), it is likely that, unlike WNK1 or WNK3, under the presented experimental conditions the kinase is inactive. Thus it should be noted that WNK1 may not be as strongly regulated by Cab39 as WNK4 in these experimental conditions. The authors suggest three different WNK-dependent activation of NKCC pathways : WNK-SPAK-OSR1 (the most well-known, which I studied) ; WNK-Cab39, with the chloride-sensing Cab39 allowing a calcium-dependent activation of the chloride-sensitive WNK proteins ; and a Cab39-SPAK signalling (more hypothetical). The prevalence of one of those pathways on the others needs to be explored in neurons to have a better understanding of the WNK-dependent pathways regulation by chloride or calcium. The WNK-Cab39-NKCC1 signalling was reported to be up-regulated in stroke injury of spontaneous hypersensitive rats (Bhuiyan et al. 2017). These results are however relying on correlations, and further investigation is required to confirm the potential causal role of Cab39 in WNK-NKCC1 activation in the 4-AP model, and eventually in pathological conditions.

2. Entanglement of KCC2 and NKCC1 phosphorylation by WNK-SPAK-OSR1

2. A. WNK-SPAK-OSR1 regulates KCC2 and NKCC1 in opposite directions

Similarly to the reported regulation of KCC2 membrane stability by $GABA_AR$ activity, NKCC1 is regulated by GABAergic inhibition *via* diffusion-capture. Both transporters undergo a change in their phosphorylation state after $GABA_AR$ activation or inhibition, in both cases following a modulation in WNK-SPAK-OSR1 activity. When studying the regulation of NKCC1 by WNK-SPAK-OSR1, I reported strong effects of WNK1 inhibition with WNKKD on NKCC1 distribution and stability at the membrane. On the other hand WNK1 activation, emulated by WNKCA transfection, did not yield any effect on NKCC1 diffusion-capture. WNKCA has been demonstrated to have little effect on chloride homeostasis (Friedel et al. 2015). The authors suggested this result reflects a high KCC2 phosphorylation under control conditions, explaining the stronger effects of WNK1 inhibition. Yet I worked on mature neurons, where WNK1 was shown to be much less active (Friedel et al. 2015). It may then be that **NKCC1 is more phosphorylated than KCC2 under baseline conditions, perhaps due to a higher phosphorylation rate of SPAK and OSR1 on NKCC1, explaining KCC2 regulation by WNK-SPAK-OSR1 activation** (Heubl et al. 2017) **and NKCC1 modulation upon the inhibition ofWNK-SPAK-OSR1**. Hence, a potential cause for WNKCA absence of effects is that a greater fraction of NKCC1 is phosphorylated compared with KCC2 under control conditions in mature hippocampal neurons.

If NKCC1 can be almost only down-regulated in our experiments and readouts, the pharmacological regulation of GABAergic using either **gabazine or muscimol both resulting in NKCC1 decreased clustering through endocytosis-dependent pathways** can be explained. The reported muscimol impact on KCC2 lateral diffusion is limited while gabazine application considerably increases its lateral diffusion, both in terms of kinetics and area (Heubl et al. 2017). On the other hand both treatments decreased NKCC1 lateral diffusion with a similar effect size, with different effects on NKCC1 clustering, notably on the structure and density of detections in

those clusters. For reasons that have been discussed (section 1. B. b), biochemistry assays on NKCC1 suffer from its expression in non-neuronal cells, and in consequence may be misleading. Nevertheless Heubl et al. reported a lighter increase in NKCC1 phosphorylation at T203/207/212 residues than KCC2 phosphorylation at T906/1007 after $GABA_AR$ blockade using gabazine. While KCC2 underwent unclustering, the expected positive effects on NKCC1 were not observed, but instead NKCC1 cluster size was reduced. Furthermore, gabazine had the same effect on NKCC1 lateral diffusion than muscimol, with a dependence on clathrin-mediated endocytosis. I hence formulate the hypothesis that, **following gabazine-dependent decrease in KCC2 transport activity, the reported subsequent increase in $[Cl^-]_i$ leads to the inhibition of WNK, resulting in effects similar to an increase in $[Cl^-]_i$.** This hypothesis would explain the similarity shared with muscimol effects (transient increase in $[Cl^-]_i$) and the increased clustering reported in the chloride depletion experiment, consistently with the idea that the WNK-SPAK-OSR1 signalling inhibition effects on NKCC1 are stronger than its stimulation.

This hypothesis relies on the idea that after KCC2 down-regulation, a significant part of membrane NKCC1 is dephosphorylated due to the decreased WNK-SPAK-OSR1 activity, leaving PP1 in control. My data suggest a rather quick reorganization, whithin minutes, due to higher dephosphorylation kinetics thanks to the multi-stage dephosphorylation mediated by PP1. However this does not come in adequation with the measured increase in NKCC1 phosphorylation 30 minutes after gabazine application, although the effect can also come from glial NKCC1 (Heubl et al. 2017). A way to interepret these results is to consider dendritic NKCC1 sub-populations, with phosphorylated NKCC1 located in non-endocytic clusters or “freely” diffusing at the membrane, while the smaller, non phosphorylated fraction would tend to be trapped in endocytic zones, decreasing their lateral diffusion. This is consistent with my super-resolution results showing that NKCC1 clusters were smaller, but not denser, after gabazine application. Hence the cluster reorganization would only be partial at this time, due to the delay in KCC2-mediated $[Cl^-]_i$ increase after gabazine application. Another supporting fact is the apparent difficulty in changing NKCC1 membrane expression, with only strong homeostatic stress, or 1 week long WNK1 inhibition leading to an increase or decrease in NKCC1 membrane pool fraction, respectively. NKCC1 undergoing limited recycling at the membrane, the rapid, muscimol-like effect of gabazine would then be indeed observable. On the other hand, KCC2 seems to be more strongly regulated by endocytosis, and consequently the gabazine-induced

$[Cl^-]_i$ increase may not impact the transporter's lateral diffusion at the time it was observed due to additional endocytosis-exocytosis steps (Chamma et al. 2013; Heubl et al. 2017). Yet the direct involvement of KCC2 remains a hypothesis, and more direct approaches are needed to assess it (see later).

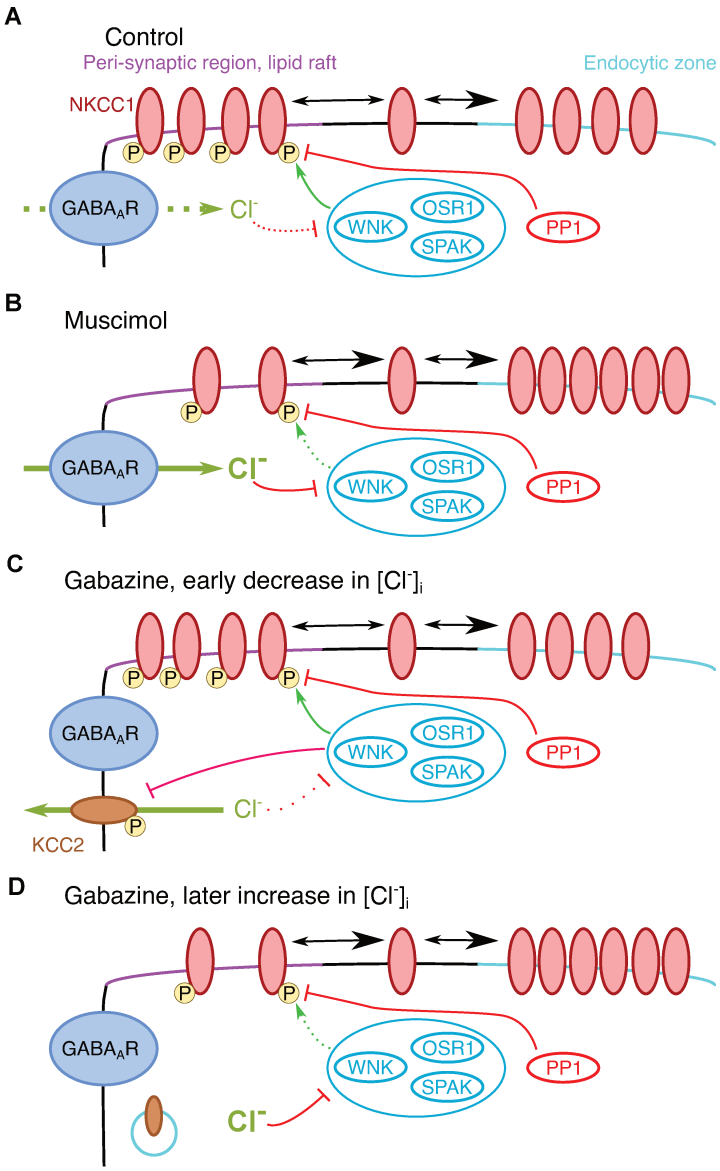

Figure 29. NKCC1 lateral diffusion regulation by WNK-SPAK-OSR1 is dynamically tuned by GABAergic neurotransmission. **A**, under the control condition, a significative portion of membrane NKCC1 is phosphorylated and localized in peri-synaptic clusters and lipid rafts. **B**, muscimol activation leads to a transient increase in $[Cl^-]_i$ from $GABA_AR$ activation. WNK are inhibited by chloride ions, leading to NKCC1 unclustering and diffusion into denser clusters in endocytic regions following dephosphorylation by PP1. **C**, gabazine application leads to a decrease in $[Cl^-]_i$ resulting from $GABA_AR$ blockade and KCC2 activity. If NKCC1 phosphorylation is already high under control conditions, gabazine would have little effects on NKCC1 diffusion-capture. **D**, as KCC2 membrane fraction is decreased by the kinases, chloride extrusion is impaired once the co-transporter has undergone endocytosis. Intracellular chloride levels increase in consequence, inhibiting the kinase pathway. Resulting from these events NKCC1 is dephosphorylated and targeted to endocytic regions.

2. B. Changes in NKCC1 lateral diffusion are correlated with its phosphorylation state

To further characterize NKCC1 regulation by GABAergic activity, I used the vbSPT (section 3. B. a. (Persson et al. 2013)) analysis tool to extract additional variables on NKCC1 lateral diffusion. The results of these analysis are presented in figure 30 for dendritic NKCC1 and figure 31 for axonal NKCC1. By including several states in the diffusion analysis, other outputs are provided. I used the obtained data with a more “vectorial” approach, analysing the colinearity of the effects of different conditions relatively to NKCC1 WT control.

In the dendrite the mutation of T203/207/212/217/230 (NKCC1 TA_5) had comparable effects polarity to NKCC1 WT after muscimol application across the different states (Fig. 30). However the amplitude of those effects is higher for NKCC1 TA5. Considering our paradigm with muscimol-triggered WNK inhibition, this result seems logical, as the consequence on NKCC1 would be a reduced phosphorylation following WNK inactivation by muscimol-mediated chloride influx. The fact that NKCC1 TA_5 exhibited stronger effects may stem from the fact that muscimol would only partially decrease the transporter’s phosphorylation. Hence a difference in NKCC1 phosphorylation seem to be a main factor influencing the co-transporter diffusion in the dendrite.

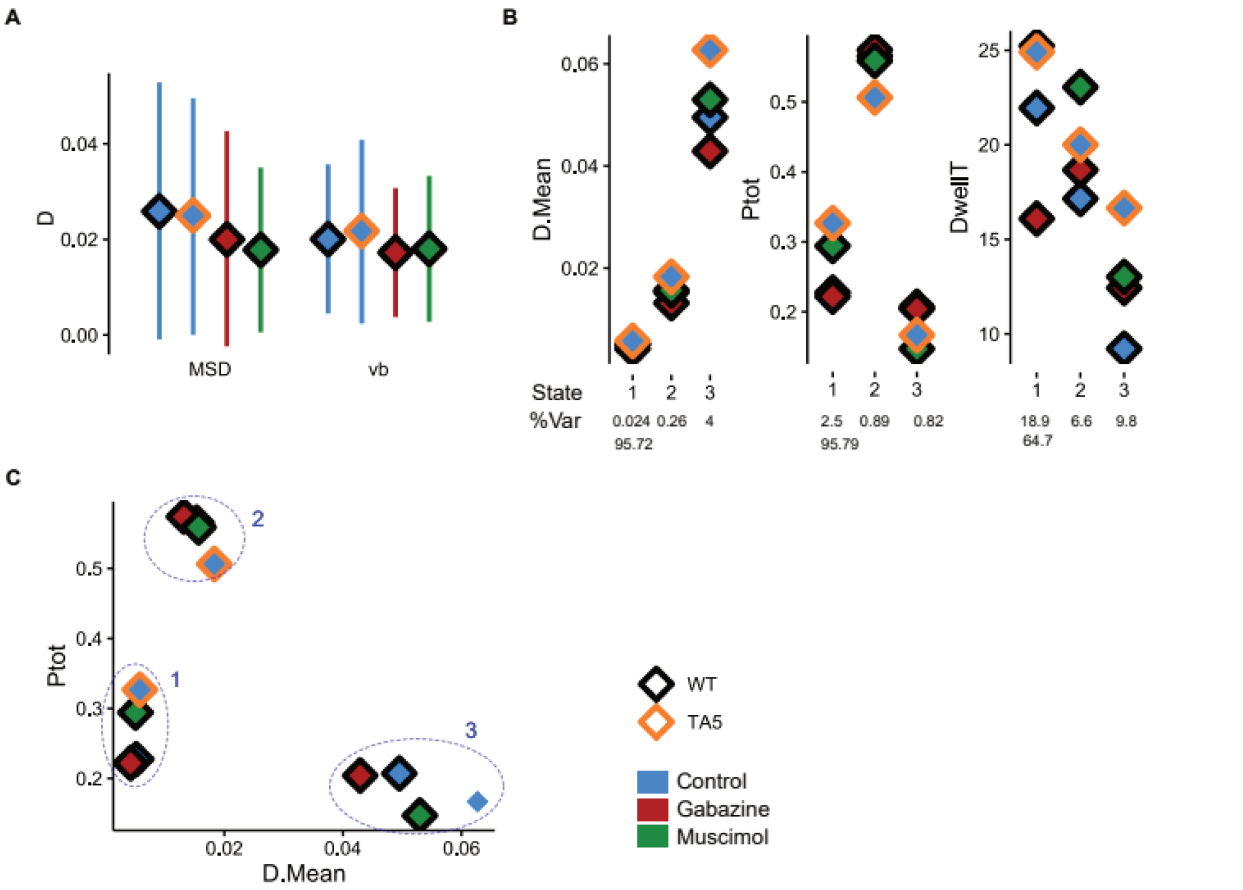

D

		Cos_D	Cos_Ptot	Cos_DwellT	L_D	L_Ptot	L_DwellT
TA5 1 Control Dendrite	WT 1 Gabazine Dendrite	-0.908804	-0.6115314	0.6966577	1.318924	15.09449537	1.8621458
TA5 1 Control Dendrite	WT 1 Muscimol Dendrite	0.7566777	0.919756	0.8817525	4.611511	1.18622994	1.4978499
WT 1 Gabazine Dendrite	WT 1 Muscimol Dendrite	-0.4194886	-0.2519131	0.5395128	3.49642	0.07858692	0.8043677

Figure 30. NKCC1 TA5 has a diffusion behaviour similar to NKCC1 WT after muscimol application in the dendrite. **A**, comparison of diffusion coefficient values obtained from MSD and variational Bayes for SPT, without inter-culture normalization. Note that for MSD-derived D values, there is 1 value per trajectory, while for vbSPT only the distribution parameters are computed. Note the recorded decrease in gabazine and muscimol conditions. **B**, principal variables obtained from vbSPT analysis, and mean values for each state (N=3) and each condition. D.Mean : mean D value for the condition and the state ; Ptot : time fraction spent in the corresponding state ; DwellT : dwell time, representing the probability to remain in the current state (different variable from dwell time at the synapses presented in my work). *Bottom :* intra-state and inter-states variance fraction. **C**, Projection on the (Ptot, D.Mean) plane depicts the consistent discrimination between states. **D**, colinearity and effect size of different conditions, with the WT control condition taken as a reference. Cos_variable quantifies the similarity of effects directionality, 1 indicates similar effects across the 3 states, -1 opposite effects. L_variable reflects the effect amplitude of the left condition relatively to the effect amplitude of the right condition. This table shows that the TA5 mutant and WT muscimol application share similar effects (cosinus values), however the amplitude of TA5 effects is greater.

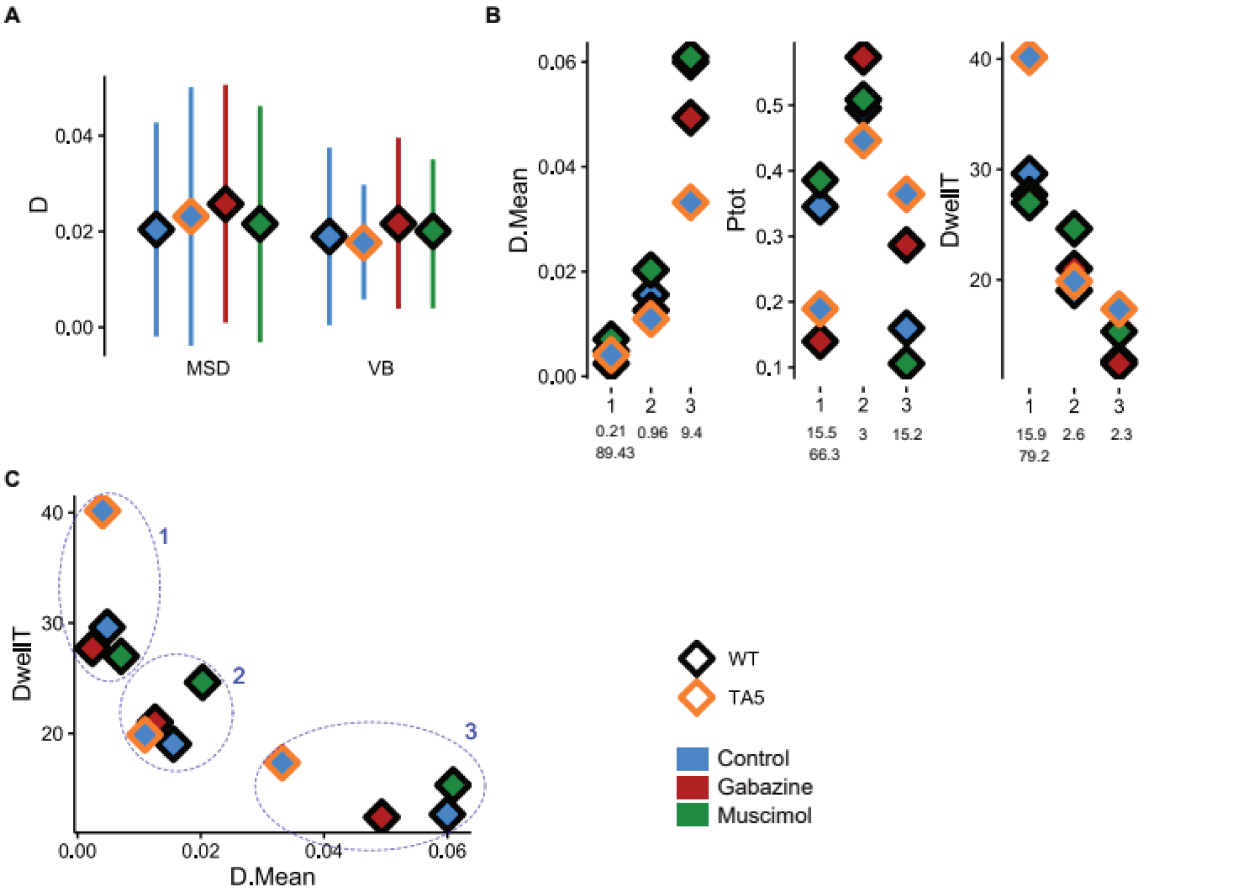

D

		Cos_D	Cos_Ptot	Cos_DwellT	L_D	L_Ptot	L_DwellT
TA5 1 Control Axon	WT 1 Gabazine Axon	0.6778145	0.9285582	-0.4052573	0.9943139	1.354021	4.1567434
TA5 1 Control Axon	WT 1 Muscimol Axon	-0.5439315	-0.9999804	0.3057866	1.0031351	3.798476	1.3871309
WT 1 Gabazine Axon	WT 1 Muscimol Axon	-0.9359859	-0.9262186	0.6953943	1.0088717	2.80533	0.3337062

Figure 31. NKCC1 TA5 behaviour is similar to NKCC1 WT under gabazine treatment in the axon. **A**, comparison of diffusion coefficient values obtained from MSD and variational Bayes for SPT, without inter-culture normalization. Note the increase in D under gabazine and muscimol conditions. **B**, principal variables obtained from vbSPT analysis, and mean values for each state (N=3) and each condition. **C**, Projection on the (DwellT, D.Mean) plane shows a less efficient clustering of the different conditions in the 3 states. This potentially arises from NKCC1 TA5 having diffusion properties quite different from WT NKCC1, notably in states 1 and 3. **D**, colinearity and effect size of different conditions, with the WT control condition taken as a reference. This table shows that WT gabazine and WT muscimol application have opposite effects on D and Ptot, while the NKCC1 TA5 and WT gabazine conditions share a quite similar behaviour.

I have briefly mentioned the regulation of NKCC1 by $GABA_AR$ activity in the axon (figure 26). Interestingly the inhibition of the receptors importantly raised NKCC1 lateral diffusion in this compartment. The tracking was performed in the distal axon, however the expression of NKCC1 and the lack of KCC2 expression suggests a higher chloride concentration, reminiscent of the AIS (Khirug et al. 2008; Rinetti-Vargas et al. 2017). Still, these hypothesis are not proofs of a WNK-SPAK-OSR1 regulation of axonal NKCC1. The analysis from vbSPT, using the same variables, show

that NKCC1 TA_5 does actually has similar effects to the gabazine treatment, notably on the diffusion coefficient. By interpreting this result like previously for dendritic NKCC1, the gabazine effect would be due to the inhibition of the signalling pathway (or a stimulation of PP1), leading to NKCC1 dephosphorylation and increased lateral diffusion. If confirmed, this result further conforts the pivotal role of WNK-SPAK-OSR1 in NKCC1 regulation in mature neurons.

2. C. KCC2 dominant transport activity in the mature hippocampus retroactively regulates NKCC1 via changes in $[Cl^-]_i$

NKCC1 would then be dynamically regulated by KCC2 transport activity, through a change in WNK-SPAK-OSR1 activity resulting from WNK auto-phosphorylation inhibition, leading to a dominant dephosphorylation mediated by PP1. This hypothesis of a **KCC2-dependent tuning of NKCC1** is suggested by the unexpected regulation of NKCC1 observed in gabazine conditions. Indeed, we initially used gabazine treatment to lower intracellular chloride and activate WNK signaling, phosphorylate NKCC1 and increase its membrane stability and clustering. In contrast, we observed that neuronal exposure to gabazine led to a comparable regulation of NKCC1 diffusion/stability/clustering than muscimol treatment i.e. to an increased confinement in endocytic zones. This could be due to the gabazine-induced increase in intracellular chloride levels consecutive to the down-regulation of KCC2 membrane stability and activity (Heubl et al., 2017).

KCC2 activity indirectly playing on NKCC1 distribution at the membrane is noteworthy, further illustrating the fine tuning of $[Cl^-]_i$ in neurons. To confirm this hypothesis one way would be to remove KCC2 from the neuronal system. However, co-transfection of shKCC2 and WT NKCC1 turned out to be toxic for the neurons, while the expression of either one was not (data not shown). This toxicity may be due to the lack of chloride extrusion capacity of the neurons combined to the activity of the recombinant WT NKCC1 resulting in the loading of the cells with high chloride. Another option is to study the WNK-dependent regulation of NKCC1 in immature neurons, where KCC2 expression is lower. However, this is a rather delicate change in paradigm, with interpolations made harder. We are however addressing this point right now. Preliminary experiments suggest that surface NKCC1 expression in immature (6 DIV) neurons is actually not

that different than in mature (21 DIV) neurons. Moreover, the membrane stability of NKCC1 in immature neurons does not seem to be significantly altered by a blockade of the WNK signaling. This suggests that either the WNK signaling pathway influences the clustering of the transporter and not its membrane stability or that other mechanisms are at play to tune NKCC1. Further work will allow to discriminate between these hypotheses.

Despite the observation of NKCC1 regulation in neurons, engaging a well-documented kinase pathway, **NKCC1 appears to have little to no impact on chloride homeostasis in basal conditions of activity** as recorded by electrophysiological and genetic tools (section 1. A. b). In adequation with these observations, I did not observe an influential role of NKCC1 and of its phosphorylation on $[Cl^-]_i$ in 21-25 DIV mature hippocampal neurons. On the other hand, modulation of KCC2 using either the antagonist VU0463271 (Heubl et al. 2017) or transfection of neurons with a mutant of KCC2 (T906/1007E) mimicking a KCC2 transporter phosphorylated by SPAK-OSR1, did impact $[Cl^-]_i$. Hence the question about the function of NKCC1 in mature neurons remains asked. While compensatory mechanisms (section 1. A. d.) can explain the lack of effects of genetic approaches (transfection, mutations), the general lack of impact of bumetanide application is quite explicit on NKCC1 role in chloride transport.

Given the wide range of functions associated with NKCC1 (Delpire and Gagnon 2018), suggesting the transporter association with a variety of molecular mechanisms, it is rather difficult to easily infer the roles the transporter serves in the mature brain. Similarly, the processes leading to NKCC1 inhibition effects in several pathological cases are tricky to decipher given the broad expression, and the numerous functions of NKCC1. Moreover, the diversity in models and effects of NKCC1 inhibition render this task challenging (R. Liu et al. 2020). Akin to the reported interaction of KCC2 with a potassium channel, an eye must be kept open for **non transport-related aspects of NKCC1**, like evoked earlier regarding its interaction with cofilin (Goutierre et al. 2019).

3. Can the WNK-SPAK-OSR1 signalling inhibition alleviate ictogenesis symptoms via the regulation of KCC2 and NKCC1 phosphorylation ?

3. A. Targetting a pathway regulating both KCC2 and NKCC1

While both NKCC1 and KCC2 expression is altered in several epilepsy models in adulthood, most works studying chloride transporters only focused on either KCC2 (Goutierre et al. 2019; Kelley et al. 2018; Magloire et al. 2019; Moore et al. 2018; Silayeva et al. 2015; S. Sivakumaran et al. 2015) or NKCC1 (Kourdougli et al. 2017; Sudhir Sivakumaran and Maguire 2016) function. Based on the data regarding its implication in the regulation of KCC2 and NKCC1 in neurons, the WNK-SPAK-OSR1 kinase cascade appears as a promising target for both KCC2 down-regulation and NKCC1 up-regulation in pathological contextes. A simple hypothesis is that WNK inhibition leads to an decrease in intracellular chloride concentration, resulting from the effects on KCC2 and NKCC1. **In a model of PTZ-induced ictogenesis, Heubl et al. report an increase in the phosphorylation of WNK1, SPAK, KCC2 and NKCC1**, demonstrating the relevance in controlling the pathway phosphorylation in the context of seizures (Heubl et al. 2017). It was then reported that **prevention of KCC2 phosphorylation by those kinases with mutations at the 906 and 1007 threonine residues limited the severity of kainate-induced seizures** (Moore et al. 2018). However as mentioned previously, this later study only focused on the potassion-chloride co-transporter. It makes sense as KCC2 is the lead CCC in the ature brain. However given the reported effects of NKCC1 in epileptogenesis, a portion of the picture is still missing.

3. B. Genetic inhibition of SPAK does not have a big impact on ictogenesis severity

To assess the relevance of inhibiting this kinase pathway in the context of ictogenesis, I used a **PTZ-induced seizure model assays with SPAK$^{243A/243A}$, who express a non-active form of SPAK**, and WT mice. Behavioural indicators (Racine's scale) and electrocorticograms (EcoG) were

recorded and analyzed. It resulted that the effects of the mutation on these variables was mild, with a **reduced death rate and a slight increase in the post-seizure signal power. On the other end, the duration of seizures was decreased, but the observed difference was not significant** (Fig. 33)**.**

Although SPAK is inactivated in the $SPAK^{243A/243A}$ mice, **OSR1 is still active**, genetic inactivation of OSR1 leading to prenatal death (Rafiqi et al. 2010, 4). The authors reported a decreased expression and phosphorylation of NKCC1, NKCC2 and NCC in the kidney, with a correlated effect on arterial blood pressure. Another work showed that the phosphorylation of N(K)CC was not always compensated by OSR1 in a SPAK-KO model, however they also report a hyperphosphorylation of NKCC1 in KO mice (Grimm et al. 2012). Hence the SPAK-OSR1 system in the kidney is more complex than it was first expected, with the presence of specific isoforms inhibiting NKCC2 and NCC phosphorylation in the thick ascending limb due to a lack of kinase domain, and acting as a dominant negative isoform (McCormick et al. 2011). In consequence, depending notably on the expression and activity of OSR1 in neurons or glial cells, the SPAK 243A mutation may not have the expected effect on NKCC1 and KCC2 phosphorylation state. Other compensatory mechanisms previously introduced (section 1. A. d.) may play a part in neuronal chloride homeostasis (e.g. AE), and other actions of SPAK inhibition outside CCC and chloride transport are indeed possible (Murillo-de-Ozores et al. 2020). To prevent these compensations, a model with an intracerebral injection of closantel or WNK463 could be developped.

A second likely cause for the reported results is the **chosen experimental model**. Indeed PTZ-induced ictogenesis leads to the pathway phosphorylation, however this increase in phosphorylation may not be influent at the time of the ictogenesis occurrence. NKCC1's proactive role on epileptic activities in the mature brain has been especially described during or after the epileptogenesis process (Huberfeld et al. 2007; Kourdougli et al. 2017; Robel et al. 2015; Sudhir Sivakumaran and Maguire 2016). NKCC1 function has been correlated with ectopia (Koyama et al. 2012) and mossy fibers sprouting (Kourdougli et al. 2017). Thus SPAK inhibition effects on NKCC1 are possibly not assessable in the ictogenesis **time window** we chose. Another, non-exclusive hypothesis, is that KCC2 activity still predominates during ictogenesis, "hiding"

NKCC1 transport activity. This hypothesis is backed by the reported crucial role of KCC2 activity in limitating kainate-induced SE (Moore et al. 2018; Silayeva et al. 2015; Sudhir Sivakumaran and Maguire 2016). In conclusion, **NKCC1 phosphorylation by SPAK is unlikely to be relevant in PTZ-induced tonico clonic seizures.**

KCC2 is at the crossroads of several pathways which were thoroughly described (Chamma et al. 2012; Kristopher T Kahle et al. 2014; Lévi 2019). Hence focusing on its phosphorylation downstream of WNK is quite reductive. KCC2 phosphorylation at **serine 940**, but also at threonines 903/1087 have been consistently described as a most crucial factor for the transporter's activity (H. H. C. Lee et al. 2011; H. H. C. Lee, Jurd, and Moss 2010; Puskarjov et al. 2012; Silayeva et al. 2015; Watanabe et al. 2009). In consequence depending on the chosen model **different regulatory mechanisms might infer with KCC2 activity**, and SPAK-mediated phosphorylation may not be as dominant as showed in studies focusing on this pathway, using a pharmacology decreasing spontaneous neuronal activity (Friedel et al. 2015; Heubl et al. 2017). Yet preventing the phosphorylation of T906/1007 in a kainate model of SE was shown to be sufficient to attenuate lethality and delay the 1st tonic seizure occurrence (Moore et al. 2018). The reported effects *in vivo* are **not visible before 30 to 60 minutes**, and the effect size is not especially striking. As PTZ is rapidly degraded, and most animals undergo a single seizure in the first 20 minutes in my experiments, the likelihood for KCC2 phosphorylation by SPAK to be effective are rather low. Furthermore **SPAK/OSR1 are known to phosphorylate KCC2 at T1007, but the kinase phosphorylating the co-transporter at T906 is still to be determined** (Alessi et al. 2014; Kristopher T. Kahle et al. 2013; Zhang et al. 2016). Hence in addition to targetting one of several molecular signallings, only one of the two kinases phosphorylating one of the two concerned residues is inhibited in this model.

In conclusion these experiments characterize the SPAK$^{243A/243A}$ strain in the context of ictogenesis, demonstrating that **SPAK genenitic inhibition is not sufficient to limitate PTZ-induced symptoms**. This is probably due to the rapid effect of PTZ injection preventing the potential phosphorylation effects on later symptoms.

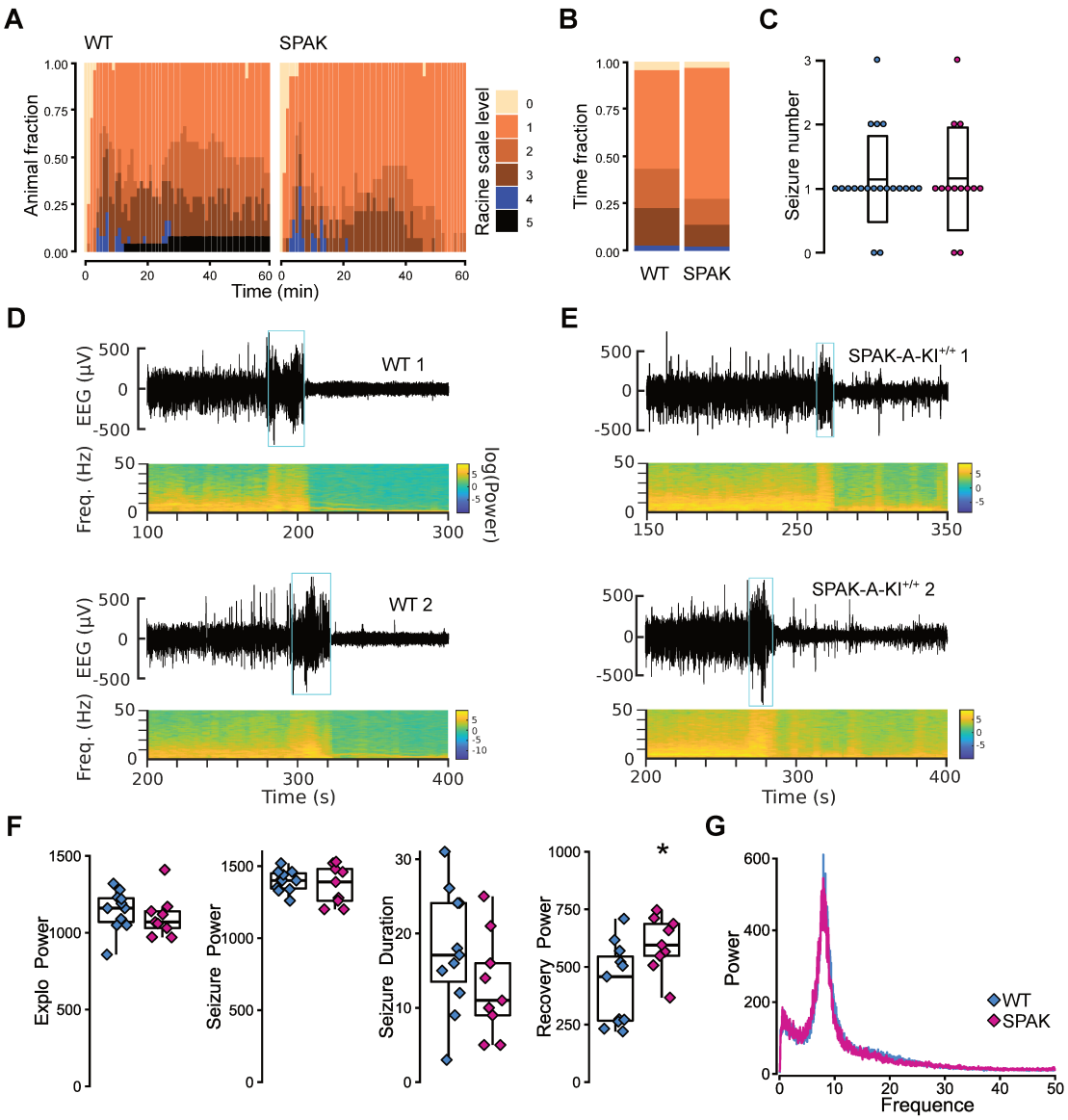

Figure 32. SPAK$^{243A/243A}$ mutants display decreased symptoms severity during epileptic seizures in a pentylenetetrazole ictogenesis model (75 mg/kg). **A**, symptoms were studied for 60 minutes after PTZ injection. Representation of the fraction of higher Racine scale level observed each minute for each animal. Scale used : 0 : no symptom, 1 : prostration, 2 : partial clonies (limbs), 3 : generalized clonies, 4 : seizure. Level 5 (death) is displayed here but will not be used for analysis. It should however be noted that only WT mice died during these assays. **B**, proportion of time spent in each Racine scale level during the 60 minutes following the injection. **C**, number of seizure per animal, box represents Mean +/- SD. Note that the number of seizure is not affected by the mutation. **D**, representative traces of epileptic seizure from 2 wild-type (WT) mice, upper panel : EEG recording (μV), lower panel : spectrogram (log function applied, μV^2). Blue rectangles represent the signal classified as a seizure. **E**, same as A with SPAK$^{243A/243A}$ mice. **F**, **G**, characteristics of EEG recordings in WT and mutant mice. Baseline exploration power does not differ between the two strains (**F1** and **G**). Similarly seizure power and duration do not change even though a tendancy is visible for the latter. A change in the recovery power was observed, being higher in mutant mice.

Number of animals used for behavioural analysis : 20 (18 during 60 min.) WT, 13 (12 during 60 min.) SPAK$^{243A/243A}$. Number of animals used for ECoG experiments : 11 WT, 9 SPAK$^{243A/243A}$.

General conclusions

NKCC1 is the main chloride importer in immature neurons, allowing GABAergic neurotransmission to be excitatory during early developmental stages. As KCC2 expression is developmentally up-regulated, NKCC1 role in the chloride homeostasis of mature neurons in the hippocampus takes a back seat. In addition to the interrogations on NKCC1 function in mature neurons, the cellular mechanisms underlying NKCC1 expression and regulation are vastly unknown. Yet, its transport activity was demonstrated to be involved in a number of pathological models, and especially under contextes of impaired neuronal inhibition. Using several imaging techniques, I characterized NKCC1 expression and diffusion at the membrane of mature hippocampal neurons.

The most important part of my work is the unravelling of activity-dependent NKCC1 regulation at the membrane, demonstrating the involvement of the chloride-sensitive WNK signalling. This regulation involves the diffusion-capture mechanism, sparked by NKCC1 dephosphorylation as the kinase activity is decreased by $GABA_AR$ activity. Hence the pathway regulating KCC2 through GABAergic activity also tunes NKCC1 distribution and endocytosis at the membrane, proving the relevance of lateral diffusion as a readout for the rapid regulation of neuronal CCC membrane pool. The study of this mechanism also highlighted the peculiar diffusion signature of NKCC1, with an apparently counter-intuitive correlation between clustering and diffusion speed or explored area.

The function of NKCC1 in mature hippocampal neurons remains largely elusive, as its transport function is overrun by KCC2 one under physiological conditions. In this context, my work provides the first in-depht characterization of an activity-dependent regulation of NKCC1 by neuronal inhibition in mature neurons. The WNK-SPAK-OSR1 signalling then appears as a homeostatic hub for chloride in mature neurons, and its study in the context of chloride-related pathological conditions could lead to convincing results .

Bibliography

Achilles, K. et al. 2007. 'Kinetic Properties of Cl Uptake Mediated by Na+-Dependent K+-2Cl Cotransport in Immature Rat Neocortical Neurons'. *Journal of Neuroscience* 27(32): 8616–27.

Acton, B. A. et al. 2012. 'Hyperpolarizing GABAergic Transmission Requires the KCC2 C-Terminal ISO Domain'. *Journal of Neuroscience* 32(25): 8746–51.

Agez, Morgane et al. 2017. 'Molecular Architecture of Potassium Chloride Co-Transporter KCC2'. *Scientific Reports* 7(1): 16452.

Akella, Radha et al. 2020. 'A Phosphorylated Intermediate in the Activation of WNK Kinases'. *Biochemistry* 59(18): 1747–55.

Akyuz, Enes. 2021. 'Revisiting the Role of Neurotransmitters in Epilepsy: An Updated Review'. *Life Sciences*: 21.

Alessi, D. R. et al. 2014. 'The WNK-SPAK/OSR1 Pathway: Master Regulator of Cation-Chloride Cotransporters'. *Science Signaling* 7(334): re3–re3.

Andrews, Katie, Sunday Solomon Josiah, and Jinwei Zhang. 2020. 'The Therapeutic Potential of Neuronal K-Cl Co-Transporter KCC2 in Huntington's Disease and Its Comorbidities'. *International Journal of Molecular Sciences* 21(23): 9142.

Anselmo, A. N. et al. 2006. 'WNK1 and OSR1 Regulate the Na+, K+, 2Cl- Cotransporter in HeLa Cells'. *Proceedings of the National Academy of Sciences* 103(29): 10883–88.

Arosio, Daniele et al. 2010. 'Simultaneous Intracellular Chloride and PH Measurements Using a GFP-Based Sensor'. *Nature Methods* 7(7): 516–18.

Arosio, Daniele, and Gian Michele Ratto. 2014. 'Twenty Years of Fluorescence Imaging of Intracellular Chloride'. *Frontiers in Cellular Neuroscience* 8. http://journal.frontiersin.org/article/10.3389/fncel.2014.00258/abstract (November 22, 2020).

Auer, Theresa, Philipp Schreppel, Thomas Erker, and Christoph Schwarzer. 2020. 'Impaired Chloride Homeostasis in Epilepsy: Molecular Basis, Impact on Treatment, and Current Treatment Approaches'. *Pharmacology & Therapeutics* 205: 107422.

Avoli, Massimo et al. 1996. 'Synchronous GABA-Mediated Potentials and Epileptiform Discharges in the Rat Limbic System ***In Vitro*** '. *The Journal of Neuroscience* 16(12): 3912–24.

Avoli, Massimo, and Paul Perreault. 'A GABAergic Depolarizing Potential in the

Hippocampus Disclosed by the ConvuIsant 4-Aminopyridine'. : 5.

Banke, T. G., and C. J. McBain. 2006. 'GABAergic Input onto CA3 Hippocampal Interneurons Remains Shunting throughout Development'. *Journal of Neuroscience* 26(45): 11720–25.

Bannai, Hiroko et al. 2006. 'Imaging the Lateral Diffusion of Membrane Molecules with Quantum Dots'. *Nature Protocols* 1(6): 2628–34.

Barberis, Andrea. 2020. 'Postsynaptic Plasticity of GABAergic Synapses'. *Neuropharmacology* 169: 107643.

Bazúa-Valenti, Silvana et al. 2015. 'The Effect of WNK4 on the Na^+–Cl^- Cotransporter Is Modulated by Intracellular Chloride'. *Journal of the American Society of Nephrology* 26(8): 1781–86.

Ben-Ari, Yehezkel. 2002. 'Excitatory Actions of Gaba during Development: The Nature of the Nurture'. *Nature Reviews Neuroscience* 3(9): 728–39.

Berglund, K. et al. 2016. 'Optogenetic Visualization of Presynaptic Tonic Inhibition of Cerebellar Parallel Fibers'. *Journal of Neuroscience* 36(21): 5709–23.

Berglund, Ken et al. 2006. 'Imaging Synaptic Inhibition in Transgenic Mice Expressing the Chloride Indicator, Clomeleon'. *Brain Cell Biology* 35(4–6): 207–28.

———. 2008. 'Imaging Synaptic Inhibition throughout the Brain via Genetically Targeted Clomeleon'. *Brain Cell Biology* 36(1–4): 101–18.

Bhuiyan, Mohammad Iqbal H et al. 2017. 'WNK-Cab39-NKCC1 Signaling Increases the Susceptibility to Ischemic Brain Damage in Hypertensive Rats'. *Journal of Cerebral Blood Flow & Metabolism* 37(8): 2780–94.

Bize, Isabel et al. 'Serine/Threonine Protein Phosphatases and Regulation of K-Cl Cotransport in Human Erythrocytes'. : 11.

Blaesse, Peter, Matti S. Airaksinen, Claudio Rivera, and Kai Kaila. 2009. 'Cation-Chloride Cotransporters and Neuronal Function'. *Neuron* 61(6): 820–38.

Boffi, Juan C., Johannes Knabbe, Michaela Kaiser, and Thomas Kuner. 2018. 'KCC2-Dependent Steady-State Intracellular Chloride Concentration and PH in Cortical Layer 2/3 Neurons of Anesthetized and Awake Mice'. *Frontiers in Cellular Neuroscience* 12: 7.

Bonar, Pamela T., and Joseph R. Casey. 2008. 'Plasma Membrane Cl^-/HCO_3^- Exchangers: Structure, Mechanism and Physiology'. *Channels* 2(5): 337–45.

Bonneau, S., M. Dahan, and L.D. Cohen. 2005. 'Single Quantum Dot Tracking Based on Perceptual Grouping Using Minimal Paths in a Spatiotemporal Volume'. *IEEE*

Transactions on Image Processing 14(9): 1384–95.

Botterill, Justin J. et al. 2019. 'An Excitatory and Epileptogenic Effect of Dentate Gyrus Mossy Cells in a Mouse Model of Epilepsy'. *Cell Reports* 29(9): 2875-2889.e6.

Brumback, A. C., and K. J. Staley. 2008. 'Thermodynamic Regulation of NKCC1-Mediated Cl- Cotransport Underlies Plasticity of GABAA Signaling in Neonatal Neurons'. *Journal of Neuroscience* 28(6): 1301–12.

Cancedda, L., H. Fiumelli, K. Chen, and M.-m. Poo. 2007. 'Excitatory GABA Action Is Essential for Morphological Maturation of Cortical Neurons In Vivo'. *Journal of Neuroscience* 27(19): 5224–35.

Chamma, Ingrid et al. 2013. 'Activity-Dependent Regulation of the K/Cl Transporter KCC2 Membrane Diffusion, Clustering, and Function in Hippocampal Neurons'. *The Journal of Neuroscience* 33(39): 15488–503.

Chamma, Ingrid, Quentin Chevy, Jean Christophe Poncer, and Sabine Lévi. 2012. 'Role of the Neuronal K-Cl Co-Transporter KCC2 in Inhibitory and Excitatory Neurotransmission'. *Frontiers in Cellular Neuroscience* 6. http://journal.frontiersin.org/article/10.3389/fncel.2012.00005/abstract (November 6, 2020).

Chen, G, P Q Trombley, and A N van den Pol. 1996. 'Excitatory Actions of GABA in Developing Rat Hypothalamic Neurones.' *The Journal of Physiology* 494(2): 451–64.

Chen, Jen-Chi et al. 2019. 'WNK4 Kinase Is a Physiological Intracellular Chloride Sensor'. *Proceedings of the National Academy of Sciences* 116(10): 4502–7.

Chen, Li-Yuan, Maxime Lévesque, and Massimo Avoli. 2020. 'KCC2 Antagonism and Gabaergic Synchronization in the Entorhinal Cortex in the Absence of Ionotropic Glutamatergic Receptor Signalling'. *Neuropharmacology* 167: 107982.

Cherubini, E. et al. 1990. 'GABA Mediated Excitation in Immature Rat CA3 Hippocampal Neurons'. *International Journal of Developmental Neuroscience* 8(4): 481–90.

Chew, Thomas A. et al. 2019. 'Structure and Mechanism of the Cation–Chloride Cotransporter NKCC1'. *Nature* 572(7770): 488–92.

Chi, Ximin et al. 2020. 'Cryo-EM Structures of the Full-Length Human KCC2 and KCC3 Cation-Chloride Cotransporters'. *Cell Research*. http://www.nature.com/articles/s41422-020-00437-x (December 2, 2020).

Cho, Hyun-Min et al. 2013. 'Recruitment of Specificity Protein 1by CpG Hypomethylation Upregulates Naþ-Kþ-2ClÀ Cotransporter 1in Hypertensive Rats'. *Journal of Hypertension* 31(7): 8.

Choquet, Daniel. 2018. ‘Linking Nanoscale Dynamics of AMPA Receptor Organization to Plasticity of Excitatory Synapses and Learning’. *The Journal of Neuroscience* 38(44): 9318–29.

Cohen, I. 2002. ‘On the Origin of Interictal Activity in Human Temporal Lobe Epilepsy in Vitro’. *Science* 298(5597): 1418–21.

Côme, Etienne, Xavier Marques, Jean Christophe Poncer, and Sabine Lévi. 2020. ‘KCC2 Membrane Diffusion Tunes Neuronal Chloride Homeostasis’. *Neuropharmacology* 169: 107571.

Currin, Christopher B., Andrew J. Trevelyan, Colin J. Akerman, and Joseph V. Raimondo. 2020. ‘Chloride Dynamics Alter the Input-Output Properties of Neurons’ ed. Hugues Berry. *PLOS Computational Biology* 16(5): e1007932.

Dahan, M. 2003. ‘Diffusion Dynamics of Glycine Receptors Revealed by Single-Quantum Dot Tracking’. *Science* 302(5644): 442–45.

Dan, Ippeita, Norinobu M. Watanabe, and Akihiro Kusumi. 2001. ‘The Ste20 Group Kinases as Regulators of MAP Kinase Cascades’. *Trends in Cell Biology* 11(5): 220–30.

Darman, Rachel B., Andreas Flemmer, and Biff Forbush. 2001. ‘Modulation of Ion Transport by Direct Targeting of Protein Phosphatase Type 1 to the Na-K-Cl Cotransporter’. *Journal of Biological Chemistry* 276(37): 34359–62.

Darman, Rachel B., and Biff Forbush. 2002. ‘A Regulatory Locus of Phosphorylation in the N Terminus of the Na-K-Cl Cotransporter, NKCC1’. *Journal of Biological Chemistry* 277(40): 37542–50.

DeFazio, R Anthony, Sotirios Keros, Michael W Quick, and John J Hablitz. ‘Potassium-Coupled Chloride Cotransport Controls Intracellular Chloride in Rat Neocortical Pyramidal Neurons’. : 8.

Deisz, Rudolf A. et al. 2011. ‘Components of Neuronal Chloride Transport in Rat and Human Neocortex: Neuronal Chloride Transport in Rat and Human Cortex’. *The Journal of Physiology* 589(6): 1317–47.

Delpire, Eric et al. 1999. ‘Deafness and Imbalance Associated with Inactivation of the Secretory Na-K-2Cl Co-Transporter’. *Nature Genetics* 22(2): 192–95.

Delpire, Eric, and Kenneth B. Gagnon. 2018. ‘Na^+-K^+-$2Cl^-$ Cotransporter (NKCC) Physiological Function in Nonpolarized Cells and Transporting Epithelia’. In *Comprehensive Physiology*, ed. Ronald Terjung. Hoboken, NJ, USA: John Wiley & Sons, Inc., 871–901. http://doi.wiley.com/10.1002/cphy.c170018 (November 6, 2020).

Delpire, Eric, and Kenneth B. E. Gagnon. 2008. ‘SPAK and OSR1: STE20 Kinases

Involved in the Regulation of Ion Homoeostasis and Volume Control in Mammalian Cells'. *Biochemical Journal* 409(2): 321–31.

Delpire, Eric, and Jiangtao Guo. 'The Cryo-EM Structures of DrNKCC1 and HKCC1: A New Milestone in the Physiology of Cation-Chloride Cotransporters'. : 41.

DelpireSOn, Eric et al. ''Molecular Cloning and Chromosome Localization of a Putative Basolateral Na+-K+-2Cl- Cotransporter from Mouse Inner Medullary Collecting Duct (MIMCD-3) Cells'. : 7.

Demian, Wael L. et al. 2019. 'The Ion Transporter NKCC1 Links Cell Volume to Cell Mass Regulation by Suppressing MTORC1'. *Cell Reports* 27(6): 1886-1896.e6.

Di Cristo, Graziella, Patricia N. Awad, Shabnam Hamidi, and Massimo Avoli. 2018. 'KCC2, Epileptiform Synchronization, and Epileptic Disorders'. *Progress in Neurobiology* 162: 1–16.

Dowd, Brian F. X., and Biff Forbush. 2003. 'PASK (Proline-Alanine-Rich STE20-Related Kinase), a Regulatory Kinase of the Na-K-Cl Cotransporter (NKCC1)'. *Journal of Biological Chemistry* 278(30): 27347–53.

Doyon, Nicolas et al. 2011. 'Efficacy of Synaptic Inhibition Depends on Multiple, Dynamically Interacting Mechanisms Implicated in Chloride Homeostasis' ed. Abigail Morrison. *PLoS Computational Biology* 7(9): e1002149.

———. 'Chloride Regulation: A Dynamic Equilibrium Crucial for Synaptic Inhibition'. : 16.

Duebel, Jens et al. 2006. 'Two-Photon Imaging Reveals Somatodendritic Chloride Gradient in Retinal ON-Type Bipolar Cells Expressing the Biosensor Clomeleon'. *Neuron* 49(1): 81–94.

Düsterwald, Kira M et al. 2018. 'Biophysical Models Reveal the Relative Importance of Transporter Proteins and Impermeant Anions in Chloride Homeostasis'. *eLife* 7: e39575.

Duy, Phan Q., Miao He, Zhigang He, and Kristopher T. Kahle. 2020. 'Preclinical Insights into Therapeutic Targeting of KCC2 for Disorders of Neuronal Hyperexcitability'. *Expert Opinion on Therapeutic Targets* 24(7): 629–37.

Dzhala, Volodymyr I et al. 2005. 'NKCC1 Transporter Facilitates Seizures in the Developing Brain'. *Nature Medicine* 11(11): 1205–13.

Dzhala, Volodymyr I., and Kevin J. Staley. 2020. 'KCC2 Chloride Transport Contributes to the Termination of Ictal Epileptiform Activity'. *eneuro*: ENEURO.0208-20.2020.

Elgueta, Claudio, and Marlene Bartos. 2019. 'Dendritic Inhibition Differentially

Regulates Excitability of Dentate Gyrus Parvalbumin-Expressing Interneurons and Granule Cells'. *Nature Communications* 10(1): 5561.

Engblom, A.Christine, and Karl E.O. Åkerman. 1993. 'Determination of the Intracellular Free Chloride Concentration in Rat Brain Synaptoneurosomes Using a Chloride-Sensitive Fluorescent Indicator'. *Biochimica et Biophysica Acta (BBA) - Biomembranes* 1153(2): 262–66.

Filippi, Beatrice M et al. 2011. 'MO25 Is a Master Regulator of SPAK/OSR1 and MST3/MST4/YSK1 Protein Kinases: MO25 Is a Master Regulator of Many STE20 Kinases'. *The EMBO Journal* 30(9): 1730–41.

Fiumelli, Hubert, Laura Cancedda, and Mu-ming Poo. 2005. 'Modulation of GABAergic Transmission by Activity via Postsynaptic Ca2+-Dependent Regulation of KCC2 Function'. *Neuron* 48(5): 773–86.

Flemmer, Andreas W. et al. 2002. 'Activation of the Na-K-Cl Cotransporter NKCC1 Detected with a Phospho-Specific Antibody'. *Journal of Biological Chemistry* 277(40): 37551–58.

Friedel, Perrine et al. 2015. 'WNK1-Regulated Inhibitory Phosphorylation of the KCC2 Cotransporter Maintains the Depolarizing Action of GABA in Immature Neurons'. *Science Signaling* 8(383): ra65–ra65.

Furusho, Taisuke, Shinichi Uchida, and Eisei Sohara. 2020. 'The WNK Signaling Pathway and Salt-Sensitive Hypertension'. *Hypertension Research* 43(8): 733–43.

Gagnon, Kenneth B., and Eric Delpire. 2010a. 'Molecular Determinants of Hyperosmotically Activated NKCC1-Mediated K^+/K^+ Exchange: Volume-Sensitive NKCC1-Mediated K^+/K^+ Exchange'. *The Journal of Physiology* 588(18): 3385–96.

———. 2010b. 'Multiple Pathways for Protein Phosphatase 1 (PP1) Regulation of Na-K-2Cl Cotransporter (NKCC1) Function: THE N-TERMINAL TAIL OF THE Na-K-2Cl COTRANSPORTER SERVES AS A REGULATORY SCAFFOLD FOR Ste20-RELATED PROLINE/ALANINE-RICH KINASE (SPAK) AND PP1'. *Journal of Biological Chemistry* 285(19): 14115–21.

Gagnon, Kenneth B. E., Roger England, and Eric Delpire. 2006a. 'Characterization of SPAK and OSR1, Regulatory Kinases of the Na-K-2Cl Cotransporter'. *Molecular and Cellular Biology* 26(2): 689–98.

———. 2006b. 'Volume Sensitivity of Cation-Cl^- Cotransporters Is Modulated by the Interaction of Two Kinases: Ste20-Related Proline-Alanine-Rich Kinase and WNK4'. *American Journal of Physiology-Cell Physiology* 290(1): C134–42.

Gagnon, Martin et al. 2013. 'Chloride Extrusion Enhancers as Novel Therapeutics for

Neurological Diseases'. *Nature Medicine* 19(11): 1524–28.

Galan, A., and F. Cervero. 2005. 'Painful Stimuli Induce in Vivo Phosphorylation and Membrane Mobilization of Mouse Spinal Cord NKCC1 Co-Transporter'. *Neuroscience* 133(1): 245–52.

Galanopoulou, A. 2003. 'Sex-Specific KCC2 Expression and GABAA Receptor Function in Rat Substantia Nigra'. *Experimental Neurology* 183(2): 628–37.

Galanopoulou, Aristea S, and Solomon L Moshé. 2003. 'Role of Sex Hormones in the Sexually Dimorphic Expression of KCC2 in Rat Substantia Nigra'. *Experimental Neurology* 184(2): 1003–9.

Gamba, Gerardo. 2005a. 'Molecular Physiology and Pathophysiology of Electroneutral Cation-Chloride Cotransporters'. *Physiological Reviews* 85(2): 423–93.

———. 2005b. 'Role of WNK Kinases in Regulating Tubular Salt and Potassium Transport and in the Development of Hypertension'. *American Journal of Physiology-Renal Physiology* 288(2): F245–52.

Gao, Jian-ling et al. 2019. 'Suppression of WNK1-SPAK/OSR1 Attenuates Bone Cancer Pain by Regulating NKCC1 and KCC2'. *The Journal of Pain* 20(12): 1416–28.

Garneau, A P et al. 2020. 'Multiple Facets and Roles of Na+-K+-Cl− Cotransport: Mechanisms and Therapeutic Implications'. 35: 15.

Gauvain, G. et al. 2011. 'The Neuronal K-Cl Cotransporter KCC2 Influences Postsynaptic AMPA Receptor Content and Lateral Diffusion in Dendritic Spines'. *Proceedings of the National Academy of Sciences* 108(37): 15474–79.

Genç, Fatma et al. 2019. 'Methylation of Cation–Chloride Cotransporters NKCC1 and KCC2 in Patients with Juvenile Myoclonic Epilepsy'. *Neurological Sciences* 40(5): 1007–13.

Gerelsaikhan, Tudevdagva, and R James Turner. 'Transmembrane Topology of the Secretory Na⁺-K⁺-2Cl⁺ Cotransporter NKCC1 Studied by in Vitro Translation'. : 8.

Gharaylou, Zeinab et al. 2019. 'Longitudinal Effects of Bumetanide on Neuro-Cognitive Functioning in Drug-Resistant Epilepsy'. *Frontiers in Neurology* 10: 483.

Gilbert, Daniel et al. 2007. 'Differential Maturation of Chloride Homeostasis in Primary Afferent Neurons of the Somatosensory System'. *International Journal of Developmental Neuroscience* 25(7): 479–89.

Glykys, J. et al. 2014a. 'Local Impermeant Anions Establish the Neuronal Chloride Concentration'. *Science* 343(6171): 670–75.

———. 2014b. ‘Response to Comments on “Local Impermeant Anions Establish the Neuronal Chloride Concentration”’. *Science* 345(6201): 1130–1130.

Glykys, Joseph et al. 2009. ‘Differences in Cortical versus Subcortical GABAergic Signaling: A Candidate Mechanism of Electroclinical Uncoupling of Neonatal Seizures’. *Neuron* 63(5): 657–72.

———. 2017. ‘Chloride Dysregulation, Seizures, and Cerebral Edema: A Relationship with Therapeutic Potential’. *Trends in Neurosciences* 40(5): 276–94.

González, Oscar C. et al. 2018. ‘Role of KCC2-Dependent Potassium Efflux in 4-Aminopyridine-Induced Epileptiform Synchronization’. *Neurobiology of Disease* 109: 137–47.

Gonzalez-Islas, Carlos, Nikolai Chub, and Peter Wenner. 2009. ‘NKCC1 and AE3 Appear to Accumulate Chloride in Embryonic Motoneurons’. *Journal of Neurophysiology* 101(2): 507–18.

Goubert, Emmanuelle et al. 2019. ‘Bumetanide Prevents Brain Trauma-Induced Depressive-Like Behavior’. *Frontiers in Molecular Neuroscience* 12: 12.

Goutierre, Marie. ‘KCC2 Regulates Neuronal Excitability and Hippocampal Activity via Interaction with Task-3 Channels’. : 21.

Gregoriades, Jeannine M C, Aaron Madaris, Francisco J Alvarez, and Francisco Javier Alvarez-Leefmans. ‘Genetic and Pharmacologic Inactivation of Apical NKCC1 in Choroid Plexus Epithelial Cells Reveals the Physiological Function of the Cotransporter’. : 73.

Grimley, J. S. et al. 2013. ‘Visualization of Synaptic Inhibition with an Optogenetic Sensor Developed by Cell-Free Protein Engineering Automation’. *Journal of Neuroscience* 33(41): 16297–309.

Grimm, P. Richard et al. 2012. ‘SPAK Isoforms and OSR1 Regulate Sodium-Chloride Co-Transporters in a Nephron-Specific Manner’. *Journal of Biological Chemistry* 287(45): 37673–90.

Gulácsi, Alexandra et al. 2003. ‘Cell Type-Specific Differences in Chloride-Regulatory Mechanisms and $GABA_A$ Receptor-Mediated Inhibition in Rat Substantia Nigra’. *The Journal of Neuroscience* 23(23): 8237–46.

Gulyás, A. I. et al. 2001. ‘The KCl Cotransporter, KCC2, Is Highly Expressed in the Vicinity of Excitatory Synapses in the Rat Hippocampus: Localization of KCC2 in the Rat Hippocampus’. *European Journal of Neuroscience* 13(12): 2205–17.

Haas, M., D. McBrayer, and C. Lytle. 1995. ‘[Cl-]i-Dependent Phosphorylation of the Na-K-Cl Cotransport Protein of Dog Tracheal Epithelial Cells’. *Journal of Biological Chemistry* 270(48): 28955–61.

Haas, Mark, and Bliss Forbush III. 2000. ‘The Na-K-Cl Cotransporter of Secretory Epithelia’. *Annual Review of Physiology* 62(1): 515–34.

Hamidi, Shabnam, and Massimo Avoli. 2015. ‘KCC2 Function Modulates in Vitro Ictogenesis’. *Neurobiology of Disease* 79: 51–58.

Hannemann, Anke, and Peter W. Flatman. 2011. ‘Phosphorylation and Transport in the Na-K-2Cl Cotransporters, NKCC1 and NKCC2A, Compared in HEK-293 Cells’ ed. Jean-Claude Dussaule. *PLoS ONE* 6(3): e17992.

Hansen, Anders S et al. 2018. ‘Robust Model-Based Analysis of Single-Particle Tracking Experiments with Spot-On’. *eLife* 7: e33125.

Hartmann, Anna-Maria et al. 2009. ‘Opposite Effect of Membrane Raft Perturbation on Transport Activity of KCC2 and NKCC1’. *Journal of Neurochemistry* 111(2): 321–31.

Hartmann, Anna-Maria, and Hans Gerd Nothwang. 2011. ‘Opposite Temperature Effect on Transport Activity of KCC2/KCC4 and N(K)CCs in HEK-293 Cells’. : 5.

———. 2015. ‘Molecular and Evolutionary Insights into the Structural Organization of Cation Chloride Cotransporters’. *Frontiers in Cellular Neuroscience* 8. http://journal.frontiersin.org/article/10.3389/fncel.2014.00470/abstract (December 3, 2020).

Henneberger, Christian et al. 2018. *LTP Induction Boosts Glutamate Spillover by Driving Withdrawal of Astroglia*. Neuroscience. preprint. http://biorxiv.org/lookup/doi/10.1101/349233 (November 6, 2020).

———. ‘LTP Induction Boosts Glutamate Spillover by Driving Withdrawal of Perisynaptic Astroglia’. *OPEN ACCESS*: 30.

de los Heros, P. et al. 2006. ‘WNK3 Bypasses the Tonicity Requirement for K-Cl Cotransporter Activation via a Phosphatase-Dependent Pathway’. *Proceedings of the National Academy of Sciences* 103(6): 1976–81.

Heubl, Martin et al. 2017. ‘GABAA Receptor Dependent Synaptic Inhibition Rapidly Tunes KCC2 Activity via the Cl−-Sensitive WNK1 Kinase’. *Nature Communications* 8(1): 1776.

Hines, Rochelle M. et al. 2018. ‘Developmental Seizures and Mortality Result from Reducing GABAA Receptor A2-Subunit Interaction with Collybistin’. *Nature Communications* 9(1): 3130.

Hu, Jiang-Jian et al. 2017. ‘Bumetanide Reduce the Seizure Susceptibility Induced by Pentylenetetrazol via Inhibition of Aberrant Hippocampal Neurogenesis in Neonatal Rats after Hypoxia-Ischemia’. *Brain Research Bulletin* 130: 188–99.

Huang, Chou-Long, and Chih-Jen Cheng. 2015. ‘A Unifying Mechanism for WNK Kinase Regulation of Sodium-Chloride Cotransporter’. *Pflügers Archiv - European Journal of Physiology* 467(11): 2235–41.

Huang, Huachen et al. 2019. ‘The WNK-SPAK/OSR1 Kinases and the Cation-Chloride Cotransporters as Therapeutic Targets for Neurological Diseases’. *Aging and disease* 10(3): 626.

Huang, Lin-Qiang et al. 2014. ‘Hypertonic Saline Alleviates Cerebral Edema by Inhibiting Microglia-Derived TNF-α and IL-1β-Induced Na-K-Cl Cotransporter up-Regulation’. *Journal of Neuroinflammation* 11(1): 102.

Huberfeld, G. et al. 2007. ‘Perturbed Chloride Homeostasis and GABAergic Signaling in Human Temporal Lobe Epilepsy’. *Journal of Neuroscience* 27(37): 9866–73.

Hübner, Christian A., Dietrich E. Lorke, and Irm Hermans-Borgmeyer. 2001. ‘Expression of the Na-K-2Cl-Cotransporter NKCC1 during Mouse Development’. *Mechanisms of Development* 102(1–2): 267–69.

Ibla, Juan C. et al. 2006. ‘Transcriptional Repression of Na-K-2Cl Cotransporter NKCC1 by Hypoxia-Inducible Factor-1’. *American Journal of Physiology-Cell Physiology* 291(2): C282–89.

Jackson, Michael F, and Barbara Esplin. 1999. ‘Activity-Dependent Enhancement of Hyperpolarizing and Depolarizing g-Aminobutyric Acid (GABA) Synaptic Responses Following Inhibition of GABA Uptake by Tiagabine’. *Epilepsy Research*: 12.

Jedlicka, Peter, Thomas Deller, Boris S. Gutkin, and Kurt H. Backus. 2010. ‘Activity-Dependent Intracellular Chloride Accumulation and Diffusion Controls GABAA Receptor-Mediated Synaptic Transmission’. *Hippocampus*: n/a-n/a.

Jeong, Kyoung Hoon et al. 2018. ‘Increased Expression of WNK3 in Dispersed Granule Cells in Hippocampal Sclerosis of Mesial Temporal Lobe Epilepsy Patients’. *Epilepsy Research* 147: 58–61.

Jiang, Yanbo. 2018. ‘Activation of Axon Initial Segmental GABAA Receptors Inhibits Action Potential Generation in Neocortical GABAergic Interneurons’. : 9.

Jonniya, Nisha Amarnath, Md Fulbabu Sk, and Parimal Kar. 2019. ‘Investigating Phosphorylation-Induced Conformational Changes in WNK1 Kinase by Molecular Dynamics Simulations’. *ACS Omega* 4(17): 17404–16.

Kahle, K. T. et al. 2005. ‘WNK3 Modulates Transport of Cl- in and out of Cells: Implications for Control of Cell Volume and Neuronal Excitability’. *Proceedings of the National Academy of Sciences* 102(46): 16783–88.

Kahle, Kristopher T et al. 2003. ‘WNK4 Regulates the Balance between Renal NaCl

Reabsorption and K+ Secretion'. *Nature Genetics* 35(4): 372–76.

Kahle, Kristopher T. et al. 2013. 'Modulation of Neuronal Activity by Phosphorylation of the K–Cl Cotransporter KCC2'. *Trends in Neurosciences* 36(12): 726–37.

Kahle, Kristopher T et al. 2014. 'Genetically Encoded Impairment of Neuronal KCC 2 Cotransporter Function in Human Idiopathic Generalized Epilepsy'. *EMBO reports* 15(7): 766–74.

Kahle, Kristopher T., and Eric Delpire. 2016. 'Kinase-KCC2 Coupling: Cl ⁻ Rheostasis, Disease Susceptibility, Therapeutic Target'. *Journal of Neurophysiology* 115(1): 8–18.

Kaila, Kai et al. 2014. 'Cation-Chloride Cotransporters in Neuronal Development, Plasticity and Disease'. *Nature Reviews Neuroscience* 15(10): 637–54.

———. 'Long-Lasting GABA-Mediated Depolarization Evoked by High- Frequency Stimulation in Pyramidal Neurons of Rat Hippocampal Slice Is Attributable to a Network-Driven, Bicarbonate-Dependent K⁺ Transient'. : 11.

Kaneko, H. 2004. 'Chloride Accumulation in Mammalian Olfactory Sensory Neurons'. *Journal of Neuroscience* 24(36): 7931–38.

Kaneko, Hiroshi, Ilva Putzier, Stephan Frings, and Thomas Gensch. 2002. 'Determination of Intracellular Chloride Concentration in Dorsal Root Ganglion Neurons by Fluorescence Lifetime Imaging'. In *Current Topics in Membranes*, Elsevier, 167–89. https://linkinghub.elsevier.com/retrieve/pii/S1063582302530337 (December 8, 2020).

Kapur, Jaideep, and Douglas A. Coulter. 1995. 'Experimental Status Epilepticus Alters ?-Aminobutyric Acid Type A Receptor Function in CA1 Pyramidal Neurons'. *Annals of Neurology* 38(6): 893–900.

Kelley, Matt R. et al. 2018. 'Locally Reducing KCC2 Activity in the Hippocampus Is Sufficient to Induce Temporal Lobe Epilepsy'. *EBioMedicine* 32: 62–71.

Kelsch, Wolfgang et al. 2001. 'Insulin-Like Growth Factor 1 and a Cytosolic Tyrosine Kinase Activate Chloride Outward Transport during Maturation of Hippocampal Neurons'. *The Journal of Neuroscience* 21(21): 8339–47.

Kharod, Shivani C., Seok Kyu Kang, and Shilpa D. Kadam. 2019. 'Off-Label Use of Bumetanide for Brain Disorders: An Overview'. *Frontiers in Neuroscience* 13: 310.

Khirug, S. et al. 2008. 'GABAergic Depolarization of the Axon Initial Segment in Cortical Principal Neurons Is Caused by the Na-K-2Cl Cotransporter NKCC1'. *Journal of Neuroscience* 28(18): 4635–39.

Khoshkhoo, Sattar, Daniel Vogt, and Vikaas S. Sohal. 2017. ‘Dynamic, Cell-Type-Specific Roles for GABAergic Interneurons in a Mouse Model of Optogenetically Inducible Seizures’. *Neuron* 93(2): 291–98.

Klein, Peter M. et al. 2018. ‘Tenuous Inhibitory GABAergic Signaling in the Reticular Thalamus’. *The Journal of Neuroscience* 38(5): 1232–48.

Kneussel, Matthias, and Torben Johann Hausrat. 2016. ‘Postsynaptic Neurotransmitter Receptor Reserve Pools for Synaptic Potentiation’. *Trends in Neurosciences* 39(3): 170–82.

Kohling, R. 1998. ‘Spontaneous Sharp Waves in Human Neocortical Slices Excised from Epileptic Patients’. *Brain* 121(6): 1073–87.

Kolbaev, Sergey N. et al. 2020. ‘NKCC-1 Mediated Cl− Uptake in Immature CA3 Pyramidal Neurons Is Sufficient to Compensate Phasic GABAergic Inputs’. *Scientific Reports* 10(1): 18399.

Konstantoudaki, Xanthippi et al. 2014. ‘Modulatory Effects of Inhibition on Persistent Activity in a Cortical Microcircuit Model’. *Frontiers in Neural Circuits* 8. http://journal.frontiersin.org/article/10.3389/fncir.2014.00007/abstract (November 26, 2020).

Kourdougli, Nazim et al. 2017. ‘Depolarizing γ-Aminobutyric Acid Contributes to Glutamatergic Network Rewiring in Epilepsy: GABA and Glu-Ergic Rewiring’. *Annals of Neurology* 81(2): 251–65.

Kovalchuk, Y., and O. Garaschuk. 2012. ‘Two-Photon Chloride Imaging Using MQAE In Vitro and In Vivo’. *Cold Spring Harbor Protocols* 2012(7): pdb.prot070037-pdb.prot070037.

Koyama, Ryuta et al. 2012. ‘GABAergic Excitation after Febrile Seizures Induces Ectopic Granule Cells and Adult Epilepsy’. *Nature Medicine* 18(8): 1271–78.

Kurihara, Kinji, Marilyn L Moore-Hoon, Masato Saitoh, and R James Turner. ‘Characterization of a Phosphorylation Event Resulting in Upregulation of the Salivary Na+-K+-2Cl−cotransporter’. : 10.

Lee, Hae-Ahm, Inji Baek, et al. 2010. ‘Promoter Hypomethylation Upregulates Na+–K+–2Cl− Cotransporter 1 in Spontaneously Hypertensive Rats’. *Biochemical and Biophysical Research Communications* 396(2): 252–57.

Lee, Hae-Ahm, Su-Hyung Hong, Jung-Wan Kim, and Il-Sung Jang. 2010. ‘Possible Involvement of DNA Methylation in NKCC1 Gene Expression during Postnatal Development and in Response to Ischemia: Epigenetic Control of NKCC1 Gene Expression by DNA Methylation’. *Journal of Neurochemistry* 114(2): 520–29.

Lee, Henry H. C. et al. 2007. ‘Direct Protein Kinase C-Dependent Phosphorylation

Regulates the Cell Surface Stability and Activity of the Potassium Chloride Cotransporter KCC2'. *Journal of Biological Chemistry* 282(41): 29777–84.

Lee, Henry H C et al. 2011. 'NMDA Receptor Activity Downregulates KCC2 Resulting in Depolarizing GABAA Receptor–Mediated Currents'. *Nature Neuroscience* 14(6): 736–43.

Lee, Henry H.C., Rachel Jurd, and Stephen J. Moss. 2010. 'Tyrosine Phosphorylation Regulates the Membrane Trafficking of the Potassium Chloride Co-Transporter KCC2'. *Molecular and Cellular Neuroscience* 45(2): 173–79.

Lee, Min et al. 2020. 'Ecm29-Mediated Proteasomal Distribution Modulates Excitatory GABA Responses in the Developing Brain'. *Journal of Cell Biology* 219(2): e201903033.

Lesept, Flavie et al. 2016. 'Tissue-Type Plasminogen Activator Controls Neuronal Death by Raising Surface Dynamics of Extrasynaptic NMDA Receptors'. *Cell Death & Disease* 7(11): e2466–e2466.

Leterrier, X Christophe. 'The Axon Initial Segment: An Updated Viewpoint'. : 11.

Lévi, Sabine. 2019. 'Reciprocal Regulation of KCC2 Trafficking and Synaptic Activity'. *Frontiers in Cellular Neuroscience* 13: 16.

Lévi, Sabine, Nicolas Le Roux, Emmanuel Eugène, and Jean Christophe Poncer. 2015. 'Benzodiazepine Ligands Rapidly Influence GABAA Receptor Diffusion and Clustering at Hippocampal Inhibitory Synapses'. *Neuropharmacology* 88: 199–208.

Lewin, Naomi, Emre Aksay, and Colleen E. Clancy. 2012. 'Computational Modeling Reveals Dendritic Origins of GABAA-Mediated Excitation in CA1 Pyramidal Neurons' ed. Maxim Bazhenov. *PLoS ONE* 7(10): e47250.

Li, Chuanchuan et al. 2014. 'Structural and Biochemical Insights into the Activation Mechanisms of Germinal Center Kinase OSR1'. *Journal of Biological Chemistry* 289(52): 35969–78.

Li, Hong et al. 2002. 'Patterns of Cation-Chloride Cotransporter Expression during Embryonic Rodent CNS Development: Cl^- Cotransporters in Embryonic Brain Development'. *European Journal of Neuroscience* 16(12): 2358–70.

Li, Hong et al. 2007. 'KCC2 Interacts with the Dendritic Cytoskeleton to Promote Spine Development'. *Neuron* 56(6): 1019–33.

Lillis, Kyle P et al. 2012. 'Pyramidal Cells Accumulate Chloride at Seizure Onset'. *Neurobiology of Disease*: 9.

Liu, Ru et al. 2020. 'Role of NKCC1 and KCC2 in Epilepsy: From Expression to

Function’. *Frontiers in Neurology* 10: 1407.

Liu, Si et al. 2019. ‘Cryo-EM Structures of the Human Cation-Chloride Cotransporter KCC1’. *Science* 366(6464): 505–8.

Lorenzo, Louis-Etienne et al. 2020. ‘Enhancing Neuronal Chloride Extrusion Rescues A2/A3 GABAA-Mediated Analgesia in Neuropathic Pain’. *Nature Communications* 11(1): 869.

Lozovaya, N. et al. 2018. ‘GABAergic Inhibition in Dual-Transmission Cholinergic and GABAergic Striatal Interneurons Is Abolished in Parkinson Disease’. *Nature Communications* 9(1): 1422.

———. 2019. ‘Early Alterations in a Mouse Model of Rett Syndrome: The GABA Developmental Shift Is Abolished at Birth’. *Scientific Reports* 9(1): 9276.

Lu, Juu-Chin, Yu-Tien Hsiao, Chung-Wei Chiang, and Chih-Tien Wang. 2014. ‘GABAA Receptor-Mediated Tonic Depolarization in Developing Neural Circuits’. *Mol Neurobiol*: 22.

de Luca, Emanuela et al. 2017. ‘Inter-Synaptic Lateral Diffusion of GABAA Receptors Shapes Inhibitory Synaptic Currents’. *Neuron* 95(1): 63-69.e5.

Lucas, Olivier, Cécile Hilaire, Eric Delpire, and Frédérique Scamps. 2012. ‘KCC3-Dependent Chloride Extrusion in Adult Sensory Neurons’. *Molecular and Cellular Neuroscience* 50(3–4): 211–20.

Luhmann, H. J., S. Kirischuk, and W. Kilb. 2014. ‘Comment on “Local Impermeant Anions Establish the Neuronal Chloride Concentration”’. *Science* 345(6201): 1130–1130.

Luhmann, H. J., and D. A. Prince. 1991. ‘Postnatal Maturation of the GABAergic System in Rat Neocortex’. *Journal of Neurophysiology* 65(2): 247–63.

Luo, Wen-di et al. 2018. ‘Vitexin Reduces Epilepsy after Hypoxic Ischemia in the Neonatal Brain via Inhibition of NKCC1’. *Journal of Neuroinflammation* 15(1): 186.

Magloire, Vincent et al. 2019. ‘KCC2 Overexpression Prevents the Paradoxical Seizure-Promoting Action of Somatic Inhibition’. *Nature Communications* 10(1): 1225.

Mahadevan, Vivek et al. 2017. ‘Native KCC2 Interactome Reveals PACSIN1 as a Critical Regulator of Synaptic Inhibition’. *eLife* 6: e28270.

Marandi, Nima, Arthur Konnerth, and Olga Garaschuk. 2002. ‘Two-Photon Chloride Imaging in Neurons of Brain Slices’. *Pfl*[illegible]*gers Archiv European Journal of Physiology* 445(3): 357–65.

Markkanen, Marika et al. 2014. ‘Distribution of Neuronal KCC2a and KCC2b Isoforms in Mouse CNS: Differential Localization of Kcc2 Isoforms’. *Journal of Comparative Neurology* 522(8): 1897–1914.

———. 2017. ‘Implications of the N-Terminal Heterogeneity for the Neuronal K-Cl Cotransporter KCC2 Function’. *Brain Research* 1675: 87–101.

McCormick, James A. et al. 2011. ‘A SPAK Isoform Switch Modulates Renal Salt Transport and Blood Pressure’. *Cell Metabolism* 14(3): 352–64.

Medina, Igor. ‘Current View on the Functional Regulation of the Neuronal K+-Cl- Cotransporter KCC2’. *Frontiers in Cellular Neuroscience*: 18.

Mejia-Gervacio, Sheyla, Kerren Murray, and Pierre-Marie Lledo. 2011. ‘NKCC1 Controls GABAergic Signaling and Neuroblast Migration in the Postnatal Forebrain’. *Neural Development* 6(1): 4.

Mele, Miranda, Rui O. Costa, and Carlos B. Duarte. 2019. ‘Alterations in GABAA-Receptor Trafficking and Synaptic Dysfunction in Brain Disorders’. *Frontiers in Cellular Neuroscience* 13: 77.

Mercado, Adriana et al. 2006. ‘A C-Terminal Domain in KCC2 Confers Constitutive K^+-Cl^- Cotransport’. *Journal of Biological Chemistry* 281(2): 1016–26.

Michalet, Xavier. 2010. ‘Mean Square Displacement Analysis of Single-Particle Trajectories with Localization Error: Brownian Motion in an Isotropic Medium’. *Physical Review E* 82(4): 041914.

Michaluk, P. et al. 2009. ‘Matrix Metalloproteinase-9 Controls NMDA Receptor Surface Diffusion through Integrin 1 Signaling’. *Journal of Neuroscience* 29(18): 6007–12.

Miesenböck, Gero, Dino A. De Angelis, and James E. Rothman. 1998. ‘Visualizing Secretion and Synaptic Transmission with PH-Sensitive Green Fluorescent Proteins’. *Nature* 394(6689): 192–95.

Milenković, I., and R. Rübsamen. 2011. ‘Development of the Chloride Homeostasis in the Auditory Brainstem’. *Physiological Research*: S15–27.

Min, Xiaoshan, Byung-Hoon Lee, Melanie H Cobb, and Elizabeth J Goldsmith. 2004. ‘Crystal Structure of the Kinase Domain of WNK1, a Kinase That Causes a Hereditary Form of Hypertension’. *Structure* 12(7): 1303–11.

Mody, Istvan. 2005. ‘Aspects of the Homeostaic Plasticity of $GABA_A$ Receptor-Mediated Inhibition: Homeostaic Plasticity of $GABA_A$ Receptor-Mediated Inhibition’. *The Journal of Physiology* 562(1): 37–46.

Mody, Istvan, and Robert A. Pearce. 2004. ‘Diversity of Inhibitory Neurotransmission

through GABAA Receptors'. *Trends in Neurosciences* 27(9): 569–75.

Moon, Thomas M. et al. 2013. 'Solution Structure of the WNK1 Autoinhibitory Domain, a WNK-Specific PF2 Domain'. *Journal of Molecular Biology* 425(8): 1245–52.

Moore, Yvonne E. et al. 2018. 'Potentiating KCC2 Activity Is Sufficient to Limit the Onset and Severity of Seizures'. *Proceedings of the National Academy of Sciences* 115(40): 10166–71.

Moore-Hoon, Marilyn L., and R. James Turner. 2000. 'The Structural Unit of the Secretory $Na^{+}-K^{+}-2Cl^{-}$ Cotransporter (NKCC1) Is a Homodimer'. *Biochemistry* 39(13): 3718–24.

Morales-Aza, Begonia M., Naomi L. Chillingworth, John A. Payne, and Lucy F. Donaldson. 2004. 'Inflammation Alters Cation Chloride Cotransporter Expression in Sensory Neurons'. *Neurobiology of Disease* 17(1): 62–69.

Moriguchi, Tetsuo et al. 2005. 'WNK1 Regulates Phosphorylation of Cation-Chloride-Coupled Cotransporters via the STE20-Related Kinases, SPAK and OSR1'. *Journal of Biological Chemistry* 280(52): 42685–93.

Murata, Yasunobu, and Matthew T. Colonnese. 2020. 'GABAergic Interneurons Excite Neonatal Hippocampus in Vivo'. *Science Advances* 6(24): eaba1430.

Murillo-de-Ozores, Adrián Rafael et al. 2018. 'C-Terminally Truncated, Kidney-Specific Variants of the WNK4 Kinase Lack Several Sites That Regulate Its Activity'. *Journal of Biological Chemistry* 293(31): 12209–21.

———. 2020. 'Physiological Processes Modulated by the Chloride-Sensitive WNK-SPAK/OSR1 Kinase Signaling Pathway and the Cation-Coupled Chloride Cotransporters'. *Frontiers in Physiology* 11: 585907.

Nickell, William T., Nancy K. Kleene, Robert C. Gesteland, and Steven J. Kleene. 2006. 'Neuronal Chloride Accumulation in Olfactory Epithelium of Mice Lacking NKCC1'. *Journal of Neurophysiology* 95(3): 2003–6.

Nickell, William T., Nancy K. Kleene, and Steven J. Kleene. 2007. 'Mechanisms of Neuronal Chloride Accumulation in Intact Mouse Olfactory Epithelium: Neuronal Chloride Accumulation in Olfactory Epithelium'. *The Journal of Physiology* 583(3): 1005–20.

Omer, Salma, Rainelli Koumangoye, and Eric Delpire. 2020. 'A Mutation in the Na-K-2Cl Cotransporter-1 Leads to Changes in Cellular Metabolism'. *Journal of Cellular Physiology* 235(10): 7239–50.

Otsu, Yo, Florian Donneger, Eric J Schwartz, and Jean Christophe Poncer. 2020. 'Cation–Chloride Cotransporters and the Polarity of GABA Signalling in Mouse Hippocampal Parvalbumin Interneurons'. *The Journal of Physiology* 598(10):

1865–80.

Owens, David F, Leslie H Boyce, Marion B E Davis, and Arnold R Kriegstein. ‘Excitatory GABA Responses in Embryonic and Neonatal Cortical Slices Demonstrated by Gramicidin Perforated-Patch Recordings and Calcium Imaging’. : 10.

Pacheco-Alvarez, Diana et al. 2020. ‘WNK3 and WNK4 Exhibit Opposite Sensitivity with Respect to Cell Volume and Intracellular Chloride Concentration’. *American Journal of Physiology-Cell Physiology* 319(2): C371–80.

Palma, E. et al. 2006. ‘Anomalous Levels of Cl- Transporters in the Hippocampal Subiculum from Temporal Lobe Epilepsy Patients Make GABA Excitatory’. *Proceedings of the National Academy of Sciences* 103(22): 8465–68.

Pan-Vazquez, Alejandro. ‘Activity-Dependent Plasticity of Axo-Axonic Synapses at the Axon Initial Segment’. : 19.

Paredes, Jose M. et al. 2016. ‘Synchronous Bioimaging of Intracellular PH and Chloride Based on LSS Fluorescent Protein’. *ACS Chemical Biology* 11(6): 1652–60.

Parvin, Most. Nahid, Tudevdagva Gerelsaikhan, and R. James Turner. 2007. ‘Regions in the Cytosolic C-Terminus of the Secretory Na^{+}-K^{+}-$2Cl^{-}$ Cotransporter NKCC1 Are Required for Its Homodimerization †’. *Biochemistry* 46(33): 9630–37.

Payne, John A. 1997. ‘Functional Characterization of the Neuronal-Specific K-Cl Cotransporter: Implications for $[K^{+}]_{o}$ Regulation’. *American Journal of Physiology-Cell Physiology* 273(5): C1516–25.

Payne, John A, Claudio Rivera, Juha Voipio, and Kai Kaila. 2003. ‘Cation–Chloride Co-Transporters in Neuronal Communication, Development and Trauma’. *Trends in Neurosciences* 26(4): 199–206.

Payne, John A., Tamara J. Stevenson, and Lucy F. Donaldson. 1996. ‘Molecular Characterization of a Putative K-Cl Cotransporter in Rat Brain: A NEURONAL-SPECIFIC ISOFORM’. *Journal of Biological Chemistry* 271(27): 16245–52.

Peng, Liang et al. 2013. ‘Methodological Limitations in Determining Astrocytic Gene Expression’. *Frontiers in Endocrinology* 4. http://journal.frontiersin.org/article/10.3389/fendo.2013.00176/abstract (December 3, 2020).

Perreault, P, and M Avoli. 1992. ‘4-Aminopyridine-Induced Epileptiform Activity and a GABA-Mediated Long- Lasting Depolarization in the Rat Hippocampus’. *The Journal of Neuroscience* 12(1): 104–15.

Perrot-Sinal, T. S. et al. 2007. ‘Sex Differences in the Chloride Cotransporters, NKCC1 and KCC2, in the Developing Hypothalamus’. *Journal of Neuroendocrinology*

19(4): 302–8.

Persson, Fredrik, Martin Lindén, Cecilia Unoson, and Johan Elf. 2013. ‘Extracting Intracellular Diffusive States and Transition Rates from Single-Molecule Tracking Data’. *Nature Methods* 10(3): 265–69.

Petrini, Enrica Maria et al. 2009. ‘Endocytic Trafficking and Recycling Maintain a Pool of Mobile Surface AMPA Receptors Required for Synaptic Potentiation’. *Neuron* 63(1): 92–105.

Petrini, Enrica Maria, and Andrea Barberis. 2014. ‘Diffusion Dynamics of Synaptic Molecules during Inhibitory Postsynaptic Plasticity’. *Frontiers in Cellular Neuroscience* 8. http://journal.frontiersin.org/article/10.3389/fncel.2014.00300/abstract (December 29, 2020).

Pfeffer, C. K. et al. 2009. ‘NKCC1-Dependent GABAergic Excitation Drives Synaptic Network Maturation during Early Hippocampal Development’. *Journal of Neuroscience* 29(11): 3419–30.

Piala, A. T. et al. 2014. ‘Chloride Sensing by WNK1 Involves Inhibition of Autophosphorylation’. *Science Signaling* 7(324): ra41–ra41.

Piechotta, Kerstin, Nicole Garbarini, Roger England, and Eric Delpire. 2003. ‘Characterization of the Interaction of the Stress Kinase SPAK with the Na^+-K^+-$2Cl^-$ Cotransporter in the Nervous System: EVIDENCE FOR A SCAFFOLDING ROLE OF THE KINASE’. *Journal of Biological Chemistry* 278(52): 52848–56.

Piechotta, Kerstin, Jianming Lu, and Eric Delpire. 2002. ‘Cation Chloride Cotransporters Interact with the Stress-Related Kinases Ste20-Related Proline-Alanine-Rich Kinase (SPAK) and Oxidative Stress Response 1 (OSR1)’. *Journal of Biological Chemistry* 277(52): 50812–19.

Pisella, Lucie I. et al. 2019. ‘Impaired Regulation of KCC2 Phosphorylation Leads to Neuronal Network Dysfunction and Neurodevelopmental Pathology’. *Science Signaling* 12(603): eaay0300.

Plotkin, M. D. et al. 1997. ‘Expression of the Na(+)-K(+)-2Cl- Cotransporter BSC2 in the Nervous System’. *American Journal of Physiology-Cell Physiology* 272(1): C173–83.

van den Pol, Anthony N., Karl Obrietan, and Gong Chen. 1996. ‘Excitatory Actions of GABA after Neuronal Trauma’. *The Journal of Neuroscience* 16(13): 4283–92.

Ponce-Coria, J. et al. 2008. ‘Regulation of NKCC2 by a Chloride-Sensing Mechanism Involving the WNK3 and SPAK Kinases’. *Proceedings of the National Academy of Sciences* 105(24): 8458–63.

Ponce-Coria, Jose et al. 2014. ‘A Novel Ste20-Related Proline/Alanine-Rich Kinase (SPAK)-Independent Pathway Involving Calcium-Binding Protein 39 (Cab39) and Serine Threonine Kinase with No Lysine Member 4 (WNK4) in the Activation of Na-K-Cl Cotransporters’. *Journal of Biological Chemistry* 289(25): 17680–88.

Pond, B. B. 2006. ‘The Chloride Transporter Na+-K+-Cl- Cotransporter Isoform-1 Contributes to Intracellular Chloride Increases after In Vitro Ischemia’. *Journal of Neuroscience* 26(5): 1396–1406.

Puskarjov, M., F. Ahmad, K. Kaila, and P. Blaesse. 2012. ‘Activity-Dependent Cleavage of the K-Cl Cotransporter KCC2 Mediated by Calcium-Activated Protease Calpain’. *Journal of Neuroscience* 32(33): 11356–64.

Qian, H., M.P. Sheetz, and E.L. Elson. 1991. ‘Single Particle Tracking. Analysis of Diffusion and Flow in Two-Dimensional Systems’. *Biophysical Journal* 60(4): 910–21.

Race, Joanne E. et al. 1999. ‘Molecular Cloning and Functional Characterization of KCC3, a New K-Cl Cotransporter’. *American Journal of Physiology-Cell Physiology* 277(6): C1210–19.

Rafiqi, Fatema H. et al. 2010. ‘Role of the WNK-activated SPAK Kinase in Regulating Blood Pressure’. *EMBO Molecular Medicine* 2(2): 63–75.

Rahmani, Behrouz et al. 2018. ‘A Novel Nonsense Mutation in WNK1/HSN2 Associated with Sensory Neuropathy and Limb Destruction in Four Siblings of a Large Iranian Pedigree’. *BMC Neurology* 18(1): 195.

Raimondo, Joseph. 2013. ‘A Genetically-Encoded Chloride and PH Sensor for Dissociating Ion Dynamics in the Nervous System’. *Frontiers in Cellular Neuroscience* 7. http://journal.frontiersin.org/article/10.3389/fncel.2013.00202/abstract (December 8, 2020).

Randall, Jeffrey, Tina Thorne, and Eric Delpire. 1997. ‘Partial Cloning and Characterization of *Slc12a2* : The Gene Encoding the Secretory Na^{+}-K^{+}-$2Cl^{-}$ Cotransporter’. *American Journal of Physiology-Cell Physiology* 273(4): C1267–77.

Reid, Michelle S, David M Kern, and Stephen Graf Brohawn. 2020. ‘Cryo-EM Structure of the Potassium-Chloride Cotransporter KCC4 in Lipid Nanodiscs’. *eLife* 9: e52505.

Renner, Marianne et al. 2017. ‘A Simple and Powerful Analysis of Lateral Subdiffusion Using Single Particle Tracking’. *Biophysical Journal* 113(11): 2452–63.

Renner, Marianne L. et al. 2009. ‘The Excitatory Postsynaptic Density Is a Size

Exclusion Diffusion Environment’. *Neuropharmacology* 56(1): 30–36.

Reuter, Dirk, Karl Zierold, Walter H. Schröder, and Stephan Frings. 1998. ‘A Depolarizing Chloride Current Contributes to Chemoelectrical Transduction in Olfactory Sensory Neurons *In Situ*’. *The Journal of Neuroscience* 18(17): 6623–30.

Richardson, C. et al. 2008. ‘Activation of the Thiazide-Sensitive Na+-Cl- Cotransporter by the WNK-Regulated Kinases SPAK and OSR1’. *Journal of Cell Science* 121(5): 675–84.

Righes Marafiga, Joseane, Mayara Vendramin Pasquetti, and Maria Elisa Calcagnotto. 2020. ‘GABAergic Interneurons in Epilepsy: More than a Simple Change in Inhibition’. *Epilepsy & Behavior*: 106935.

Rinehart, J. et al. 2005. ‘WNK3 Kinase Is a Positive Regulator of NKCC2 and NCC, Renal Cation-Cl- Cotransporters Required for Normal Blood Pressure Homeostasis’. *Proceedings of the National Academy of Sciences* 102(46): 16777–82.

Rinehart, Jesse et al. 2009. ‘Sites of Regulated Phosphorylation That Control K-Cl Cotransporter Activity’. *Cell* 138(3): 525–36.

———. 2011. ‘WNK2 Kinase Is a Novel Regulator of Essential Neuronal Cation-Chloride Cotransporters’. *Journal of Biological Chemistry* 286(34): 30171–80.

Rinetti-Vargas, Gina, Khanhky Phamluong, Dorit Ron, and Kevin J. Bender. 2017. ‘Periadolescent Maturation of GABAergic Hyperpolarization at the Axon Initial Segment’. *Cell Reports* 20(1): 21–29.

Rivera, Claudio et al. 1999. ‘The K+/ClÐ Co-Transporter KCC2 Renders GABA Hyperpolarizing during Neuronal Maturation’. 397: 5.

Rivière, Jean-Baptiste et al. 2004. ‘A Mutation in the *HSN2* Gene Causes Sensory Neuropathy Type II in a Lebanese Family: Mutation in *HSN2* Causes HSN II’. *Annals of Neurology* 56(4): 572–75.

Robel, Stefanie et al. ‘Reactive Astrogliosis Causes the Development of Spontaneous Seizures’. : 16.

Russell, John M. 2000. ‘Sodium-Potassium-Chloride Cotransport’. 80: 66.

Saxton, Michael J., and Ken Jacobson. 1997. ‘SINGLE-PARTICLE TRACKING:Applications to Membrane Dynamics’. *Annual Review of Biophysics and Biomolecular Structure* 26(1): 373–99.

Saxton, M.J. 1993. ‘Lateral Diffusion in an Archipelago. Single-Particle Diffusion’. *Biophysical Journal* 64(6): 1766–80.

Schiapparelli, Paula et al. 2017. ‘NKCC1 Regulates Migration Ability of Glioblastoma Cells by Modulation of Actin Dynamics and Interacting with Cofilin’. *EBioMedicine* 21: 94–103.

Schmidt, Tobias et al. 2018. ‘Differential Regulation of Chloride Homeostasis and GABAergic Transmission in the Thalamus’. *Scientific Reports* 8(1): 13929.

Schulte, Joran T., Corette J. Wierenga, and Hilgo Bruining. 2018. ‘Chloride Transporters and GABA Polarity in Developmental, Neurological and Psychiatric Conditions’. *Neuroscience & Biobehavioral Reviews* 90: 260–71.

Sedmak, Goran et al. 2016. ‘Developmental Expression Patterns of KCC2 and Functionally Associated Molecules in the Human Brain’. *Cerebral Cortex* 26(12): 4574–89.

Shekarabi, Masoud et al. 2008. ‘Mutations in the Nervous System–Specific HSN2 Exon of WNK1 Cause Hereditary Sensory Neuropathy Type II’. *Journal of Clinical Investigation*: JCI34088.

———. 2017. ‘WNK Kinase Signaling in Ion Homeostasis and Human Disease’. *Cell Metabolism* 25(2): 285–99.

Silayeva, Liliya et al. 2015. ‘KCC2 Activity Is Critical in Limiting the Onset and Severity of Status Epilepticus’. *Proceedings of the National Academy of Sciences* 112(11): 3523–28.

Sipilä, Sampsa T. et al. 2006. ‘The Cation-Chloride Cotransporter NKCC1 Promotes Sharp Waves in the Neonatal Rat Hippocampus: NKCC1 Promotes Early Sharp Waves’. *The Journal of Physiology* 573(3): 765–73.

Sivakumaran, S. et al. 2015. ‘Selective Inhibition of KCC2 Leads to Hyperexcitability and Epileptiform Discharges in Hippocampal Slices and In Vivo’. *Journal of Neuroscience* 35(21): 8291–96.

Sivakumaran, Sudhir, and Jamie Maguire. 2016. ‘Bumetanide Reduces Seizure Progression and the Development of Pharmacoresistant Status Epilepticus’. *Epilepsia* 57(2): 222–32.

Smalley, Joshua L. et al. 2020. ‘Isolation and Characterization of Multi-Protein Complexes Enriched in the K-Cl Co-Transporter 2 From Brain Plasma Membranes’. *Frontiers in Molecular Neuroscience* 13: 563091.

Smart, Trevor G, and F Anne Stephenson. 2019. ‘A Half Century of γ-Aminobutyric Acid’. *Brain and Neuroscience Advances* 3: 239821281985824.

Starke, L. C., and M. L. Jennings. 1993. ‘K-Cl Cotransport in Rabbit Red Cells: Further Evidence for Regulation by Protein Phosphatase Type 1’. *American Journal of Physiology-Cell Physiology* 264(1): C118–24.

Stefanits, Harald et al. 2019. ‘Alterations in GABAA Receptor Subunit Expression in the Amygdala and Entorhinal Cortex in Human Temporal Lobe Epilepsy’. *Journal of Neuropathology & Experimental Neurology* 78(11): 1022–48.

Steffensen, Annette B. et al. 2018. ‘Cotransporter-Mediated Water Transport Underlying Cerebrospinal Fluid Formation’. *Nature Communications* 9(1): 2167.

Stein, Valentin, Irm Hermans-Borgmeyer, Thomas J. Jentsch, and Christian A. Hübner. 2004. ‘Expression of the KCl Cotransporter KCC2 Parallels Neuronal Maturation and the Emergence of Low Intracellular Chloride: Temporal Expression of KCC2’. *Journal of Comparative Neurology* 468(1): 57–64.

Stenesen, Drew et al. 2019. ‘The Glial Sodium-Potassium-2-Chloride Cotransporter Is Required for Synaptic Transmission in the Drosophila Visual System’. *Scientific Reports* 9(1): 2475.

Strange, Kevin, Thomas D. Singer, Rebecca Morrison, and Eric Delpire. 2000. ‘Dependence of KCC2 K-Cl Cotransporter Activity on a Conserved Carboxy Terminus Tyrosine Residue’. *American Journal of Physiology-Cell Physiology* 279(3): C860–67.

Succol, Francesca et al. 2012. ‘Intracellular Chloride Concentration Influences the GABAA Receptor Subunit Composition’. *Nature Communications* 3(1): 738.

Sulis Sato, Sebastian et al. 2017. ‘Simultaneous Two-Photon Imaging of Intracellular Chloride Concentration and PH in Mouse Pyramidal Neurons in Vivo’. *Proceedings of the National Academy of Sciences* 114(41): E8770–79.

Sun, Dandan, and Sangita G. Murali. 1999. ‘Na^+-K^+-$2Cl^-$ Cotransporter in Immature Cortical Neurons: A Role in Intracellular Cl^- Regulation’. *Journal of Neurophysiology* 81(4): 1939–48.

Sun, Qifei et al. 2018. ‘Intracellular Chloride and Scaffold Protein Mo25 Cooperatively Regulate Transepithelial Ion Transport through WNK Signaling in the Malpighian Tubule’. *Journal of the American Society of Nephrology* 29(5): 1449–61.

Sung, Ki-Wug et al. 2000. ‘Abnormal $GABA_A$ Receptor-Mediated Currents in Dorsal Root Ganglion Neurons Isolated from Na–K–2Cl Cotransporter Null Mice’. *The Journal of Neuroscience* 20(20): 7531–38.

Taira, Tomi, Karri Lamsa, and Kai Kaila. 1997. ‘Posttetanic Excitation Mediated by $GABA_A$ Receptors in Rat CA1 Pyramidal Neurons’. *Journal of Neurophysiology* 77(4): 2213–18.

Tang, Bor Luen. 2020. ‘The Expanding Therapeutic Potential of Neuronal KCC2’. *Cells* 9(1): 240.

Tanimura, Akihiko, Kinji Kurihara, Stephan J Reshkin, and R James Turner.

‘Involvement of Direct Phosphorylation in the Regulation of the Rat Parotid Na⁺-K⁺-2Cl⁻ Cotransporter’. : 8.

Tao-Cheng, Jung-Hwa. 2020. ‘Stimulation-Induced Differential Redistributions of Clathrin and Clathrin-Coated Vesicles in Axons Compared to Soma/Dendrites’. *Molecular Brain* 13(1): 141.

Taylor-Burds, Carol, Paul Cheng, and Susan Wray. 2015. ‘Chloride Accumulators NKCC1 and AE2 in Mouse GnRH Neurons: Implications for GABAA Mediated Excitation’ ed. Andrew Wolfe. *PLOS ONE* 10(6): e0131076.

Thastrup, Jacob O. et al. 2012. ‘SPAK/OSR1 Regulate NKCC1 and WNK Activity: Analysis of WNK Isoform Interactions and Activation by T-Loop Trans-Autophosphorylation’. *Biochemical Journal* 441(1): 325–37.

Titz, Stefan, Esther M. Sammler, and Sheriar G. Hormuzdi. 2015. ‘Could Tuning of the Inhibitory Tone Involve Graded Changes in Neuronal Chloride Transport?’ *Neuropharmacology* 95: 321–31.

Toulme, Estelle, and Baljit S. Khakh. 2012. ‘Imaging P2X4 Receptor Lateral Mobility in Microglia: REGULATION BY CALCIUM AND P38 MAPK’. *Journal of Biological Chemistry* 287(18): 14734–48.

Treiman, David M. 2001. ‘GABAergic Mechanisms in Epilepsy’. *Epilepsia* 42: 8–12.

Triller, Antoine, and Daniel Choquet. 2008. ‘New Concepts in Synaptic Biology Derived from Single-Molecule Imaging’. *Neuron* 59(3): 359–74.

Tyzio, Roman et al. 2008. ‘Postnatal Changes in Somatic γ-Aminobutyric Acid Signalling in the Rat Hippocampus’. *European Journal of Neuroscience* 27(10): 2515–28.

Ushiro, Hiroshi et al. 1998. ‘Molecular Cloning and Characterization of a Novel Ste20-Related Protein Kinase Enriched in Neurons and Transporting Epithelia’. *Archives of Biochemistry and Biophysics* 355(2): 233–40.

Uvarov, Pavel et al. 2007. ‘A Novel N-Terminal Isoform of the Neuron-Specific K-Cl Cotransporter KCC2’. *Journal of Biological Chemistry* 282(42): 30570–76.

———. 2009. ‘Coexpression and Heteromerization of Two Neuronal K-Cl Cotransporter Isoforms in Neonatal Brain’. *Journal of Biological Chemistry* 284(20): 13696–704.

Verkman, A.S. et al. 1989. ‘Synthesis and Characterization of Improved Chloride-Sensitive Fluorescent Indicators for Biological Applications’. *Analytical Biochemistry* 178(2): 355–61.

Vibat, Cecile Rose T. et al. 2001. ‘Quantitation of Na+-K+-2Cl− Cotransport Splice

Variants in Human Tissues Using Kinetic Polymerase Chain Reaction'. *Analytical Biochemistry* 298(2): 218–30.

Vida, Imre, Marlene Bartos, and Peter Jonas. 2006. 'Shunting Inhibition Improves Robustness of Gamma Oscillations in Hippocampal Interneuron Networks by Homogenizing Firing Rates'. *Neuron* 49(1): 107–17.

Vidal-Petiot, E. et al. 2013. 'WNK1-Related Familial Hyperkalemic Hypertension Results from an Increased Expression of L-WNK1 Specifically in the Distal Nephron'. *Proceedings of the National Academy of Sciences* 110(35): 14366–71.

Viitanen, Tero, Eva Ruusuvuori, Kai Kaila, and Juha Voipio. 2010. 'The K^+-Cl^- Cotransporter KCC2 Promotes GABAergic Excitation in the Mature Rat Hippocampus: GABA Excitation and KCC2'. *The Journal of Physiology* 588(9): 1527–40.

Villa, Fabrizio et al. 2007. 'Structural Insights into the Recognition of Substrates and Activators by the OSR1 Kinase'. *EMBO reports* 8(9): 839–45.

Virtanen, Mari A., Pavel Uvarov, Christian A. Hübner, and Kai Kaila. 2020. 'NKCC1, an Elusive Molecular Target in Brain Development: Making Sense of the Existing Data'. *Cells* 9(12): 2607.

Vitari, Alberto C, Maria Deak, Nick A Morrice, and Dario R Alessi. 2005. 'The WNK1 and WNK4 Protein Kinases That Are Mutated in Gordon's Hypertension Syndrome Phosphorylate and Activate SPAK and OSR1 Protein Kinases'. : 8.

Vitari, Alberto C. et al. 2006. 'Functional Interactions of the SPAK/OSR1 Kinases with Their Upstream Activator WNK1 and Downstream Substrate NKCC1'. *Biochemical Journal* 397(1): 223–31.

Voipio, J. et al. 2014. 'Comment on "Local Impermeant Anions Establish the Neuronal Chloride Concentration"'. *Science* 345(6201): 1130–1130.

Wang, Cong et al. 2002. 'Developmental Changes in KCC1, KCC2, and NKCC1 MRNA Expressions in the Rat Brain'. *Developmental Brain Research* 139(1): 59–66.

Wang, Doris D., and Arnold R. Kriegstein. 2011. 'Blocking Early GABA Depolarization with Bumetanide Results in Permanent Alterations in Cortical Circuits and Sensorimotor Gating Deficits'. *Cerebral Cortex* 21(3): 574–87.

Wang, S. et al. 2015. 'In Vivo Effects of Bumetanide at Brain Concentrations Incompatible with NKCC1 Inhibition on Newborn DGC Structure and Spontaneous EEG Seizures Following Hypoxia-Induced Neonatal Seizures'. *Neuroscience* 286: 203–15.

Wang, Ying, Yi Wang, and Zhong Chen. 2018. 'Double-Edged GABAergic Synaptic Transmission in Seizures: The Importance of Chloride Plasticity'. *Brain Research*

1701: 126–36.

Warmuth, Stefan, Iwan Zimmermann, and Raimund Dutzler. 2009. ‘X-Ray Structure of the C-Terminal Domain of a Prokaryotic Cation-Chloride Cotransporter’. *Structure* 17(4): 538–46.

Watanabe, Miho et al. 2019. ‘Developmentally Regulated KCC2 Phosphorylation Is Essential for Dynamic GABA-Mediated Inhibition and Survival’. *Science Signaling* 12(603): eaaw9315.

Watanabe, Miho, and Atsuo Fukuda. 2015. ‘Development and Regulation of Chloride Homeostasis in the Central Nervous System’. *Frontiers in Cellular Neuroscience* 9. http://journal.frontiersin.org/Article/10.3389/fncel.2015.00371/abstract (November 6, 2020).

Watanabe, Miho, Hiroaki Wake, Andrew J. Moorhouse, and Junichi Nabekura. 2009. ‘Clustering of Neuronal K^+-Cl^- Cotransporters in Lipid Rafts by Tyrosine Phosphorylation’. *Journal of Biological Chemistry* 284(41): 27980–88.

Weimann, Laura et al. 2013. ‘A Quantitative Comparison of Single-Dye Tracking Analysis Tools Using Monte Carlo Simulations’ ed. Attila Szolnoki. *PLoS ONE* 8(5): e64287.

Wilson, Corinne S., and Alexander A. Mongin. 2019. ‘The Signaling Role for Chloride in the Bidirectional Communication between Neurons and Astrocytes’. *Neuroscience Letters* 689: 33–44.

Wilson, F. H. 2001. ‘Human Hypertension Caused by Mutations in WNK Kinases’. *Science* 293(5532): 1107–12.

———. 2003. ‘Molecular Pathogenesis of Inherited Hypertension with Hyperkalemia: The Na-Cl Cotransporter Is Inhibited by Wild-Type but Not Mutant WNK4’. *Proceedings of the National Academy of Sciences* 100(2): 680–84.

Witte, M. et al. 2014. ‘Depolarizing Chloride Gradient in Developing Cochlear Nucleus Neurons: Underlying Mechanism and Implication for Calcium Signaling’. *Neuroscience* 261: 207–22.

Wright, Rebecca et al. 2017. ‘Neuronal Chloride Regulation via KCC2 Is Modulated through a $GABA_B$ Receptor Protein Complex’. *The Journal of Neuroscience* 37(22): 5447–62.

Wu, Degang et al. 2020. ‘Activated WNK3 Induced by Intracerebral Hemorrhage Deteriorates Brain Injury Maybe via WNK3/SPAK/NKCC1 Pathway’. *Experimental Neurology* 332: 113386.

Wu, Zi-Zhen, De-Pei Li, Shao-Rui Chen, and Hui-Lin Pan. 2009. ‘Aminopyridines Potentiate Synaptic and Neuromuscular Transmission by Targeting the Voltage-

Activated Calcium Channel β Subunit'. *Journal of Biological Chemistry* 284(52): 36453–61.

Xu, Bing-e et al. 2002. 'Regulation of WNK1 by an Autoinhibitory Domain and Autophosphorylation'. *Journal of Biological Chemistry* 277(50): 48456–62.

———. 'WNK1, a Novel Mammalian Serine/Threonine Protein Kinase Lacking the Catalytic Lysine in Subdomain II'. : 8.

Xu, J. C. et al. 1994. 'Molecular Cloning and Functional Expression of the Bumetanide-Sensitive Na-K-Cl Cotransporter.' *Proceedings of the National Academy of Sciences* 91(6): 2201–5.

Xu, Wangshu et al. 2017. 'Chloride Co-Transporter NKCC1 Inhibitor Bumetanide Enhances Neurogenesis and Behavioral Recovery in Rats After Experimental Stroke'. *Molecular Neurobiology* 54(4): 2406–14.

Yamada, Junko et al. 2004. 'Cl $^{-}$ Uptake Promoting Depolarizing GABA Actions in Immature Rat Neocortical Neurones Is Mediated by NKCC1: NKCC-1 Mediated Cl $^{-}$ Uptake Promoting Depolarizing GABA Actions'. *The Journal of Physiology* 557(3): 829–41.

Yang, Xiaoyong, Qinzhe Wang, and Erhu Cao. 2020. 'Structure of the Human Cation–Chloride Cotransporter NKCC1 Determined by Single-Particle Electron Cryo-Microscopy'. *Nature Communications* 11(1): 1016.

Yang, Xing-Liang et al. 2019. 'NFAT5 and HIF-1α Coordinate to Regulate NKCC1 Expression in Hippocampal Neurons After Hypoxia-Ischemia'. *Frontiers in Cell and Developmental Biology* 7: 339.

Yelhekar, Tushar D., Michael Druzin, and Staffan Johansson. 2017. 'Contribution of Resting Conductance, $GABA_A$-Receptor Mediated Miniature Synaptic Currents and Neurosteroid to Chloride Homeostasis in Central Neurons'. *eneuro* 4(2): ENEURO.0019-17.2017.

Zagórska, Anna et al. 2007. 'Regulation of Activity and Localization of the WNK1 Protein Kinase by Hyperosmotic Stress'. *Journal of Cell Biology* 176(1): 89–100.

Zarepour, Leila. 2020. 'Preliminary Study of Analgesic Effect of Bumetanide on Neuropathic Pain in Patients with Spinal Cord Injury'. *Journal of Clinical Neuroscience*: 8.

Zhang, Jinwei et al. 2016. 'Functional Kinomics Establishes a Critical Node of Volume-Sensitive Cation-Cl− Cotransporter Regulation in the Mammalian Brain'. *Scientific Reports* 6(1): 35986.

———. 2020. 'Modulation of Brain Cation-Cl− Cotransport via the SPAK Kinase Inhibitor ZT-1a'. *Nature Communications* 11(1): 78.

Zimanyi, Christina M. ‘Structure of the Regulatory Cytosolic Domain of a Eukaryotic Potassium-Chloride Cotransporter’. : 15.

Zions, Michael et al. 2020. ‘Nest Carbon Dioxide Masks GABA-Dependent Seizure Susceptibility in the Naked Mole-Rat’. *Current Biology* 30(11): 2068-2077.e4.

Neuronal Excitability

Activity-Dependent Inhibitory Synapse Scaling Is Determined by Gephyrin Phosphorylation and Subsequent Regulation of $GABA_A$ Receptor Diffusion

Sereina Battaglia,[4] Marianne Renner,[1,2,3] Marion Russeau,[1,2,3] Etienne Côme,[1,2,3] Shiva K. Tyagarajan,[4,5,*] and Sabine Lévi[1,2,3,*]

DOI:http://dx.doi.org/10.1523/ENEURO.0203-17.2017

[1]INSERM UMR-S, Paris, 75005, France, [2]Université Pierre et Marie Curie, Paris, 75005, France, [3]Institut du Fer a Moulin, Paris, 75005, France, [4]Institute of Pharmacology and Toxicology, University of Zürich, Zurich, 8057, Switzerland, and [5]Center for Neuroscience Zurich, Zurich, 8057, Switzerland

Abstract

Synaptic plasticity relies on the rapid changes in neurotransmitter receptor number at postsynaptic sites. Using superresolution photoactivatable localization microscopy imaging and quantum dot–based single-particle tracking in rat hippocampal cultured neurons, we investigated whether the phosphorylation status of the main scaffolding protein gephyrin influenced the organization of the gephyrin scaffold and $GABA_A$ receptor ($GABA_AR$) membrane dynamics. We found that gephyrin phosphorylation regulates gephyrin microdomain compaction. Extracellular signal–regulated kinase 1/2 and glycogen synthase kinase 3β (GSK3β) signaling alter the gephyrin scaffold mesh differentially. Differences in scaffold organization similarly affected the diffusion of synaptic $GABA_ARs$, suggesting reduced gephyrin receptor–binding properties. In the context of synaptic scaling, our results identify a novel role of the GSK3β signaling pathway in the activity-dependent regulation of extrasynaptic receptor surface trafficking and GSK3β, protein kinase A, and calcium/calmodulin-dependent protein kinase IIα pathways in facilitating adaptations of synaptic receptors.

Key words: GABAA receptor; homeostatic plasticity; PALM; post-translation modification; single particle tracking

Significance Statement

Our data identify phosphorylation as a key mechanism controlling the gephyrin scaffold mesh, and hence, the diffusion capture of $GABA_A$ receptors at inhibitory synapses. We further show how critical this mechanism is for inhibitory synaptic scaling.

Introduction

Fast synaptic inhibition mediated by $GABA_A$ receptors ($GABA_ARs$) plays an essential role in information transfer between neurons. In recent years GABAergic inhibition has been shown to be dynamic, allowing flexible adaptations (Chen et al., 2012). Within the paradigm of *in vitro*

Received June 9, 2017; accepted December 21, 2017; First published January 11, 2018.

Authors report no conflict of interest.

Author contributions: SL and SKT conceptualized the project and designed the experiments. SL supervised the experimental work. SB, EC, and MRu performed immunofluorescence and SPT experiments and analyzed the data together with SL. MRu prepared primary hippocampal neurons. MRe performed the superresolution experiments, developed data analysis tools, and analyzed the data. SL and SKT wrote the manuscript.

This work was supported in part by INSERM, Sorbonne Université-UPMC, LabEx Biopsy to SL, Olgamyenfisch Grant to SKT, and University of Zurich internal funding to SKT. EC is the recipient of a doctoral fellowship from the Université Pierre and Marie Curie. STORM/PALM equipment at the IFM was supported by DIM NeRF from Région Ile-de-France and by the FRC/Rotary 'Espoir en tête.' The Lévi lab is affiliated with the Paris School of Neuroscience (ENP) and the Bio-Psy Laboratory of Excellence.

*S.K.T. and S.L. are co-senior authors.

synaptic scaling, wherein the neuronal activity is pharmacologically manipulated for several hours to days, the effects of chronic changes in activity are still poorly understood at inhibitory synapses.

Neuronal inhibition is dynamically regulated by the amount of network activity. $GABA_AR$ stability at synaptic sites and subsequent proteasomal degradation is an essential component of synaptic homeostasis that strongly influences amplitude and frequency of miniature inhibitory postsynaptic currents (mIPSCs; Saliba et al., 2007). Similarly, lasting depolarization decreases $GABA_AR$ internalization on principal neurons and increases GAD65 cluster size at presynaptic GABAergic terminals (Rannals and Kapur, 2011). These observations highlight that multiple systems and pathways facilitate inhibitory synapse adjustments in response to chronic changes in activity.

At postsynaptic sites, lateral diffusion in and out of synapses can also rapidly alter receptor availability on acute activity elevation (Bannai et al., 2009, 2015). Chemical-induced long-term potentiation (iLTP) enhances phosphorylation of the $GABA_AR$ β3 subunit at serine 383 (S383) by calcium/calmodulin-dependent protein kinase IIα (CaMKIIα), resulting in reduced surface mobility of $GABA_ARs$, synaptic enrichment of receptors, and increased inhibitory neurotransmission (Petrini et al., 2014). Hence, apart from endocytosis and exocytosis, lateral diffusion of receptors could also be an effective mechanism of synaptic plasticity.

In recent years, it has become evident that the main scaffolding protein at the GABAergic synapse, gephyrin, is dynamically regulated, and this contributes to input-specific adaptations at postsynaptic sites (Chen et al., 2012; van Versendaal et al., 2012; Villa et al., 2016). Identification of signaling pathways that converge onto gephyrin scaffolds by causing posttranslational modifications of specific residues has shed new light on the molecular mechanisms underlying GABAergic synaptic plasticity. It was revealed that gephyrin phosphorylation by extracellular signal–regulated kinase 1/2 (ERK1/2) at serine 268 (S268) reduces scaffold size and GABAergic mIPSC amplitude (Tyagarajan et al., 2013). Similarly, blocking glycogen synthase kinase 3β (GSK3β) phosphorylation of gephyrin at serine 270 via the transgenic expression of the phospho-null mutant (S270A) significantly increases mIPSC frequency and amplitude (Tyagarajan et al., 2011). Theta burst stimulation (TBS) of CA3 Schaffer collaterals has been reported to induce gephyrin-mediated remodeling of GABAergic synapses in CA1 pyramidal cells (Flores et al., 2015). Although gephyrin phosphorylation at CaMKIIα sites is involved in this form of structural plasticity (Flores et al., 2015), the molecular basis for gephyrin phosphorylation–induced $GABA_AR$ synapse dynamics remains to be further explored.

To address this, we rendered gephyrin insensitive to ERK1/2 and GSK3β signaling pathways and studied their influence on $GABA_AR$ membrane diffusion properties. We report structural organization differences within gephyrin scaffolds based on phosphorylation status. Furthermore, cooperation between gephyrin and $GABA_ARs$ is differentially regulated by gephyrin phosphorylation status and changes in activity.

Material and Methods

Neuronal culture

Primary cultures of hippocampal neurons were prepared from hippocampi dissected at embryonic day 18 or 19 from Sprague-Dawley rats of either sex. Tissue was trypsinized (0.25% vol/vol) and mechanically dissociated in 1× HBSS (Invitrogen) containing 10 mM Hepes (Invitrogen). Neurons were plated at a density of 120 × 10^3 cells/ml onto 18-mm-diameter glass coverslips (Assistent) precoated with 50 μg/ml poly-D,L-ornithine (Sigma-Aldrich) in plating medium composed of minimum essential medium (MEM, Sigma-Aldrich) supplemented with horse serum (10% vol/vol, Invitrogen), L-glutamine (2 mM), and Na^+ pyruvate (1 mM; Invitrogen). After attachment for 3–4 h, cells were incubated in culture medium that consists of Neurobasal medium supplemented with B27 (1×), L-glutamine (2 mM), and antibiotics (penicillin 200 units/ml, streptomycin, 200 μg/ml; Invitrogen) for up to 4 wk at 37°C in a 5% CO_2 humidified incubator. Each week, one-fifth of the culture medium volume was replaced.

DNA constructs

The following constructs were used: *GEPHN* 3′-UTR shRNA and control shRNA-3m (Yu et al., 2007), DsRed-homer1c (Bats et al., 2007; provided by D. Choquet, IIN, Bordeaux, France), eGFP-gephyrin P1 variant (Lardi-Studler et al., 2007). eGFP- or pDendra2-WT, -S268E, -S270A, -DN, -S303A/S305A (SSA), and –SSA/S270A point mutants were generated using the eGFP-gephryin P1 variant as template for site-directed mutagenesis (Tyagarajan et al., 2011, 2013; Flores et al., 2015).

Neuronal transfection

Transfections were conducted at 14–15 days *in vitro* (DIV) using Lipofectamine 2000 (Invitrogen) or Transfectin (Bio-Rad), according to the manufacturers' instructions (DNA:transfectin ratio 1 μg:3 μl), with 1–1.2 μg of plasmid DNA per 20-mm well. The following ratio of plasmid DNA was used in cotransfection experiments: 0.5:0.5:0.3 μg for eGFP-S268E/eGFP-S270A/eGFP-DN/eGFP-SSA/eGFP-SSA/S270A:*GEPHN* 3′ UTR shRNA/*GEPHN* 3′ UTR-3m shRNA:DsRed-homer1c. Experiments were performed 6–9 d after transfection.

Pharmacology

4-Aminopyridine (4-AP, 100 mM, Sigma-Aldrich) was directly added to the culture medium, and the neurons

Acknowledgments: We are grateful to the Cell and Tissue Imaging Facility of Institut du Fer à Moulin (IFM).

Correspondence should be addressed to either of the following: Sabine Lévi, INSERM-UPMC UMR-S 839, 17 rue du Fer a Moulin, 75005 Paris, France. E-mail: sabine.levi@inserm.fr; or Shiva Tyagarajan, Institute of Pharmacology and Toxicology, University of Zürich, Winterthurerstrasse 190, 8057 Zurich, CH, Switzerland. E-mail: tyagarajan@pharma.uzh.ch.

DOI:http://dx.doi.org/10.1523/ENEURO.0203-17.2017

Copyright © 2018 Battaglia et al.

This is an open-access article distributed under the terms of the Creative Commons Attribution 4.0 International license, which permits unrestricted use, distribution and reproduction in any medium provided that the original work is properly attributed.

were returned to a 5% CO_2 humidified incubator for 8 or 48 h before use. For SPT experiments, neurons were labeled at 37°C in imaging medium (see below for composition) in the presence of 4-AP, transferred to a recording chamber, and recorded within 45 min at 31°C in imaging medium in the presence of 4-AP. The imaging medium consisted of phenol red–free MEM supplemented with glucose (33 mM; Sigma-Aldrich) and Hepes (20 mM), glutamine (2 mM), Na^+-pyruvate (1 mM), and B27 (1×) from Invitrogen.

Immunocytochemistry

Cells were fixed for 15 min at room temperature (RT) in paraformaldehyde (PFA, 4% wt/vol, Sigma-Aldrich) and sucrose (14% wt/vol, Sigma) solution prepared in PBS (1×). After washes in PBS, cells were permeabilized with Triton (0.25% vol/vol, Sigma-Aldrich) diluted in PBS. Cells were washed again in PBS and incubated for 1 h at RT in Triton (0.1% vol/vol, Sigma-Aldrich) and goat serum (GS, 10% vol/vol, Invitrogen) in PBS to block nonspecific staining. Subsequently, neurons were incubated for 1 h with a primary antibody mix consisting of guinea pig antibodies against $GABA_AR$ $\alpha2$ subunit (1:2000, provided by J.M. Fritschy, University of Zurich) and rabbit anti-VGAT (1:400, provided by B. Gasnier, University Paris Descartes, Paris) in PBS supplemented with GS (10% vol/vol, Invitrogen) and Triton (0.1% vol/vol, Sigma-Aldrich). After washes, cells were incubated for 60 min at RT with a secondary antibody mix containing biotinylated F(ab′)2 anti-guinea pig (1:300, Jackson Immunoresearch) and AMCA350-conjugated goat anti-rabbit (1:100, Jackson Laboratory) in PBS-GS-Triton blocking solution, washed, incubated for another 45 min with streptavidin-CY5 (1:300, Thermo Fisher Scientific), and finally mounted on glass slides using Mowiol 4-88 (48 mg/ml, Sigma-Aldrich). Sets of neurons compared for quantification were labeled simultaneously.

Fluorescence image acquisition and analysis

Image acquisition was performed using a 63× objective (NA 1.32) on a Leica DM6000 upright epifluorescence microscope with a 12-bit cooled CCD camera (Micromax, Roper Scientific) run by MetaMorph software (Roper Scientific). Quantification was performed using MetaMorph software. Image exposure time was determined on bright cells to obtain the best fluorescence-to-noise ratio and avoid pixel saturation. All images from a given culture were then acquired with the same exposure time and acquisition parameters. For each image, several dendritic regions of interest were manually chosen, and a user-defined intensity threshold was applied to select clusters and avoid their coalescence. For quantification of gephyrin or $GABA_AR$ $\alpha2$ synaptic clusters, gephyrin or receptor clusters comprising at least 3 pixels and colocalized on at least 1 pixel with VGAT clusters were considered. The integrated fluorescence intensities of clusters were measured.

Live-cell staining for single-particle imaging

Neurons were incubated for 3–5 min at 37°C with primary antibodies against extracellular epitopes of $GABA_AR$ $\alpha2$ subunit (guinea pig, 1:750/1:1000, provided by J.M. Fritschy), washed, and incubated for 3–5 min at 37°C with biotinylated Fab secondary antibodies (goat anti–guinea pig, 4–12 μg/ml; Jackson Immunoresearch) in imaging medium. After washes, cells were incubated for 1 min with streptavidin-coated quantum dots (QDs) emitting at 605 nm (1 nM; Invitrogen) in borate buffer (50 mM) supplemented with sucrose (200 mM) or in PBS (1 M; Invitrogen) supplemented with 10% casein (vol/vol; Sigma-Aldrich). Washing and incubation steps were all done in imaging medium. To assess the membrane dynamics of $GABA_AR$ $\alpha2$ subunit at inhibitory synapses in neurons expressing the eGFP-DN mutant, inhibitory synapses were stained by incubating live neurons for 48 h at 37°C in a 5% CO_2 humidified incubator with a primary VGAT antibody directly coupled to Oyster550 (1:200, Synaptic Systems) diluted in conditioned maintenance medium.

Single-particle tracking and analysis

Cells were imaged using an Olympus IX71 inverted microscope equipped with a 60× objective (NA 1.42; Olympus) and a Lambda DG-4 monochromator (Sutter Instrument). Individual images of gephyrin-eGFP and homer1c-GFP, and QD real time recordings (integration time of 75 ms over 600 consecutive frames) were acquired with Hamamatsu ImagEM EMCCD camera and MetaView software (Meta Imaging 7.7). Cells were imaged within 45 min after labeling.

QD tracking and trajectory reconstruction were performed with Matlab software (The Mathworks). One to two subregions of dendrites were quantified per cell. In cases of QD crossing, the trajectories were discarded from analysis. Trajectories were considered synaptic when overlapping with the synaptic mask of gephyrin-eGFP or VGAT-Oyster550 clusters, or extrasynaptic for spots 2 pixels (380 nm) away (Lévi et al., 2008). Values of the mean square displacement (MSD) plot versus time were calculated for each trajectory by applying the relation

$$MSD(n\tau) = \frac{1}{N-n}\sum_{i=1}^{N-n}(\{x[(i+n)\tau - x(i\tau)]^2\} + \{y[(i+n)\tau] - y(i\tau)\}^2),$$

(Saxton and Jacobson, 1997), where τ is the acquisition time, N is the total number of frames, and n and i are positive integers with n determining the time increment. Diffusion coefficients (D) were calculated by fitting the first four points without origin of the MSD versus time curves with the equation:$MSD(n\tau) = 4Dn\tau + b$, where b is a constant reflecting the spot localization accuracy. Synaptic dwell time was defined as the duration of detection of QDs at synapses on a recording divided by the number of exits as detailed previously (Ehrensperger et al., 2007; Charrier et al., 2010). Dwell times ≤5 frames were not retained. The explored area of each trajectory was defined as the MSD value of the trajectory at two different time intervals of 0.42 and 0.45 s (Renner et al., 2012).

PALM imaging

Photoactivatable localization microscopy (PALM) imaging on fixed samples was conducted on an inverted N-STORM Nikon Eclipse Ti microscope with a 100× oil-immersion objective (NA 1.49) and an Andor iXon Ultra EMCCD camera (image pixel size, 160 nm), using specific lasers for PALM imaging of Dendra2 (405 and 561 nm). Videos of 10,000 frames were acquired at frame rates of 50 ms. The *z* position was maintained during acquisition by a Nikon perfect focus system. Single-molecule localization and 2D image reconstruction was conducted as described in Specht et al. (2013) by fitting the PSF of spatially separated fluorophores to a 2D Gaussian distribution. The position of fluorophore were corrected by the relative movement of the synaptic cluster by calculating the center of mass of the cluster throughout the acquisition using a partial reconstruction of 2000 frames with a sliding window (Specht et al., 2013). PALM images were rendered by superimposing the coordinates of single-molecule detections, which were represented with 2D Gaussian curves of unitary intensity and SDs representing the localization accuracy ($\sigma = 20$ nm). To correct multiple detections coming from the same pDendra2 molecule (Specht et al., 2013), we identified detections occurring in the vicinity of space ($2\times \sigma$) and time (15 s) as belonging to the same molecule. The surface of gephyrin clusters and the densities of gephyrin molecules per square micrometer were measured in reconstructed 2D images through cluster segmentation based on detection densities. The threshold to define the border was set to 1000 detections/μm^2, taking into account the reported gephyrin densities in synapses (Specht et al., 2013; Fig. 3*B*). Briefly, all pixels (PALM pixel size = 20 nm) containing <2 detections were considered empty, and their intensity value was set to 0. The intensity of pixels with ≥ 2 detections was set to 1. The resulting binary image was analyzed with the function "regionprops" of Matlab to extract the surface area of each cluster identified by this function. Density was calculated as the total number of detections in the pixels belonging to a given cluster, divided by the area of the cluster.

Statistics

Sampling corresponds to the number of quantum dots for SPT, the number of cells for ICC, and the number of synapses for PALM. Sample size selection for experiments was based on published experiments, pilot studies, and in-house expertise. All results were used for analysis except in a few cases. Cells with signs of suffering (apparition of blobs, fragmented neurites) were discarded from the analysis. Means ± SEM are shown, and median values are indicated with their interquartile range (IQR, 25%–75%). Means were compared using the nonparametric Mann–Whitney test (immunocytochemistry, dwell time comparison, PALM quantifications) using SigmaPlot 12.5 (Systat Software). For diffusion coefficient and explored area values having nonnormal distributions, a nonparametric Kolmogorov–Smirnov test was run in Matlab. Differences were considered significant for *p*-values $<5\%$.

Results

eGFP-gephyrin mutants exhibit different clustering properties in culture

Signaling pathways that converge onto gephyrin scaffolding properties influence $GABA_AR$ synaptic transmission. Hence, mimicking phosphorylation/dephosphorylation events that influence gephyrin clustering can help gain critical insights into nanoscale regulation of $GABA_ARs$ at synaptic sites. ERK1/2 phosphorylation at the S268 residue results in smaller gephyrin clusters (Tyagarajan et al., 2013); hence, we selected phosphomimetic eGFP-gephyrin-S268E mutant to study the impact of smaller clusters on receptor diffusion. Similarly, pharmacological blockade of the GSK3β pathway or eGFP-gephyrin-S270A mutant expression increases gephyrin cluster number and size (Tyagarajan et al., 2011). We selected the eGFP-S270A mutant to understand how larger clusters would impact receptor diffusion. eGFP-gephyrin dominant negative (DN) mutant in primary neurons not only abolishes gephyrin clustering and reduces surface expression of $GABA_ARs$, but also significantly decreases GABAergic mIPSC amplitude and frequency (Ghosh et al., 2016). Hence, we selected eGFP-DN mutant to evaluate how cluster disruption would impact synaptic anchoring and surface diffusion of $GABA_ARs$.

Primary hippocampal neurons were cotransfected at 14 DIV with eGFP-gephyrin WT (eGFP-WT), eGFP-S268E, eGFP-S270A, or eGFP-DN along with shRNA targeting the gephyrin 3′ UTR (to minimize the influence of endogenous gephyrin expression on mutant phenotypes). Before studying the influence of altered gephyrin clustering on $GABA_AR$ diffusion properties, we confirmed the respective gephyrin mutant morphology 6–9 d after transfection. Representative images of neurons expressing either eGFP-WT or eGFP-S268E, eGFP-S270A, eGFP-DN variants are shown (Fig. 1*A*). We stained for the $\alpha 2$ $GABA_AR$ subunit to study the relation of eGFP-gephyrin with receptors. Quantification for eGFP-gephyrin cluster density (Nb), cluster size (area), and intensity (Int) showed a tendency for reduced clustering for the S268E mutant and increased clustering for the S270A mutant (Fig 1*B*). The impact of the gephyrin S270A mutation on gephyrin cluster area and intensity was more pronounced, in comparison to the S268E mutant. As expected, eGFP-DN failed to cluster (data not shown). Similar to the observed changes in eGFP-gephyrin morphology, quantification of cluster intensity for $\alpha 2$ $GABA_AR$ showed a significant increase in neurons expressing eGFP-S270A, whereas eGFP-S268E expressing neurons showed only a modest reduction in $\alpha 2$ (Fig. 1*C*). The neurons expressing eGFP-DN showed very little $\alpha 2$ $GABA_AR$ staining (data not shown).

Influence of eGFP-gephyrin mutants on $GABA_AR$ surface diffusion

$GABA_ARs$ are known to exhibit faster mobility at extrasynaptic sites compared with synaptic sites. Because of their interaction with the main scaffolding molecule gephyrin, $GABA_ARs$ are slowed down and confined at synapses. This diffusion-capture of $GABA_ARs$ is modu-

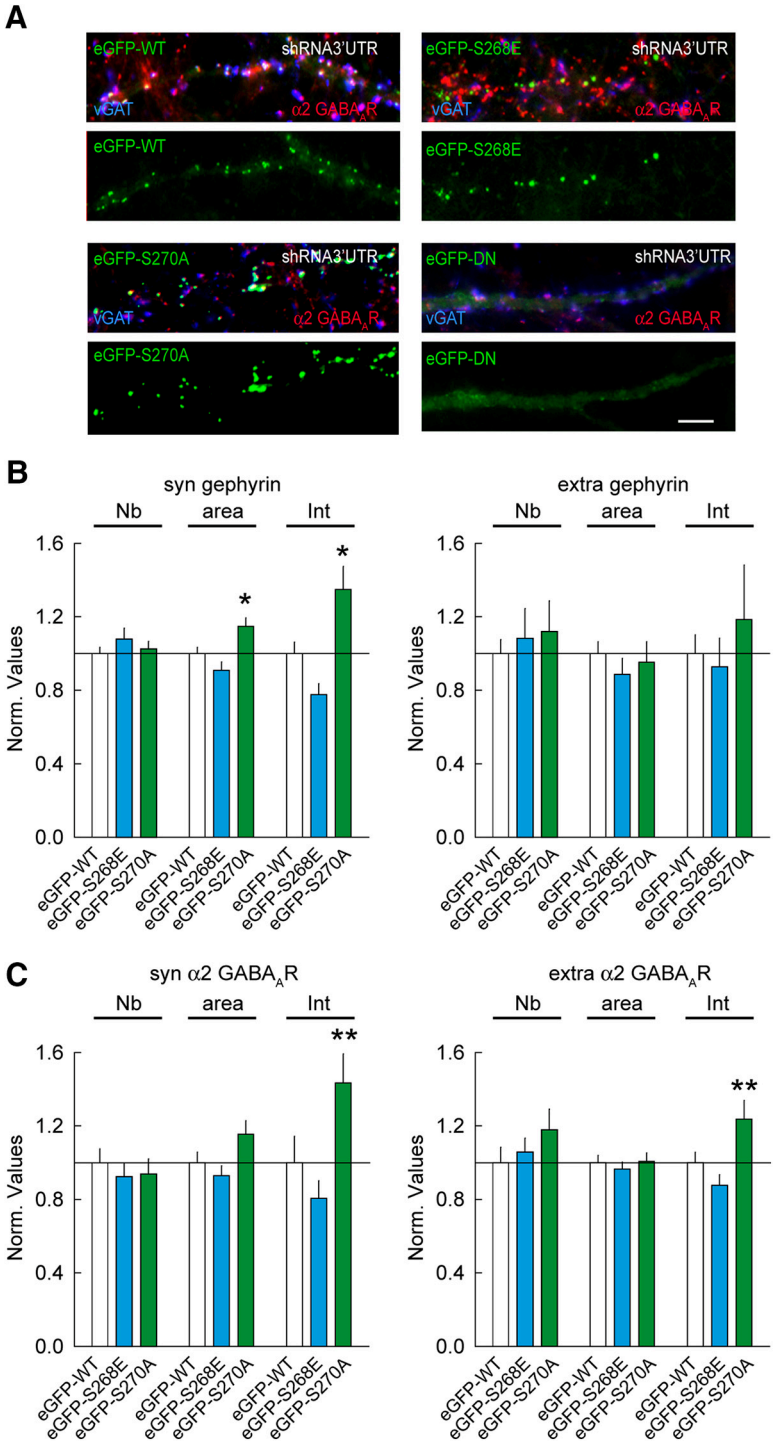

Figure 1. Morphologic characterization of eGFP-gephyrin and its mutant variants. ***A***, Representative images of primary hippocampal neurons cotransfected with eGFP-WT, eGFP-S268E, eGFP-S270A, or eGFP-DN and shRNA-3′UTR. eGFP-gephyrin clusters (green), α2 GABA$_A$Rs (red), and VGAT (blue) are shown. Scale bar, 10 μm. ***B***, Quantification of eGFP-gephyrin cluster density, cluster area, and intensity shows larger eGFP-S270A clusters compared with eGFP-WT at synapses. S268E: WT $n = 66$ cells, S268E $n = 60$ cells, 4 cultures. Syn: Cluster Number (Nb) $p = 0.42$, area $p = 0.22$, intensity $p = 0.05$. Extra: Nb $p = 0.99$, Area $p = 0.66$, Intensity $p = 0.44$. S270A: WT $n = 86$ cells, S270A: $n = 74$ cells, 6 cultures. Syn: Nb $p = 0.77$, Area $p = 0.02$, Intensity $p = 0.02$. Extra: Nb $p = 0.39$, Area $p = 0.42$, Intensity $p = 0.15$. ***C***, Quantification for α2 GABA$_A$R clusters shows significantly more receptors in eGFP-S270A mutant clusters. S268E: WT $n = 52$ cells, S268E $n = 47$ cells, 3 cultures. Syn: Nb $p = 0.48$, Area $p = 0.46$, Intensity $p = 0.6$. Extra: Nb $p = 0.46$, area $p = 0.63$, intensity $p = 0.22$. S270A: WT $n = 52$ cells, S270A $n = 39$ cells, 3 cultures. Syn: Nb $p = 0.56$, Area $p = 0.08$, Intensity $p = 0.008$. Extra: Nb $p = 0.008$, Area $p = 0.81$, Intensity $p = 0.29$. Data shown as mean ± SEM. Values were normalized to the corresponding control values. Statistics $*$, $p \leq 0.05$, $**$, $p \leq 0.01$ (Mann–Whitney rank sum test).

lated by neuronal activity and constitutes an important basis for synaptic plasticity (Petrini and Barberis, 2014). The expression of specific eGFP-gephyrin mutations allows us to lock the scaffold into different conformations and study its influence on $GABA_AR$ surface diffusion. To achieve this, we assessed the lateral mobility of $\alpha2$ $GABA_AR$ using quantum dot–based single-particle tracking (QD-SPT). Live imaging over 600 constitutive frames at 75 Hz was used to record individual trajectories, and the trajectories were later analyzed using custom software (Fig. 2*A*; see Methods). As a proof of concept, we first tested the effect of total gephyrin cluster removal on $\alpha2$ $GABA_AR$ surface dynamics by expressing the eGFP-DN mutant. However, given that eGFP-DN has a diffuse expression, to distinguish synaptic and extrasynaptic $\alpha2$ clusters we preloaded presynaptic GABAergic terminals using VGAT-Oyster550 antibody. The expression of the eGFP-DN mutant increased the surface exploration of QDs at both extrasynaptic and synaptic sites compared with control eGFP-WT. Quantification of the $\alpha2$ $GABA_AR$ diffusion coefficient showed a 1.4-fold increase for extrasynaptic receptors and a 1.2-fold increase for synaptic receptors in eGFP-DN–expressing neurons (Fig. 2*B*). Areas explored by $\alpha2$ $GABA_ARs$ also showed a 1.6-fold increase at extrasynaptic sites and a 1.3-fold increase at synaptic sites in eGFP-DN–expressing neurons (Fig. 2*C*). These observations support the notion that gephyrin slows down and confines $GABA_ARs$ not only at synapses but also at extrasynaptic sites (Ehrensperger et al., 2007).

Synaptic dwell time values can be discriminated from "trapped" receptors (dwell time >5.9 s) and "passing" receptors (dwell time ≤5.9 s; Renner et al., 2012). Quantification of $\alpha2$ $GABA_AR$ dwell time confirmed a 1.3-fold faster escape time of receptors in neurons expressing the eGFP-DN mutant (Fig. 2*D*). We did not observe any difference in this rate for passing receptors. This is an indication that the observed reduction of trapped receptors is not due to increased membrane viscosity, but rather to gephyrin scaffold's influence on $GABA_AR$ surface mobility. Thus, we concluded that the diffuse DN gephyrin relieved $GABA_AR$ $\alpha2$ diffusion constraints, leading to synaptic escape of receptors.

If gephyrin clustering can indeed influence receptor diffusion, then S268E and S270A modifications must have an influence on $\alpha2$ $GABA_AR$ surface mobility. To test this, we transfected the eGFP-S268E or eGFP-S270A mutants and measured surface mobility at extrasynaptic and synaptic locations. Superimposition of trajectories with fluorescent images of eGFP-gephyrin allowed us to distinguish synaptic versus extrasynaptic $\alpha2$ $GABA_ARs$. Neurons transfected with eGFP-S268E exhibited an increase in surface exploration of individual trajectories (Fig. 2*A*). This was consistent with the observed increase in diffusion coefficients at both extrasynaptic and synaptic sites (Fig. 2*E*). Similarly, quantification of explored areas at both extrasynaptic and synaptic sites showed significant increases (Fig. 2*F*). If reducing gephyrin cluster size facilitates $\alpha2$ diffusion, then we would expect shorter dwell time at synaptic sites. Indeed, we report reduced dwell time for trapped $\alpha2$ $GABA_ARs$ in eGFP-S268E–transfected neurons (Fig. 2*G*). Therefore the use of eGFP-S268E gephyrin mutant shows that the reduction in gephyrin cluster size causes an increase in $GABA_AR$ diffusion, while reducing synaptic dwell time.

On the other hand, in eGFP-S270A–transfected neurons, the $\alpha2$ $GABA_ARs$ showed increased surface exploration of individual trajectories at synapses (Fig. 2*A*). Unexpectedly, diffusion coefficients and surface exploration of $\alpha2$ extrasynaptic and synaptic $GABA_ARs$ were significantly increased in eGFP-S270A–transfected neurons (Fig. 2*E*,*F*). However, analysis showed no reduction in $\alpha2$ $GABA_AR$ dwell time at synaptic sites (Fig. 2*G*). We thus concluded that the increase in receptor mobility at synapses in S270A-transfected neurons does not correlate with what we may expect from a larger scaffold, suggesting additional regulations are at play.

Superresolution PALM microscopy reveals differential packing of gephyrin scaffold

We turned to quantitative nanoscopic imaging to understand the influence of phosphorylation on gephyrin scaffold organization. Using photoactivated localization microscopy (PALM), we estimated localization accuracy from several detections of the same fluorophore from subsequent image frames (Specht et al., 2013). The spatial resolution of PALM is within the range of ~25–30 nm; hence, image segmentation of the rendered PALM images can resolve substructure organization within a gephyrin cluster that are not discernable using diffraction-limited imaging (Specht et al., 2013).

Employing fluorescence imaging on primary hippocampal neurons cotransfected with photoconvertible pDendra2-WT, pDendra2-S268E, or pDendra2-S270A and shRNA 3′ UTR showed a clustering phenotype consistent with eGFP-gephyrin and its mutant variants (Fig. 3*A*). PALM image cluster segmentation was established based on local density of detections using a threshold of 1000 detections/μm^2 (Fig. 3*B*). Image segmentation allows us to estimate the mean surface area of a given pDendra2-WT cluster. In this case, quantification showed pDendra2-WT clusters to be 0.054 ± 0.003 μm^2, corresponding to the mean diameter of 262 nm as has been reported earlier (Specht et al., 2013). pDendra2-S268E quantifications showed a significant reduction in mean surface area to 0.035 ± 0.002 μm^2, and consistent with our expectations, pDendra2-S270A showed an increase in cluster area of 0.078 ± 0.005 μm^2 (Fig. 3*C*).

We next tried to correlate the estimated size of gephyrin clusters to their respective densities. Our analysis showed 3919.7 ± 227.9 molecules/μm^2 of pDendra2-WT within a cluster (Fig. 3*D*). pDendra2-S268E showed a significantly increased molecular density (4457.5 ± 221.6) despite having a smaller cluster area. In contrast, pDendra2-S270A mutant shows a significantly reduced molecular density (2819.8 ± 117.6), despite having a larger surface area (Fig. 3*D*).

Our data indicate that there is no correlation between the diffusion properties of $GABA_ARs$ despite the relative size difference between S268E and S270A gephyrin clusters. However, there is a strong correlation between

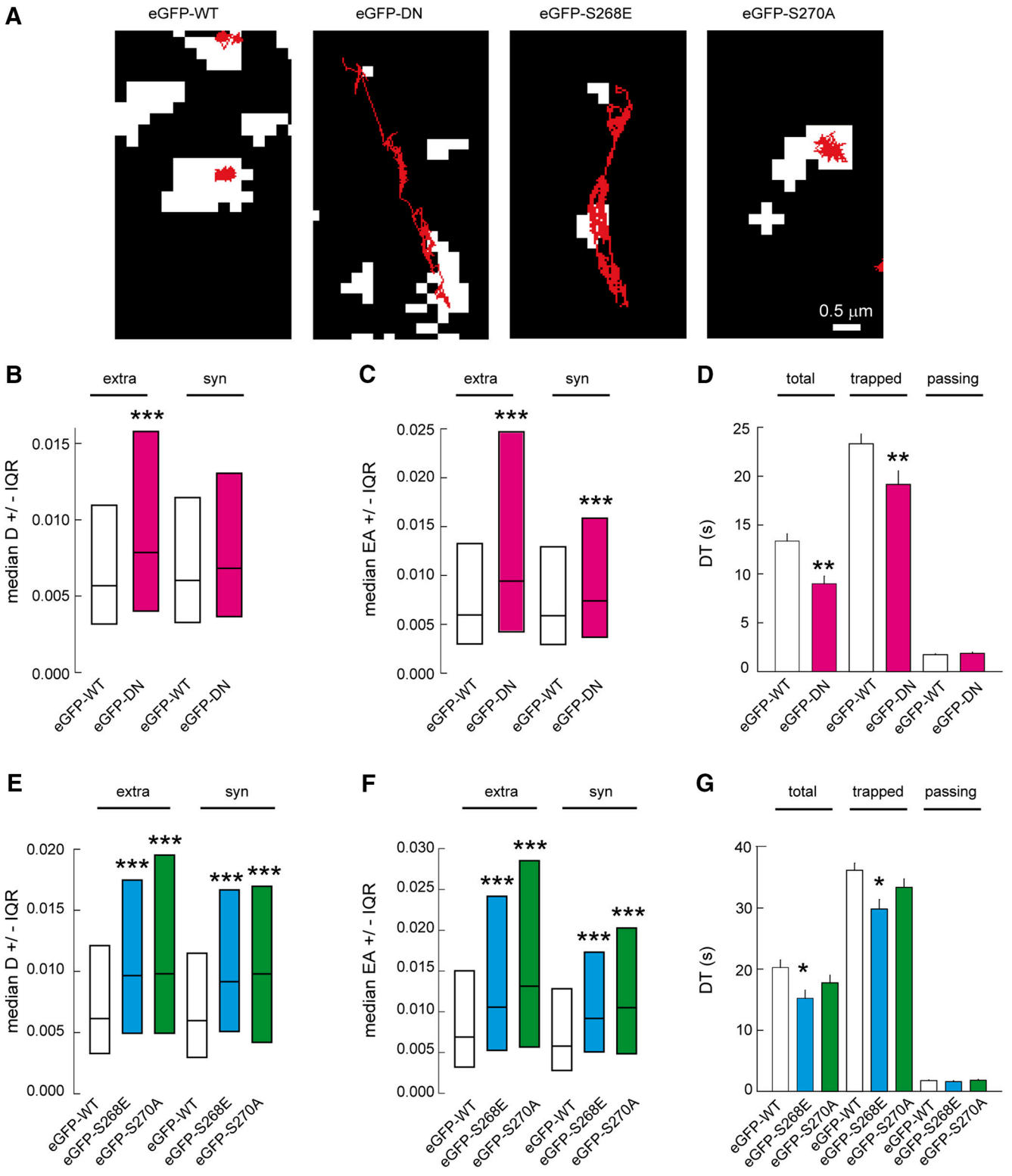

Figure 2. Membrane dynamics of α2 $GABA_AR$ is influenced by gephyrin phosphorylation. ***A***, Example traces of QD trajectories (red) overlaid with fluorescent synaptic clusters (white) of VGAT-Oyster550 for eGFP-DN transfected neurons or with eGFP-gephyrin clusters for eGFP-WT, eGFP-S268E, or eGFP-S270A expressing cells. Scale bar, 0.5 μm. ***B***, Median diffusion coefficients D of α2 $GABA_AR$ in neurons transfected with either eGFP-WT or eGFP-DN. Extra: WT $n = 975$ QDs, DN $n = 491$ QDs, $p = 4.5 \times 10^{-34}$; Syn: WT $n = 306$ QDs, DN $n = 173$ QDs, $p = 0.36$. ***C***, Quantification of explored area EA of α2 $GABA_AR$, Extra: WT $n = 2925$ QDs, DN $n = 1473$ QDs, $p = 3.8 \times 10^{-23}$; Syn: WT $n = 918$ QDs, DN $n = 519$ QDs, $p = 4.4 \times 10^{-4}$. ***D***, Dwell time DT of α2 $GABA_AR$ at synapses in neurons transfected with either eGFP-WT or eGFP-DN. Quantification of all QDs (total), trapped (DT < 5.9 s), and passing (DT > 5.9 s) QDs at inhibitory synapses. Significant decrease in synaptic dwell time for total and trapped QDs was observed but not for

continued

passing ones. Total: WT $n = 436$ QDs, DN $n = 262$ QDs, $p = 0.001$; Trapped: WT $n = 235$ QDs, DN $n = 108$ QDs, $p = 8.0 \times 10^{-3}$; Passing: WT $n = 201$ QDs, DN $n = 154$ QDs, $p = 0.19$. ***E***, Quantification of diffusion coefficients of α2 $GABA_AR$ showing increased receptor mobility at extrasynaptic (extra) and synaptic (syn) sites in neurons transfected with eGFP-S268E or eGFP-S270A, compared with eGFP-WT expressing cells. Extra: WT $n = 1820$ QDs, S268E $n = 1273$ QDs, $p = 1.1 \times 10^{-22}$, S270A $n = 1658$, $p = 2.9 \times 10^{-27}$. Syn: WT $n = 461$ QDs, S268E $n = 326$ QDs, $p = 2.4 \times 10^{-8}$, S270A $n = 340$, $p = 1.8 \times 10^{-8}$. ***F***, Quantification of α2 $GABA_AR$ explored area EA, Extra: WT $n = 5460$ QDs, S268E $n = 3807$ QDs, $p = 6.8 \times 10^{-52}$, S270A $n = 5355$, $p = 2.2 \times 10^{-101}$. Syn: WT $n = 1383$ QDs, S268E $n = 978$ QDs, $p = 7.4 \times 10^{-23}$, S270A $n = 2208$, $p = 1.2 \times 10^{-33}$. ***G***, Quantification of α2 $GABA_AR$ dwell time DT in neurons expressing eGFP-WT, eGFP-S268E, or eGFP-S270A. Calculations were done for all QDs (total), (trapped), or (passing) QDs at inhibitory synapses. Decrease in dwell time for the whole or trapped population of QDs was seen in synapses expressing eGFP-S268E but not in synapses containing eGFP-S270A. Total: WT $n = 251$ QDs, S268E $n = 176$ QDs, $p = 0.013$, S270A $n = 216$ QDs, $p = 0.31$; Trapped: WT $n = 135$ QDs, S268E $n = 85$ QDs, $p = 0.002$, S270A $n = 109$ QDs, $p = 0.28$; Passing: WT $n = 116$ QDs, S268E $n = 91$ QDs, $p = 0.24$, S270A $n = 107$ QDs, $p = 0.98$. All data are from six independent experiments. In ***B***, ***C***, ***E***, and ***F***, data are presented as median values ± 25%–75% IQR, ***, $p \leq 0.001$ (Kolmogorov–Smirnov test). In ***D*** and ***G***, data are presented as mean ± SEM. *, $p \leq 0.05$, **, $p \leq 0.01$ (Mann–Whitney rank sum test). D in $\mu m^2/s$, EA in μm^2, DT in s.

gephyrin phosphorylation and cluster microdomain compaction. The compaction of the scaffold or the increased spacing between gephyrin molecules may perturb the organization of the gephyrin microdomain, thereby altering gephyrin-receptor binding properties. We cannot exclude the possibility that the mutations directly affect

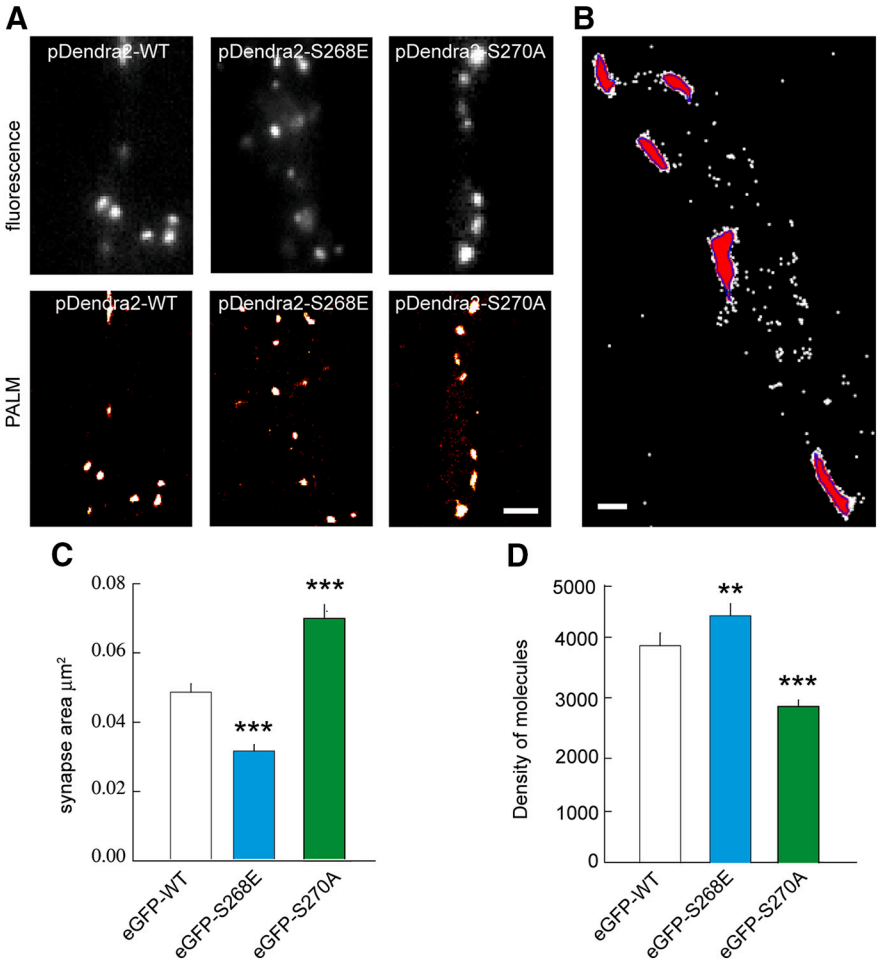

Figure 3. PALM imaging showing gephyrin phosphorylation influences scaffold packing. ***A***, Epifluorescence (top) and PALM (bottom) imaging of the same dendritic regions in neurons expressing pDendra2-WT, -S268E, or -S270A mutant. Scale bar, 1 μm. ***B***, Representative image of cluster segmentation (red) based on local density of molecules detected (white dots) using a threshold of 1000 detections/μm^2 (blue). Scale bar, 200 nm. ***C***, Quantification of eGFP cluster area using PALM shows reduction in cluster size for eGFP-S268E and increase in cluster size for eGFP-S270A compared with eGFP-WT. WT $n = 313$ synapses, S268E $n = 277$ synapses, S270A $n = 290$ synapses, $p < 0.001$, 4 cultures. ***D***, Quantification of density of gephyrin molecules per square micrometer using PALM in transfected neurons. Neurons expressing eGFP-S268E exhibit denser gephyrin packing, and neurons expressing eGFP-S270A exhibit less dense packing of gephyrin compared with eGFP-WT. Data are presented as mean ± SEM. **, $p = 0.006$; ***, $p \leq 0.001$ (Mann–Whitney rank sum test).

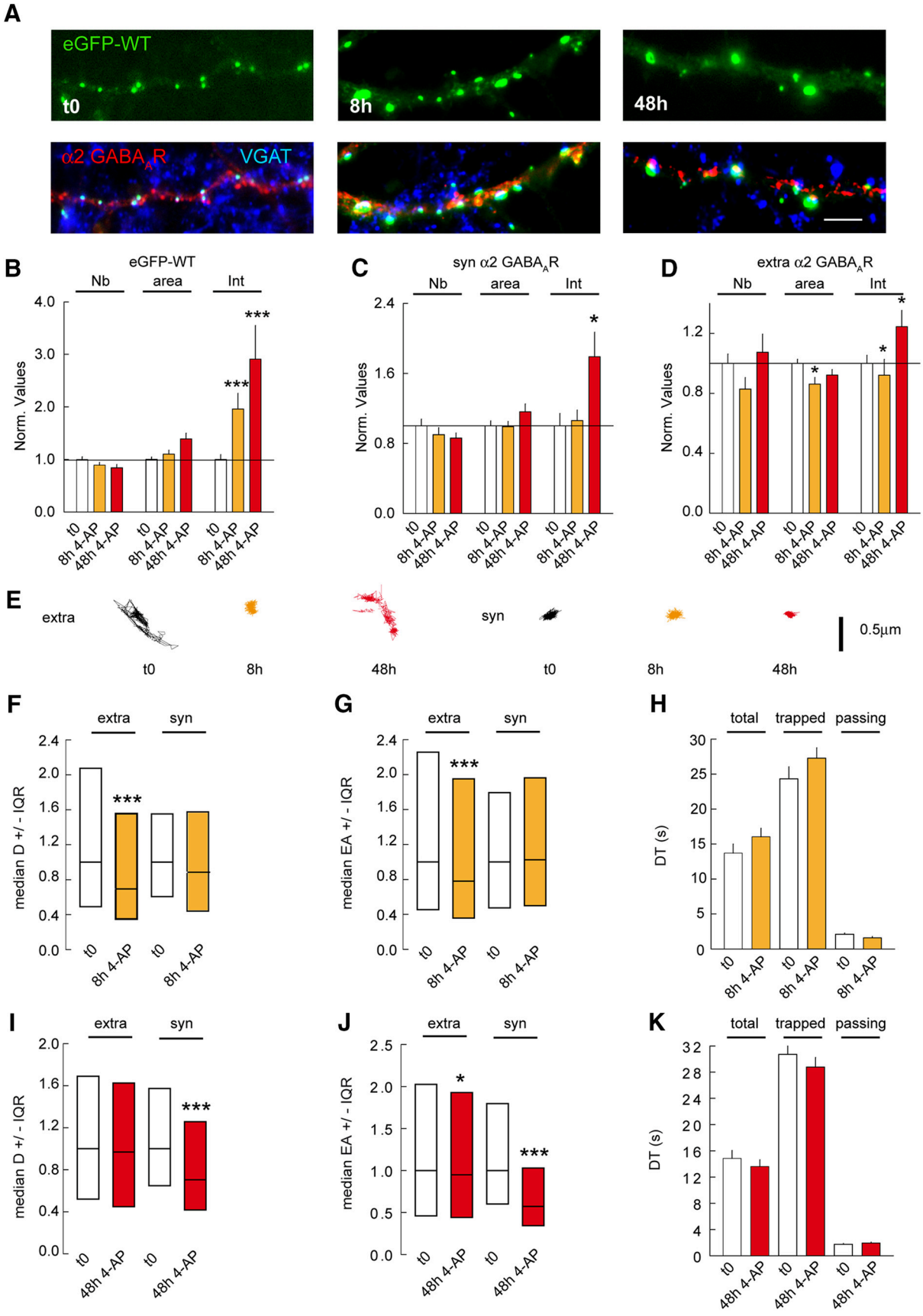

Figure 4. Gephyrin clustering influences GABA$_A$R lateral diffusion. ***A***, Morphology of eGFP-WT (green) after 8 and 48 h of 4-AP

continued

application; VGAT (blue), $GABA_AR$ $\alpha2$ (red) at 21 DIV. Scale bar, 10 μm. ***B***, Quantification of eGFP-WT clusters after 8 and 48 h of 4-AP application. t0 $n = 55$ cells, 8 h $n = 46$ cells, 48 h $n = 55$ cells, 3 cultures. Cluster Nb: 0–8 h: $p = 0.13$, 0–48 h: $p = 0.002$; Area: 0–8 h: $p = 0.5$, 0–48 h: $p = 0.001$; Intensity: 0–8 h: $p < 0.001$, 0–48 h: $p < 0.001$. ***C***, Quantification of synaptic $\alpha2$ $GABA_AR$ clusters after 8 and 48 h of 4-AP compared with mock treated control. t0 $n = 52$ cells, 8 h $n = 43$ cells, 48 h $n = 53$ cells, 3 cultures. Cluster Nb: 0–8 h: $p = 0.4$, 0–48 h: $p = 0.3$; Area: 0–8 h: $p = 0.8$, 0–48 h: $p = 0.8$; Intensity: 0–8 h: $p = 0.5$, 0–48 h: $p = 0.03$. ***D***, Quantification of extrasynaptic $\alpha2$ $GABA_AR$ clusters after 8 and 48 h of 4-AP compared with mock treated control. t0 $n = 52$ cells, 8 h $n = 43$ cells, 48 h $n = 53$ cells, 3 cultures. Cluster Nb: 0–8 h: $p = 0.2$, 0–48 h: $p = 0.9$; Area: 0–8 h: $p = 0.02$, 0–48 h: $p = 0.3$; Intensity: 0–8 h: $p = 0.05$, 0–48 h: $p = 0.022$. ***E***, Example trace of $\alpha2$ $GABA_AR$ trajectories showing surface exploration of extrasynaptic and synaptic receptors after 8 and 48 h of 4-AP exposure. Scale bar, 0.5 μm. ***F***, Quantification of diffusion coefficients of $\alpha2$ $GABA_AR$ after 8 h of 4-AP exposure. Extra; t0 $n = 450$ QDs, WT 4AP 8 h $n = 961$ QDs, $p = 1.96\ 10^{-7}$. Syn; t0 $n = 103$ QDs, 8 h $n = 138$ QDs, $p = 0.22$; 2 cultures. ***G***, Quantification of explored area EA of $\alpha2$ $GABA_AR$ after 8 h of 4-AP application. Extra; t0 $n = 1347$ QDs, 8 h $n = 5265$ QDs, $p = 6.4 \times 10^{-9}$. Syn; t0 $n = 308$ QDs, 8 h $n = 708$ QDs, $p = 0.63$. ***H***, Quantification of synaptic dwell time DT of $\alpha2$ $GABA_AR$ showing no impact after 8 h of 4-AP for total, trapped, or passing receptor population. Total: t0 $n = 151$ QDs, 8 h $n = 206$ QDs, $p = 0.073$; Trapped: t0 $n = 80$ QDs, 8 h $n = 116$ QDs, $p = 0.36$; Passing: t0 $n = 78$ QDs, 8 h $n = 90$ QDs, $p = 0.02$. ***I***, Quantification of diffusion coefficients of $\alpha2$ $GABA_AR$ after 48 h of 4-AP application. Extra: t0 $n = 777$ QDs, 48 h $n = 174$ QDs, $p = 0.69$. Syn: t0 $n = 126$ QDs, 48 h $n = 213$ QDs, $p = 1.4 \times 10^{-4}$. ***J***, Quantification of explored area EA of $\alpha2$ $GABA_AR$ after 48 h of 4-AP application. Extra: t0 $n = 2331$ QDs, 48 h $n = 5508$ QDs, $p = 0.045$. Syn: t0 $n = 378$ QDs, 48 h $n = 717$ QDs, $p = 2.2 \times 10^{-20}$. ***K***, Quantification of $\alpha2$ $GABA_AR$ dwell time after 48 h of 4-AP application. Total: t0 $n = 201$ QDs, 48 h $n = 254$ QDs, $p = 0.74$. Trapped: t0 $n = 91$ QDs, 48 h $n = 110$ QDs, $p = 0.99$. Passing: t0 $n = 110$ QDs, 48 h $n = 144$ QDs, $p = 0.81$. In ***B–D***, ***H***, and ***K***, data are presented as mean ± SEM, $*$, $p \leq 0.05$; $***$, $p \leq 0.001$ (Mann–Whitney rank sum test). In ***F***, ***G***, ***I***, and ***J***, data are presented as median values ± 25%–75% IQR, $*$, $p \leq 0.05$; $***$, $p \leq 0.001$ (Kolmogorov–Smirnov test). In ***B–G***, ***I***, and ***J***, values were normalized to the corresponding control values. In ***H*** and ***K***, DT in s.

receptor-binding properties independently of their effect on the mesh.

Prolonged neuronal activity influences gephyrin and $GABA_AR$ clustering as well as $GABA_AR$ diffusion

Activity-dependent regulation of receptor lateral diffusion is an essential contributor to synapse adaptation (Lüscher et al., 2011). This phenomenon has been explored within the experimental paradigm of short-term (1- to 60-min) drug applications (Bannai et al., 2009, 2015; Muir et al., 2010; Niwa et al., 2012; Petrini et al., 2014). There is accumulating evidence that synaptic adaptations at GABAergic synapses also occur in response to prolonged changes in activity (Rannals and Kapur, 2011; Vlachos et al., 2013; Flores et al., 2015). Hence, we examined whether gephyrin phosphorylation regulates activity-dependent membrane diffusion and synaptic recruitment of $\alpha2$ $GABA_ARs$. To test this hypothesis, we chronically elevated synaptic activity by treating our primary hippocampal neurons with the potassium channel blocker 4-aminopyridine (4-AP; 100 μM; Chamma et al., 2013) for 8 or 48 h. We used immunocytochemistry to determine the impact of a prolonged activity increase on gephyrin and $\alpha2$ $GABA_AR$ clustering (Fig. 4*A*). Quantification across independent experiments showed that fluorescence intensity of eGFP-WT gephyrin clusters increased by 1.95-fold after 8 h and 2.3-fold after 48 h of 4-AP treatment (Fig. 4*B*). Quantification for $\alpha2$ $GABA_AR$ cluster intensity after 8 h of 4-AP–induced neuronal activity did not show an increase in receptor accumulation at synapses; however, after 48 h of 4-AP treatment, we found a 1.7-fold increase in receptor density at synaptic sites (Fig. 4*C*). Thus, gephyrin recruitment at synapses precedes that of the receptor in response to chronic changes in activity. In contrast to synaptic clusters, extrasynaptic $\alpha2$ clusters decreased in size and intensity after 8 h of 4-AP application (Fig. 4*D*). This transient decrease in extrasynaptic $\alpha2$ clusters intensity is reversed after 48 h of 4-AP, similar to synaptic receptor clusters (Fig. 4*C*,*D*). Therefore, a chronic increase in activity regulates both extrasynaptic and synaptic receptor clustering.

It has been reported that acute 4-AP treatment increases $GABA_AR$ mobility between synaptic and extrasynaptic sites (Bannai et al., 2009). Hence, we analyzed $\alpha2$ $GABA_AR$ surface diffusion at extrasynaptic and synaptic sites after either 8 or 48 h of 4-AP treatment using QD-SPT (Fig. 4*E*). Quantification of the receptor diffusion coefficient showed a 1.3-fold reduction for extrasynaptic receptors; however, the synaptic receptors were not influenced by 8 h of 4-AP treatment (Fig. 4*F*). Consistently, 8 h of 4-AP treatment reduced the explored area for only the extrasynaptic receptors by 1.2-fold (Fig. 4*G*). The receptor dwell time at synaptic sites was also unchanged after 8 h of activity change (Fig. 4*H*). This is consistent with a lack of receptor accumulation at synapses after 8 h of 4-AP treatment.

Contrary to the 8-h 4-AP treatment, 48-h treatment significantly reduced the diffusion coefficients of synaptic $\alpha2$ receptors by 1.3-fold, while having no effect on the extrasynaptic receptors (Fig. 4*I*). We also observed a 1.3-fold reduction in explored area for synaptic $\alpha2$ $GABA_ARs$, with only a modest reduction for extrasynaptic receptors (Fig. 4*J*). Unexpectedly, the reduction in the diffusion rate and explored area of synaptic $\alpha2$ receptors had no influence on the dwell time at synaptic sites (Fig. 4*K*). Therefore, pools of extrasynaptic and synaptic receptor are regulated independently of each other over prolonged activity change.

Altogether, our data show that $GABA_AR$ lateral diffusion can be regulated on a time scale of days. We observe a decrease in synaptic $GABA_AR$ diffusion at the 48-h time point and not at 8 h, which is in direct correlation to cluster intensity change observed after 48 h. Therefore, regulation of $GABA_AR$ diffusion capture accounts for the change

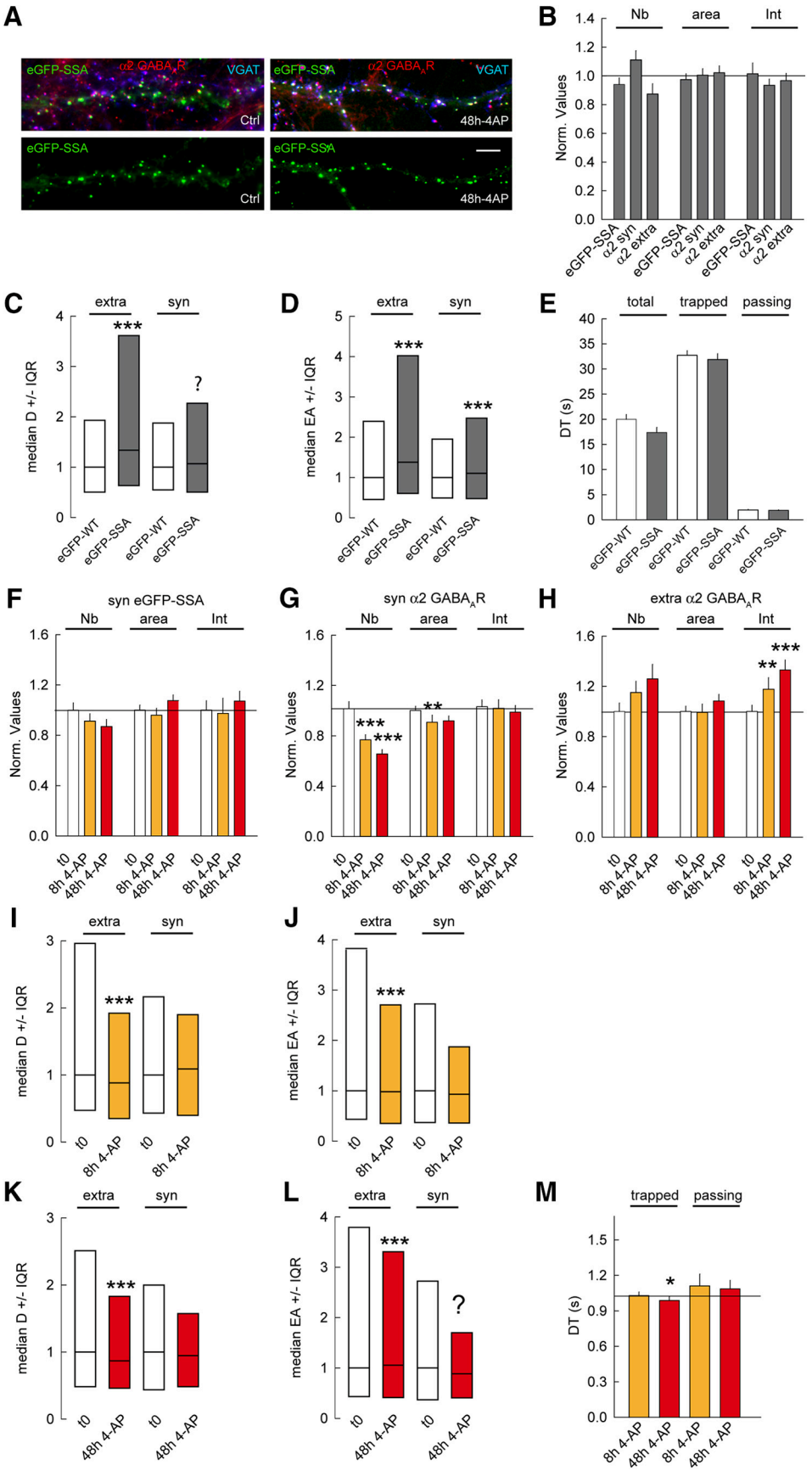

Figure 5. PKA and CaMKIIα signaling pathways regulate gephyrin clustering and α2 GABA$_A$R membrane dynamics in conditions of

continued

chronic changes of activity. ***A***, Morphologic analysis of neurons transfected with eGFP-S303A/S305A (eGFP-SSA) gephyrin double mutant insensitive to PKA and CaMKIIα signaling pathways. Double staining of VGAT (blue) and α2 $GABA_AR$ (red) at 21 DIV under control condition (t0) or in the presence of 4-AP for 48 h. Scale bar, 10 μm. ***B***, Quantifications of synaptic eGFP-SSA clusters and synaptic (α2 syn) and extrasynaptic (α2 extra) α2 $GABA_AR$ clusters in relation to eGFP-WT show minor impact of eGFP-SSA under control condition. eGFP-WT: $n = 89$ cells, eGFP-SSA $n = 95$ cells, 6 cultures. eGFP-SSA: Cluster Nb: $p = 0.3$; Area: $p = 0.9$; Intensity: $p = 0.5$. α2 syn: Cluster Nb: $p = 0.4$; Area: $p = 0.5$; Intensity: $p = 0.8$. α2 extra: Cluster Nb: $p = 0.2$; Area: $p = 0.4$; Intensity: $p = 0.2$. ***C***, Quantification of median diffusion coefficient D of α2 $GABA_AR$ in neurons expressing eGFP-WT or eGFP-SSA under control condition. Extra: WT $n = 1166$ QDs, SSA $n = 989$ QDs, $p = 1.5 \times 10^{-12}$; Syn: WT $n = 312$ QDs, SSA $n = 245$ QDs, $p = 0.08$; 4 cultures. ***D***, Quantification of median explored area EA of α2 $GABA_AR$ in neurons expressing eGFP-WT or eGFP-SSA under control condition. Extra: WT $n = 3510$ QDs, SSA $n = 2778$ QDs, $p = 3.9 \times 10^{-18}$; Syn: WT $n = 932$ QDs, SSA $n = 735$ QDs, $p = 3.1 \times 10^{-4}$. ***E***, Quantification of α2 $GABA_AR$ dwell time DT at synaptic sites in neurons expressing either eGFP-WT or eGFP-SSA. Calculations were done for all QDs (total), (trapped), or (passing) QDs at inhibitory synapses. No significant differences were found between eGFP-WT and eGFP-SSA. Total: WT $n = 390$ QDs, SSA $n = 335$ QDs, $p = 0.2$; Trapped: WT $n = 229$ QDs, SSA $n = 173$ QDs, $p = 0.4$; Passing: WT $n = 161$ QDs, SSA $n = 162$ QDs, $p = 0.9$. ***F***, Quantification of eGFP-SSA clusters after 8 and 48 h of 4-AP application. t0 $n = 61$ cells, 8 h $n = 52$ cells, 48 h $n = 93$ cells, 3–6 cultures. Cluster Nb: 0–8 h: $p = 0.2$, 0–48 h: $p < 0.001$; Area: 0–8 h: $p = 0.8$, 0–48 h: $p = 0.3$; intensity: 0–8 h: $p = 0.8$, 0–48 h: $p = 0.2$. ***G***, Quantification of synaptic α2 $GABA_AR$ clusters after 8 and 48 h of 4-AP compared with mock treated control. t0 $n = 53$ cells, 8 h $n = 50$ cells, 48 h $n = 69$ cells, 3–6 cultures. Cluster Nb: 0–8 h: $p < 0.001$, 0–48 h: $p < 0.001$; Area: 0–8 h: $p = 0.002$, 0–48 h: $p = 0.09$; Intensity: 0–8 h: $p = 0.5$, 0–48 h: $p = 0.5$. ***H***, Quantification of extrasynaptic α2 $GABA_AR$ clusters after 8 and 48 h of 4-AP compared with mock treated control. Cluster Nb: 0–8 h: $p = 0.2$, 0–48 h: $p = 0.1$; Area: 0–8 h: $p = 0.01$, 0–48 h: $p = 0.9$; Intensity: 0–8 h: $p = 0.002$, 0–48 h: $p < 0.001$. ***I***, Quantification of α2 $GABA_AR$ diffusion coefficients in eGFP-SSA expressing cells after 8 h of 4-AP exposure. Extra: t0 $n = 787$ QDs, 4AP 8 h $n = 365$ QDs, $p = 3.6 \times 10^{-4}$. Syn: t0 $n = 212$ QDs, 8 h $n = 187$ QDs, $p = 0.4$; 5 cultures. ***J***, Quantification of explored area EA of α2 $GABA_AR$ after 8 h of 4-AP application. Extra: t0 $n = 1869$ QDs, 8 h $n = 1092$ QDs, $p = 0.002$. Syn: t0 $n = 753$ QDs, 8 h $n = 558$ QDs, $p = 0.09$. ***K***, Quantification of α2 $GABA_AR$ diffusion coefficients in eGFP-SSA expressing cells after 48 h of 4-AP exposure. Extra: t0 $n = 1098$ QDs, 4AP 48 h $n = 734$ QDs, $p = 0.002$. Syn: t0 $n = 287$ QDs, 48 h $n = 198$ QDs, $p = 0.2$; 5 cultures. ***L***, Quantification of explored area EA of α2 $GABA_AR$ after 48 h of 4-AP application. Extra: t0 $n = 2169$ QDs, 48 h $n = 1500$ QDs, $p = 0.04$. Syn; t0 $n = 633$ QDs, 48 h $n = 510$ QDs, $p = 0.002$. ***M***, Quantification of α2 $GABA_AR$ dwell time DT in neurons expressing eGFP-SSA after 8 or 48 h of 4-AP application. Calculations were done for trapped or passing QDs at inhibitory synapses. Trapped: 8 h: $n = 189$ QDs, $p = 0.3$; 48 h: $n = 166$ QDs, $p = 0.1$; Passing: 8 h: $n = 76$ QDs, $p = 0.3$; 48 h: $n = 132$ QDs, $p = 0.9$. In ***B***, ***E***, ***F–H***, and ***M***, data are presented as mean ± SEM. **, $p < 0.01$; ***, $p \leq 0.001$ (Mann–Whitney rank sum test). In ***C***, ***D***, ***I***, and ***L***, data are presented as median values ± 25%–75% IQR; ***, $p \leq 0.001$ (Kolmogorov–Smirnov test). In all graphs except ***E***, values were normalized to the corresponding control values.

in receptor density at synapses on chronic changes in activity.

PKA and CaMKIIα pathways regulate synaptic scaling at GABAergic postsynaptic sites through gephyrin phosphorylation

To identify signaling cascades that couple the gephyrin scaffold to $GABA_ARs$ for activity-dependent synaptic recruitment, we focused on the protein kinase A (PKA) and CaMKIIα pathways. NMDA receptor–dependent compensatory adaptations at the GABAergic postsynaptic sites have been reported to be facilitated by gephyrin phosphorylation at PKA and CaMKIIα locations (Flores et al., 2015). We thus transfected the eGFP-S303A/S305A (SSA) mutant (insensitive to PKA- and CaMKIIα-dependent phosphorylation) into our primary hippocampal neurons and treated the neurons for 8 or 48 h with 4-AP. We did not observe differences between eGFP-WT and eGFP-SSA cluster number, cluster size, and fluorescence intensity in control conditions (Fig. 5*A*,*B*). Similarly, the SSA mutant did not significantly influence the synaptic or extrasynaptic clustering of α2 $GABA_ARs$ (Fig. 5*B*). In contrast, the SSA mutation increased the diffusion coefficient and explored area of α2 $GABA_ARs$ at both extrasynaptic and synaptic sites (Fig. 5*C*,*D*). This increase in receptor mobility did not correlate with what we expected from a normal-size scaffold. However, the α2 $GABA_ARs$ dwell time at inhibitory synapses did not differ between eGFP-SSA– and eGFP-WT–transfected neurons (Fig. 5*E*), indicating that the increase in receptor mobility was not accompanied by a faster synaptic escape of receptors. This is consistent with a lack of effect of the SSA mutant on α2 $GABA_ARs$ clustering at synapses.

The expression of the eGFP-SSA mutant was sufficient to prevent the 4-AP (8- or 48-h) induced gephyrin and α2 $GABA_ARs$ cluster growth at synapses (Fig. 5*A*,*F*,*G*). Interestingly, 8 and 48 h after 4-AP application, extrasynaptic α2 cluster intensity increased in eGFP-SSA–transfected neurons (Fig. 5*H*). This indicated that receptor clustering at extrasynaptic sites at the 8-h treatment time point is dependent on PKA and CaMKIIα phosphorylation. However, at 48 h, receptor accumulation is independent of these two pathways. Hence, an additional pathway permits $GABA_AR$ recruitment, in particular at extrasynaptic sites, after chronic changes in activity.

We also analyzed the effect of the SSA mutant on α2 $GABA_ARs$ surface diffusion. Similar to wild-type gephyrin, SSA reduced diffusion coefficient and surface exploration of α2 $GABA_ARs$ at extrasynaptic sites after 8 h of 4-AP (Fig. 5*I*,*J*). This effect was maintained also after 48-h treatment (Fig. 5*K*,*L*). In contrast to wild-type gephyrin, SSA mutant increased α2 $GABA_AR$ confinement and decreased dwell time of $GABA_ARs$ at synapses after 48 h of 4-AP (Fig. 5*K–M*). The passing α2 $GABA_ARs$ remained unchanged at synapses after 8 or 48 h of 4-AP (Fig. 5*M*). Hence, our results indicate that gephyrin scaffold reorga-

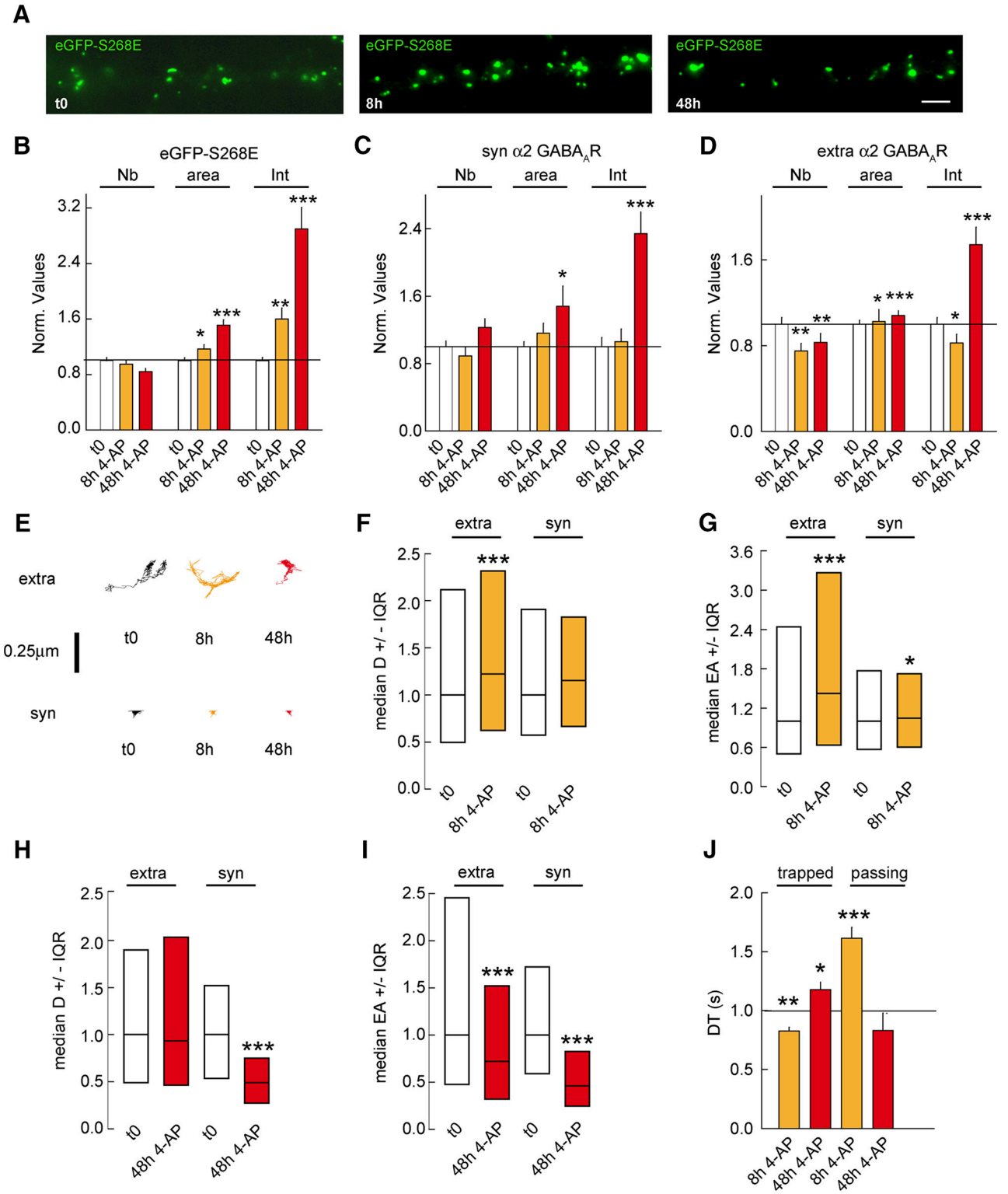

Figure 6. The ERK1/2 pathway does not influence structural synaptic adaptation. ***A***, Morphologic analysis of eGFP-S268E in control (t0) or after 4-AP application for 8 or 48 h. Scale bar, 10 μm. ***B***, Quantification of eGFP-S268E clusters after 8 or 48 h of 4-AP application. t0 $n = 50$ cells, 8 h $n = 54$ cells, 48 h $n = 55$ cells, 3 cultures. Cluster Nb: 0–8 h: $p = 0.2$, 0–48 h: $p = 0.004$; Area: 0–8 h: $p = 0.02$, 0–48 h: $p < 0.001$; Intensity: 0–8 h: $p = 0.003$, 0–48 h: $p < 0.001$. 3 cultures. ***C***, Quantification of synaptic α2 GABA$_A$R clusters after 8 h and 48 h of 4-AP compared with mock treated control. t0 $n = 47$ cells, 8 h $n = 50$ cells, 48 h $n = 62$ cells, 3-4 cultures. Cluster Nb: 0–8 h: $p = 0.08$, 0–48 h: $p = 0.5$; Area: 0–8 h: $p = 0.8$, 0–48 h: $p = 0.03$; Intensity: 0–8 h: $p = 0.5$, 0–48 h: $p < 0.001$. ***D***, Quantification of extrasynaptic α2 GABA$_A$R clusters after 8 and 48 h of 4-AP compared with mock treated control. Cluster Nb: 0–8 h: $p = 0.006$, 0–48 h: $p = 0.007$; Area: 0–8 h: $p = 0.02$, 0–48 h: $p < 0.001$; Intensity: 0–8 h: $p = 0.04$, 0–48 h: $p < 0.001$. ***E***, Example

continued

traces of α2 $GABA_AR$ trajectories at extrasynaptic (extra) and synaptic (syn) sites under control condition (t0) or after 8 or 48 h of 4-AP application. Scale bar, 0.25 μm. ***F***, Quantification of α2 $GABA_AR$ diffusion coefficients after 8 h of 4-AP exposure. Extra: t0 $n = 1230$ QDs, 4AP 8 h $n = 1855$ QDs, $p = 3.4 \times 10^{-6}$. Syn: t0 $n = 281$ QDs, 8 h $n = 378$ QDs, $p = 0.2$; 3 cultures. ***G***, Quantification of explored area EA of α2 $GABA_AR$ after 8 h of 4-AP application. Extra: t0 $n = 3402$ QDs, 8 h $n = 2454$ QDs, $p = 3.2 \times 10^{-23}$. Syn: t0 $n = 843$ QDs, 8 h $n = 984$ QDs, $p = 0.02$. ***H***, Quantification of α2 $GABA_AR$ diffusion coefficients after 48 h of 4-AP exposure. Extra: t0 $n = 687$ QDs, 4AP 48 h $n = 1611$ QDs, $p = 0.4$. Syn: t0 $n = 73$ QDs, 48 h $n = 46$ QDs, $p = 1.6 \times 10^{-4}$. ***I***, Quantification of explored area EA of α2 $GABA_AR$ after 48 h of 4-AP application. Extra: t0 $n = 2061$ QDs, 48 h $n = 546$ QDs, $p = 2.9 \times 10^{-6}$. Syn; t0 $n = 219$ QDs, 48 h $n = 74$ QDs, $p = 6.6 \times 10^{-7}$. ***J***, Quantification of α2 $GABA_AR$ dwell time DT after 8 or 48 h of 4-AP application. Calculations were done for trapped or passing QDs at inhibitory synapses. Trapped: t0: $n = 130$ QDs, 8 h: $n = 194$ QDs, $p = 0.007$; t0: $n = 85$ QDs, 48 h: $n = 51$ QDs, $p = 0.02$; Passing: t0: $n = 91$ QDs, 8 h: $n = 161$ QDs, $p < 0.001$; t0: $n = 91$ QDs, 48 h: $n = 31$ QDs, $p = 0.6$. In ***B–D*** and ***J***, data are presented as mean ± SEM. ∗, $p \leq 0.05$; ∗∗, $p \leq 0.01$; ∗∗∗, $p \leq 0.001$ (Mann–Whitney rank sum test). In ***F–I***, data are presented as median values ± 25%–75% IQR. ∗, $p \leq 0.05$; ∗∗∗, $p \leq 0.001$ (Kolmogorov–Smirnov test). In all graphs, values were normalized to the corresponding control values.

nization via PKA- and CaMKIIα-dependent phosphorylation at S303 and S305 is essential for $GABA_AR$ diffusion at synapses but not at extrasynaptic sites in response to chronic changes in activity.

Synapse scaling is independent of the ERK1/2 pathway

It has been reported that gephyrin clustering is also influenced by the ERK1/2 pathway. We thus assessed whether ERK1/2 signaling influences gephyrin cluster size during chronic changes in network activity. Transgenic expression of eGFP-S268E gephyrin mutant renders gephyrin scaffold insensitive to the ERK1/2 signaling pathway (Tyagarajan et al., 2013). We therefore transfected cultured neurons with eGFP-S268E mutant and treated them with 4-AP for 8 or 48 h. Immunocytochemical analysis showed an increase in eGFP-S268E mutant cluster size after 4-AP treatment (Fig. 6*A*). Quantification of changes in eGFP-S268E cluster intensity confirmed an increase of 1.6- and 2.2-fold after 8 and 48 h of 4-AP treatment, respectively (Fig. 6*B*). This was associated with increases of 1.2- and 1.3-fold in eGFP-S268E cluster size after 8 and 48 h of 4-AP treatment (Fig. 6*B*). Analysis for α2 $GABA_AR$ cluster intensity at synapses and at extrasynaptic sites showed a respective 2.2- and 1.8-fold increase after 48 h of 4-AP treatment, but not after 8 h (Fig. 6*C*,*D*). We conclude that the eGFP-S268E mutant is not required for the activity-dependent recruitment of gephyrin and $GABA_AR$ within synaptic and extrasynaptic clusters. We wondered whether 4-AP induced chronic activity would impact the surface diffusion of $GABA_ARs$. We checked α2 $GABA_AR$ diffusion coefficients after 8 or 48 h of 4-AP. Individual receptor trajectories for extrasynaptic and synaptic α2 $GABA_AR$ suggested increased confinement after 48 h of enhanced activity (Fig. 6*E*). The α2 diffusion coefficients and explored area were increased by 1.2- and 1.4-fold for extrasynaptic receptors after 8 h of 4-AP (Fig. 6*F*,*G*). However, 48 h after 4-AP application, extrasynaptic receptors diffusion coefficients were unchanged (Fig 6*H*), whereas QDs were more confined at extrasynaptic sites (Fig. 6*I*). Interestingly, 48 h of 4-AP treatment reduced synaptic α2 $GABA_AR$ diffusion coefficients and explored areas at eGFP-S268E synapses (Fig. 6*H*,*I*), as observed at synapses containing eGFP-WT (Fig. 4*I*,*J*). In agreement with an increased number of α2 $GABA_ARs$ at synapses, α2 dwell time increased at eGFP-S268E synapses (Fig. 6*J*).

Therefore, we conclude that although ERK1/2 signaling is not necessary for the activity-dependent regulation of the diffusive behavior of synaptic $GABA_ARs$, it controls the mobility of receptors at extrasynaptic sites. These observations further confirm that synaptic and extrasynaptic receptor pools are independently regulated, and that adaptations observed at GABAergic postsynapses are independent of the ERK1/2 pathway.

GSK3β phosphorylation of gephyrin facilitates $GABA_AR$ diffusion after activity change

It has been reported that the GSK3β signaling pathway postsynaptically regulates the density and size of GABAergic synapses via gephyrin phosphorylation. Pharmacological blockade of the GSK3β pathway or expression of the S270A gephyrin mutant is sufficient to increase gephyrin cluster size (Tyagarajan et al., 2011). Hence, it is plausible that the GSK3β pathway acts in addition to PKA and CaMKIIα signaling to regulate homeostatic adaptations at GABAergic synapses. To address this question, we treated neurons transfected with eGFP-S270A gephyrin mutant with 4-AP for 8 and 48 h. Morphologic characterization showed that the GSK3β signaling is not essential for gephyrin accumulation at synapses on chronic changes in activity (Fig. 7*A*,*B*). In contrast, the eGFP-S270A mutant fully abolished the synaptic and extrasynaptic increase in α2 $GABA_AR$ clustering after 48 h of 4-AP application (Fig. 7*C*,*D*). After 8 h of 4-AP treatment, extrasynaptic α2 $GABA_AR$ cluster density, size, and intensity were respectively reduced by 1.4-, 1.2-, and 1.4-fold in eGFP-S270A–expressing cells (Fig. 7*D*). These results implicate the GSK3β pathway in the regulation of activity-induced $GABA_AR$ clustering at both synaptic and extrasynaptic sites.

If the GSK3β signaling is important for $GABA_ARs$ accumulation at synapses in response to chronic changes in activity, then eGFP-S270A mutant expression should have no impact on α2 diffusion rates. However, 8 h after 4-AP application, α2 diffusion coefficients and explored areas were reduced by 1.3- and 1.1-fold at synaptic sites (Fig. 7*E–G*). This increased confinement was counterbalanced by a decrease in the time trapped receptors spent at synapses (Fig. 7*J*), explaining why α2 clustering was

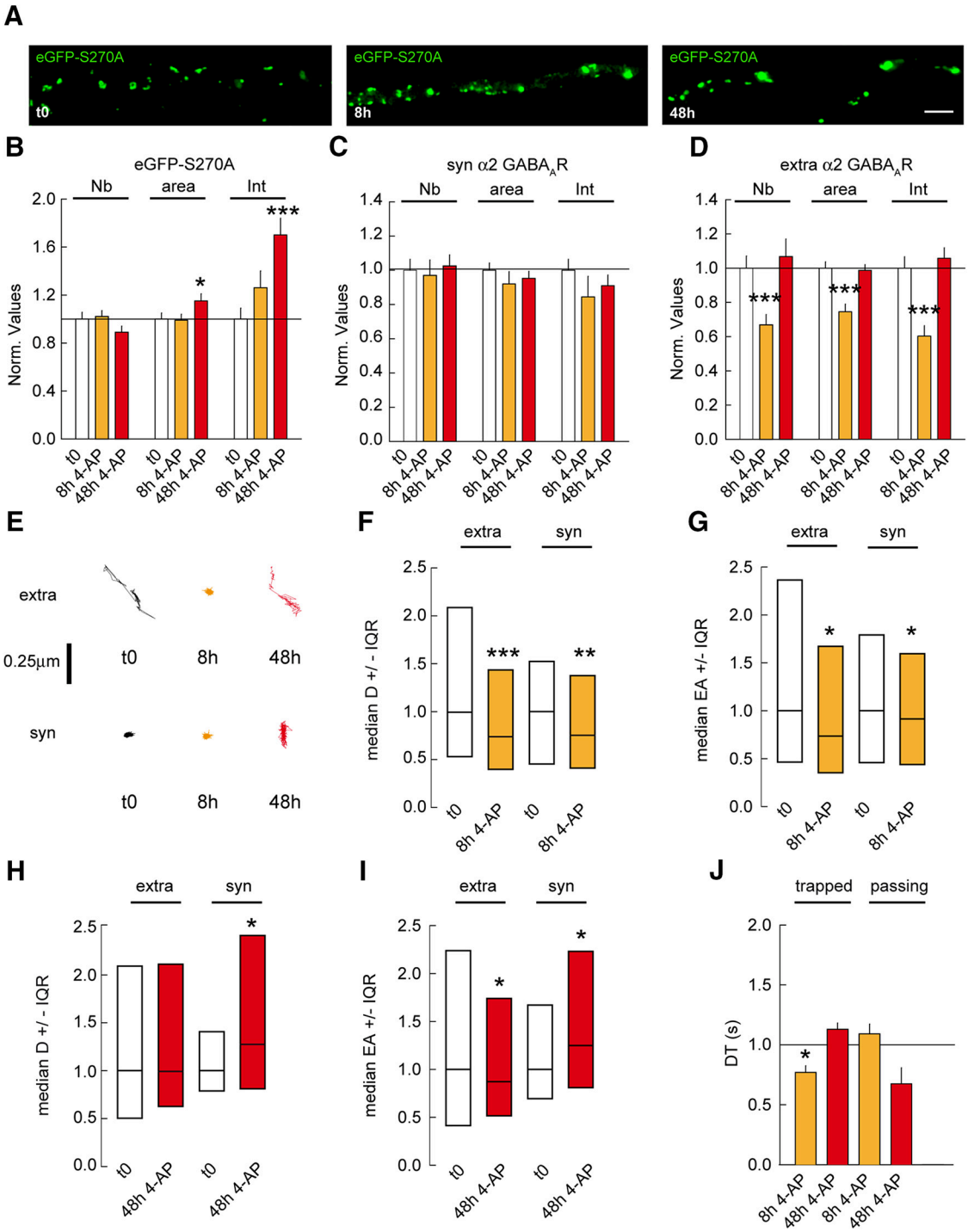

Figure 7. GSK3β pathway influences gephyrin scaffold and $GABA_A$Rs after changes in chronic activity. ***A***, Morphology of neuron transfected with eGFP-S270A under control condition (t0) or in the presence of 4-AP after 8 or 48 h. Scale bar, 10 μm. ***B***, Quantification of eGFP-S270A clusters after 8 or 48 h of 4-AP application. t0 $n = 43$ cells, 8 h $n = 50$ cells; 48 h $n = 50$ cells, 3 cultures. Cluster Nb: 0–8 h: $p = 0.8$, 0–48 h: $p = 0.14$; Area: 0–8 h: Mann–Whitney test $p = 0.7$, 0–48 h: $p = 0.04$; Intensity: 0–8 h: $p = 0.12$, 0–48 h: $p < 0.001$. ***C***, Quantification of synaptic α2 $GABA_A$R clusters after 8 and 48 h of 4-AP compared with mock treated control. t0 $n = 40$ cells, 8 h $n = 47$ cells; t0: $n = 59$ cells, 48 h $n = 52$ cells, 3–5 cultures. Cluster Nb: 0–8 h: $p = 0.8$, 0–48 h: $p = 0.7$; Area: 0–8 h: $p = 0.14$, 0–48 h: $p = 0.6$; Intensity: 0–8 h: $p = 0.03$, 0–48 h: $p = 0.4$. ***D***, Quantification of extrasynaptic α2 $GABA_A$R clusters after 8 and 48 h of 4-AP compared with mock treated control. Cluster Nb: 0–8 h: $p < 0.001$, 0–48 h: $p = 0.7$; Area: 0–8 h: $p < 0.001$, 0–48 h: $p = 0.7$; Intensity: 0–8 h: $p < 0.001$, 0–48 h: $p = 0.3$. ***E***, Example traces of α2 $GABA_A$R trajectories at extrasynaptic (extra) and synaptic (syn) sites under control conditions (t0) or after 8 or 48 h of 4-AP application. Scale bar, 0.25 μm. ***F***, Quantification of α2 $GABA_A$R diffusion coefficients after 8 h of 4-AP exposure. Extra: t0 $n = 1580$ QDs, 4AP 8 h $n = 1892$ QDs, $p = 1.4 \times 10^{-13}$. Syn: t0 $n = 229$ QDs, 8 h $n = 307$ QDs, $p = 8.8 \times 10^{-3}$; 3 cultures. ***G***, Quantification of explored area EA of α2 $GABA_A$R after 8 h of 4-AP

continued

application. Extra: t0 $n = 4575$ QDs, 8 h $n = 4041$ QDs, $p = 0.02$. Syn: t0 $n = 687$ QDs, 8 h $n = 663$ QDs, $p = 0.04$. ***H***, Quantification of α2 $GABA_AR$ diffusion coefficients after 48 h of 4-AP exposure. Extra: t0 $n = 314$ QDs, 4AP 48 h $n = 338$ QDs, $p = 0.05$. Syn: t0 $n = 46$ QDs, 48 h $n = 51$ QDs, $p = 0.04$. 3 cultures. ***I***, Quantification of explored area EA of α2 $GABA_AR$ after 48 h of 4-AP application. Extra: t0 $n = 939$ QDs, 48 h $n = 771$ QDs, $p = 0.02$. Syn; t0 $n = 138$ QDs, 48 h $n = 153$ QDs, $p = 0.04$. ***J***, Quantification of α2 $GABA_AR$ dwell time DT after 8 or 48 h of 4-AP application. Calculations were done for trapped or passing QDs at inhibitory synapses. Trapped: t0: $n = 82$ QDs, 8 h: $n = 97$ QDs, $p = 0.04$; t0: $n = 191$ QDs, 48 h: $n = 45$ QDs, $p = 0.5$; Passing: t0: $n = 104$ QDs, 8 h: $n = 131$ QDs, $p = 0.5$; t0: $n = 211$ QDs, 48 h: $n = 23$ QDs, $p = 0.1$. In ***B–D*** and ***J***, data are presented as mean ± SEM. ∗, $p \leq 0.05$; ∗∗∗, $p \leq 0.001$ (Mann–Whitney rank sum test). In ***F–I***, data are presented as median values ± 25%–75% IQR. ∗, $p \leq 0.05$; ∗∗, $p \leq 0.01$; ∗∗∗, $p \leq 0.001$ (Kolmogorov–Smirnov test). In all graphs, values were normalized to the corresponding control values.

unchanged at synapses after 8 h of 4-AP application. On the other hand, 48 h of 4-AP application increased α2 diffusion coefficients by 1.3-fold as well as explored areas at synaptic sites (Fig. 7*E*,*H*,*I*). This was, however, not accompanied by a change in synaptic receptor dwell time (Fig. 7*J*). The reduction of extrasynaptic α2 clustering coincided with a 1.3-fold reduced explored area in eGFP-S270A–expressing cells after 8 h of 4-AP (Fig. 7*E–G*). Nevertheless, 48 h after 4-AP application, α2 diffusion coefficients and explored areas returned to baseline levels at extrasynaptic sites (Fig. 7*H*,*I*). These observations are consistent with the receptor clustering returning to control levels at extrasynaptic sites after 48 h of 4-AP (Fig. 7*D*). Altogether, these results show that GSK3β signaling in addition to PKA and CaMKIIα pathways tune $GABA_ARs$ at synapses in response to chronic changes in activity.

Impairment of PKA, CAMKIIα, and GSK3β phosphorylation of gephyrin abolishes the activity-dependent regulation of $GABA_ARs$ mobility

The analysis of the SSA and S270A mutants indicated that PKA, CAMKIIα, and GSK3β phosphorylation of gephyrin have complementary effects on gephyrin and α2 $GABA_ARs$ clustering in conditions of synaptic plasticity. To show it more directly, we generated eGFP-SSA/S270A mutant, expressed it in hippocampal neurons, and treated the neurons for 8 or 48 h with 4-AP.

We found that overexpressing eGFP-SSA/S270A increased eGFP cluster size and intensity (Fig. 8*A*). The gephyrin cluster growth was, however, not accompanied by synaptic recruitment of α2 $GABA_ARs$ (Fig. 8*A*). Although the density of α2 $GABA_ARs$ clusters was reduced in eGFP-SSA/S270A–transfected cells, there was no major impact of the mutant on α2 $GABA_ARs$ cluster size and intensity at synaptic and extrasynaptic sites (Fig. 8*A*).

We then characterized α2 $GABA_AR$ diffusion in SSA/S270A-transfected neurons. Diffusion coefficients showed a 1.4-fold increase for extrasynaptic receptors and no significant change for synaptic receptors (Fig. 8*B*). This effect was consistent with the observation that α2 $GABA_AR$ spent the same time at eGFP-SSA/S270A and eGFP-WT synapses (Fig. 8*C*). Therefore the eGFP-SSA/S270A mutant can recapitulate many of the observed phenotypes seen with SSA or S270A individual mutations.

We then characterized how chronic activity affects eGFP-SSA/S270A mutant behavior. Although the extrasynaptic $GABA_ARs$ cluster density increased after 48 h of 4-AP in eGFP-SSA/S270A transfected cells, the triple mutant prevented the synaptic increase in gephyrin and $GABA_ARs$ cluster size and intensity in response to 4-AP treatment (Fig. 8*D–F*). The diffusion coefficient and explored area of α2 $GABA_ARs$ showed no change after 8 or 48 h of 4-AP application (Fig. 8*G–J*). There was also no impact on receptor dwell time at synapses after chronic changes in activity (Fig. 8*K*).

Our results uncover a role for several signaling pathways in chronic activity-dependent modulation of gephyrin clustering and $GABA_ARs$ surface diffusion at synapses. Our data also show that distinct signaling pathways regulate synaptic and extrasynaptic receptor clustering. Together, these results identify a novel role of GSK3β signaling in the regulation of extrasynaptic receptor surface trafficking and GSK3β, PKA, and CaMKIIα pathways in facilitating adaptations of synaptic receptors.

Discussion

In the current study, we investigate the molecular basis for gephyrin scaffold–induced $GABA_AR$ membrane dynamics. We identify a novel role for gephyrin posttranslational modification involving phosphorylation and dephosphorylation in regulating $GABA_AR$ lateral diffusion. By tracking α2 $GABA_ARs$ within and outside synaptic sites using QD-SPT, we demonstrate that gephyrin phosphorylation by ERK1/2 at S268, and inhibition of GSK3β phosphorylation on gephyrin at S270, while exhibiting opposite effects on synaptic morphology, similarly influence $GABA_AR$ diffusion properties. We analyze gephyrin scaffold organization at the nanoscale level using PALM and uncover that phosphorylation also controls gephyrin molecule packing.

Over the past decade, several independent studies have documented changes in lateral diffusion of $GABA_ARs$ after pharmacological alteration of neuronal function within a time scale of minutes to a few hours (Lévi et al., 2008; Bannai et al., 2009; Niwa et al., 2012; Petrini et al., 2014). 4-AP application within minutes induces NMDA receptor–mediated calcium influx and calcineurin activation, leading to dephosphorylation of the $GABA_AR$ γ2 subunit S327 residue (Wang et al., 2003). In this context, an increase in $GABA_AR$ diffusion constraint results from receptor dephosphorylation, whereas gephyrin scaffold loss is a secondary effect in response to receptor dispersal (Niwa et al., 2012). We identify gephyrin phosphorylation as an essential facilitator of $GABA_AR$ diffusion dynamics in response to chronic changes in activity. More specifically, we identify a central role for PKA and CaMKIIα pathways along with GSK3β signaling in phosphorylating gephyrin to regulate activity-dependent inhibitory synapse remodeling.

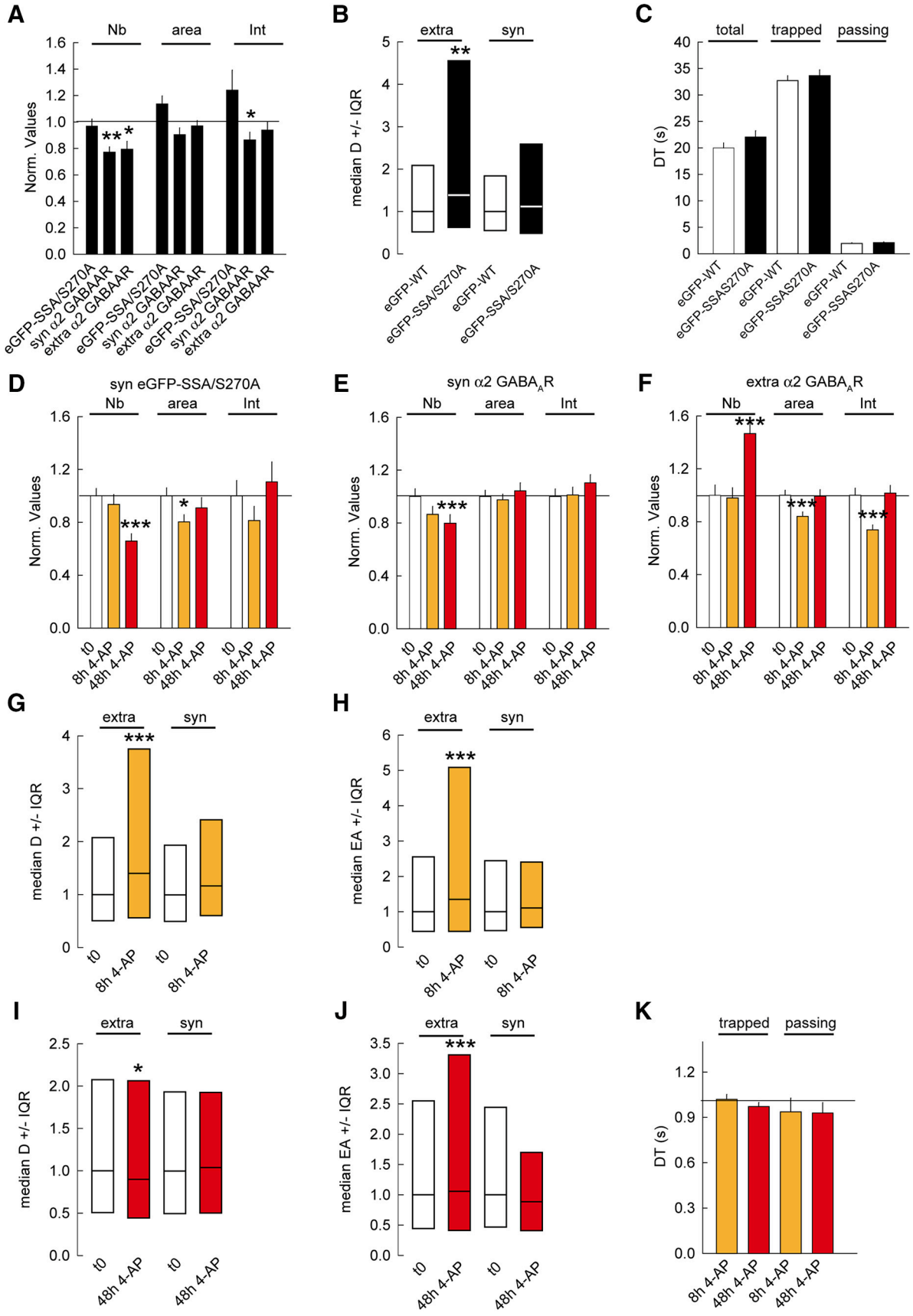

Figure 8. PKA, CAMKIIα, and GSK3β pathways are required to tune the inhibitory synapse. ***A***, Quantifications of synaptic eGFP-SSA/S270 clusters and synaptic (α2 syn) and extrasynaptic (α2 extra) α2 GABA$_A$R clusters in relation to eGFP-WT show minor

continued

impact of the mutant under control condition. eGFP-WT $n = 58$ cells, eGFP-SSA/S270A $n = 62$ cells, 3 cultures. eGFP-SSA: Cluster Nb: $p = 0.6$; Area: $p = 0.1$; Intensity: $p = 0.7$. $\alpha 2$ syn: Cluster Nb: $p = 0.001$; Area: $p = 0.1$; Intensity: $p = 0.02$. $\alpha 2$ extra: Cluster Nb: $p = 0.03$; Area: $p = 0.5$; Intensity: $p = 0.2$. ***B***, Quantification of median diffusion coefficient D of $\alpha 2$ $GABA_AR$ in neurons expressing eGFP-WT or eGFP-SSA/S270A under control condition. Extra: WT $n = 823$ QDs, SSA/S270A $n = 786$ QDs, $p = 0.004$; Syn: WT $n = 261$ QDs, SSA/S270A $n = 211$ QDs, $p = 0.3$, 2 cultures. ***C***, Quantification of $\alpha 2$ $GABA_AR$ dwell time DT at synaptic sites in neurons expressing either eGFP-WT or eGFP-SSA/S270A. Calculations were done for all QDs (total), (trapped), or (passing) QDs at inhibitory synapses. No significant differences were found between eGFP-WT and eGFP-SSA/S270A. Total: WT $n = 165$ QDs, SSA/S270A $n = 183$ QDs, $p = 0.1$; Trapped: WT $n = 95$ QDs, SSA/S270A $n = 116$ QDs, $p = 0.5$; Passing: WT $n = 70$ QDs, SSA/S270A $n = 67$ QDs, $p = 0.2$. ***D***, Quantification of eGFP-SSA/S270A clusters after 8 or 48 h of 4-AP application. t0 $n = 53$ cells, 8 h $n = 45$ cells, 48 h $n = 51$ cells, 3 cultures. Cluster Nb: 0–8 h: $p = 0.3$, 0–48 h: $p < 0.001$; Area: 0–8 h: $p = 0.03$, 0–48 h: $p = 0.2$; Intensity: 0–8 h: $p = 0.3$, 0–48 h: $p = 0.9$. ***E***, Quantification of synaptic $\alpha 2$ $GABA_AR$ clusters after 8 and 48 h of 4-AP compared with mock treated control. t0 $n = 49$ cells, 8 h $n = 49$ cells, 48 h $n = 39$ cells, 3 cultures. Cluster Nb: 0–8 h: $p = 0.2$, 0–48 h: $p < 0.001$; Area: 0–8 h: $p = 0.8$, 0–48 h: $p = 0.6$; Intensity: 0–8 h: $p = 0.2$, 0–48 h: $p = 0.9$. ***F***, Quantification of extrasynaptic $\alpha 2$ $GABA_AR$ clusters after 8 and 48 h of 4-AP compared with mock treated control. Cluster Nb: 0–8 h: $p = 0.8$, 0–48 h: $p = 0.001$; Area: 0–8 h: $p < 0.001$, 0–48 h: $p = 0.7$; Intensity: 0–8 h: $p = 0.8$, 0–48 h: $p = 0.8$. ***G***, Quantification of $\alpha 2$ $GABA_AR$ diffusion coefficients after 8 h of 4-AP exposure. Extra: t0 $n = 624$ QDs, 4AP 8 h $n = 421$ QDs, $p = 5.4 \times 10^{-7}$. Syn: t0 $n = 252$ QDs, 8 h $n = 173$ QDs, $p = 0.2$, 2 cultures. ***H***, Quantification of explored area EA of $\alpha 2$ $GABA_AR$ after 8 h of 4-AP application. Extra: t0 $n = 1869$ QDs, 8 h $n = 1092$ QDs, $p = 7.8 \times 10^{-14}$. Syn: t0 $n = 753$ QDs, 8 h $n = 516$ QDs, $p = 0.07$. ***I***, Quantification of $\alpha 2$ $GABA_AR$ diffusion coefficients after 48 h of 4-AP exposure. Extra: t0 $n = 624$ QDs, 4AP 48 h $n = 631$ QDs, $p = 0.04$. Syn: t0 $n = 252$ QDs, 48 h $n = 251$ QDs, $p = 0.8$. 2 cultures. ***J***, Quantification of explored area EA of $\alpha 2$ $GABA_AR$ after 48 h of 4-AP application. Extra: t0 $n = 1092$ QDs, 48 h $n = 1890$ QDs, $p = 1.5 \times 10^{-6}$. Syn; t0 $n = 558$ QDs, 48 h $n = 750$ QDs, $p = 0.3$. ***K***, Quantification of $\alpha 2$ $GABA_AR$ dwell time DT after 8 or 48 h of 4-AP application. Calculations were done for trapped or passing QDs at inhibitory synapses. Trapped: t0: $n = 116$ QDs, 8 h: $n = 84$ QDs, 48 h: $n = 43$ QDs, 0–8 h: $p = 0.2$; 0–48 h: $p = 0.02$; Passing: t0: $n = 67$ QDs, 8 h: $n = 46$ QDs, 48 h: $n = 43$ QDs, 0–8 h: $p = 0.2$; 0–48 h: $p = 0.1$. In ***A***, ***C–F***, and ***K***, data are presented as mean ± SEM. ∗, $p \leq 0.05$; ∗∗∗, $p \leq 0.001$ (Mann–Whitney rank sum test). In ***G–J***, data are presented as median values ± 25%–75% IQR. ∗, $p \leq 0.05$; ∗∗∗, $p \leq 0.001$ (Kolmogorov–Smirnov test). In all graphs except ***C***, values were normalized to the corresponding control values.

Structure of the gephyrin scaffold requires phosphoregulation of gephyrin molecules

At GABAergic synapses, the role of phosphorylation for gephyrin scaffold compaction has yet to be reported. The fluorescence microscopy data (Fig. 1*B*) inform us about average area and intensity per cluster. PALM microscopy informs us about the actual density of molecules per surface area (Fig. 3). The number of molecules per synapse using PALM imaging can be roughly estimated by multiplying the mean surface area of the cluster by the density of gephyrin molecules per surface unit. Values of ~212, 156, and 220 were found for the gephyrin WT, S268E, and S270A respectively. Interestingly, these estimations are consistent with the measurements of the mean cluster fluorescence intensity for the S268E and S270A mutants.

The hexameric gephyrin lattice model was proposed based on G and E domain crystal structures available at the time. However, in recent years, atomic force microscopy (AFM) and small-angle X-ray scattering (SAXS) structure of full-length gephyrin has shown that gephyrin only exists as trimers, as individual E domains are in an open extended confirmation (Sander et al., 2013). Pennacchietti et al. (2017) have shown that after iLTP, gephyrin reorganizes itself into distinct subsynaptic nanodomains. Full-length gephyrin can exist in open or closed confirmations based on the linker domain folding (Sander et al., 2013). All the gephyrin phosphorylation sites have been mapped to the linker domain, suggesting that phosphorylation is a strong candidate for determining open and closed states within gephyrin nanodomains. This could in turn determine the distance between two nanodomains and/or total number of nanodomains within a given synapse.

Gephyrin-independent $GABA_AR$ adaptations at synaptic sites

It has long been assumed that alterations in $GABA_AR$ and/or gephyrin cluster intensity are indicative of the number of molecules found at the synapse, and thereby a direct correlate for changes in synapse structure and function. Here we report that disrupting gephyrin scaffold via the expression of the eGFP-DN mutant does not increase the diffusion properties of $GABA_ARs$ at synaptic sites. This observation was unexpected, as loss of the scaffolding apparatus should have increased receptor diffusion also at synaptic sites. It has been reported that eGFP-DN expression significantly reduces mIPSC amplitude and frequency, without leading to a complete loss of GABAergic synaptic transmission (Ghosh et al., 2016). Our observation suggests that a pool of gephyrin-independent $GABA_ARs$ are present in neurons. Recently, the GIT1/βPIX/Rac1/PAK signaling pathway was shown to contribute to GABAergic transmission. βPIX is a guanine nucleotide exchange factor (GEF) for Rac1 activating PAK and contributes to $GABA_AR$ stability (Smith et al., 2014). Similar signaling mechanisms could be operational even in the absence of gephyrin scaffold to maintain the membrane pool of $GABA_ARs$.

Independent behavior of $GABA_ARs$ at synaptic and extrasynaptic sites

Postsynaptic receptor trapping is adaptable depending on phosphorylation events that impinge on scaffold–scaffold or receptor–scaffold interactions (Choquet and Triller, 2013). It became clear with the development of SPT approaches that receptors are also hindered in their diffusion outside synapses via molecular crowding but also through specific protein–protein interactions. A receptor–

gephyrin interaction outside inhibitory synapses has been reported earlier (Ehrensperger et al., 2007). $GABA_A$Rs also colocalize and interact with clathrin-enriched endocytic zones (EZs) that are mostly localized extrasynaptically (Smith et al., 2012). Receptors in EZs do not necessarily undergo internalization. They can be part of a reserve pool of receptors rapidly available upon increase in synaptic activity (Petrini et al., 2014). Conversely, the $GABA_A$R–AP2 interaction within EZs has been shown to indirectly control receptor mobility and number at synapses (Smith et al., 2012).

However, our data show independent behavior of $GABA_A$Rs at synaptic and extrasynaptic sites. After 8 h of 4-AP treatment, α2 $GABA_A$Rs were confined at extrasynaptic sites without influencing the diffusion property of synaptic receptors. In contrast, after 48 h of 4-AP treatment, α2 $GABA_A$R confinement at extrasynaptic sites was ceased, and this was followed by an increase in receptor confinement at synapses, suggesting that $GABA_A$R retention at extrasynaptic sites prevents their synaptic capture/accumulation. However, after 8 h of 4-AP treatment, neurons expressing eGFP-S268E mutant show a reduction in receptor confinement at extrasynaptic locations, without affecting synaptic receptor diffusion. Therefore, removing diffusion constraints onto extrasynaptic $GABA_A$Rs does not facilitate receptor recruitment at synapses. In addition, after 8 h of 4-AP treatment, neurons expressing eGFP-S270A mutant show increased confinement of $GABA_A$Rs at both extrasynaptic and synaptic locations, indicating that confining $GABA_A$Rs at extrasynaptic locations does not prevent diffusion-capture of receptors.

Synaptic adaptation is facilitated by gephyrin phosphorylation

We present evidence for a biphasic model for activity-dependent plasticity at GABAergic postsynapse. Acute 4-AP treatment increases and chronic 4-AP treatment decreases α2 $GABA_A$R lateral diffusion. The observed increase in $GABA_A$R diffusion after acute 4-AP treatment can be explained by an increase in synaptic escape of receptors, leading to reduced postsynaptic clustering and dispersal of gephyrin molecules away from the synapse (Bannai et al., 2009). On the contrary, we show here that chronic 4-AP treatment leads to synaptic immobilization and recruitment of $GABA_A$R α2 and gephyrin. These discrepancies are probably due to the distinct signaling pathways activated by the acute and chronic changes in activity. Short-term 4-AP application induces NMDAR-mediated calcium influx and calcineurin activation, leading to dephosphorylation of $GABA_A$R γ2 subunit S327 residue (Bannai et al., 2009). In this context, the relief in $GABA_A$R diffusion constraints arises from receptor dephosphorylation, whereas gephyrin loss is a consequence of receptor dispersal (Niwa et al., 2012). In contrast, we show that chronic changes in activity affect first the recruitment of gephyrin at synapses, and then allow the recruitment of $GABA_A$Rs. PKA and CaMKIIα signaling act downstream of NMDA receptor to facilitate compensatory postsynaptic adaptations at GABAergic synapses (Flores et al., 2015). Our data extends this understanding by demonstrating a role for the GSK3β pathway in addition to PKA and CaMKIIα pathways in facilitating gephyrin scaffold organization of individual $GABA_A$Rs after prolonged changes in activity.

References

Bannai H, Lévi S, Schweizer C, Inoue T, Launey T, Racine V, Sibarita J-B, Mikoshiba K, Triller A (2009) Activity-dependent tuning of inhibitory neurotransmission based on GABAAR diffusion dynamics. Neuron 62:670–682. CrossRef Medline

Bannai H, Niwa F, Sherwood MW, Shrivastava AN, Arizono M, Miyamoto A, Sugiura K, Lévi S, Triller A, Mikoshiba K (2015) Bidirectional control of synaptic GABAAR clustering by glutamate and calcium. Cell Rep 13:2768–2780. CrossRef Medline

Bats C, Groc L, Choquet D (2007) The interaction between Stargazin and PSD-95 regulates AMPA receptor surface trafficking. Neuron 53:719–734. CrossRef Medline

Chamma I, Heubl M, Chevy Q, Renner M, Moutkine I, Eugène E, Poncer JC, Lévi S (2013) Activity-dependent regulation of the K/Cl transporter KCC2 membrane diffusion, clustering, and function in hippocampal neurons. J Neurosci 33:15488–15503. CrossRef

Charrier C, Machado P, Tweedie-Cullen RY, Rutishauser D, Mansuy IM, Triller A (2010) A crosstalk between β1 and β3 integrins controls glycine receptor and gephyrin trafficking at synapses. Nat Neurosci 13:1388–1395. CrossRef Medline

Chen JL, Villa KL, Cha JW, So PTC, Kubota Y, Nedivi E (2012) Clustered dynamics of inhibitory synapses and dendritic spines in the adult neocortex. Neuron 74:361–373. CrossRef Medline

Choquet D, Triller A (2013) The dynamic synapse. Neuron 80:691–703. CrossRef Medline

Ehrensperger M-V, Hanus C, Vannier C, Triller A, Dahan M (2007) Multiple association states between glycine receptors and gephyrin identified by SPT analysis. Biophys JI 92:3706–3718. CrossRef Medline

Flores CE, Nikonenko I, Mendez P, Fritschy J-M, Tyagarajan SK, Muller D (2015) Activity-dependent inhibitory synapse remodeling through gephyrin phosphorylation. Proc Natl Acad Sci USA 112:E65–E72. CrossRef

Ghosh H, Auguadri L, Battaglia S, Simone Thirouin Z, Zemoura K, Messner S, Acuña MA, Wildner H, Yévenes GE, Dieter A, Kawasaki H, O Hottiger M, Zeilhofer HU, Fritschy J-M, Tyagarajan SK (2016) Several posttranslational modifications act in concert to regulate gephyrin scaffolding and GABAergic transmission. Nat Commun 7:13365CrossRef Medline

Lardi-Studler B, Smolinsky B, Petitjean CM, Koenig F, Sidler C, Meier JC, Fritschy JM, Schwarz G (2007) Vertebrate-specific sequences in the gephyrin E-domain regulate cytosolic aggregation and postsynaptic clustering. J Cell Sci 120:1371–1382. CrossRef Medline

Lévi S, Schweizer C, Bannai H, Pascual O, Charrier C, Triller A (2008) Homeostatic regulation of synaptic GlyR numbers driven by lateral diffusion. Neuron 59:261–273. CrossRef Medline

Lüscher B, Fuchs T, Kilpatrick CL (2011) GABAA receptor trafficking-mediated plasticity of inhibitory synapses. Neuron 70:385–409. CrossRef Medline

Muir J, Arancibia-Carcamo IL, MacAskill AF, Smith KR, Griffin LD, Kittler JT (2010) NMDA receptors regulate GABAA receptor lateral mobility and clustering at inhibitory synapses through serine 327 on the γ2 subunit. Proc Natl Acad Sci USA 107:16679–16684. CrossRef

Niwa F, Bannai H, Arizono M, Fukatsu K, Triller A, Mikoshiba K (2012) Gephyrin-independent GABA(A)R mobility and clustering during plasticity. PLoS ONE 7:e36148. CrossRef Medline

Pennacchietti F, Vascon S, Nieus T, Rosillo C, Das S, Tyagarajan SK, Diaspro A, Del Bue A, Petrini EM, Barberis A, Cella Zanacchi F (2017) Nanoscale molecular reorganization of the inhibitory postsynaptic density is a determinant of GABAergic synaptic potentiation. J Neurosci 37:1747–1756. CrossRef Medline

Petrini EM, Barberis A (2014) Diffusion dynamics of synaptic molecules during inhibitory postsynaptic plasticity. Front Cell Neurosci 8:300. CrossRef Medline

Petrini EM, Ravasenga T, Hausrat TJ, Iurilli G, Olcese U, Racine V, Sibarita J-B, Jacob TC, Moss SJ, Benfenati F, Medini P, Kneussel M, Barberis A (2014) Synaptic recruitment of gephyrin regulates surface GABAA receptor dynamics for the expression of inhibitory LTP. Nat Commun 5:3921. CrossRef

Rannals MD, Kapur J (2011) Homeostatic strengthening of inhibitory synapses is mediated by the accumulation of GABA(A) receptors. J Neurosci 31:17701–17712. CrossRef Medline

Renner M, Schweizer C, Bannai H, Triller A, Lévi S (2012) Diffusion barriers constrain receptors at synapses. PLoS ONE 7:e43032. CrossRef

Saliba RS, Michels G, Jacob TC, Pangalos MN, Moss SJ (2007) Activity-dependent ubiquitination of GABA(A) receptors regulates their accumulation at synaptic sites. J Neurosci 27:13341–13351. CrossRef

Sander B, Tria G, Shkumatov AV, Kim EY, Grossmann JG, Tessmer I, Svergun DI, Schindelin H (2013) Structural characterization of gephyrin by AFM and SAXS reveals a mixture of compact and extended states. Acta Crystallogr D Biol Crystallogr 69:2050–2060. CrossRef Medline

Smith KR, Davenport EC, Wei J, Li X, Pathania M, Vaccaro V, Yan Z, Kittler JT (2014) GIT1 and βPIX are essential for GABA(A) receptor synaptic stability and inhibitory neurotransmission. Cell Rep 9:298–310. CrossRef Medline

Smith KR, Muir J, Rao Y, Browarski M, Gruenig MC, Sheehan DF, Haucke V, Kittler JT (2012) Stabilization of GABA(A) receptors at endocytic zones is mediated by an AP2 binding motif within the GABA(A) receptor β3 subunit. J Neurosci 32:2485–2498. CrossRef Medline

Specht CG, Izeddin I, Rodriguez PC, Beheiry El M, Rostaing P, Darzacq X, Dahan M, Triller A (2013) Quantitative nanoscopy of inhibitory synapses: counting gephyrin molecules and receptor binding sites. Neuron 79:308–321. CrossRef

Tyagarajan SK, Ghosh H, Yévenes GE, Imanishi SY, Zeilhofer HU, Gerrits B, Fritschy J-M (2013) Extracellular signal-regulated kinase and glycogen synthase kinase 3β regulate gephyrin postsynaptic aggregation and GABAergic synaptic function in a calpain-dependent mechanism. J Biol Chem 288:9634–9647. CrossRef

Tyagarajan SK, Ghosh H, Yévenes GE, Nikonenko I, Ebeling C, Schwerdel C, Sidler C, Zeilhofer HU, Gerrits B, Muller D, Fritschy J-M (2011) Regulation of GABAergic synapse formation and plasticity by GSK3beta-dependent phosphorylation of gephyrin. Proc Natl Acad Sci USA 108:379–384. CrossRef

van Versendaal D, Rajendran R, Saiepour MH, Klooster J, Smit-Rigter L, Sommeijer J-P, De Zeeuw CI, Hofer SB, Heimel JA, Levelt CN (2012) Elimination of inhibitory synapses is a major component of adult ocular dominance plasticity. Neuron 74:374–383. CrossRef Medline

Villa KL, Berry KP, Subramanian J, Cha JW, Oh WC, Kwon H-B, Kubota Y, So PTC, Nedivi E (2016) Inhibitory synapses are repeatedly assembled and removed at persistent sites in vivo. Neuron 89:756–769. CrossRef

Vlachos A, Reddy-Alla S, Papadopoulos T, Deller T, Betz H (2013) Homeostatic regulation of gephyrin scaffolds and synaptic strength at mature hippocampal GABAergic postsynapses. Cereb Cortex 23:2700–2711. CrossRef Medline

Wang J, Liu S, Haditsch U, Tu W, Cochrane K, Ahmadian G, Tran L, Paw J, Wang Y, Mansuy I, Salter MM, Lu YM (2003) Interaction of calcineurin and type-A GABA receptor gamma 2 subunits produces long-term depression at CA1 inhibitory synapses. J Neurosci 23:826–836. Medline

Yu W, Jiang M, Miralles CP, Li R-W, Chen G, De Blas AL (2007) Gephyrin clustering is required for the stability of GABAergic synapses. Mol Cell Neurosci 36:484–500. CrossRef Medline

frontiers in Cellular Neuroscience

REVIEW
published: 20 February 2019
doi: 10.3389/fncel.2019.00048

Reciprocal Regulation of KCC2 Trafficking and Synaptic Activity

Etienne Côme[1,2,3†], *Martin Heubl*[1,2,3†], *Eric J. Schwartz*[1,2,3], *Jean Christophe Poncer*[1,2,3] *and Sabine Lévi*[1,2,3*]

[1]INSERM UMR-S 1270, Paris, France, [2]Sorbonne Université, Paris, France, [3]Institut du Fer à Moulin, Paris, France

The main inhibitory neurotransmitter receptors in the adult central nervous system (CNS) are type A γ-aminobutyric acid receptors ($GABA_A$Rs) and glycine receptors (GlyRs). Synaptic responses mediated by GlyR and $GABA_A$R display a hyperpolarizing shift during development. This shift relies mainly on the developmental up-regulation of the K^+-Cl^- co-transporter KCC2 responsible for the extrusion of Cl^-. In mature neurons, altered KCC2 function—mainly through increased endocytosis—leads to the re-emergence of depolarizing GABAergic and glycinergic signaling, which promotes hyperexcitability and pathological activities. Identifying signaling pathways and molecular partners that control KCC2 surface stability thus represents a key step in the development of novel therapeutic strategies. Here, we present our current knowledge on the cellular and molecular mechanisms governing the plasma membrane turnover rate of the transporter under resting conditions and in response to synaptic activity. We also discuss the notion that KCC2 lateral diffusion is one of the first parameters modulating the transporter membrane stability, allowing for rapid adaptation of Cl^- transport to changes in neuronal activity.

Keywords: $GABA_A$R, chloride homeostasis, membrane turnover, lateral diffusion, clustering

OPEN ACCESS

Edited by:
Enrica Maria Petrini, Fondazione Istituto Italiano di Tecnologia, Italy

Reviewed by:
Igor Medina, Institut National de la Santé et de la Recherche Médicale (INSERM), France
Tarek Deeb, Tufts University School of Medicine, United States

***Correspondence:**
Sabine Lévi
sabine.levi@inserm.fr

†These authors have contributed equally to this work

Received: *01 August 2018*
Accepted: *01 February 2019*
Published: *20 February 2019*

Citation:
Côme E, Heubl M, Schwartz EJ, Poncer JC and Lévi S (2019) Reciprocal Regulation of KCC2 Trafficking and Synaptic Activity. Front. Cell. Neurosci. 13:48. doi: 10.3389/fncel.2019.00048

INTRODUCTION

Excitatory and inhibitory neurotransmission depend on the electrochemical ion gradients across the plasma membrane. The activation of postsynaptic ionotropic glutamate receptors leads to an influx of positively charged ions and thereby generates a depolarizing, excitatory postsynaptic potential (EPSP). In contrast, the net effect of activation of ionotropic anion permeable channels, such as type A γ-aminobutyric acid receptors ($GABA_A$Rs) or glycine receptors (GlyRs), depends on the gradient of anions across the plasma membrane, predominantly chloride (Cl^-) and bicarbonate (HCO_3^-; Bormann et al., 1987; Kaila and Voipio, 1987). The chloride gradient is mainly established by two secondary active transporters: the K^+-Cl^- cotransporter KCC2 that extrudes chloride out of the neuron using the potassium gradient (generated by the Na^+/K^+ ATPase), and the Na^+-K^+-Cl^- cotransporter NKCC1 which usually transports chloride into the neuron based on transmembrane sodium and potassium gradients also generated by the Na^+/K^+ ATPase (**Figure 1**). Hence, the balance of expression and activity of these transporters influence intracellular chloride concentration ($[Cl^-]_i$) and the efficacy and polarity of GABAergic and glycinergic transmission. In immature neurons, where NKCC1 expression

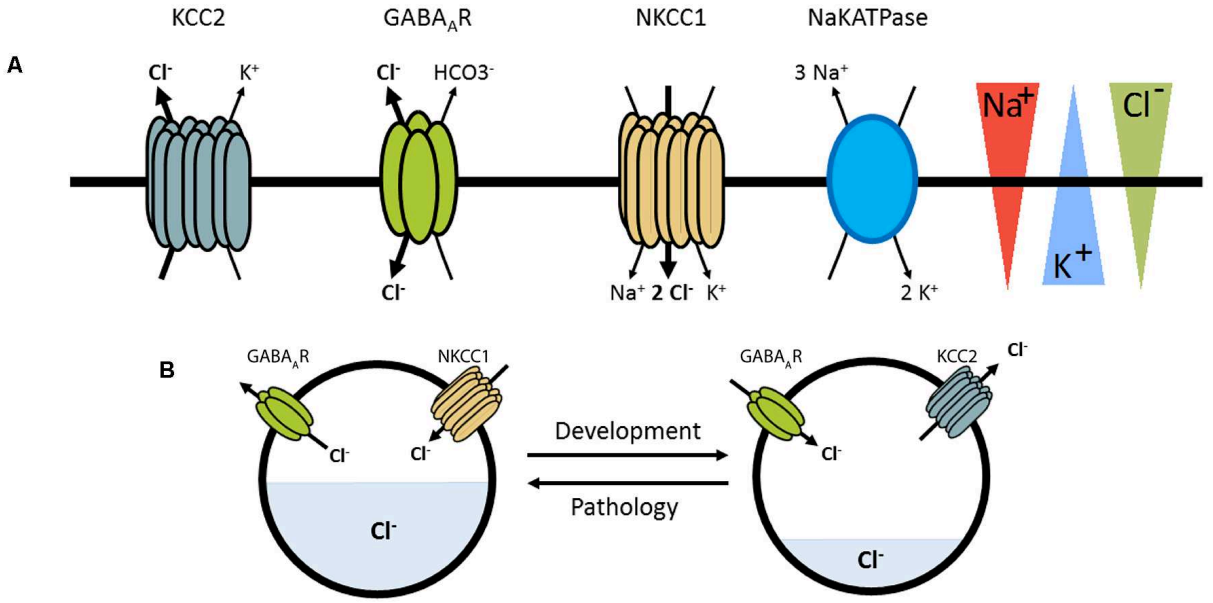

FIGURE 1 | Pivotal role of KCC2 and NKCC1 in the regulation of $[Cl]_i$. **(A)** KCC2 and NKCC1 transport chloride across the plasma membrane according to the Na^+ and K^+ gradients imposed by the Na^+K^+ ATPase. γ-aminobutyric acid receptor ($GABA_AR$) are primarily permeable to chloride ions and thus GABAergic transmission depends on KCC2 and NKCC1 regulation. **(B)** Depending on pathological conditions or developmental stages, GABAergic transmission may be depolarizing, correlated with an increased NKCC1/KCC2 functional ratio.

predominates, high $[Cl^-]_i$ is associated with depolarizing responses to GABA and glycine reflecting Cl^- efflux. In contrast, an increased expression of KCC2 in mature neurons lowers $[Cl^-]_i$ leading to an influx of Cl^- ions and hyperpolarizing responses upon $GABA_AR$/GlyR activation.

In addition to its role in maintaining low $[Cl^-]_i$, KCC2 regulates the formation (Li et al., 2007), functional maintenance and plasticity (Gauvain et al., 2011; Fiumelli et al., 2013; Chevy et al., 2015; Llano et al., 2015) of glutamatergic synapses. Consistent with its key role in regulating inhibitory and excitatory neurotransmission, alterations in KCC2 expression and function have emerged as a common mechanism underlying pathological activity in a variety of neurological and psychiatric disorders (Medina et al., 2014; Kahle and Delpire, 2016; Moore et al., 2017; Wang et al., 2018). Understanding the mechanisms regulating KCC2 expression and function is therefore crucial to develop novel and efficient therapeutic strategies. Here, we will review the cellular and molecular mechanisms controlling KCC2 turnover and describe how these mechanisms are rapidly tuned when neuronal activity is challenged.

KCC2 STRUCTURE AND REGULATORY SEQUENCES

KCC2 is one of nine members of the cation-chloride co-transporter (CCC) family encoded by the genes *Slc12a1-9*. KCC2 is a glycoprotein of 120 kDa with a predicted structure of 12 transmembrane segments (TMs), six extracellular loops flanked by a short intracellular amino terminal domain (NTD; amino acids 1–103) and a long intracellular carboxy-terminal domain (CTD; last 500 amino acids; Hartmann and Nothwang, 2015; **Figure 2**).

Two different KCC2 isoforms, KCC2a and KCC2b, are produced by use of alternative promoters of the *Slc12a5* gene encoding KCC2 (Uvarov et al., 2007). The NTD of KCC2a is 23 amino acids longer than the KCC2b one (Uvarov et al., 2007) and contains a putative SPAK (STE20/SPS1-related, proline alanine-rich kinase) and OSR1 kinase (Oxydative stress response 1) interaction site (de Los Heros et al., 2014; **Table 1**). Both isoforms show similar ion transport properties when expressed in human embryonic kidney (HEK) 293 cells and cultured hippocampal and cortical neurons (Uvarov et al., 2007; Markkanen et al., 2017), but have different subcellular localization *in vivo* (in neurons of the deep cerebellar nucleus, the pons and the medulla) and *in vitro* (cultured hippocampal neurons; Markkanen et al., 2014, 2017), suggesting a contribution of the NTD to the subcellular targeting of the transporter in given cells, probably *via* the binding to selective partners.

Based on a study of KCC1 (Casula et al., 2001), the KCC2 NTD has been suggested to be mandatory for KCC2 function (Li et al., 2007). Several groups have therefore used KCC2 lacking the NTD (KCC2-ΔNTD) to study ion-transport independent roles of KCC2 (Li et al., 2007; Horn et al., 2010; Fiumelli et al., 2013). The group of Igor Medina recently described altered exocytosis by truncation of the NTD in N2a cells, HEK 293 cells and cultured hippocampal neurons (Friedel et al., 2017).

In addition to five short extracellular loops, KCC2 contains a long extracellular loop (LEL) between TM5 and TM6 of around 100 amino acids (Williams et al., 1999). Based on

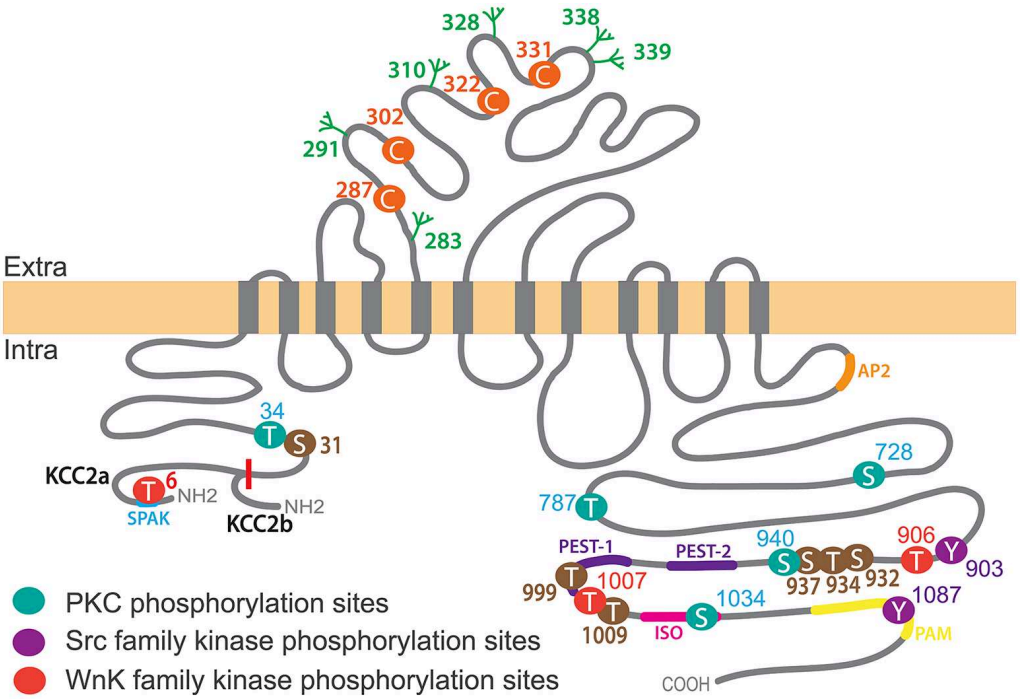

FIGURE 2 | KCC2 structure, key phosphorylation residues and regulatory domains. The KCC2 co-transporter is a ~140 kDa protein with a predicted topology of 12 membrane spanning segments, an extracellular domain between transmembrane domains 5 and 6 containing N-glycosylation sites (green) and key Cysteine residues for ion transport (orange), and is flanked by two cytoplasmic carboxy- and amino- terminal domains. All residues (besides Threonine T6 which is only present in KCC2a) are numbered according to human KCC2b. Note that the mouse sequence lacks amino acid 1,000 and thus beyond this residue the numbering is shifted (e.g., T1007 in human corresponds to T1006 in mice). KCC2a and KCC2b isoforms differ from their intracellular amino-terminal domain with KCC2a having a 23 amino acids longer sequence bearing a SPAK-binding domain (blue). Other regulatory sequences of KCC2 are located within the large intracellular carboxy-terminal domain (CTD), such as protein kinase C (PKC) phosphorylation sites (Serine S728, T787, S940 and S1034), Src family kinase phosphorylation sites (Tyrosine Y903, Y1087) and WNK-SPAK-OSR1 kinases (T906, T1007). Other regulatory sequences are present on this region: the ISO domain (pink) allowing for KCC2 activity under isotonic conditions, and protein associated with Myc (PAM; yellow), Proline/E/S/T (PEST; purple), SPAK (blue) and adaptor protein-2 (AP2; orange) binding sequences. Note that KCC2 activators staurosporine and N-ethylmaleimide (NEM) act by controlling (de)phosphorylation of series of residues (brown).

TABLE 1 | Key regulatory sites and sequences on KCC2.

Site	Localization	References
Protein Associated with Myc (PAM) LVLLNMPGPPRNRNGDENYM	1069-1088	Garbarini and Delpire (2008)
PEST sequence	PEST-1: 949-966 PEST-2: 974-1002	Mercado et al. (2006)
ISO domain PSPVSSEGIKDFFSM	1021-1035	Mercado et al. (2006)
AP-2 interaction domain LLRLEE	657-662	Zhao et al. (2008)
SPAK-OSR1 interaction domain		
RFTV	4–7	Piechotta et al. (2002)
Cysteines	287-302-322-331	Hartmann et al. (2010)
N-Glycosylation sites	283-291-310-328-338-339	Agez et al. (2017)
Tyrosines	34-787-906-1007	Rinehart et al. (2009), de Los Heros et al. (2014), Weber et al. (2014) and Cordshagen et al. (2018)
	34, 999, 1009	
	34, 1009	
Serines	728-940-1,034	Lee et al. (2007), Weber et al. (2014) and Cordshagen et al. (2018)
	31, 913, 932, 988	
	25, 26, 937, 1022, 1025, 1026	

Positions are shown relative to the human KCC2b protein.

KCC4 studies, N-linked glycosylation in the KCC2 LEL was proposed to be crucial for the membrane targeting of KCC2 (Hartmann and Nothwang, 2015). Six glycosylation sites on KCC2 were subsequently identified (Agez et al., 2017). Three human KCC2 mutations associated with severe early-onset epileptic encephalopathy showed reduced protein glycosylation and cell surface KCC2 (Stödberg et al., 2015), implicating KCC2 glycosylation in the control of its membrane expression. In addition, four highly conserved cysteine residues within the LEL were shown to be important for KCC2 activity but not membrane expression in HEK 293 cells probably due to their implication in inter- or intra-molecular di-sulfide bonds and correct protein folding (Hartmann et al., 2010).

The KCC2 CTD contains most of the KCC2 regulatory sequences. Complete truncation of the CTD reduces membrane expression of KCC1, 2 and 3 in *Xenopus laevis* oocytes and HEK 293 cells (Payne, 1997; Casula et al., 2001; Howard et al., 2002). Using live-cell surface labeling, Friedel et al. (2017) recently showed in cultured hippocampal neurons that KCC2 CTD is dispensable for membrane delivery of the transporter but is required for its membrane stabilization. Consistent with these observations, truncation of the KCC2 CTD by the Ca^{2+}-dependent protease calpain at an unknown site leads to the internalization and lysosomal degradation of KCC2 in rat brain slices (Puskarjov et al., 2012). Moreover, the interaction of KCC2 CTD with the clathrin-binding adaptor protein-2 (AP-2) *via* a di-leucine motif induces a constitutive, dynamin-dependent and clathrin-mediated endocytosis of KCC2 in HEK 293 cells (Zhao et al., 2008). The CTD also hosts the majority of KCC2 phosphorylation residues (**Figure 2**) which influence KCC2 membrane stability and thereby function through regulation of the transporter's lateral diffusion, oligomerization, clustering, and endocytosis (see below).

In contrast to other KCCs, KCC2 is constitutively active under isotonic conditions (Payne, 1997). A short sequence called ISO domain (1,022–1,037) located in the CTD has been shown to be responsible for this specific feature in Xenopus oocytes and hippocampal neurons (Mercado et al., 2006; Acton et al., 2012). Thus, replacement of this sequence by the corresponding KCC4 amino acids abolished constitutive KCC2 activity (Acton et al., 2012). Interestingly, KCC2 transporters lacking the ISO domain can still be activated under hypotonic conditions, indicating that two distinct domains are involved in KCC2 activation under isotonic vs. hypotonic conditions.

TEMPORAL AND SPATIAL EXPRESSION PATTERN OF KCC2

KCC2 expression can be observed throughout the central nervous system (CNS) including spinal cord (Hübner et al., 2001), thalamus (Barthó et al., 2004), cerebellum (Williams et al., 1999), hippocampus (Rivera et al., 1999), cortical structures (Gulyás et al., 2001) and the auditory brainstem (Blaesse et al., 2006). Although KCC2 expression is very broad in the CNS, the reversal potential of $GABA_AR$-mediated currents (E_{GABA}) varies among neuronal populations and brain structures (Chavas and Marty, 2003; Watanabe and Fukuda, 2015). These differences are thought to reflect changes in CCC expression and function.

Developmental Expression

Developmental upregulation of KCC2 expression has been described in different systems including human (Dzhala et al., 2005; Sedmak et al., 2016), mouse (Hübner et al., 2001), rat (Gulyás et al., 2001), zebrafish (Zhang et al., 2010), *C. elegans* (Tanis et al., 2009) and other species (for review Blaesse et al., 2009; Kaila et al., 2014). The KCC2 expression profile is well correlated with the sequential maturation of different brain regions (Watanabe and Fukuda, 2015), and follows the rostro-caudal axis of neuronal maturation (Li et al., 2002; Stein et al., 2004). Interestingly only the KCC2b isoform is developmentally upregulated, while KCC2a expression remains constant over brain maturation (Yeo et al., 2009). In the neonatal mouse brainstem KCC2a therefore contributes to about 20%–50% of the total KCC2 mRNA expression, while in the mature cortex its contribution decreases down to 5%–10% (Uvarov et al., 2009). KCC2a is expressed in the basal forebrain, hypothalamus and spinal cord, but is absent from the hippocampus (Markkanen et al., 2014). In contrast to full KCC2 knockout mice, which die at birth due to respiratory failure (Hübner et al., 2001), KCC2b knockout mice are viable until postnatal age 15 (P15; Woo et al., 2002). This suggests that both KCC2a and KCC2b isoforms are essential but contribute differentially to brain development and the establishment of inhibitory neurotransmission. Indeed, Dubois et al. (2018) recently showed a transient role of KCC2a at birth controlling the pontine neuromodulation of the respiratory motor circuits.

Subcellular Expression

At the cellular level, KCC2 expression can be found in the somatodendritic plasma membrane in most brain regions, such as cerebellum (Williams et al., 1999), hippocampus (Rivera et al., 1999; Gulyás et al., 2001) or cortex (Szabadics et al., 2006). KCC2 membrane expression is enriched near inhibitory and excitatory synapses and in spine heads of hippocampal neurons (Gulyás et al., 2001; Hübner et al., 2001; Blaesse et al., 2006; Gauvain et al., 2011; Chamma et al., 2012). At the presynaptic level, only developing photoreceptor cells (Zhang et al., 2006) and retinal bipolar cells (Vardi et al., 2000) exhibit KCC2 expression. Axonal exclusion of KCC2 from CNS axons, including axon initial segment (Williams et al., 1999; Hübner et al., 2001; Chamma et al., 2012), leads to higher $[Cl^-]_i$ in axons than in the somatodendritic compartment (Price and Trussell, 2006). As a consequence, activation of $GABA_AR$ by GABA spillover or axo-axonic GABAergic synapses leads to increased axonal excitability (Stell et al., 2007; Ruiz et al., 2010; Pugh and Jahr, 2011, 2013; Stell, 2011).

Association of KCC2 with the plasma membrane increases during neuronal maturation. Hence, immature neurons show brighter intracellular labeling than mature neurons (Gulyás et al., 2001; Szabadics et al., 2006) and KCC2 forms clusters at the surface of mature neurons (Gulyás et al., 2001; Hübner et al., 2001; Barthó et al., 2004; Watanabe et al., 2009; Chamma et al., 2012, 2013; Heubl et al., 2017). In primary

cultures of hippocampal neurons, KCC2 protein expression can be observed already at 3 days *in vitro* (div) in the soma, while the somatodendritic labeling peaks only at div 15 (Ludwig et al., 2003).

Markkanen and colleagues were the first to compare the subcellular distribution of the two KCC2 isoforms, KCC2a and KCC2b, in the deep cerebellar nucleus, the pons and the medulla, in hippocampal cultured neurons (Markkanen et al., 2014, 2017). The authors showed that in these neurons, KCC2a and KCC2b only partly colocalize and that the two isoforms are not localized in the same subcellular compartments in mature neurons (with stronger labeling of KCC2b on the soma and plasma membrane in general). The functional consequence of this distinct isoform localization however remains unclear.

MOLECULAR AND CELLULAR MECHANISMS OF REGULATION OF KCC2

KCC2 is regulated at the transcriptional and post-transcriptional level (e.g., through phosphorylation/dephosphorylation of key residues) which in turn influence its cellular trafficking (cell surface delivery, membrane diffusion-trapping, clustering, surface removal and intracellular degradation).

Transcriptional Regulation of KCC2

The neuron-specific KCC2 expression pattern is tightly regulated by transcription factors and neuron-restrictive silencing elements (NRSE) in the KCC2 gene *Slc12a5* (Karadsheh and Delpire, 2001; Uvarov et al., 2005, 2006; Yeo et al., 2009). Two NRSE sequences were found in intron 1 of the *Slc12a5* gene (Karadsheh and Delpire, 2001) and in the upstream regulatory region (Yeo et al., 2009). Binding of each of the restrictive elements to a neuron-restrictive silencing factor/repressor-element transcription factor (NRSF/REST) is sufficient to repress gene transcription (Yeo et al., 2009). In addition to these negative regulatory elements, two positive regulatory regions in the *Slc12a5* gene have been reported. Binding of the neuron specific transcription factor Egr4 (early growth response 4) to the Egr (early growth response) binding site activates KCC2 transcription (Uvarov et al., 2006). Similarly, Markkanen et al. (2008) found that binding of upstream stimulation factors, USF1 and 2, to an enhancer box (E-box) activates KCC2 expression.

The brain-derived neurotrophic factor (BDNF) has been shown to modulate KCC2 expression (Poo, 2001; Rivera et al., 2002; Aguado et al., 2003; Gottmann et al., 2009; Watanabe and Fukuda, 2015). While BDNF promotes KCC2 expression in immature neurons, exposure of mature CA1 pyramidal neurons to BDNF leads to decreased chloride extrusion (Rivera et al., 2004). Conversely, GABA increases BDNF expression in immature hippocampal and cerebrocortical neurons but not in mature hippocampal neurons, indicating a synergistic effect of GABAergic maturation and BDNF (Berninger et al., 1995; Kuczewski et al., 2011; Porcher et al., 2011). However, BDNF depletion (as shown in BDNF knockout mice) does not affect the developmental upregulation of KCC2 expression and function (Puskarjov et al., 2015). These results contrast with the reduced hippocampal KCC2 expression observed in TrkB knockout mice (Carmona et al., 2006) and the BDNF-induced increase in KCC2 mRNA expression in immature hippocampal neurons (Aguado et al., 2003; Rivera et al., 2004; Ludwig et al., 2011). Altogether, these results support a role of BDNF and TrkB in the developmental upregulation of KCC2.

Other trophic factors such as insulin-like growth factor 1 (Kelsch et al., 2001) and neurturin (Ludwig et al., 2011) have been implicated in the regulation of KCC2 expression. These data indicate that several signals control KCC2 expression and interact to increase KCC2 expression during neuronal development. The correlation of synaptic maturation with KCC2 upregulation therefore suggests their reciprocal influence.

Posttranslational Regulatory Mechanisms

Ion-transport activity of KCC2 does not only depend on KCC2 expression levels but also on the abundance and activity of numerous other proteins such as scaffolding proteins, cytoskeleton interactors/regulators, kinases and phosphatases that regulate its cellular trafficking.

Exocytosis

Consistent with the developmental switch of GABA/glycine neurotransmission, translocation of KCC2 from the cytoplasm to the plasma membrane indicates that exocytosis contributes to the control of KCC2-mediated chloride extrusion. Dynamic visualization of membrane insertion or internalization using recombinant proteins linked to pH-sensitive fluorophores helped to determine exocytosis-endocytosis trafficking of several neurotransmitter receptors (Petrini et al., 2014; Zhang et al., 2015). Since the NTD and CTD of KCC2 are both cytosolic, a pH-sensitive pHluorin tag was inserted in the second or third extracellular loop of the transporter (Friedel et al., 2015, 2017). Insertion of the tag loop of the transporter did not perturb the function of the protein and therefore this construct constitutes a useful tool to study KCC2 trafficking (Friedel et al., 2017). The expression of pHluorin-tagged KCC2 mutants with deletions of the N terminal (ΔNTD) or C terminal (ΔCTD) domain and the use of live-cell surface immunolabeling of heterologous cells or cultured hippocampal neurons revealed that the NTD is essential for KCC2 plasma membrane delivery whereas the CTD is critical to its membrane stability (Friedel et al., 2017).

Recently, insights into the regulatory mechanisms of KCC2 exocytosis were obtained as transforming growth factor β2 (TGF-β2) was shown to mediate translocation of KCC2 from intracellular pools to the plasma membrane in developing and mature hippocampal neurons (Roussa et al., 2016). The mechanism for TGF-β2-mediated KCC2 membrane translocation involves the Ras-associated binding protein 11b (Rab11b). KCC2-Rab11b interaction was recently confirmed in a native KCC2 interactome study (Mahadevan et al., 2017).

Oligomerization

Multimeric assembly has been demonstrated for a large number of members of the CCC family (Moore-Hoon and Turner, 2000; Casula et al., 2001, 2009; Starremans et al., 2003; Blaesse et al., 2006; Simard et al., 2007; Warmuth et al., 2009). KCC2 was shown to form KCC2a and KCC2b homo-dimers,

as well as KCC2a-KCC2b, KCC2-KCC4 and KCC2-NKCC1 hetero-dimers, in biochemical assays from neuronal and heterologous cell lysates (Blaesse et al., 2006; Simard et al., 2007; Uvarov et al., 2009).

There are discrepancies in the literature regarding the proportions of KCC2 monomers, dimers and higher-order oligomers in neurons. Blaesse et al. (2006) showed that an increase of KCC2 oligomers parallels transporter activation in the developing brainstem (between P2 and P30) whereas Uvarov et al. (2009) found oligomerization already at P2 in various brain regions. Mahadevan et al. (2014, 2017) using native PAGE reported that KCC2 form monomers, dimers as well as higher molecular mass complexes. However, using similar approaches, Agez et al. (2017) detected KCC2 monomers and dimers but not higher-order oligomers. These discrepancies may arise from differences in both experimental assays (native perfluorooctanoate-PAGE vs. 3%–8% Tris-acetate NuPAGE; Blaesse et al., 2006; Uvarov et al., 2009) as well as detergents used for sample preparation (CALX-R3 vs. C12E9; Agez et al., 2017; Mahadevan et al., 2017). These limitations also apply to SDS-PAGE studies, as differences in sample preparation influence the proportion of KCC2 dimer-like complexes (Medina et al., 2014). In conclusion, it is not possible to compare the relative abundance of KCC2 monomers, dimers and higher-order oligomers between studies.

The oligomerization domain has not been identified to date. However, several studies showed self-assembling capability for the CTD of NKCC1 and an Archean CCC (Simard et al., 2004; Warmuth et al., 2009) and decreased oligomerization of KCCs truncated on the C-terminus, or mutated on tyrosine residue 1087 (Simard et al., 2007; Watanabe et al., 2009). This observation suggests that KCC2 CTD might be involved in the assembly of the transporters as observed in Xenopus oocytes and hippocampal cultures (Simard et al., 2007; Watanabe et al., 2009). Whether the monomeric KCC2 is active remains unclear. Several studies reported a correlation between decreased KCC2 oligomerization and reduced transport activity (Watanabe et al., 2009; Mahadevan et al., 2014). For instance, neuropilin and tolloid like-2 (Neto-2) assemble with the oligomeric forms of KCC2 and this interaction increases KCC2-mediated Cl^- extrusion in cultured hippocampal neurons (Ivakine et al., 2013). Similarly, the kainate receptor GluK2 subunit interacts with KCC2 and is critical to KCC2 oligomerization, surface expression and ion-transport function in hippocampal neurons (Mahadevan et al., 2014; Pressey et al., 2017). However, since changes in KCC2 oligomerization and surface expression occur in parallel, these observations do not demonstrate a causal link between KCC2 oligomerization and Cl^- transport.

Clustering

KCC2 forms clusters in the neuronal plasma membrane (Gulyás et al., 2001; Hübner et al., 2001; Barthó et al., 2004; Watanabe et al., 2009; Chamma et al., 2012, 2013; Heubl et al., 2017). Interestingly the majority of KCC2 clusters are found at excitatory and inhibitory synapses in hippocampal cultures, without preferential accumulation at one type of synapses (Chamma et al., 2013). Ultrastructural studies indicate that KCC2 accumulates at the periphery of synapses in dendritic spines as well as on the dendritic shaft (Gulyás et al., 2001; Báldi et al., 2010).

KCC2 clustering could help to localize and/or stabilize transporters in sub-membrane compartments (e.g., near excitatory and inhibitory synapses), and to form a barrier in dendritic spines surrounding glutamatergic postsynaptic densities. Moreover, KCC2 clustering has been proposed to regulate the cotransporter function. Watanabe et al. (2009) showed that inhibition of tyrosine phosphorylation or deletion of a nearby region (Δ1089–1116) both lead to disruption of KCC2 clustering and transport activity without any change in the neuronal membrane pool. This suggests that the KCC2 CTD is involved in cluster formation and that clustering and function of the transporter are tightly correlated. Overexpression of the CTD on the other hand causes a decrease in KCC2 cluster size with no alteration of cluster density or chloride transport in hippocampal neurons (Chamma et al., 2013), suggesting KCC2 clustering does not rely exclusively on its CTD binding to the cytoskeleton. Association of KCC2 with lipid rafts was proposed to influence KCC2 clustering. Watanabe et al. (2009) observed that association with lipid rafts increases KCC2 clustering and function in neuronal cultures, while Hartmann et al. (2009) found larger clusters and enhanced transport activity after disruption of lipid rafts. The later study, however, was performed in HEK 293 cells and showed an overall increase in KCC2 surface expression. It therefore remains unclear how clustering of KCC2 in lipid rafts modifies its transport activity in neurons.

Lateral Diffusion

Lateral diffusion is a key mechanism controlling rapid activity-dependent changes in neurotransmitter receptor number (and therefore clustering) at synapses, a phenomenon underlying the tuning of synaptic transmission and plasticity (Choquet and Triller, 2013). Receptors constantly alternate between periods of free Brownian-type motion outside synapses and constrained diffusion at synapses. They are captured and confined at synapses by transient interactions with postsynaptic scaffolding molecules that anchor them to the underlying cytoskeleton. A reduced density of scaffolding proteins at synapses and/or a weakening of receptor-scaffold interactions increases the escape of receptors from synapses and thereby clustering and synapse efficacy. Since KCC2 is similarly clustered near excitatory and inhibitory synapses, we addressed the role of lateral diffusion on KCC2 subcellular distribution and function. This was analyzed using Quantum-based Single Particle Tracking (QD-SPT) in hippocampal cultures (Chamma et al., 2012, 2013; Heubl et al., 2017).

These experiments showed that KCC2 displays free Brownian-type motion outside clusters while it is slowed down and confined within clusters located near excitatory and inhibitory synapses (Chamma et al., 2012, 2013). However, KCC2 escapes clusters faster near inhibitory synapses than excitatory synapses, reflecting stronger molecular constraints at excitatory synapses. Further investigations suggested specific tethering of KCC2 near excitatory synapses through actin-

binding of the CTD of KCC2 *via* the actin binding protein 4.1 N, whereas KCC2 is confined at inhibitory synapses by a distinct mechanism (Chamma et al., 2013). Therefore, KCC2 undergoes a diffusion-trap mechanism similar to neurotransmitter receptors.

KCC2 lateral diffusion is rapidly tuned by activity. Enhancing glutamatergic excitation or reducing GABAergic inhibition both increased KCC2 membrane diffusion (Chamma et al., 2013; Heubl et al., 2017) through reduced phosphorylation of S940 and increased phosphorylation of T906/1007, respectively. Changes in transporter diffusion were accompanied by cluster dispersion and increased membrane turnover of the transporter. Therefore, we propose that different subpopulations of transporters exist in the plasma membrane: freely moving KCC2 outside clusters and transporters confined in clusters in the vicinity of synapses. These two pools of transporters are in a dynamic equilibrium that can vary in response to changes in synaptic activity. The extra-cluster pool of transporters can be considered as a reserve pool in equilibrium with the perisynaptic pool. Transitions between these compartments by lateral diffusion may then participate in the fine tuning of synapses in response to local fluctuations of synaptic activity (**Figure 3**). Since changes in KCC2 mobility occur within tens of seconds (Heubl et al., 2017), lateral diffusion is probably the first cellular mechanism modulating the transporter membrane stability. This may represent a rapid mechanism for adapting Cl- homeostasis to changes in synaptic activity.

Endocytosis

While activity-dependent KCC2 endocytosis was shown to rapidly decrease its neuronal membrane pool (Lee et al., 2011; Chamma et al., 2013; Heubl et al., 2017), KCC2 turn-over rate under basal conditions is controversial. Two studies showed a high turn-over rate (of about 20 min) of the transporter in neuronal cultures (Lee et al., 2010) and rat hippocampal slices (Rivera et al., 2004). In contrast, Puskarjov et al. (2012) observed no change in KCC2 membrane pool in hippocampal slices after 4 h inhibition of protein synthesis (by cycloheximide) or degradation (by leupeptin). Although the authors concluded that KCC2 has a rather low turnover, what they were testing in this study was the lifetime of the transporter. Once KCC2 is synthesized and inserted in the membrane, it undergoes several cycles of endocytosis and exocytosis until final degradation. The lifetime of the transporter therefore seems to be >4 h whereas KCC2 turn-over rate at the membrane is in the range of 20–30 min.

Lee et al. (2010) reported increased surface expression of endogenous KCC2 in hippocampal cultured neurons after a 45 min exposure to dynasore, a cell-permeable inhibitor of dynamin. Using co-immunoprecipitation experiments, Zhao et al. (2008) showed that endogenous KCC2 interacts with the clathrin-binding AP2, suggesting that KCC2 internalization may be controlled by the clathrin-mediated endocytic pathway. Then, they identified in HEK293 cells a constitutive, non-canonical endocytic 657LLRLEE662 motif in the KCC2 CTD. Both di-leucine residues are required to mediate efficient transporter endocytosis but the L658 residue is the most important. The two glutamic acid residues downstream regulate the function of the di-leucine endocytic motif. This motif is highly conserved among KCC family members but not in NKCC1, NKCC2 or NCC proteins (Zhao et al., 2008). Furthermore, protein kinase C (PKC) and casein kinase substrate in neurons protein 1 (PACSIN1), which are involved in clathrin-mediated endocytosis and vesicle transport in neurons (Schael et al., 2013), were recently identified in a KCC2 interactome study (Mahadevan et al., 2017). Altogether these results suggest that KCC2 membrane retrieval may require AP2 and PACSIN1. PACSIN1 has been shown to regulate the activity-dependent AMPAR surface recycling in cerebellar neurons (Anggono et al., 2013; Widagdo et al., 2016). More work is now needed to test whether PACSIN1 plays a similar role in activity-dependent membrane recycling of KCC2.

However, regarding clathrin-dependence of KCC2 endocytosis, it is important to mention that the motif identified by Zhao et al. (2008) in an artificial overexpression system is non-canonical. Whether this motif plays a role in neurons and whether other regions on KCC2 are critical for internalization remains to be tested. Endocytosis of most transmembrane molecules involves post-translational modifications favoring interaction with the clathrin pathway that have not been clearly demonstrated for KCC2.

Degradation

Constitutively internalized transporters are not targeted for lysosomal degradation in HEK 293 cells (Zhao et al., 2008). Only upon increased glutamatergic activity does KCC2 undergo lysosomal degradation. This has been shown in spinal cord neurons following peripheral nerve injury (Zhou et al., 2012), in cultured hippocampal neurons and hippocampal slices upon application of the glutamate receptor agonist NMDA (Lee et al., 2011; Puskarjov et al., 2012) or interictal-like activity induced by Mg^{2+} depletion (Puskarjov et al., 2012). This process has been shown to require Ca^{2+}-activated calpain cleavage of the KCC2 CTD (Puskarjov et al., 2012; Zhou et al., 2012). The exact location of the proteolytic cleavage site remains unknown. However, since it was proposed that KCC2 S940 dephosphorylation is a pre-requisite for calpain cleavage (Chamma et al., 2013), the calpain cleavage site may be positioned near the S940 residue.

Phospho-Regulation of KCC2

Phosphorylation or dephosphorylation of KCC2 key tyrosine, serine or threonine residues tune KCC2 activity mainly by controlling its membrane stability. KCC2 stability and clustering at the plasma membrane is directly regulated *via* its CTD and notably Y1087 and Y903 residues in HEK 293 cells, GT1-7 cells and hippocampal neurons (Watanabe et al., 2009; Lee et al., 2010). Other pathways have also been identified, and their consequences on KCC2 membrane stability and function characterized (Lee et al., 2007; Rinehart et al., 2009; Heubl et al., 2017). Thus, PKC-dependent phosphorylation of KCC2 S940 was shown to increase the transporter membrane stabilization in HEK 293 cells and in hippocampal neurons (Lee et al., 2007). Interestingly, S940 phosphorylation and calpain-mediated cleavage have been negatively correlated in cultured hippocampal neurons (Chamma et al., 2013). Studies in HEK 293 cells reported that T1007 phosphorylation is mediated by

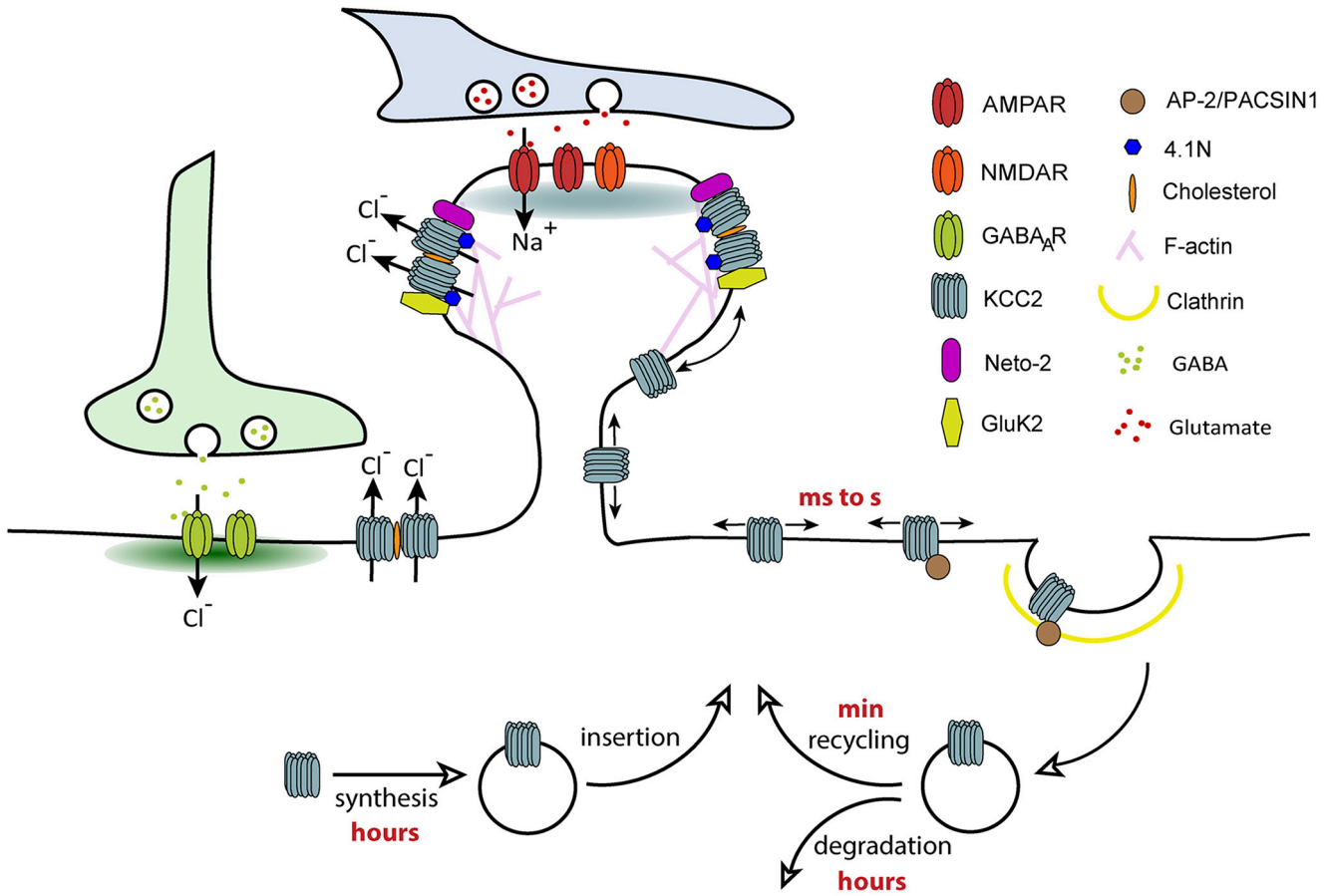

FIGURE 3 | Regulation of KCC2 membrane trafficking by lateral diffusion, clustering and endocytosis. Different subpopulations of KCC2 exist in the plasma membrane: freely moving KCC2 outside of clusters and confined KCC2 in membrane clusters. KCC2 clustering probably results from its accumulation in lipid-rafts, interaction with the cytoskeleton *via* protein 4.1N and oligomerization of the transporter. Freely moving molecules are more susceptible to interact with molecules involved in clathrin-dependent endocytosis such as AP-2. Confinement of KCC2 in membrane clusters may therefore prevent transporter endocytosis, a mechanism favoring chloride extrusion. The balance between "freely moving" and "clustered" pools of KCC2 can be rapidly changed by activity through phosphoregulations, which regulate the overall density of transporters localized at the membrane.

the serine/threonine kinase WNK1 [With No lysine (K) serine-threonine kinase 1] and its downstream effectors SPAK and OSR1 (Rinehart et al., 2009; de Los Heros et al., 2014). In contrast, T906 is not the target of WNK, SPAK or OSR1 in HEK 293 cells (de Los Heros et al., 2014; Zhang et al., 2016). The nature of the kinase phosphorylating T906 is still unknown (Zhang et al., 2016). The phosphorylation of T906 and T1007 keeps E_{GABA} depolarized by decreasing the membrane pool of KCC2 both in immature neurons (Friedel et al., 2015) as well as in mature neurons in response to reduced $GABA_AR$ activation (Heubl et al., 2017).

Other KCC2 phospho-sites have been identified in large-scale phospho-proteomics studies: S31, T34, S913, S932, S988, T999, T1009 (according to human sequence; Cordshagen et al., 2018), and S25, S26, T34, S937, T1009, S1022, S1025 and S1026 (Weber et al., 2014). Several of these sites tune KCC2 transport activity but unlike Y1087, S940, T906 and T1007, this regulation does not involve changes in total or surface expression levels of the transporter. Phosphorylation of S932, T934, S937 and dephosphorylation of T1009 enhance KCC2 transport function in HEK 293 cells (Weber et al., 2014; Cordshagen et al., 2018). Moreover, two potent KCC2 activators, N-Ethylmaleimide (NEM) and staurosporine, differentially impact KCC2 transport activity through a complex mechanism of (de)phosphorylation of several of these phospho-sites (Weber et al., 2014; Conway et al., 2017; Cordshagen et al., 2018). Staurosporine triggers phosphorylation of S932 and dephosphorylation of T1009. The action of staurosporine on T1009 occurs indirectly by inhibiting a kinase while its effect on S932 would be due to an indirect inhibition of a phosphatase (Cordshagen et al., 2018). NEM increases the phosphorylation of S940 while it decreases the phosphorylation of T1007 (Conway et al., 2017). NEM is thought to dephosphorylate T1007 through the control of SPAK phosphorylation/activity (Conway et al., 2017). Furthermore, a complex regulatory mechanism of KCC2 activity by staurosporine and NEM likely involves a change in the transporter conformational state through the (de)phosphorylation of several, partly overlapping phospho-sites

that include S31, T34 and T999 for staurosporine and S31, T34 and S932 for NEM (Cordshagen et al., 2018). The function of other phosphorylation sites (e.g., S25, S26, S1022, S1025 and S1026), however, remains unclear.

REGULATION OF KCC2 CELLULAR TRAFFICKING BY NEURONAL ACTIVITY

KCC2 mRNA, protein, and surface expression are known to be down-regulated under pathological conditions such as epilepsy or in experimental paradigms leading to enhanced excitatory activity, including long term potentiation (LTP; Wang et al., 2006a), rebound burst activity (Wang et al., 2006b), repetitive postsynaptic spiking activity (Fiumelli et al., 2005), coincident pre- and post- synaptic spiking (Woodin et al., 2003), NMDAR activation (Kitamura et al., 2008; Lee et al., 2011), and epileptiform activity (Reid et al., 2001; Rivera et al., 2004; Pathak et al., 2007; Li et al., 2008; Shimizu-Okabe et al., 2011). Most of these paradigms result in a depolarizing shift in E_{GABA} due to a reduced KCC2 function and/or expression. Recently, KCC2 down-regulation was also observed in conditions of reduced GABAergic inhibition in mature neurons (Heubl et al., 2017). This raises questions about the cellular and molecular mechanisms controlling KCC2 activity. A mechanism has emerged that involves phospho-regulation of key KCC2 serine and threonine residues that in turn influence the membrane dynamics, clustering, endocytosis, recycling and/or degradation of the transporter (Lee et al., 2011; Puskarjov et al., 2012; Zhou et al., 2012; Chamma et al., 2013; Heubl et al., 2017).

KCC2 Downregulation by Neuronal Excitation

Under conditions of increased neuronal activity, KCC2 diffusion is rapidly increased leading to the dispersal of KCC2 clusters, transporter internalization, degradation and ultimately deficits in chloride transport (Lee et al., 2011; Puskarjov et al., 2012; Zhou et al., 2012; Chamma et al., 2013). These effects are mediated by NMDAR-dependent Ca^{2+} influx, Ca^{2+}-induced protein phosphatase 1 (PP1) dephosphorylation of KCC2 S940 and Ca^{2+}-activated calpain protease cleavage of KCC2 CTD. These data suggest that deficits in KCC2 activity induced by dephosphorylation of S940 may contribute to the development of status epilepticus *in vivo*. However, the importance of KCC2 S940 phospho-regulation *in vivo* remains unclear. KCC2 dephospho-mimetic S940 (S940A) knock-in mice display normal basal KCC2 expression levels and activity in the hippocampus and do not exhibit any overt behavioral abnormality. Only in conditions of hyperactivity, S940 mice showed increased lethality to kainate-induced seizures (Silayeva et al., 2015). It remains to be determined whether increased lethality reflects enhanced seizure severity due to altered chloride transport or a brainstem-mediated respiratory arrest. On the other hand, phosphorylation of T906/1007 inhibits KCC2 function (Rinehart et al., 2009). Mice in which T906/1007 phospho-dependent inactivation was prevented by mutation into alanine showed increased KCC2 transport function in basal conditions (Moore et al., 2018). This effect was not associated with increased KCC2 surface expression but seems to involve changes in the intrinsic properties of the transporter. Importantly, increased KCC2 function attenuates chemically-induced epileptiform activity in T906A/1007A mice, both in acute hippocampal slices and *in vivo* (Moore et al., 2018), suggesting that enhancing KCC2 activity through T906/1007 dephosphorylation may be an effective approach in epilepsy treatment.

Implication in Glutamatergic Long-Term Potentiation

LTP of glutamatergic synapses in cortical neurons relies mainly on NMDAR activation and Ca^{2+}-dependent activation of intracellular kinases such as Ca^{2+}/calmodulin-dependent protein kinase II (CaMKII; Poncer, 2003). Consistent with the Ca^{2+}-dependent regulation of the transporter, persistent (>1 h) KCC2 downregulation has been reported during hippocampal LTP (Wang et al., 2006a). Reduced KCC2 function was then hypothesized to dampen GABAergic transmission and to promote LTP at excitatory synapses (e.g., Ferando et al., 2016), although this hypothesis has not been tested experimentally. Instead, chronic KCC2 knockdown by RNA interference was shown to preclude LTP expression in hippocampal neurons (Chevy et al., 2015). This effect was independent of Ca^{2+} and CaMKII activation but instead involved the direct interaction of KCC2 with the Rac1-specific guanilyl exchange factor betaPIX. Loss of this interaction upon KCC2 suppression led to enhanced activation of Rac1 and its downstream effectors PAK1 and LIM kinase, which inhibit the actin-severing protein cofilin (Chevy et al., 2015; Llano et al., 2015). Thus, KCC2 suppression prevented actin depolymerization required for activity-driven AMPAR exocytosis during LTP (Gu et al., 2010). This effect however was observed upon chronic KCC2 knockdown. How acute downregulation of KCC2 upon physiologically induced LTP influences subsequent plasticity therefore remains to be tested.

Regulation of KCC2 by GABAergic Inhibition

Several studies have shown that KCC2 can be rapidly downregulated by enhanced neuronal activity and glutamatergic neurotransmission (see above). However, little was known until recently about the regulation of KCC2 by synaptic inhibition. A study by Woodin et al. (2003) reported that increased GABAergic transmission also leads to KCC2 downregulation. However, this study was carried out in immature neurons displaying mainly depolarizing excitatory $GABA_AR$-mediating synaptic responses associated with activation of voltage-dependent Ca^{2+} channels (VDCCs) and intracellular Ca^{2+} signaling pathways (Woodin et al., 2003). Therefore, this study did not reveal regulation of KCC2 by synaptic inhibition *per se* but instead by excitatory GABAergic transmission.

A recent study from our group investigated the direct contribution of GABAergic inhibition in the regulation of KCC2 and chloride homeostasis in mature neurons (Heubl et al., 2017). In order to isolate the effect of GABAergic inhibition on KCC2 diffusion and membrane stability, we

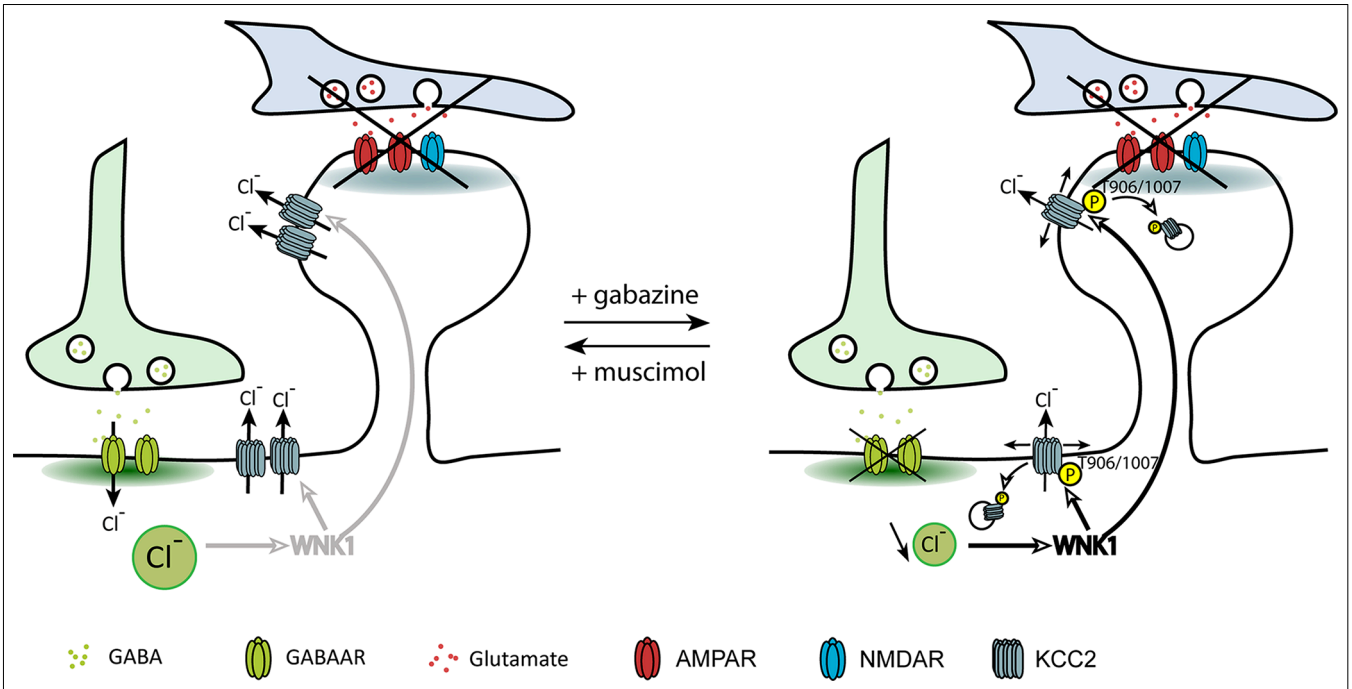

FIGURE 4 | Regulation of KCC2 diffusion and membrane stability by GABAergic inhibition. The impact of inhibitory activity on KCC2 diffusion was explored while blocking neuronal activity and glutamate receptors activity with the Na^+ channel blocker tetrodotoxin, the ionotropic glutamate receptor antagonist kynurenic acid, and the group I/group II mGluR antagonist R, S-MCPG. Chloride influx through $GABA_A$Rs inhibits WNK1, leading to KCC2 dephosphorylation on threonines 906/1007 and membrane stabilization. Upon $GABA_A$R blockade, reduced intracellular chloride activates WNK1 leading to KCC2 phosphorylation on threonines 906/1007 and increased KCC2 diffusion and subsequent internalization. From Heubl et al. (2017).

adjusted neuronal inhibition while blocking action potentials and glutamate receptors. In these conditions, increasing neuronal $GABA_A$R-mediated synaptic inhibition with muscimol enhanced KCC2 diffusion constraints and membrane stability. On the other hand, $GABA_A$R activity blockade with gabazine increased KCC2 diffusion while reducing its membrane clustering and stability (**Figure 4**). Although these observations reflect the influence of bath application of $GABA_A$R agonists and antagonists on KCC2 membrane diffusion and stability, one could imagine that such regulation may also take place locally near GABAergic synapses.

The search for the signaling pathway underlying the $GABA_A$R-dependent regulation of KCC2 demonstrated for the first time that Cl^- acts as a genuine second intracellular messenger to rapidly tune inhibitory synaptic transmission (Heubl et al., 2017). Thus, lowering intracellular Cl^- levels activates the Cl^--sensing WNK1 kinase which in turn phosphorylates and activates the SPAK and OSR1 kinases. Activated SPAK and OSR1 phosphorylate KCC2 T1007, leading to decreased KCC2 activity (Heubl et al., 2017). Conversely, increasing $[Cl^-]_i$ *via* photostimulation of halorhodopsin eNpHR, the light-activated microbial chloride pump, significantly reduced diffusion coefficients and increased the confinement of KCC2 transporters. This mechanism would therefore allow neurons to locally increase or decrease their KCC2 pools to match GABAergic synaptic activity and subsequent need to extrude Cl^- (**Figure 5**). We concluded that GABAergic inhibition in mature neurons tunes itself *via* rapid regulation of KCC2-mediated changes in intracellular Cl^- levels. Since the effect of eNpHR was observed 10 s after light exposure, diffusion-trap of KCC2 appears to be a very rapid mechanism to control Cl^- homeostasis in neurons.

However, the published values of the Cl^- sensitivity of WNK1 measured in an *in vitro* kinase assay (Piala et al.,

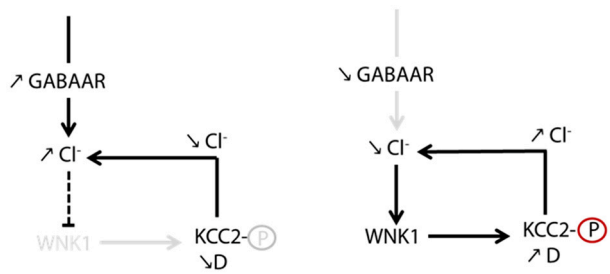

FIGURE 5 | Homeostatic regulation of intracellular chloride *via* WNK1-dependent KCC2 phosphorylation. $GABA_A$R-dependent chloride influx inhibits WNK1 kinase activity and stabilizes KCC2 in the membrane. Increased KCC2-dependent chloride extrusion can therefore counteract efficiently chloride influx due to activation of GABAergic synapses. In conditions of decreased $GABA_A$R activation, a decrease in the intracellular chloride level activates WNK1. Subsequent increase in KCC2 diffusion (D) and loss of KCC2 in the membrane contribute to restore intracellular chloride concentration. From Heubl et al. (2017).

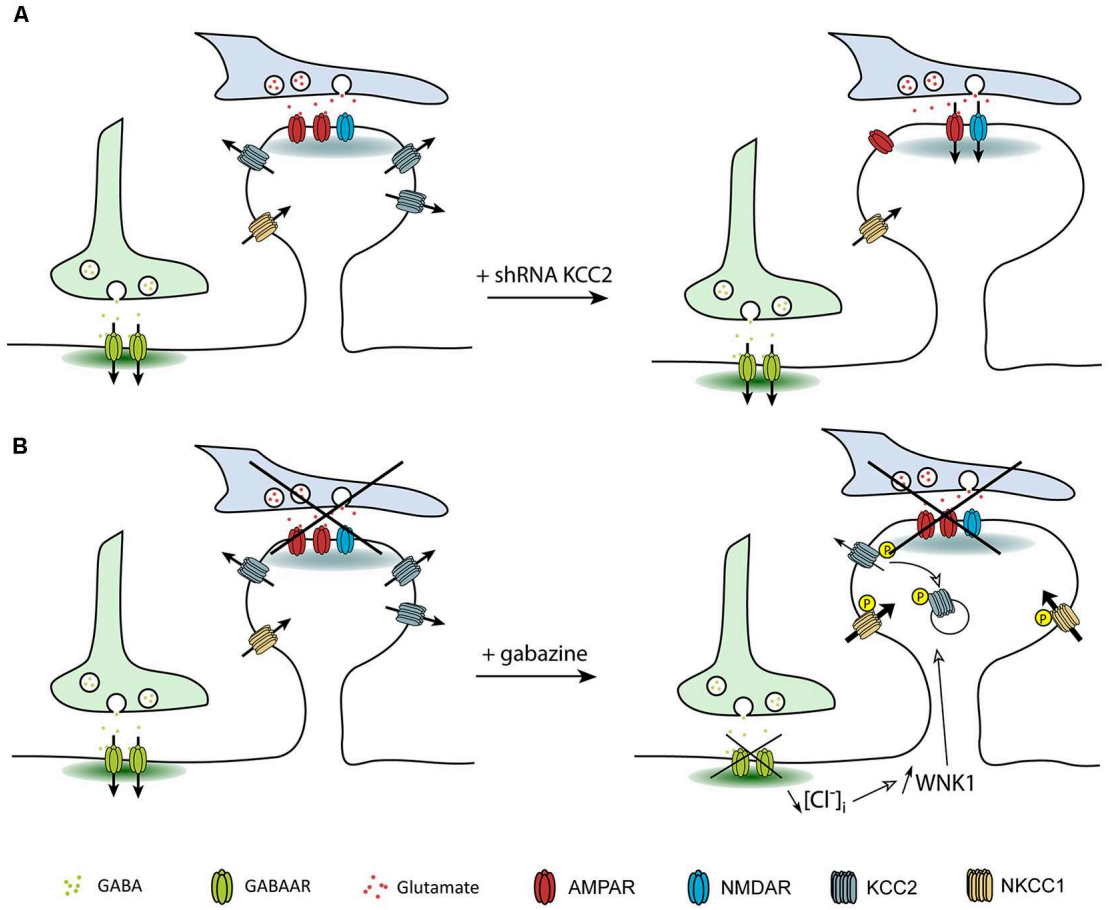

FIGURE 6 | Regulation of dendritic spine head volume upon changes in KCC2 membrane expression. Arrows indicate water fluxes associated with the activity of secondary active transporters and ionotropic receptors. **(A)** Suppression of KCC2 expression leads to increased spine head volume due to the loss of KCC2-associated water extrusion. **(B)** Activation of WNK1 upon $GABA_AR$ blockade leads to KCC2 and NKCC1 phosphorylation and subsequent decrease and increase in the membrane stability of KCC2 and NKCC1, respectively. Increased water influx associated with NKCC1 activity cannot be counteracted by KCC2, leading to spine head swelling.

2014) cannot account for the activation of this signaling pathway upon $GABA_AR$ activity changes in neurons (Heubl et al., 2017). Indeed, intracellular chloride levels in these cells are expected to be in the range of 5–10 mM under control conditions, down to 4–6 mM after $GABA_AR$ blockade and up to 10–15 mM upon $GABA_AR$ activation. The IC50 of chloride was about 20 mM for WNK1 autophosphorylation (Piala et al., 2014) and 100 mM for phosphorylation of its target SPAK in an *in vitro* kinase assay (Terker et al., 2016). If transposable *in situ*, these values would suggest WNK1 would be constantly activated in neurons. Instead, we showed modulation of WNK1 activity even upon subtle intracellular chloride changes (Heubl et al., 2017). The chloride sensitivity of WNK1 in neurons remains to be determined. Additional mechanisms such as membrane translocation (Zagórska et al., 2007) or interaction with other ion-sensitive molecules could modulate the chloride sensitivity of WNK1 upon $GABA_AR$ blockade. Further characterization of WNK1 localization and activity in neurons would therefore provide invaluable insights into how changes in osmolarity and ion concentration can tune its kinase activity.

This signaling pathway may also participate in the onset of pathological conditions. Indeed, a single subcutaneous injection of the $GABA_AR$ antagonist pentylenetetrazole (PTZ) to elicit epileptic seizures *in vivo* increased WNK1, SPAK and OSR1 phosphorylation/activities and promoted KCC2 T906/1007 phosphorylation, which resulted in KCC2 inhibition in neuronal cells (Heubl et al., 2017). Interestingly, PTZ injection also increased NKCC1 T203/T207/T212 phosphorylation. Considering threonine phosphorylation was shown to have opposite effects on KCC2 vs. NKCC1 activity (McCormick and Ellison, 2011), the downregulation of the WNK/SPAK/OSR1 pathway could be a very efficient mechanism to adjust neuronal Cl^- homeostasis in disorders associated with altered inhibition like epilepsy, schizophrenia, autism and neuropathic pain.

Since KCC2 S940 residue is crucial for the regulation of KCC2 transport activity (see above), one may wonder

about the interplay between KCC2 T906/1007 and S940. KCC2 diffusion was increased upon gabazine application even when S940 was mutated to aspartate, indicating that threonine phosphorylation can destabilize KCC2 in the membrane independently of its S940 phospho-status (Heubl et al., 2017). On the other hand, NMDAR-dependent S940 dephosphorylation in neurons in which KCC2 T906/1007 were mutated into alanine also destabilizes KCC2 independently of the threonine phosphorylation status. Hence, the kinase pathways involved in KCC2 regulation by GABAergic inhibition and neuronal excitation appear to be largely independent.

Impact at Glutamatergic Synapses

Several studies showed that, in addition to its role in setting $[Cl^-]_i$ in mature neurons, KCC2 also influences spine head volume as well as the efficacy of glutamatergic neurotransmission (e.g., Gauvain et al., 2011; Chevy et al., 2015). KCC2-mediated spine head volume regulation may rely on water fluxes associated with ion transport, as demonstrated for KCC- (Zeuthen, 1991a,b) and NKCC-mediated transport in epithelial cells (Hamann et al., 2005). Instead, the effect of KCC2 on glutamatergic transmission was shown to depend on its interaction with actin-related proteins (Gauvain et al., 2011). Thirty minutes of $GABA_AR$ blockade with gabazine also induced dendritic spine swelling while $GABA_AR$ activation with muscimol had no effect on dendritic spines (Heubl et al., 2017). The effect of gabazine is reminiscent of what was observed upon chronic KCC2 knockdown or pharmacological blockade. Spine swelling upon KCC2 blockade may thus result from ion and water influx associated with ionotropic receptor activation. Under basal activity, the number of opened receptors is low in hippocampal cultures, with spontaneous EPSP frequency ranging 20–50 Hz. However, gabazine-induced spine swelling occurred on a much faster time scale than with ionotropic glutamate receptors blockade (Gauvain et al., 2011; Heubl et al., 2017). Another mechanism could therefore be at play in the gabazine effect. WNK kinases regulate KCC2 and NKCC1 in opposite directions. Activation of WNK1 in conditions of reduced neuronal inhibition possibly leads to KCC2 removal from the plasma membrane while in the meantime NKCC1 is stabilized at the membrane (Vitari et al., 2006; McCormick and Ellison, 2011). Therefore, spine head swelling observed upon gabazine application may primarily involve increased NKCC1 membrane stabilization and water influx (Zeuthen and Macaulay, 2012). NKCC1 being very efficient in mediating water influx, this might explain the rapidity of the gabazine effect on dendritic spines as compared to that observed upon KCC2 blockade only (**Figure 6**). It would be interesting to directly test NKCC1 involvement in spine swelling upon gabazine application, for instance using the NKCC1 blocker bumetanide.

KCC2 knockdown leads to actin reorganization in spine heads (Chevy et al., 2015). Thus, reduced KCC2 content at the plasma membrane potentially weakens the molecular barrier formed by KCC2 in dendritic spines. This could in turn increase AMPAR escape from spines and reduce the efficacy of glutamatergic synapses as shown upon KCC2 knockdown (Gauvain et al., 2011). Therefore, we predict that KCC2 membrane removal upon reduced $GABA_AR$ activity may act to homeostatically adjust GABAergic and glutamatergic synaptic transmission.

Implication in Energy Loss

The regulation of KCC2 may not only permit a rapid reaction to changes in $[Cl^-]_i$ but also preserve energy consumption. Thus, the loss of KCC2 in conditions of decreased $GABA_AR$-dependent Cl^- influx would maintain membrane KCC2 at minimal levels required to keep E_{GABA} hyperpolarized. Indeed, for every Cl^- ion extruded by KCC2, the transporter uses the energy of the electrochemical gradient of one potassium ion. The Na^+/K^+ ATPase that generates the potassium transmembrane gradient is the main energy consumer in the brain (Buzsáki et al., 2007; Harris et al., 2012; de Lores Arnaiz and Ordieres, 2014). Even though the highest energetic cost of the Na^+/K^+-ATPase is used to restore transmembrane potential upon action potential discharge (Harris et al., 2012; Howarth et al., 2012), maintaining low $[Cl^-]_i$ is associated with high metabolic cost (Kaila et al., 2014). Kaila et al. (2014) raising the hypothesis that "the downregulation of KCC2 following neuronal trauma may be part of a general adaptive cellular response that facilitates neuronal survival by reducing the energetic costs that are needed to preserve low $[Cl^-]_i$". Under physiological conditions, rapid redistribution of KCC2 in the membrane could allow neurons to save energy by keeping surface KCC2 molecules at the minimum required density.

In conclusion, normal and pathological excitatory and inhibitory activities rapidly tune KCC2 function at both inhibitory and excitatory synapses. This regulation occurs through phosphorylation-induced changes in KCC2 membrane diffusion, clustering, endocytosis, recycling or degradation. Although alterations in excitatory and inhibitory signaling might have similar effects on KCC2 cellular trafficking and function, the underlying molecular mechanisms are distinct and involve Ca^{2+} vs. Cl^- signaling cascades and key serine and threonine KCC2 residues. The recent discovery of activity-dependent regulation of KCC2 by the Cl^--dependent WNK/SPAK/OSR1 signaling pathway is of particular interest in the pathology since it controls simultaneously KCC2 and NKCC1 in opposite directions. Further investigation will tell whether targeting this signaling pathway efficiently restores chloride homeostasis and synaptic inhibition in epilepsy, neuropathic pain and various neuropsychiatric disorders.

AUTHOR CONTRIBUTIONS

SL supervised the writing of the review and corrected the manuscript. JP gave advice. EC and MH participated equally in the writing of the review and ES wrote sub-sections of the manuscript.

FUNDING

This work was supported by Fondation Française pour la Recherche sur l'Épilepsie, Fédération pour la Recherche sur le Cerveau and Fondation pour la Recherche Médicale.

REFERENCES

Acton, B. A., Mahadevan, V., Mercado, A., Uvarov, P., Ding, Y., Pressey, J., et al. (2012). Hyperpolarizing GABAergic transmission requires the KCC2 C-terminal ISO domain. *J. Neurosci.* 32, 8746–8751. doi: 10.1523/JNEUROSCI.6089-11.2012

Agez, M., Schultz, P., Medina, I., Baker, D. J., Burnham, M. P., Cardarelli, R. A., et al. (2017). Molecular architecture of potassium chloride co-transporter KCC2. *Sci. Rep.* 7:16452. doi: 10.1038/s41598-017-15739-1

Aguado, F., Carmona, M. A., Pozas, E., Aguiló, A., Martínez-Guijarro, F. J., Alcantara, S., et al. (2003). BDNF regulates spontaneous correlated activity at early developmental stages by increasing synaptogenesis and expression of the K^+/Cl^- co-transporter KCC2. *Development* 130, 1267–1280. doi: 10.1242/dev.00351

Anggono, V., Koç-Schmitz, Y., Widagdo, J., Kormann, J., Quan, A., Chen, C.-M., et al. (2013). PICK1 interacts with PACSIN to regulate AMPA receptor internalization and cerebellar long-term depression. *Proc. Natl. Acad. Sci. U S A* 110, 13976–13981. doi: 10.1073/pnas.1312467110

de Lores Arnaiz, G. R., and Ordieres, M. G. (2014). Brain Na^+, K^+-ATPase activity in aging and disease. *Int. J. Biomed. Sci.* 10, 85–102.

Báldi, R., Varga, C., and Tamás, G. (2010). Differential distribution of KCC2 along the axo-somato-dendritic axis of hippocampal principal cells. *Eur. J. Neurosci.* 32, 1319–1325. doi: 10.1111/j.1460-9568.2010.07361.x

Barthó, P., Payne, J. A., Freund, T. F., and Acsády, L. (2004). Differential distribution of the KCl cotransporter KCC2 in thalamic relay and reticular nuclei. *Eur. J. Neurosci.* 20, 965–975. doi: 10.1111/j.1460-9568.2004.03562.x

Berninger, B., Marty, S., Zafra, F., da Penha Berzaghi, M., Thoenen, H., and Lindholm, D. (1995). GABAergic stimulation switches from enhancing to repressing BDNF expression in rat hippocampal neurons during maturation *in vitro*. *Development* 121, 2327–2335.

Blaesse, P., Airaksinen, M. S., Rivera, C., and Kaila, K. (2009). Cation-chloride cotransporters and neuronal function. *Neuron* 61, 820–838. doi: 10.1016/j.neuron.2009.03.003

Blaesse, P., Guillemin, I., Schindler, J., Schweizer, M., Delpire, E., Khiroug, L., et al. (2006). Oligomerization of KCC2 correlates with development of inhibitory neurotransmission. *J. Neurosci.* 26, 10407–10419. doi: 10.1523/JNEUROSCI.3257-06.2006

Bormann, J., Hamill, O. P., and Sakmann, B. (1987). Mechanism of anion permeation through channels gated by glycine and gamma-aminobutyric acid in mouse cultured spinal neurones. *J. Physiol.* 385, 243–286. doi: 10.1113/jphysiol.1987.sp016493

Buzsáki, G., Kaila, K., and Raichle, M. (2007). Inhibition and brain work. *Neuron* 56, 771–783. doi: 10.1016/j.neuron.2007.11.008

Carmona, M. A., Pozas, E., Martínez, A., Espinosa-Parrilla, J. F., Soriano, E., and Aguado, F. (2006). Age-dependent spontaneous hyperexcitability and impairment of GABAergic function in the hippocampus of mice lacking *trkB*. *Cereb. Cortex* 16, 47–63. doi: 10.1093/cercor/bhi083

Casula, S., Shmukler, B. E., Wilhelm, S., Stuart-Tilley, A. K., Su, W., Chernova, M. N., et al. (2001). A dominant negative mutant of the KCC1 K-Cl cotransporter: both N- and C-terminal cytoplasmic domains are required for K-Cl cotransport activity. *J. Biol. Chem.* 276, 41870–41878. doi: 10.1074/jbc.M107155200

Casula, S., Zolotarev, A. S., Stuart-Tilley, A. K., Wilhelm, S., Shmukler, B. E., Brugnara, C., et al. (2009). Chemical crosslinking studies with the mouse Kcc1 K-Cl cotransporter. *Blood Cells Mol. Dis.* 42, 233–240. doi: 10.1016/j.bcmd.2009.01.021

Chamma, I., Chevy, Q., Poncer, J. C., and Lévi, S. (2012). Role of the neuronal K-Cl co-transporter KCC2 in inhibitory and excitatory neurotransmission. *Front. Cell. Neurosci.* 6:5. doi: 10.3389/fncel.2012.00005

Chamma, I., Heubl, M., Chevy, Q., Renner, M., Moutkine, I., Eugène, E., et al. (2013). Activity-dependent regulation of the K/Cl transporter KCC2 membrane diffusion, clustering and function in hippocampal neurons. *J. Neurosci.* 33, 15488–15503. doi: 10.1523/JNEUROSCI.5889-12.2013

Chavas, J., and Marty, A. (2003). Coexistence of excitatory and inhibitory GABA synapses in the cerebellar interneuron network. *J. Neurosci.* 23, 2019–2031. doi: 10.1523/jneurosci.23-06-02019.2003

Chevy, Q., Heubl, M., Goutierre, M., Backer, S., Moutkine, I., Eugène, E., et al. (2015). KCC2 gates activity-driven AMPA receptor traffic through cofilin phosphorylation. *J. Neurosci.* 35, 15772–15786. doi: 10.1523/JNEUROSCI.1735-15.2015

Choquet, D., and Triller, A. (2013). The dynamic synapse. *Neuron* 80, 691–703. doi: 10.1016/j.neuron.2013.10.013

Conway, L. C., Cardarelli, R. A., Moore, Y. E., Jones, K., McWilliams, L. J., Baker, D. J., et al. (2017). *N*-Ethylmaleimide increases KCC2 cotrans- porter activity by modulating transporter phosphorylation. *J. Biol. Chem.* 292, 21253–21263. doi: 10.1074/jbc.m117.817841

Cordshagen, A., Busch, W., Winklhofer, M., Nothwang, H. G., and Hartmann, A. M. (2018). Phosphoregulation of the intracellular termini of K^+-Cl^- cotransporter 2 (KCC2) enables flexible control of its activity. *J. Biol. Chem.* 293, 16984–16993. doi: 10.1074/jbc.RA118.004349

de Los Heros, P., Alessi, D. R., Gourlay, R., Campbell, D. G., Deak, M., Macartney, T. J., et al. (2014). The WNK-regulated SPAK/OSR1 kinases directly phosphorylate and inhibit the K^+-Cl^- co-transporters. *Biochem. J.* 458, 559–573. doi: 10.1042/BJ20131478

Dubois, C. J., Cardoit, L., Schwarz, V., Markkanen, M., Airaksinen, M. S., Uvarov, P., et al. (2018). Role of the K^+-Cl^- cotransporter KCC2a isoform in Mammalian respiration at birth. *eNeuro* 5:ENEURO.0264-18.2018. doi: 10.1523/ENEURO.0264-18.2018

Dzhala, V. I., Talos, D. M., Sdrulla, D. A., Brumback, A. C., Mathews, G. C., Benke, T. A., et al. (2005). NKCC1 transporter facilitates seizures in the developing brain. *Nat. Med.* 11, 1205–1213. doi: 10.1038/nm1301

Ferando, I., Faas, G. C., and Mody, I. (2016). Diminished KCC2 confounds synapse specificity of LTP during senescence. *Nat. Neurosci.* 19, 1197–1200. doi: 10.1038/nn.4357

Fiumelli, H., Briner, A., Puskarjov, M., Blaesse, P., Belem, B. J., Dayer, A. G., et al. (2013). An ion transport-independent role for the cation-chloride cotransporter kcc2 in dendritic spinogenesis *in vivo*. *Cereb. Cortex* 23, 378–388. doi: 10.1093/cercor/bhs027

Fiumelli, H., Cancedda, L., and Poo, M. (2005). Modulation of GABAergic transmission by activity via postsynaptic Ca^{2+}-dependent regulation of KCC2 function. *Neuron* 48, 773–786. doi: 10.1016/j.neuron.2005.10.025

Friedel, P., Kahle, K. T., Zhang, J., Hertz, N., Pisella, L. I., Buhler, E., et al. (2015). WNK1-regulated inhibitory phosphorylation of the KCC2 cotransporter maintains the depolarizing action of GABA in immature neurons. *Sci. Signal.* 8:ra65. doi: 10.1126/scisignal.aaa0354

Friedel, P., Ludwig, A., Pellegrino, C., Agez, M., Jawhari, A., Rivera, C., et al. (2017). A novel view on the role of intracellular tails in surface delivery of the potassium-chloride cotransporter KCC2. *eNeuro* 4:ENEURO.0055-17.2017. doi: 10.1523/ENEURO.0055-17.2017

Garbarini, N., and Delpire, E. (2008). The RCC1 domain of protein associated with myc (PAM) interacts with and regulates KCC2. *Cell. Physiol. Biochem.* 22, 31–44. doi: 10.1159/000149781

Gauvain, G., Chamma, I., Chevy, Q., Cabezas, C., Irinopoulou, T., Bodrug, N., et al. (2011). The neuronal K-Cl cotransporter KCC2 influences postsynaptic AMPA receptor content and lateral diffusion in dendritic spines. *Proc. Natl. Acad. Sci. U S A* 108, 15474–15479. doi: 10.1073/pnas.1107893108

Gottmann, K., Mittmann, T., and Lessmann, V. (2009). BDNF signaling in the formation, maturation and plasticity of glutamatergic and GABAergic synapses. *Exp. Brain Res.* 199, 203–234. doi: 10.1007/s00221-009-1994-z

Gu, J., Lee, C. W., Fan, Y., Komlos, D., Tang, X., Sun, C., et al. (2010). ADF/cofilin-mediated actin dynamics regulate AMPA receptor trafficking during synapticplasticity. *Nat. Neurosci.* 10, 1208–1215. doi: 10.1038/nn.2634

Gulyás, A. I., Sík, A., Payne, J. A., Kaila, K., and Freund, T. F. (2001). The KCl cotransporter, KCC2, is highly expressed in the vicinity of excitatory synapses in the rat hippocampus. *Eur. J. Neurosci.* 13, 2205–2217. doi: 10.1046/j.0953-816x.2001.01600.x

Hamann, S., Herrera-Perez, J. J., Bundgaard, M., Alvarez-Leefmans, F. J., and Zeuthen, T. (2005). Water permeability of Na^+-K^+-$2Cl^-$cotransporters in mammalian epithelial cells. *J. Physiol.* 568, 123–135. doi: 10.1113/jphysiol.2005.093526

Harris, J. J., Jolivet, R., and Attwell, D. (2012). Synaptic energy use and supply. *Neuron* 75, 762–777. doi: 10.1016/j.neuron.2012.08.019

Hartmann, A.-M., Blaesse, P., Kranz, T., Wenz, M., Schindler, J., Kaila, K., et al. (2009). Opposite effect of membrane raft perturbation on transport activity of KCC2 and NKCC1. *J. Neurochem.* 111, 321–331. doi: 10.1111/j.1471-4159.2009.06343.x

Hartmann, A.-M., and Nothwang, H. G. (2015). Molecular and evolutionary insights into the structural organization of cation chloride cotransporters. *Front. Cell. Neurosci.* 8:470. doi: 10.3389/fncel.2014.00470

Hartmann, A.-M., Wenz, M., Mercado, A., Störger, C., Mount, D. B., Friauf, E., et al. (2010). Differences in the large extracellular loop between the K^+-Cl^- cotransporters KCC2 and KCC4. *J. Biol. Chem.* 285, 23994–24002. doi: 10.1074/jbc.m110.144063

Heubl, M., Zhang, J., Pressey, J. C., Al Awabdh, S., Renner, M., Gomez-Castro, F., et al. (2017). GABAAreceptor dependent synaptic inhibition rapidly tunes KCC2 activity via the Cl^--sensitive WNK1 kinase. *Nat. Commun.* 8:1776. doi: 10.1038/s41467-017-01749-0

Horn, Z., Ringstedt, T., Blaesse, P., Kaila, K., and Herlenius, E. (2010). Premature expression of KCC2 in embryonic mice perturbs neural development by an ion transport-independent mechanism. *Eur. J. Neurosci.* 31, 2142–2155. doi: 10.1111/j.1460-9568.2010.07258.x

Howarth, C., Gleeson, P., and Attwell, D. (2012). Updated energy budgets for neural computation in the neocortex and cerebellum. *J. Cereb. Blood Flow Metab.* 32, 1222–1232. doi: 10.1038/jcbfm.2012.35

Howard, H. C., Mount, D. B., Rochefort, D., Byun, N., Dupré, N., Lu, J., et al. (2002). The K-Cl cotransporter KCC3 is mutant in a severe peripheral neuropathy associated with agenesis of the corpus callosum. *Nat. Genet.* 32, 384–392. doi: 10.1038/ng1002

Hübner, C. A., Stein, V., Hermans-Borgmeyer, I., Meyer, T., Ballanyi, K., and Jentsch, T. J. (2001). Disruption of KCC2 reveals an essential role of K-Cl cotransport already in early synaptic inhibition. *Neuron* 30, 515–524. doi: 10.1016/s0896-6273(01)00297-5

Ivakine, E. A., Acton, B. A., Mahadevan, V., Ormond, J., Tang, M., Pressey, J. C., et al. (2013). Neto2 is a KCC2 interacting protein required for neuronal Cl^- regulation in hippocampal neurons. *Proc. Natl. Acad. Sci. U S A* 110, 3561–3566. doi: 10.1073/pnas.1212907110

Kahle, K. T., and Delpire, E. (2016). Kinase-KCC2 coupling: Cl^- rheostasis, disease susceptibility, therapeutic target. *J. Neurophysiol.* 115, 8–18. doi: 10.1152/jn.00865.2015

Kaila, K., Price, T. J., Payne, J. A., Puskarjov, M., and Voipio, J. (2014). Cation-chloride cotransporters in neuronal development, plasticity and disease. *Nat. Rev. Neurosci.* 15, 637–654. doi: 10.1038/nrn3819

Kaila, K., and Voipio, J. (1987). Postsynaptic fall in intracellular pH induced by GABA-activated bicarbonate conductance. *Nature* 330, 163–165. doi: 10.1038/330163a0

Karadsheh, M. F., and Delpire, E. (2001). Neuronal restrictive silencing element is found in the KCC2 gene: molecular basis for KCC2-specific expression in neurons. *J. Neurophysiol.* 85, 995–997. doi: 10.1152/jn.2001.85.2.995

Kelsch, W., Hormuzdi, S., Straube, E., Lewen, A., Monyer, H., and Misgeld, U. (2001). Insulin-like growth factor 1 and a cytosolic tyrosine kinase activate chloride outward transport during maturation of hippocampal neurons. *J. Neurosci.* 21, 8339–8347. doi: 10.1523/jneurosci.21-21-08339.2001

Kitamura, A., Ishibashi, H., Watanabe, M., Takatsuru, Y., Brodwick, M., and Nabekura, J. (2008). Sustained depolarizing shift of the GABA reversal potential by glutamate receptor activation in hippocampal neurons. *Neurosci. Res.* 62, 270–277. doi: 10.1016/j.neures.2008.09.002

Kuczewski, N., Fuchs, C., Ferrand, N., Jovanovic, J. N., Gaiarsa, J. L., and Porcher, C. (2011). Mechanism of $GABA_B$ receptor-induced BDNF secretion and promotion of $GABA_A$ receptor membrane expression. *J. Neurochem.* 118, 533–545. doi: 10.1111/j.1471-4159.2011.07192.x

Lee, H. H. C., Deeb, T. Z., Walker, J. A., Davies, P. A., and Moss, S. J. (2011). NMDA receptor activity downregulates KCC2 resulting in depolarizing $GABA_A$ receptor-mediated currents. *Nat. Neurosci.* 14, 736–743. doi: 10.1038/nn.2806

Lee, H. H. C., Jurd, R., and Moss, S. J. (2010). Tyrosine phosphorylation regulates the membrane trafficking of the potassium chloride co-transporter KCC2. *Mol. Cell. Neurosci.* 45, 173–179. doi: 10.1016/j.mcn.2010.06.008

Lee, H. H. C., Walker, J. A., Williams, J. R., Goodier, R. J., Payne, J. A., and Moss, S. J. (2007). Direct protein kinase C-dependent phosphorylation regulates the cell surface stability and activity of the potassium chloride cotransporter KCC2. *J. Biol. Chem.* 282, 29777–29784. doi: 10.1074/jbc.M705053200

Li, H., Khirug, S., Cai, C., Ludwig, A., Blaesse, P., Kolikova, J., et al. (2007). KCC2 interacts with the dendritic cytoskeleton to promote spine development. *Neuron* 56, 1019–1033. doi: 10.1016/j.neuron.2007.10.039

Li, H., Tornberg, J., Kaila, K., Airaksinen, M. S., and Rivera, C. (2002). Patterns of cation-chloride cotransporter expression during embryonic rodent CNS development. *Eur. J. Neurosci.* 16, 2358–2370. doi: 10.1046/j.1460-9568.2002.02419.x

Li, X., Zhou, J., Chen, Z., Chen, S., Zhu, F., and Zhou, L. (2008). Long-term expressional changes of Na^+-K^+-Cl^- co-transporter 1 (NKCC1) and K^+-Cl^- co-transporter 2 (KCC2) in CA1 region of hippocampus following lithium-pilocarpine induced status epilepticus (PISE). *Brain Res.* 1221, 141–146. doi: 10.1016/j.brainres.2008.04.047

Llano, O., Smirnov, S., Soni, S., Golubtsov, A., Guillemin, I., Hotulainen, P., et al. (2015). KCC2 regulates actin dynamics in dendritic spines via interaction with β-PIX. *J. Cell Biol.* 209, 671–686. doi: 10.1083/jcb.201411008

Ludwig, A., Li, H., Saarma, M., Kaila, K., and Rivera, C. (2003). Developmental up-regulation of KCC2 in the absence of GABAergic and glutamatergic transmission. *Eur. J. Neurosci.* 18, 3199–3206. doi: 10.1111/j.1460-9568.2003.03069.x

Ludwig, A., Uvarov, P., Pellegrino, C., Thomas-Crusells, J., Schuchmann, S., Saarma, M., et al. (2011). Neurturin evokes MAPK-dependent upregulation of Egr4 and KCC2 in developing neurons. *Neural Plast.* 2011, 1–8. doi: 10.1155/2011/641248

Mahadevan, V., Khademullah, C. S., Dargaei, Z., Chevrier, J., Uvarov, P., Kwan, J., et al. (2017). Native KCC2 interactome reveals PACSIN1 as a critical regulator of synaptic inhibition. *Elife* 6:e28270. doi: 10.7554/eLife.28270

Mahadevan, V., Pressey, J. C., Acton, B. A., Uvarov, P., Huang, M. Y., Chevrier, J., et al. (2014). Kainate receptors coexist in a functional complex with KCC2 and regulate chloride homeostasis in hippocampal neurons. *Cell Rep.* 7, 1762–1770. doi: 10.1016/j.celrep.2014.05.022

Markkanen, M., Karhunen, T., Llano, O., Ludwig, A., Rivera, C., Uvarov, P., et al. (2014). Distribution of neuronal KCC2a and KCC2b isoforms in mouse CNS. *J. Comp. Neurol.* 522, 1897–1914. doi: 10.1002/cne.23510

Markkanen, M., Ludwig, A., Khirug, S., Pryazhnikov, E., Soni, S., Khiroug, L., et al. (2017). Implications of the N-terminal heterogeneity for the neuronal K-Cl cotransporter KCC2 function. *Brain Res.* 1675, 87–101. doi: 10.1016/j.brainres.2017.08.034

Markkanen, M., Uvarov, P., and Airaksinen, M. S. (2008). Role of upstream stimulating factors in the transcriptional regulation of the neuron-specific K-Cl cotransporter KCC2. *Brain Res.* 1236, 8–15. doi: 10.1016/j.brainres.2008.08.007

McCormick, J. A., and Ellison, D. H. (2011). The WNKs: atypical protein kinases with pleiotropic actions. *Physiol. Rev.* 91, 177–219. doi: 10.1152/physrev.00017.2010

Medina, I., Friedel, P., Rivera, C., Kahle, K. T., Kourdougli, N., Uvarov, P., et al. (2014). Current view on the functional regulation of the neuronal K^+-Cl^- cotransporter KCC2. *Front. Cell. Neurosci.* 8:27. doi: 10.3389/fncel.2014.00027

Mercado, A., Broumand, V., Zandi-Nejad, K., Enck, A. H., and Mount, D. B. (2006). A C-terminal domain in KCC2 confers constitutive K^+-Cl^- cotransport. *J. Biol. Chem.* 281, 1016–1026. doi: 10.1074/jbc.M509972200

Moore, Y. E., Deeb, T. Z., Chadchankar, H., Brandon, N. J., and Moss, S. J. (2018). Potentiating KCC2 activity is sufficient to limit the onset and severity of seizures. *Proc. Natl. Acad. Sci. U S A* 115, 10166–10171. doi: 10.1073/pnas.1810134115

Moore, Y. E., Kelley, M. R., Brandon, N. J., Deeb, T. Z., and Moss, S. J. (2017). Seizing control of KCC2: a new therapeutic target for epilepsy. *Trends Neurosci.* 40, 555–571. doi: 10.1016/j.tins.2017.06.008

Moore-Hoon, M. L., and Turner, R. J. (2000). The structural unit of the secretory Na^+-K^+-$2Cl^-$ cotransporter (NKCC1) is a homodimer. *Biochemistry* 39, 3718–3724. doi: 10.1021/bi992301v

Pathak, H. R., Weissinger, F., Terunuma, M., Carlson, G. C., Hsu, F.-C., Moss, S. J., et al. (2007). Disrupted dentate granule cell chloride regulation enhances synaptic excitability during development of temporal lobe epilepsy. *J. Neurosci.* 27, 14012–14022. doi: 10.1523/JNEUROSCI.4390-07.2007

Payne, J. A. (1997). Functional characterization of the neuronal-specific K-Cl cotransporter: implications for $[K^+]_o$ regulation. *Am. J. Physiol.* 273, C1516–C1525. doi: 10.1152/ajpcell.1997.273.5.c1516

Petrini, E. M., Ravasenga, T., Hausrat, T. J., Iurilli, G., Olcese, U., Racine, V., et al. (2014). Synaptic recruitment of gephyrin regulates surface GABAA

receptor dynamics for the expression of inhibitory LTP. *Nat. Commun.* 5:3921. doi: 10.1038/ncomms4921

Piala, A. T., Moon, T. M., Akella, R., He, H., Cobb, M. H., and Goldsmith, E. J. (2014). Chloride sensing by WNK1 involves inhibition of autophosphorylation. *Sci. Signal.* 7:ra41. doi: 10.1126/scisignal.2005050

Piechotta, K., Lu, J., and Delpire, E. (2002). Cation chloride cotransporters interact with the stress-related kinases Ste20-related proline-alanine-rich kinase (SPAK) and oxidative stress response 1 (OSR1). *J. Biol. Chem.* 277, 50812–50819. doi: 10.1074/jbc.M208108200

Poncer, J. C. (2003). Hippocampal long term potentiation: silent synapses and beyond. *J. Physiol. Paris* 97, 415–422. doi: 10.1016/j.jphysparis.2004.01.003

Poo, M. M. (2001). Neurotrophins as synaptic modulators. *Nat. Rev. Neurosci.* 2, 24–32. doi: 10.1038/35049004

Porcher, C., Hatchett, C., Longbottom, R. E., McAinch, K., Sihra, T. S., Moss, S. J., et al. (2011). Positive feedback regulation between gamma-aminobutyric acid type A ($GABA_A$) receptor signaling and brain-derived neurotrophic factor (BDNF) release in developing neurons. *J. Biol. Chem.* 286, 21667–21677. doi: 10.1074/jbc.M110.201582

Pressey, J. C., Mahadevan, V., Khademullah, C. S., Dargaei, Z., Chevrier, J., Ye, W., et al. (2017). A kainate receptor subunit promotes the recycling of the neuron-specific K^+-Cl^- co-transporter KCC2 in hippocampal neurons. *J. Biol. Chem.* 292, 6190–6201. doi: 10.1074/jbc.M116.767236

Price, G. D., and Trussell, L. O. (2006). Estimate of the chloride concentration in a central glutamatergic terminal: a gramicidin perforated-patch study on the calyx of held. *J. Neurosci.* 26, 11432–11436. doi: 10.1523/JNEUROSCI.1660-06.2006

Pugh, J. R., and Jahr, C. E. (2011). Axonal $GABA_A$ receptors increase cerebellar granule cell excitability and synaptic activity. *J. Neurosci.* 31, 565–574. doi: 10.1523/JNEUROSCI.4506-10.2011

Pugh, J. R., and Jahr, C. E. (2013). Activation of axonal receptors by GABA spillover increases somatic firing. *J. Neurosci.* 33, 16924–16929. doi: 10.1523/JNEUROSCI.2796-13.2013

Puskarjov, M., Ahmad, F., Kaila, K., and Blaesse, P. (2012). Activity-dependent cleavage of the K-Cl cotransporter KCC2 mediated by calcium-activated protease calpain. *J. Neurosci.* 32, 11356–11364. doi: 10.1523/JNEUROSCI.6265-11.2012

Puskarjov, M., Ahmad, F., Khirug, S., Sivakumaran, S., Kaila, K., and Blaesse, P. (2015). BDNF is required for seizure-induced but not developmental up-regulation of KCC2 in the neonatal hippocampus. *Neuropharmacology* 88, 103–109. doi: 10.1016/j.neuropharm.2014.09.005

Reid, K. H., Li, G. Y., Payne, R. S., Schurr, A., and Cooper, N. G. F. (2001). The mRNA level of the potassium-chloride cotransporter KCC2 covaries with seizure susceptibility in inferior colliculus of the post-ischemic audiogenic seizure-prone rat. *Neurosci. Lett.* 308, 29–32. doi: 10.1016/s0304-3940(01)01973-5

Rinehart, J., Maksimova, Y. D., Tanis, J. E., Stone, K. L., Hodson, C. A., Zhang, J., et al. (2009). Sites of regulated phosphorylation that control K-Cl cotransporter activity. *Cell* 138, 525–536. doi: 10.1016/j.cell.2009.05.031

Rivera, C., Li, H., Thomas-Crusells, J., Lahtinen, H., Viitanen, T., Nanobashvili, A., et al. (2002). BDNF-induced TrkB activation down-regulates the K^+-Cl^- cotransporter KCC2 and impairs neuronal Cl^- extrusion. *J. Cell Biol.* 159, 747–752. doi: 10.1083/jcb.200209011

Rivera, C., Voipio, J., Payne, J. A., Ruusuvuori, E., Lahtinen, H., Lamsa, K., et al. (1999). The K^+/Cl^- co-transporter KCC2 renders GABA hyperpolarizing during neuronal maturation. *Nature* 397, 251–255. doi: 10.1038/16697

Rivera, C., Voipio, J., Thomas-Crusells, J., Li, H., Emri, Z., Sipilä, S., et al. (2004). Mechanism of activity-dependent downregulation of the neuron-specific K-Cl cotransporter KCC2. *J. Neurosci.* 24, 4683–4691. doi: 10.1523/jneurosci.5265-03.2004

Roussa, E., Speer, J. M., Chudotvorova, I., Khakipoor, S., Smirnov, S., Rivera, C., et al. (2016). The membrane trafficking and functionality of the K^+-Cl^- co-transporter KCC2 is regulated by TGF-β2. *J. Cell Sci.* 129, 3485–3498. doi: 10.1242/jcs.189860

Ruiz, A., Campanac, E., Scott, R. S., Rusakov, D. A., and Kullmann, D. M. (2010). Presynaptic $GABA_A$ receptors enhance transmission and LTP induction at hippocampal mossy fiber synapses. *Nat. Neurosci.* 13, 431–438. doi: 10.1038/nn.2512

Schael, S., Nüchel, J., Müller, S., Petermann, P., Kormann, J., Pérez-Otaño, I., et al. (2013). Casein kinase 2 phosphorylation of protein kinase C and casein kinase 2 substrate in neurons (PACSIN) 1 protein regulates neuronal spine formation. *J. Biol. Chem.* 288, 9303–9312. doi: 10.1074/jbc.m113.461293

Sedmak, G., Jovanov-Miloševic, N., Puskarjov, M., Ulamec, M., Krušlin, B., Kaila, K., et al. (2016). Developmental expression patterns of KCC2 and functionally associated molecules in the human brain. *Cereb. Cortex* 26, 4574–4589. doi: 10.1093/cercor/bhv218

Shimizu-Okabe, C., Tanaka, M., Matsuda, K., Mihara, T., Okabe, A., Sato, K., et al. (2011). KCC2 was downregulated in small neurons localized in epileptogenic human focal cortical dysplasia. *Epilepsy Res.* 93, 177–184. doi: 10.1016/j.eplepsyres.2010.12.008

Silayeva, L., Deeb, T. Z., Hines, R. M., Kelley, M. R., Munoz, M. B., Lee, H. H. C., et al. (2015). KCC2 activity is critical in limiting the onset and severity of status epilepticus. *Proc. Natl. Acad. Sci. U S A* 112, 3523–3528. doi: 10.1073/pnas.1415126112

Simard, C. F., Bergeron, M. J., Frenette-Cotton, R., Carpentier, G. A., Pelchat, M.-E., Caron, L., et al. (2007). Homooligomeric and heterooligomeric associations between K^+-Cl^- cotransporter isoforms and between K^+-Cl^- and Na^+-K^+-Cl^- cotransporters. *J. Biol. Chem.* 282, 18083–18093. doi: 10.1074/jbc.m607811200

Simard, C. F., Brunet, G. M., Daigle, N. D., Montminy, V., Caron, L., and Isenring, P. (2004). Self-interacting domains in the C terminus of a cation-Cl^- cotransporter described for the first time. *J. Biol. Chem.* 279, 40769–40777. doi: 10.1074/jbc.m406458200

Starremans, P. G. J. F., Kersten, F. F. J., Van Den Heuvel, L. P. W. J., Knoers, N. V. A. M., and Bindels, R. J. M. (2003). Dimeric architecture of the human bumetanide-sensitive Na-K-Cl co-transporter. *J. Am. Soc. Nephrol.* 14, 3039–3046. doi: 10.1097/01.asn.0000097370.29737.5b

Stein, V., Hermans-Borgmeyer, I., Jentsch, T. J., and Hübner, C. A. (2004). Expression of the KCl cotransporter KCC2 parallels neuronal maturation and the emergence of low intracellular chloride. *J. Comp. Neurol.* 468, 57–64. doi: 10.1002/cne.10983

Stell, B. M. (2011). Biphasic action of axonal GABA-A receptors on presynaptic calcium influx. *J. Neurophysiol.* 105, 2931–2936. doi: 10.1152/jn.01125.2010

Stell, B. M., Rostaing, P., Triller, A., and Marty, A. (2007). Activation of presynaptic $GABA_A$ Receptors Induces glutamate release from parallel fiber synapses. *J. Neurosci.* 27, 9022–9031. doi: 10.1523/jneurosci.1954-07.2007

Stödberg, T., McTague, A., Ruiz, A. J., Hirata, H., Zhen, J., Long, P., et al. (2015). Mutations in SLC12A5 in epilepsy of infancy with migrating focal seizures. *Nat. Commun.* 6:8038. doi: 10.1038/ncomms9038

Szabadics, J., Varga, C., Molnár, G., Oláh, S., Barzó, P., and Tamás, G. (2006). Excitatory effect of GABAergic axo-axonic cells in cortical microcircuits. *Science* 311, 233–235. doi: 10.1126/science.1121325

Tanis, J. E., Bellemer, A., Moresco, J. J., Forbush, B., and Koelle, M. R. (2009). The potassium chloride cotransporter KCC-2 coordinates development of inhibitory neurotransmission and synapse structure in *Caenorhabditis elegans*. *J. Neurosci.* 29, 9943–9954. doi: 10.1523/jneurosci.1989-09.2009

Terker, A. S., Zhang, C., Erspamer, K. J., Gamba, G., Yang, C.-L., and Ellison, D. H. (2016). Unique chloride-sensing properties of WNK4 permit the distal nephron to modulate potassium homeostasis. *Kidney Int.* 89, 127–134. doi: 10.1038/ki.2015.289

Uvarov, P., Ludwig, A., Markkanen, M., Pruunsild, P., Kaila, K., Delpire, E., et al. (2007). A novel N-terminal isoform of the neuron-specific K-Cl cotransporter KCC2. *J. Biol. Chem.* 282, 30570–30576. doi: 10.1074/jbc.M705095200

Uvarov, P., Ludwig, A., Markkanen, M., Rivera, C., and Airaksinen, M. S. (2006). Upregulation of the neuron-specific K^+/Cl^- cotransporter expression by transcription factor early growth response 4. *J. Neurosci.* 26, 13463–13473. doi: 10.1523/jneurosci.4731-06.2006

Uvarov, P., Ludwig, A., Markkanen, M., Soni, S., Hübner, C. A., Rivera, C., et al. (2009). Coexpression and heteromerization of two neuronal K-Cl cotransporter isoforms in neonatal brain. *J. Biol. Chem.* 284, 13696–13704. doi: 10.1074/jbc.m807366200

Uvarov, P., Pruunsild, P., Timmusk, T., and Airaksinen, M. S. (2005). Neuronal K^+/Cl^- co-transporter (KCC2) transgenes lacking neurone restrictive silencer element recapitulate CNS neurone-specific expression and developmental up-regulation of endogenous KCC2 gene. *J. Neurochem.* 95, 1144–1155. doi: 10.1111/j.1471-4159.2005.03434.x

Vardi, N., Zhang, L. L., Payne, J. A., and Sterling, P. (2000). Evidence that different cation chloride cotransporters in retinal neurons allow opposite responses to GABA. *J. Neurosci.* 20, 7657–7663. doi: 10.1523/jneurosci.20-20-07657.2000

Vitari, A. C., Thastrup, J., Rafiqi, F. H., Deak, M., Morrice, N. A., Karlsson, H. K. R., et al. (2006). Functional interactions of the SPAK/OSR1 kinases with their upstream activator WNK1 and downstream substrate NKCC1. *Biochem. J.* 397, 223–231. doi: 10.1042/bj20060220

Wang, W., Gong, N., and Xu, T. L. (2006a). Downregulation of KCC2 following LTP contributes to EPSP-spike potentiation in rat hippocampus. *Biochem. Biophys. Res. Commun.* 343, 1209–1215. doi: 10.1016/j.bbrc.2006.03.038

Wang, L., Kitai, S. T., and Xiang, Z. (2006b). Activity-dependent bidirectional modification of inhibitory synaptic transmission in rat subthalamic neurons. *J. Neurosci.* 26, 7321–7327. doi: 10.1523/jneurosci.4656-05.2006

Wang, Y., Wang, Y., and Chen, Z. (2018). Double-edged GABAergic synaptic transmission in seizures: the importance of chloride plasticity. *Brain Res.* 1701, 126–136. doi: 10.1016/j.brainres.2018.09.008

Warmuth, S., Zimmermann, I., and Dutzler, R. (2009). X-ray structure of the C-terminal domain of a prokaryotic cation-chloride cotransporter. *Structure* 17, 538–546. doi: 10.1016/j.str.2009.02.009

Watanabe, M., and Fukuda, A. (2015). Development and regulation of chloride homeostasis in the central nervous system. *Front. Cell. Neurosci.* 9:371. doi: 10.3389/fncel.2015.00371

Watanabe, M., Wake, H., Moorhouse, A. J., and Nabekura, J. (2009). Clustering of neuronal K^+-Cl^- cotransporters in lipid rafts by tyrosine phosphorylation. *J. Biol. Chem.* 284, 27980–27988. doi: 10.1074/jbc.m109.043620

Weber, M., Hartmann, A.-M., Beyer, T., Ripperger, A., and Nothwang, H. G. (2014). A novel regulatory locus of phosphorylation in the C-terminus of the potassium chloride cotransporter KCC2 that interferes with N-ethylmaleimide or staurosporine mediated activation. *J. Biol. Chem.* 289, 18668–18679. doi: 10.1074/jbc.M114.567834

Widagdo, J., Fang, H., Jang, S. E., and Anggono, V. (2016). PACSIN1 regulates the dynamics of AMPA receptor trafficking. *Sci. Rep.* 6:31070. doi: 10.1038/srep 31070

Williams, J. R., Sharp, J. W., Kumari, V. G., Wilson, M., and Payne, J. A. (1999). The neuron-specific K-Cl cotransporter, KCC2: antibody development and initial characterization of the protein. *J. Biol. Chem.* 274, 12656–12664. doi: 10.1074/jbc.274.18.12656

Woo, N.-S., Lu, J., England, R., McClellan, R., Dufour, S., Mount, D. B., et al. (2002). Hyperexcitability and epilepsy associated with disruption of the mouse neuronal-specific K-Cl cotransporter gene. *Hippocampus* 12, 258–268. doi: 10.1002/hipo.10014

Woodin, M. A., Ganguly, K., and Poo, M. M. (2003). Coincident pre- and postsynaptic activity modifies GABAergic synapses by postsynaptic changes in Cl^- transporter activity. *Neuron* 39, 807–820. doi: 10.1016/s0896-6273(03)00507-5

Yeo, M., Berglund, K., Augustine, G., and Liedtke, W. (2009). Novel repression of Kcc2 transcription by REST-RE-1 controls developmental switch in neuronal chloride. *J. Neurosci.* 29, 14652–14662. doi: 10.1523/JNEUROSCI.2934-09.2009

Zagórska, A., Pozo-Guisado, E., Boudeau, J., Vitari, A. C., Rafiqi, F. H., Thastrup, J., et al. (2007). Regulation of activity and localization of the WNK1 protein kinase by hyperosmotic stress. *J. Cell Biol.* 176, 89–100. doi: 10.1083/jcb.200605093

Zeuthen, T. (1991a). Water permeability of ventricular cell membrane in choroid plexus epithelium from necturus maculosus. *J. Physiol.* 444, 133–151. doi: 10.1113/jphysiol.1991.sp018870

Zeuthen, T. (1991b). Secondary active transport of water across ventricular cell membrane of choroid plexus epithelium of Necturus maculosus. *J. Physiol.* 444, 153–173. doi: 10.1113/jphysiol.1991.sp018871

Zeuthen, T., and Macaulay, N. (2012). Cotransport of water by Na^+-K^+-$2Cl^-$ cotransporters expressed in Xenopus oocytes: NKCC1 versus NKCC2. *J. Physiol.* 590, 1139–1154. doi: 10.1113/jphysiol.2011.226316

Zhang, Y., Cudmore, R. H., Lin, D.-T., Linden, D. J., and Huganir, R. L. (2015). Visualization of NMDA receptor-dependent AMPA receptor synaptic plasticity *in vivo*. *Nat. Neurosci.* 18, 402–407. doi: 10.1038/nn.3936

Zhang, L. L., Fina, M. E., and Vardi, N. (2006). Regulation of KCC2 and NKCC during development: membrane insertion and differences between cell types. *J. Comp. Neurol.* 499, 132–143. doi: 10.1002/cne.21100

Zhang, J., Gao, G., Begum, G., Wang, J., Khanna, A. R., Shmukler, B. E., et al. (2016). Functional kinomics establishes a critical node of volume-sensitive cation-Cl^-cotransporter regulation in the mammalian brain. *Sci. Rep.* 6:35986. doi: 10.1038/srep35986

Zhang, R., Wei, H., Xia, Y., and Du, J. (2010). Development of light response and GABAergic excitation-to-inhibition switch in zebrafish retinal ganglion cells. *J. Physiol.* 588, 2557–2569. doi: 10.1113/jphysiol.2010.187088

Zhao, B., Wong, A. Y. C., Murshid, A., Bowie, D., Presley, J. F., and Bedford, F. K. (2008). Identification of a novel di-leucine motif mediating K^+/Cl^- cotransporter KCC2 constitutive endocytosis. *Cell. Signal.* 20, 1769–1779. doi: 10.1016/j.cellsig.2008.06.011

Zhou, H.-Y., Chen, S.-R., Byun, H.-S., Chen, H., Li, L., Han, H.-D., et al. (2012). *N*-methyl-D-aspartate receptor- and calpain-mediated proteolytic cleavage of K^+-Cl^- cotransporter-2 impairs spinal chloride homeostasis in neuropathic pain. *J. Biol. Chem.* 287, 33853–33864. doi: 10.1074/jbc.m112.395830

Conflict of Interest Statement: The authors declare that the research was conducted in the absence of any commercial or financial relationships that could be construed as a potential conflict of interest.

Copyright © 2019 Côme, Heubl, Schwartz, Poncer and Lévi. This is an open-access article distributed under the terms of the Creative Commons Attribution License (CC BY). The use, distribution or reproduction in other forums is permitted, provided the original author(s) and the copyright owner(s) are credited and that the original publication in this journal is cited, in accordance with accepted academic practice. No use, distribution or reproduction is permitted which does not comply with these terms.

Neuropharmacology xxx (xxxx) xxxx

Contents lists available at ScienceDirect

Neuropharmacology

journal homepage: www.elsevier.com/locate/neuropharm

Invited review

KCC2 membrane diffusion tunes neuronal chloride homeostasis

Etienne Côme[a,b,c], Xavier Marques[a,b,c], Jean Christophe Poncer[a,b,c], Sabine Lévi[a,b,c,*]

[a] INSERM UMR-S 1270, 75005, Paris, France
[b] Sorbonne Université, 75005, Paris, France
[c] Institut du Fer à Moulin, 75005, Paris, France

HIGHLIGHTS

- KCC2 and NKCC1 transporters control intra-neuronal chloride concentrations.
- Alterations of KCC2 and NKCC1 membrane expression levels in epilepsy.
- Lateral diffusion controls KCC2 membrane stability.
- Neuronal activity tunes KCC2 surface mobility, stability and function.

ARTICLE INFO

Keywords:
KCC2
NKCC1
GABAergic transmission
Chloride homeostasis
Epilepsy
Lateral diffusion
Clustering

ABSTRACT

Neuronal Cl^- homeostasis is regulated by the activity of two cation chloride co-transporters (CCCs), the K^+-Cl^- cotransporter KCC2 and the Na^+-K^+-Cl^- cotransporter NKCC1, which are primarily extruding and importing chloride in neurons, respectively. Several neurological and psychiatric disorders including epilepsy, neuropathic pain, schizophrenia and autism are associated with altered neuronal chloride (Cl^-) homeostasis. A current view is that the accumulation of intracellular Cl^- in neurons as a result of KCC2 down-regulation and/or NKCC1 up-regulation may weaken inhibitory GABA signaling and thereby promote the development of pathological activities. CCC activity is determined mainly by their level of expression in the plasma membrane. Furthermore, CCCs undergo "diffusion-trapping" in the membrane, a mechanism that is rapidly adjusted by activity-dependent post-translational modifications i.e. phosphorylation/dephosphorylation of key serine and threonine residues. This represents probably the most rapid cellular mechanism for adapting CCC function to changes in neuronal activity. Therefore, interfering with these mechanisms may help restoring Cl^- homeostasis and inhibition under pathological conditions.

1. Introduction

The main inhibitory neurotransmitter receptors in the central nervous system (CNS) are type A γ-aminobutyric acid receptors ($GABA_AR$) and glycine receptors (GlyR). Upon activation, $GABA_AR$ and GlyR selectively conduct Cl^- - and, to a lesser extent, bicarbonate - through their pore. The direction of Cl^- flux through the channels depends on the transmembrane electrochemical chloride gradient. Two members of the cation-chloride co-transporter (CCC) family (which is composed of nine members encoded by the genes *Slc12a1-9)* play a prominent role in controlling intra-neuronal chloride concentration ($[Cl^-]_i$): the Na^+/K^+/$2Cl^-$ co-transporter 1 (NKCC1) and the K^+/Cl^- co-transporter 2 (KCC2). NKCC1 and KCC2 are secondary active transporters, using the electrochemical gradients generated by the Na^+/K^+ ATPase (Fig. 1). Therefore, the net ion flux they carry primarily depends on transmembrane Na^+, K^+ and Cl^- gradients and should be expected to be reversible. However, whereas KCC2 functions near thermodynamic equilibrium and may extrude or import chloride depending on extracellular K^+ and intracellular Cl^- concentration, NKCC1 mediates ion influx in most cell types and under most physiological conditions (Russell, 2000). Therefore, it is generally assumed that NKCC1 and KCC2 are primarily a chloride importer and extruder, respectively, at least under resting conditions.

The structural organization of KCC2 and NKCC1 is similar and comprises 12 transmembrane domains (TMs), six extracellular loops (ECL), as well as intracellular N- and C- termini (Hartmann and Nothwang, 2015) (Fig. 1). TMs are required for ion translocation and are therefore highly conserved in KCC2 and NKCC1 (Gamba, 2005; Payne et al., 1995, 1996; Somasekharan et al., 2012). In contrast, KCC2 and NKCC1 differ by the position of a long extracellular loop (LEL)

* Corresponding author. INSERM UMR-S 1270, Sorbonne Université, 17 rue du Fer a Moulin, 75005, Paris, France.
E-mail address: sabine.levi@inserm.fr (S. Lévi).

https://doi.org/10.1016/j.neuropharm.2019.03.014
Received 5 October 2018; Received in revised form 26 February 2019; Accepted 10 March 2019
0028-3908/ © 2019 Elsevier Ltd. All rights reserved.

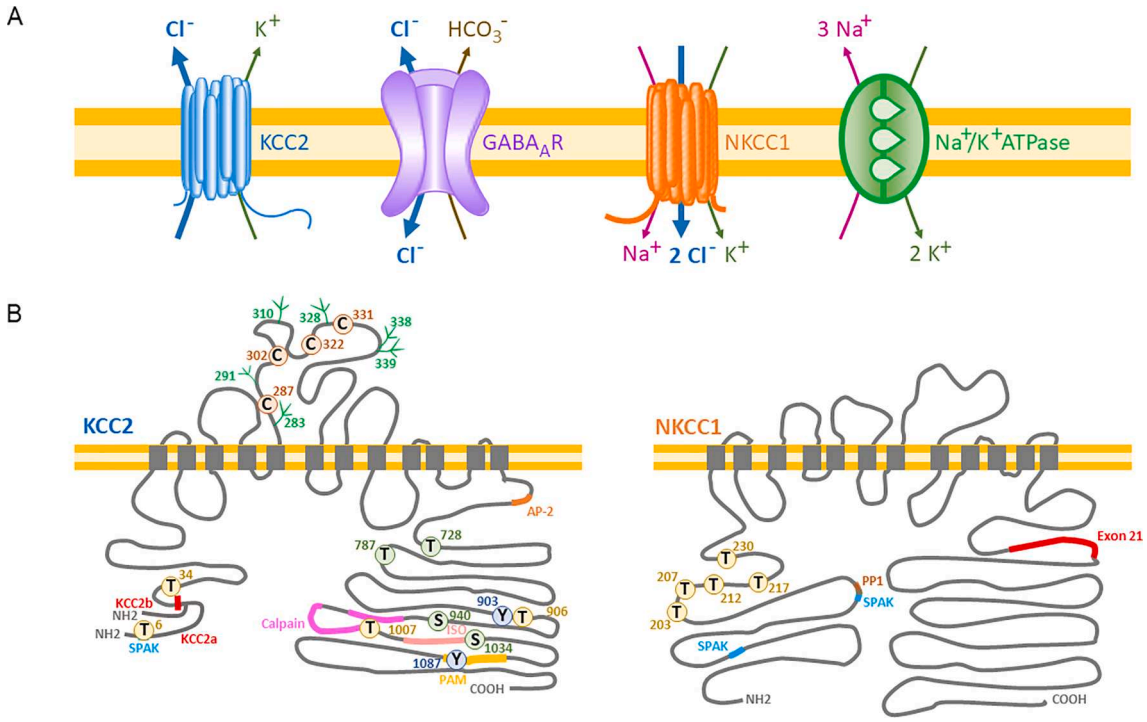

Fig. 1. CCC activity influences the direction of chloride flux through $GABA_AR$s.
A, KCC2 extrudes chloride out of the cell using the electrochemical potassium gradient generated by the Na^+/K^+ ATPase. NKCC1, in contrast, transports chloride into neurons using the electrochemical gradient of sodium ions. In mature neurons, KCC2 transport dominates over NKCC1 function, leading to low intra-neuronal chloride concentration. Hence, under resting conditions in most neurons, $GABA_AR$ activation usually induces a hyperpolarizing influx of chloride ions. ***B***, KCC2 (left) and NKCC1 (right) structure, key phosphorylation residues and domains. KCC2 and NKCC1 a and b isoforms differ by the presence of additional amino acid sequences in KCC2a and NKCC1a (exon 21). Note that most regulatory domains and phosphorylation sites of KCC2 are present in the large intracellular C-terminal domain while those of NKCC1 are located in the N-terminus. The ISO-domain, calpain and AP-2 binding domains in KCC2 are highlighted in orange, pink and salmon respectively. Key KCC2 and NKCC1 Serine (S), Tyrosine (Y) and Threonine (T) phosphorylation residues are shown. They are targeted by PKC and PP1 (green), Src family kinase (dark blue) and WNK-SPAK-OSR1 kinases (yellow). SPAK-binding domains in KCC2 and NKCC1 are also highlighted (blue).

between TM5 and TM6 in KCC2, and between TM7 and TM8 in NKCC1 (Gamba, 2005; Payne et al., 1995, 1996). The intracellular N- and C-termini of KCC2 and NKCC1 carry regulatory sequences and phosphorylation sites. In addition, the C-terminus of KCC2 contains a motif responsible for the isotonic activity of the transporter (Acton et al., 2012; Bergeron et al., 2006; Mercado et al., 2006). KCC2 and NKCC1 N- and C- termini also participate in the regulation of membrane trafficking (Lee et al., 2010, 2007; Zhao et al., 2008), basolateral and apical sorting in polarized cells (Carmosino et al., 2008) and oligomerization (Casula et al., 2009, 2001; Parvin et al., 2007; Simard et al., 2004; Warmuth et al., 2009). Furthermore, two KCC2 and NKCC1 (a and b) isoforms have been identified, which differ by the presence of additional amino acid sequences in KCC2a and NKCC1a on their N- and C-termini respectively (Fig. 1).

While other CCCs such as NKCC2 and NCC are mostly expressed in the kidney where they regulate salt re-absorption (Kahle et al., 2010; Russell, 2000), NKCC1 is ubiquitously expressed (Plotkin et al., 1997). In the CNS, NKCC1 is highly expressed in immature neurons and its expression level decreases during neuronal maturation in some but not all brain regions including the hippocampus (reviewed in Watanabe and Fukuda, 2015). In fact, the relatively high level of NKCC1 detected at adult stage is contentious with the global idea of a downregulation of NKCC1 during development (Yamada et al., 2004, reviewed by Kaila et al., 2014). In contrast to other KCCs, KCC2 is almost exclusively restricted to the CNS and is constitutively active under isotonic conditions (Acton et al., 2012; Mercado et al., 2006; Strange et al., 2000). The developmental upregulation of KCC2 expression is responsible for the early postnatal depolarizing shift in the polarity of GABAergic and glycinergic transmission in the CNS (Rivera et al., 1999). In addition to its function in inhibitory neurotransmission, KCC2 has been shown to play a role in dendritic spine formation and maturation (Li et al., 2007a; Fiumelli et al., 2005; Awad et al., 2018) as well as in excitatory glutamatergic synaptic transmission and plasticity (Gauvain et al., 2011; Chevy et al., 2015).

In the adult CNS, pathological alterations of KCC2 and NKCC1 expression and/or function lead to a depolarizing shift in GABA signaling, which may underlie anomalous network activities. Several studies have reported a down-regulation of KCC2 and an up-regulation of NKCC1, resulting in increased $[Cl^-]_i$ that promote depolarization/excitation in several neurological disorders such as neuropathic pain, spinal cord injury and epileptic disorders (reviewed in (Di Cristo et al., 2017)). Drugs aimed at reducing neuronal $[Cl^-]_i$ therefore represent a promising therapeutic strategy. Although the expression of CCCs is regulated both at the transcriptional and posttranslational levels, mechanisms controlling their membrane stability also rapidly influence their net function and therefore offer novel opportunities for pharmacological intervention. Here we will review experimental evidence supporting the role of lateral diffusion and clustering in the functional regulation of the KCC2 transporter and discuss how similar mechanisms may apply to other CCCs such as NKCC1.

2. KCC2 clustering

KCC2 is clustered in the somato-dendritic plasma membrane of cortical neurons (Gauvain et al., 2011; Barthó et al., 2004; Chamma et al., 2013, 2012; Gulyás et al., 2001; Heubl et al., 2017; Hübner et al., 2001; Watanabe et al., 2009). In these cells, most clusters are found near both excitatory and inhibitory synapses, with no preferential enrichment at one vs. the other (Chamma et al., 2013). Ultrastructural studies reported transporter accumulation at the periphery of excitatory

synapses within dendritic spines as well as along the dendritic shaft (Báldi et al., 2010; Gulyás et al., 2001). However, these studies lacked a quantitative analysis. The use of quantitative electron microscopy or super-resolution microscopy is thus required to more precisely evaluate the subcellular localization of KCC2 in the neuronal membrane.

2.1. Clustering mechanisms

2.1.1. Oligomerization and actin-binding

Several mechanisms may account for KCC2 aggregation. Oligomerization-induced trapping was proposed to be involved in - or result from - protein activation (for review see (Kusumi et al., 2005)). KCC2 is known to form homo- and hetero-oligomers with other CCC family members (Blaesse et al., 2006; Simard et al., 2007; Uvarov et al., 2009). The expression of KCC2 Tyrosine 1087 phosphorylation mutants induced a loss of transporter oligomerization and function without a change in its membrane expression (Watanabe et al., 2009), suggesting a link between oligomerization, clustering and function. Multimeric assembly of KCC2 with other membrane proteins via low-energy interactions could also regulate KCC2 function in neuronal plasma membrane (Goldman et al., 2004; Marguet et al., 2006). For instance, KCC2 assembly with the kainate-sensitive glutamate receptor GluK2 subunit or with Neuropilin and tolloid like-2 (Neto-2), the auxiliary subunit of the kainate receptor, increases its oligomerization and Cl^- transport function in hippocampal neurons (Ivakine et al., 2013; Mahadevan et al., 2014; Pressey et al., 2017). However, it is difficult to conclude that the formation of a multimeric complex increases KCC2 function since it is always associated with an increase of its surface expression.

KCC2 binds to the actin cytoskeleton in neurons through interaction of its carboxy-terminal domain (CTD) with protein 4.1N (Li et al., 2007a). The relief of KCC2 diffusion constraints observed upon either 4.1N knockdown by RNA interference, overexpression of the KCC2-CTD, or actin depolymerisation with Latrunculin A suggests that a sub-population of transporters may be anchored near excitatory synapses via KCC2-4.1N-actin interaction (Chamma et al., 2013). However, cytoskeleton tethering to the membrane does not appear to be responsible for KCC2 cluster formation *per se*, and might instead influence the specific localization of a sub-population of KCC2 clusters (Chamma et al., 2013).

2.1.2. Lipid rafts

What molecular mechanism other than actin anchoring may be responsible for KCC2 clustering? KCC2 has been shown to associate with lipid rafts (Hartmann et al., 2009; Watanabe et al., 2009), as do numerous synaptic transmembrane proteins such as $GABA_A$Rs (Li et al., 2007b) or AMPARs (Hou et al., 2008). Lipid raft-dependent segregation is thought to provide mobile signaling platforms that influence clustering and function of plasma membrane molecules (Pike, 2009; Tillman and Cascio, 2003). A study on the modulation of the serotonin reuptake transporter (SERT) by lipid raft association and cytoskeleton tethering showed increased transport activity when SERT was localized into lipid rafts. Interestingly, actin filament disruption increased the lateral diffusion of the transporter that however remained localized in lipid rafts (Chang et al., 2012). The cytoskeleton anchoring of SERT-containing lipid rafts was shown to rely on SERT interaction with intracellular partners, which can be modulated by phosphorylation. Hence, a complex interplay between phosphorylation, cytoskeleton tethering and lipid raft association seems to regulate the localization, diffusion and function of the transporter. Regarding KCC2, two studies focused on the interplay between KCC2 clustering and lipid raft association (Watanabe et al., 2009; Hartmann et al., 2009). Both groups found the transporter within lipid rafts but reached opposing conclusions regarding its functional impact. Thus, Watanabe et al. showed that KCC2 distribution in neurons switched from punctate to diffuse upon lipid raft disruption while KCC2 activity decreased, suggesting that localization in lipid rafts increases KCC2 transport activity (Watanabe et al., 2009). Hartmann et al. on the other hand observed increased KCC2 transport and aggregation upon lipid raft disruption in HEK-293 cells (Hartmann et al., 2009). In these cells, however, lipid raft disruption also increased KCC2 surface expression, which complicates the interpretation of these observations. Therefore, how KCC2 clustering in lipid rafts influences its transport function remains unclear.

Collectively, these data suggest that distinct KCC2 subpopulations may differentially associate with lipid rafts. In addition, interaction between KCC2 and actin cytoskeleton may tether KCC2-containing lipid-raft platforms to specific plasma membrane domains where local molecular partners form functional complexes. Phosphorylation of the transporter may then regulate KCC2 binding to intracellular partners and targeting to lipid rafts. It would be interesting to characterize in more detail how and under which conditions KCC2 accumulates in lipid rafts and whether KCC2-containing lipid rafts are associated with synaptic or extrasynaptic markers, as shown for $GABA_A$Rs (Li et al., 2007b).

2.2. Clustering function

Clustering may help to localize and/or stabilize transporters in submembrane compartments e.g. near excitatory synapses or to form a barrier in dendritic spines surrounding glutamatergic PSDs. The enrichment of KCC2 near excitatory synapses raises the question of whether the transporter is active in dendritic spines? Addressing the function of an electroneutral transporter at the subcellular level is extremely challenging. However, we have obtained indirect evidence that KCC2 is functional in dendritic spines. In experiments where KCC2 function was blocked using a specific KCC2 antagonist, we observed spine head swelling with no change in spine length or density (Gauvain et al., 2011). This effect is consistent with local changes in osmotic pressure due to the loss of solute export in spine heads. Importantly, this effect was independent of the structural role of KCC2 on spine actin cytoskeleton, as this effect was not observed by preventing KCC2 interaction with actin. Whether and to which extent dendritic shaft chloride concentration is influenced by KCC2 function in spines remains unknown. However, it is remarkable that modeling data suggest that the presence of dendritic spines impacts chloride diffusion in dendritic compartments (Mohapatra et al., 2016). How KCC2 further contributes to this effect remains unknown.

Could KCC2 clustering modulation account for local changes in intra-neuronal chloride concentrations? Chloride is not uniformly distributed along neurites (Doyon et al., 2011; Price and Trussell, 2006; Waseem et al., 2010). Using computational models and N-(ethoxycarbonylmethyl)-6-methoxy-quinolinium bromide (MQAE) - based fluorescence life time imaging microscopy (FLIM) in mature neurons, Doyon et al. showed that $[Cl^-]_i$ increased proportionally to the distance from the soma. They suggested that the specific geometry of the dendrites may hinder chloride diffusion, while chloride concentration at the soma remains clamped. This somato-dendritic chloride gradient was abolished by inhibition of KCC2 or blockade of GABAergic neurotransmission (Doyon et al., 2011), suggesting that KCC2 function is necessary to establish the gradient.

Simulation of intra-neuronal chloride concentrations suggested that the activation of a single GABAergic synapse can lead to a local change in $[Cl^-]_i$ of about 5 mM (Doyon et al., 2011). A single focal synapse activation at 50 Hz could therefore influence the response of neighbouring GABAergic synapses within a distance of 50 µm (Doyon et al., 2011; Jedlicka et al., 2010). In these simulations however chloride diffusion was assumed to be similar to that measured in water (2.03 μm^2/ms). In addition, the influence of intracellular or extracellular matrix proteins on $[Cl^-]_i$ via the Gibbs-Donan effect (Glykys et al., 2014) as well as local chloride attraction by positive charges such as polyamines were ignored. Estimated diffusion may then be overestimated in these models, suggesting that even stronger local chloride

accumulation may occur near activated inhibitory synapses. Therefore, increasing or decreasing CCC clustering near synapses may rapidly and efficiently modulate $[Cl^-]_i$.

3. Lateral diffusion regulates membrane protein trafficking

Protein diffusion in the neuronal plasma membrane was first evidenced for neurotransmitter receptors and this mechanism was shown to be of particular interest in the context of synaptic transmission and plasticity (Choquet and Triller, 2013; Triller and Choquet, 2008). In brief, receptors are randomly exocytosed in the plasma membrane where they diffuse until they get trapped by the postsynaptic scaffold that anchors them to the sub-membrane cytoskeleton. Pools of synaptic and extrasynaptic receptors undergo a continuous and reciprocal exchange that can be rapidly regulated by neuronal activity, thereby modulating the density of synaptic receptors. Here, we will discuss the relevance of lateral diffusion as a novel mechanism to regulate KCC2 activity, and the importance of cluster formation and maintenance in this context.

3.1. Brownian-type motion and confinement

KCC2 membrane diffusion was studied using quantum-dot-based single particle tracking (QD-SPT) (Chamma et al., 2013). SPT is an immunocytochemistry-based method which allows following the movements of individual molecules at the surface of living cells, and to detect heterogeneities in the diffusion behaviors of independent molecules. This technique therefore provides accurate information about the influence of microstructures that restrict diffusion, and of local interactions that retain proteins and confines them to a given space (Triller and Choquet, 2008). SPT consists in following fluorescent markers that are bound to the protein of interest in a specific manner through a linker, usually an antibody recognizing an extracellular epitope of the endogenous protein or a tag (e.g. HA, Flag, GFP) inserted in the extracellular region of the recombinant protein. Several criteria are required for efficient protein-linker coupling: nanomolar affinity between the protein, the linker, and the marker to ensure the stability of the protein-linker-marker complex, and a stoichiometry that enables one-to-one interaction between the protein of interest and the marker (Triller and Choquet, 2008; Pinaud et al., 2010). Moreover, the photostability of the fluorescent marker determines the maximal time of acquisition (due to photobleaching). The high photostability and signal-to-noise-ratio of QDs allow to follow single molecules for long duration with a QD localization accuracy of 5–10 nm (Dahan et al., 2003). Following QD labeling, real time movies are acquired and QD tracking and trajectory reconstructions are performed with homemade software (MATLAB; MathWorks) as described previously (Bonneau et al., 2005). Then, the center of the fluorescence spots is determined with a spatial accuracy of 5–10 nm by cross-correlating the image with a Gaussian fit of the point spread function (for details, see Triller and Choquet, 2008). Trajectories are classified as synaptic when they overlapped with the synaptic mask of gephyrin or homer1c fluorescent clusters to identify excitatory and inhibitory synapses, respectively, or extrasynaptic for spots two pixels (~380 nm) away. Analysis of reconstructed trajectories gives access to diffusion speed, confinement index and dwell time of tracked molecules in a given sub-cellular compartment.

Analysis of hundreds of KCC2 trajectories at the surface of hippocampal cultured neurons revealed a reduced diffusion coefficient and an increased confinement of the transporter near both excitatory glutamatergic and inhibitory GABAergic synapses as compared to extrasynaptic areas where transporters display Brownian-type motion (Chamma et al., 2013, 2012; Heubl et al., 2017) (Fig. 2). Transporters are temporarily immobilized near synapses and can escape the perisynaptic zone by lateral diffusion to explore neighbouring membrane areas. This is reminiscent of the neurotransmitter receptors diffusive behaviour (Choquet and Triller, 2013; Triller and Choquet, 2008). KCC2, however, diffused faster at excitatory and inhibitory synapses (~1.9 fold and 1.6 fold, respectively) as compared to AMPARs and $GABA_A$Rs (Table 1).

Increased confinement near excitatory and inhibitory synapses may lead to local KCC2 accumulation. Interestingly, the vast majority of KCC2 clusters are detected near synapses, where KCC2 confinement is also the highest (Chamma et al., 2013). Furthermore, most experimental paradigms (see below) known to increase KCC2 diffusion also induce cluster dispersion and loss. Therefore, KCC2 clustering requires a constant exchange between pools of mobile transporters in the extrasynaptic membrane and pools of less mobile transporters near synapses. A dynamic equilibrium between these pools of transporters may be rapidly modified to locally increase or decrease transporter clustering and thereby influence local, intra-neuronal chloride levels.

3.2. Molecular crowding and anchoring to cytoskeleton

Several factors are hindering the diffusion of trans-membrane proteins in biological membranes. These include transient interactions with proteins present in the membrane (Marguet et al., 2006), direct immobilization through stable molecular interactions (Gerrow and Triller, 2010), and/or corralling of membrane proteins by matrix-bound or aggregating proteins (Lippincott-Schwartz et al., 2001). Lateral diffusion of a protein also depends on its size (Ramadurai et al., 2009). Thus, the diffusion of a protein within an oligomeric complex will be reduced compared to that of a freely-moving molecule. Furthermore, lateral diffusion is limited by the concentration of obstacles in the plasma membrane (Saxton and Jacobson, 1997). In a very crowded environment, such as the postsynaptic membrane, most particles are slowed down and confined (Renner et al., 2009a; Renner et al., 2012; Renner et al., 2009b). Some proteins may also undergo specific interaction with scaffolding molecules that anchor them to the sub-membrane cytoskeleton. In this case, diffusion speed is also reduced, and confinement increased (Choquet and Triller, 2013).

To gain insight into the influence of obstacles and interactions with scaffolding molecules on KCC2 diffusion, the diffusion properties of KCC2 were compared to that of NCAM120, a glycosylphosphatidyl inositol (GPI)- anchored neural cell adhesion protein, that lacks intracellular domain (Rønn et al., 1998) and displays no preferential synaptic accumulation. Compared to KCC2, NCAM120 diffusion coefficient was increased by ~2 fold near glutamatergic and GABAergic synapses, but NCAM120 still showed reduced diffusion and increased confinement at inhibitory and excitatory synapses as compared to extrasynaptic zone, indicative of molecular crowding (Renner et al. 2009a, 2012) (Table 1). The synaptic dwell time which informs on protein-scaffold tethering (Renner et al., 2012) revealed that KCC2 spends more time near excitatory synapses than near inhibitory synapses, suggesting higher tethering near glutamatergic synapses. Compared to NCAM120, which is not specifically enriched at excitatory synapses, KCC2 dwell time was drastically increased (~5 fold), indicating KCC2 tethering near glutamatergic synapses. Although the diffusion coefficient of KCC2 was significantly (~2 fold) higher than that of AMPARs, KCC2 dwell time was only slightly lower (~1.6 fold) than that of AMPARs. There is no correlation between the diffusion coefficient and the dwell time (Renner et al., 2012). The lateral diffusion of a protein is hindered by the presence of diffusion barriers such as pickets and fences. The explored area and dwell time, but not diffusion coefficient, are correlated with the synaptic trapping and concentration of molecules. This means that although KCC2 moves rapidly in the membrane (faster than AMPARs), transporters are captured by the scaffold enriched at/near excitatory synapses (almost as efficiently as AMPARs which are known to interact with actin scaffold). In contrast, the dwell times of KCC2 and of NCAM120 did not significantly differ near inhibitory synapses (Table 1). Collectively, these results show that KCC2 specifically interacts with scaffolding molecules at excitatory glutamatergic synapses. Therefore, KCC2 undergoes a

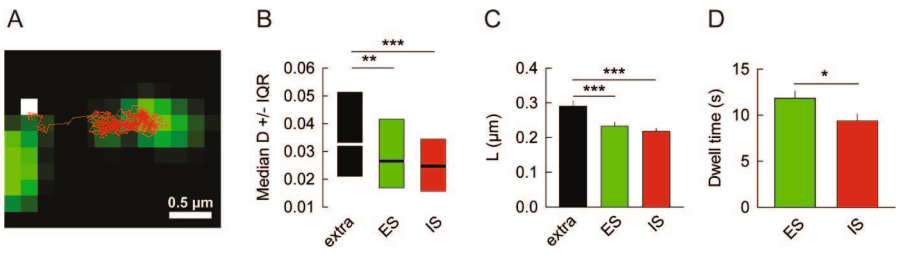

Fig. 2. KCC2 membrane dynamics studied with QD-based SPT.

A, Representative trajectory (red) of QD-bound Flag-tagged recombinant KCC2 overlaid with fluorescent clusters of recombinant gephyrin–mRFP (green) to identify inhibitory (IS) synapses. The white spot indicates the starting point of the trajectory. Scale bar, 0.5 µm. ***B***, Median QD diffusion coefficients D values ± 25–75% IQR in the extrasynaptic membrane (black) or near excitatory (green) or inhibitory (red) synapses identified by homer1c–GFP and gephyrin–mRFP clusters, respectively. Note the reduced diffusion near synapses (**$\boldsymbol{p} = 2 \times 10^{-3}$, ***$\boldsymbol{p} < 10^{-3}$). ***C***, Decreased size of the confinement domain ***L*** for synaptic versus extrasynaptic QDs (***$\boldsymbol{p} < 10^{-3}$). ***D,*** Mean KCC2 dwell times near excitatory synapses (green) and inhibitory synapses (red) showing increased time spent near excitatory synapses (*$\boldsymbol{p} < 5 \times 10^{-2}$). Adapted from (Chamma et al., 2013).

Table 1
KCC2 diffusion properties compared to that of AMPAR, $GABA_AR$ and NCAM120.

Molecules	Location	Median D (10^{-2} µm^{2}s^{-1})	Mean DT (s)
KCC2	ES.	2.7 (281, 5)	11.9 ± 0.8
	IS.	2.5 (202, 5)	9.4 ± 0.8
	Extra.	3.3 (367, 5)	N.A.
AMPAR GluA1	ES.	1.4 (40, 2)	19.5 ± 2.6
	IS.	1.6 (39, 2)	14.5 ± 2.6
	Extra.	2.1 (126, 2)	N.A.
$GABA_AR$ γ2	ES.	N.D.	N.D.
	IS.	1.6 (171, 4)	15.5 ± 0.9
	Extra.	3.1 (546, 4)	N.A.
NCAM120	ES.	5.9 (76, 2)	2.8 ± 0.6 (380)
	IS.	5.8 (68, 2)	6.2 ± 1.2 (288)
	Extra.	8.1 (183, 2)	N.A.

Quantifications from 2 to 5 independent experiments. Numbers between brackets indicate the numbers of QDs and experiments analyzed. Data for KCC2 and $GABA_AR$ are from (Chamma et al., 2013; Lévi et al., 2015); those for NCAM120 and AMPAR (unpublished data from our laboratory). N.D. not determined; N.A. not applicable.

diffusion-trapping mechanism at/near excitatory synapses but not at/near inhibitory synapses. This is consistent with the recent characterization of the KCC2 interactome showing that KCC2 interacts with more proteins located at excitatory synapses than at inhibitory synapses (Mahadevan et al., 2017).

Excitatory and inhibitory synapses differ in the composition of their associated cytoskeleton, with filamentous actin highly enriched in dendritic spines, which harbour most excitatory synapses (Korobova and Svitkina, 2010). Interactions with sub-membrane actin cytoskeleton likely contributes to hinder KCC2 diffusion near excitatory synapses. An initial study by Li et al. showed that the CTD of KCC2 interacts with actin via protein 4.1N and that this interaction is involved in spine morphogenesis (Li et al., 2007a). Overexpression of KCC2-CTD as a dominant negative inhibitor of KCC2-4.1N interaction, knockdown of 4.1N by RNA interference or inhibition of actin polymerization using Latrunculin A increased KCC2 diffusion and decreased its dwell time near excitatory (~2–5 fold) but not inhibitory synapses (Chamma et al., 2013). This indicates that KCC2 is tethered near excitatory synapses and in dendritic spines, but not near inhibitory synapses, via interaction of its CTD with 4.1N and the actin cytoskeleton. Since the discovery of the KCC2-4.1N interaction, several actin-related proteins have been shown to interact with KCC2 (Chevy et al., 2015; Llano et al., 2015; Mahadevan et al., 2017), suggesting that additional KCC2 interactors may participate in KCC2 recruitment at excitatory synapses at rest and upon synaptic activity.

What is the implication of a dynamic regulation of KCC2 tethering at the periphery of glutamatergic synapses? This may contribute to both dendritic spine morphology and excitatory synaptic function and plasticity. Direct KCC2 interaction with actin-associated proteins (such as 4.1N) contributes to form a molecular barrier hindering the lateral diffusion of transmembrane proteins within dendritic spines (Gauvain et al., 2011). Disrupting this barrier by knocking down KCC2 expression or preventing its interaction with intracellular partners promotes AMPA receptor lateral diffusion and disperses the perisynaptic reserve pool of receptors and, subsequently, the synaptic pool, leading to reduced efficacy of glutamatergic synapses. On the other hand, KCC2 binding to proteins controlling actin polymerization (such as the guanine exchange factor βPIX) controls spine actin cytoskeleton (Chevy et al., 2015; Llano et al., 2015). Changes in KCC2 diffusion and clustering near excitatory synapses are then likely to further influence synaptic plasticity at active synapses (Chevy et al., 2015). Therefore, the dynamic regulation of KCC2 may be particularly relevant for the physiological regulation of excitatory glutamatergic transmission.

4. Activity-dependent regulation of KCC2

KCC2 expression and function are regulated by both excitatory and inhibitory synaptic activity. In most cases, enhanced physiological (Lee et al., 2011; Kitamura et al., 2008; Wang et al., 2006; Fiumelli et al., 2005; Woodin et al., 2003) or pathological (Shimizu-Okabe et al., 2011; Li et al., 2008; Pathak et al., 2007; Rivera et al., 2004; Reid et al., 2001) neuronal activity have been shown to down-regulate KCC2 expression and activity, further altering the excitation/inhibition balance and promoting pathological activities. Recently, KCC2 down-regulation was also observed in conditions of reduced GABAergic inhibition in mature neurons (Heubl et al., 2017). Several cellular and molecular mechanisms underlying activity-dependent KCC2 down-regulation have been identified and lateral diffusion was shown to represent a rapid mechanism for adapting cell surface KCC2 function to changes in activity (Chamma et al., 2013; Heubl et al., 2017).

4.1. Regulation by glutamatergic activity

KCC2 is rapidly down-regulated by enhanced neuronal activity and glutamatergic neurotransmission in mature hippocampal neurons (Chamma et al., 2013; Lee et al., 2011; Wang et al., 2006). NMDAR-induced Ca^{2+}-influx leads to PP1-dependent KCC2 Serine 940 (S940) dephosphorylation and KCC2-CTD cleavage by Ca^{2+}-activated protease calpain (Lee et al., 2011; Puskarjov et al., 2012; Zhou et al., 2012). This in turn increases endocytosis and degradation of KCC2 and intra-neuronal chloride concentration. In this context, lateral diffusion contributes to the regulation of KCC2 membrane stability and neuronal Cl^- homeostasis (Chamma et al., 2013) (Fig. 3). Increasing glutamatergic synaptic activity enhanced KCC2 mobility within minutes while reducing its confinement. This effect was blocked by preventing S940 dephosphorylation or calpain-dependent cleavage of the transporter, suggesting S940 dephosphorylation and dispersion of KCC2 clusters may be a prerequisite for Ca^{2+}-activated calpain cleavage. Interestingly, even in the presence of a membrane-permeable dynamin inhibitory peptide which blocked KCC2 endocytosis, KCC2 diffusion still increased upon enhanced glutamatergic synaptic activity, indicating that altered transporter diffusion precedes its removal from the membrane.

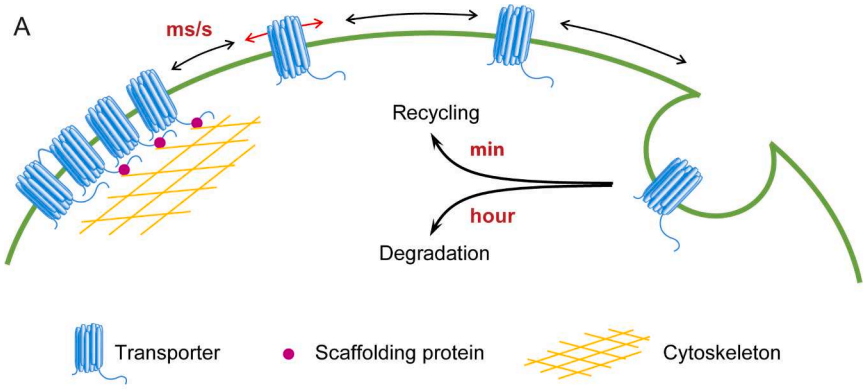

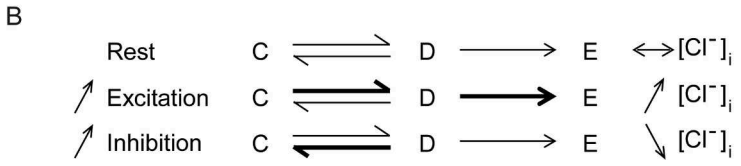

Fig. 3. Regulation of KCC2 membrane trafficking.
A, KCC2 is mobile outside of clusters and confined within clusters. KCC2 clustering probably involves a multiple step process including transporter oligomerization, accumulation in lipid-rafts, and cytoskeleton interaction. Freely moving transporters are more susceptible to interact with molecules implicated in endocytosis. ***B,*** Activity-dependent tuning of KCC2 membrane trafficking: the balance between "freely moving" and "clustered" KCC2 pools can be rapidly modified by neuronal activity. Changes in the phosphorylation state of the transporter then influence its clustering and internalization rate, and in turn affect intracellular chloride concentration. C, clustered; D, diffusing; E, endocytosed transporters.

4.2. Regulation by GABAergic inhibition

A rapid regulation of KCC2 membrane trafficking and function by $GABA_AR$-dependent inhibition was also recently demonstrated in hippocampal neurons (Heubl et al., 2017). $GABA_AR$ activation decreases KCC2 diffusion coefficient thereby increasing its membrane confinement and stability. Conversely, $GABA_AR$ blockade increases KCC2 mobility while reducing its surface clustering, stability and activity (Heubl et al., 2017). This mechanism may serve for "self-tuning" GABAergic signaling via rapid regulation of KCC2-mediated Cl^- export (Fig. 3). The underlying molecular mechanism was shown to be independent of Ca^{2+} signaling and KCC2 S940 phosphorylation but instead involved Cl^- itself acting as a second intracellular messenger in this regulation. Thus, increasing $[Cl]_i$ using the selective KCC2 inhibitor VU0463271 or local photo-stimulation of the chloride pump halorhodopsin confined KCC2 in the neuronal membrane. Reciprocally, lowering $[Cl]_i$ by substituting extracellular Cl^- with methanesulfonate relieved KCC2 diffusion constraints. Since KCC2 confinement increased within tens of seconds after halorhodopsin photo-stimulation (Heubl et al., 2017), lateral diffusion is probably among the first cellular mechanisms modulating chloride homeostasis. $GABA_AR$-dependent modulation of KCC2 diffusion involved the Cl^--sensing serine/threonine kinase WNK1 (With No lysine (K) serine-threonine kinase 1) and its effectors, the kinases SPAK (STE20/SPS1-related, proline alanine-rich kinase) and OSR1 (Oxydative stress response 1). The $GABA_AR$-mediated activation of the WNK1/SPAK/OSR1 signaling pathway in turn promoted the phosphorylation of KCC2 at positions T906 and T1007 (Heubl et al., 2017), which is known to result in KCC2 inhibition (Rinehart et al., 2009; Inoue et al., 2012, de Los Heros et al., 2014).

Therefore, enhanced NMDAR-mediated excitation or reduced $GABA_AR$-mediated inhibition both act to increase KCC2 lateral diffusion through altered phosphorylation of specific residues (S940 dephosphorylation upon increased excitation; T906/1007 phosphorylation upon $GABA_AR$ blockade). KCC2 phosphorylation/dephosphorylation may then induce conformational changes (Groban et al., 2006), thereby altering transporter-scaffold interactions and promoting cluster dispersion. This may in turn facilitate KCC2 interaction with the endocytic machinery, a process that occurs at distance from the postsynaptic zone (Blanpied et al., 2002). Endocytosed transporters may then be recycled back to the membrane or sent to lysosomes for degradation. Inversely, KCC2 confinement in the plasma membrane may protect transporters from endocytosis. Interfering with transporter diffusion/endocytosis could then help to restore KCC2 membrane expression and function under pathological conditions (Fig. 3).

4.3. Putative contribution of NKCC1 lateral diffusion to chloride homeostasis

The increase in $[Cl^-]_i$ and subsequent depolarizing shift in the reversal potential of $GABA_AR$-mediated currents (E_{GABA}) observed in the epileptic brain is most often attributed to a reduction in KCC2-dependent Cl^- export (reviewed in (Di Cristo et al., 2017)). However, an up-regulation of NKCC1 may also contribute to increased $[Cl^-]_i$ and depolarized E_{GABA} (Kourdougli et al., 2017; Wang et al., 2017). Although the mechanisms regulating KCC2 membrane expression and function have been extensively studied, the cellular and molecular mechanisms controlling NKCC1 membrane turnover are less well understood. Phosphorylation-dependent alteration of NKCC1 diffusion may regulate its membrane turnover and function. QD-SPT experiments in mature hippocampal neurons support a contribution of lateral diffusion to NKCC1 regulation at the plasma membrane (unpublished work from our laboratory). SPT experiments require labeling live neurons with an antibody targeting an extracellular epitope of NKCC1. In the absence of such antibody, we expressed a recombinant human NKCC1a transporter bearing a 2xHA tag at position Histidine 398 in its second extracellular loop (i.e. the NT931 construct in Somasekharan et al., 2013). The recombinant transporter also carries a 3xFlag tag and a monomeric Venus tag inserted at the N-terminus after the initiation codon (Somasekharan et al., 2013). The insertion of these tags did not alter the membrane expression and transport function of the NKCC1 protein as checked by HA surface labeling and ^{86}Rb influx studies in HEK 293 cells (Somasekharan et al., 2013). In agreement with these results, we reported using surface labeling that the recombinant transporter is well expressed in mature hippocampal cultured neurons and is targeted to both the axonal and somato-dendritic plasma membrane (Fig. 4), in a similar way than the endogenous protein (not shown). Confocal microscopy further indicated that the recombinant NKCC1a transporter formed clusters near both excitatory and inhibitory synapses (Fig. 4). The cellular and sub-cellular distributions of NKCC1b were indistinguishable from that of NKCC1a (data not shown). We thus focused on NKCC1a. We explored the membrane dynamics of NKCC1a by QD-SPT. As shown in Fig. 4, NKCC1a transporters explored large areas of the axonal and somato-dendritic extrasynaptic plasma membrane while others were confined near excitatory and inhibitory synapses. The

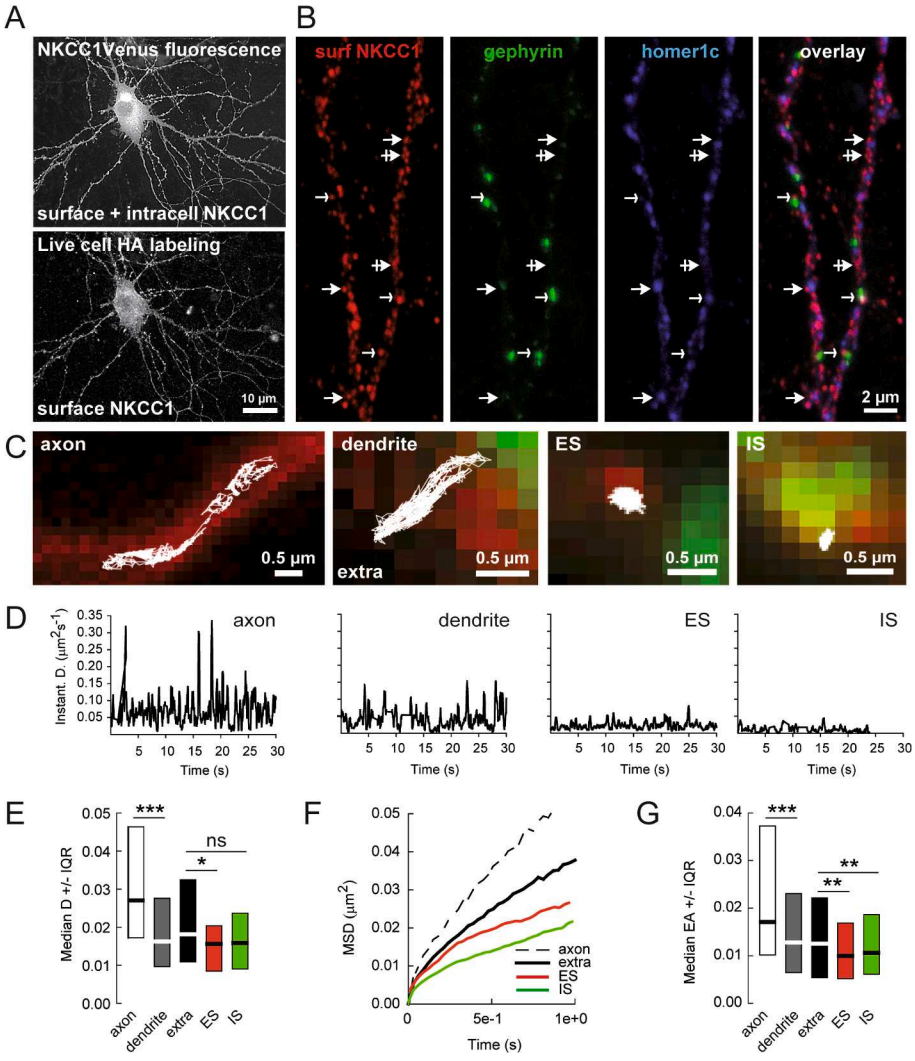

Fig. 4. NKCC1 also undergoes diffusion-trapping at the plasma membrane.

A, Total (Venus) and surface (HA tag) labeling of recombinant HA-Venus-NKCC1 transporter in 21 DIV hippocampal neurons showing that a large amount of the recombinant transporter traffics to the somato-dendritic and axonal plasma membrane. Scale bar, 10 µm. **B**, NKCC1 surface staining (red) in neurons cotransfected with HA-NKCC1 transporter, gephyrin-FingerGFP (green) and homer1c-mRFP (blue), two markers of inhibitory (IS) and excitatory (ES) synapses. Scale bar, 2 µm. Note that some NKCC1 clusters are surrounding inhibitory (open arrows) and excitatory (closed arrows) synapses, whereas others are associated with the extrasynaptic membrane (crossed arrows). **C**, Representative trajectories (white) of QD-bound HA-tagged recombinant NKCC1 overlaid with either cytoplasmic eGFP (red) to identify axons, or with recombinant homer1c–GFP (green) and gephyrin–mRFP (red) to identify ES and IS, respectively. Scale bars, 0.5 µm. **D**, Instantaneous diffusion coefficients of the trajectories shown in (C). **E**, Median diffusion coefficient D values ± 25–75% IQR in axons (white), dendrites (grey), extrasynaptic (extra, black), at/near excitatory synapses (red), and at/near inhibitory synapses (green). Axon, n = 94 QDs, dendrite, n = 234 QDs, extra, n = 153 QDs, ES, n = 47 QDs, IS, n = 36 QDs, 2 cultures. axon vs. dendrite KS test $p < 0.001$, extra vs. ES KS test $p = 0.05$, extra vs. IS KS test $p = 0.4$. **F**, Time-averaged MSD functions of axonal QDs (dashed), extrasynaptic QDs (black), QDs at ES (red), and QDs at IS (green). The MSD versus time relationships show a steeper initial slope for axonal vs extrasynaptic trajectories and for extrasynaptic vs synaptic trajectories, suggesting that trajectories are less confined. **G**, Median explored area EA ± 25–75% IQR in axons (white), dendrites (grey), extrasynaptic (black), at/near ES (red), and at/near IS (green). Axon, n = 276 QDs, dendrite, n = 408 QDs, extra, n = 488 QDs, ES, n = 89 QDs, IS, n = 95 QDs, 2 cultures. axon vs. dendrite KS test $p < 0.001$, extra vs. ES KS test $p = 0.001$, extra vs. IS KS test $p = 0.001$. Note that NKCC1 moved faster and explored a larger surface of the axonal membrane compared to the extrasynaptic dendritic membrane. NKCC1 is also slower and more confined near synapses as compared to extrasynaptic sites.

transporter mobility was significantly higher at the surface of the axon as compared to the dendrites, suggestive of lower diffusion constraints in the axon. Transitions between significant NKCC1 confinement at/near synapses and less constrained diffusion in extrasynaptic areas is reminiscent of KCC2 diffusion behaviour (Chamma et al., 2013, 2012; Heubl et al., 2017). Therefore, we concluded that NKCC1 also responds to the diffusion-trapping mechanism. Unlike KCC2, we found that NKCC1 diffused along the axon (Fig. 4) suggesting functional differences between the two transporters. This is in agreement with the fact that E_{GABA} is depolarized at the axon initial segment (AIS) due to NKCC1 expression (Khirug et al., 2008) and KCC2 exclusion from CNS axons (Hübner et al., 2001; Williams et al., 1999). Clearly, more work is needed to examine whether NKCC1a and NKCC1b membrane dynamics and clustering are modulated by normal and pathological activities in the axonal and somato-dendritic compartments. An activity-dependent regulation of NKCC1 diffusion/clustering, similar to that described for KCC2, may then locally affect its function, and in turn chloride homeostasis and GABA signaling.

In conclusion, different subpopulations of CCCs exist in the plasma membrane: freely moving transporters outside of clusters and confined transporters in clusters near synapses. KCC2 and NKCC1 clustering probably results from accumulation in lipid-rafts, interaction with the cytoskeleton via scaffolding proteins and oligomerization. Freely moving transporters are probably more susceptible to interaction with molecules involved in clathrin-dependent endocytosis. The balance between “freely moving” and “clustered” pools of KCC2 and NKCC1 might be rapidly changed by activity through phosphoregulation and impact the overall density of transporters at the plasma membrane. Since activity-induced changes in KCC2 mobility occurs within seconds - i.e. well before transporter internalization, which occurs within tens of minutes - lateral diffusion is probably among the first cellular mechanism modulating chloride transporter membrane stability.

Acknowledgments

Our work is supported in part by Inserm, Sorbonne Université as well as the Fondation pour la Recherche Médicale (Equipe FRM DEQ20140329539 to JCP), the Fondation Française pour la Recherche sur l'Épilepsie (to JCP) and the Fondation pour la Recherche sur le Cerveau (to SL). Equipment at the IFM is supported by DIM NeRF from Région Ile-de-France and by the FRC/Rotary ‘Espoir en tête’. EC is the recipient of a doctoral fellowship from Sorbonne Université. The Poncer/Lévi lab is affiliated with the Paris School of Neuroscience (ENP) and the Bio-Psy Laboratory of excellence.

References

Acton, B.A., Mahadevan, V., Mercado, A., Uvarov, P., Ding, Y., Pressey, J., Airaksinen, M.S., Mount, D.B., Woodin, M.A., 2012. Hyperpolarizing GABAergic transmission

requires the KCC2 C-terminal ISO domain. J. Neurosci. 32, 8746–8751. https://doi.org/10.1523/JNEUROSCI.6089-11.2012.
Awad, P.N., Amegandjin, C.A., Szczurkowska, J., Carriço, J.N., Fernandes do Nascimento, A.S., Baho, E., Chattopadhyaya, B., Cancedda, L., Carmant, L., Di Cristo, G., 2018. KCC2 regulates dendritic spineformation in a brain-region specific and BDNF dependent manner. Cereb. Cortex 28, 4049–4062. https://doi.org/10.1093/cercor/bhy198.
Báldi, R., Varga, C., Tamás, G., 2010. Differential distribution of KCC2 along the axo-somato-dendritic axis of hippocampal principal cells. Eur. J. Neurosci. 32, 1319–1325. https://doi.org/10.1111/j.1460-9568.2010.07361.x.
Barthó, P., Payne, J.A., Freund, T.F., Acsády, L., 2004. Differential distribution of the KCl cotransporter KCC2 in thalamic relay and reticular nuclei. Eur. J. Neurosci. 20, 965–975. https://doi.org/10.1111/j.1460-9568.2004.03562.x.
Bergeron, M.J., Gagnon, E., Caron, L., Isenring, P., 2006. Identification of key functional domains in the C terminus of the K+-Cl- cotransporters. J. Biol. Chem. 281, 15959–15969. https://doi.org/10.1074/jbc.M600015200.
Blaesse, P., Guillemin, I., Schindler, J., Schweizer, M., Delpire, E., Khiroug, L., Friauf, E., Nothwang, H.G., 2006. Oligomerization of KCC2 correlates with development of inhibitory neurotransmission. J. Neurosci. 26, 10407–10419. https://doi.org/10.1523/JNEUROSCI.3257-06.2006.
Blanpied, T.A., Scott, D.B., Ehlers, M.D., 2002. Dynamics and regulation of clathrin coats at specialized endocytic zones of dendrites and spines. Neuron 36, 435–449. https://doi.org/10.1016/S0896-6273(02)00979-0.
Bonneau, S., Dahan, M., Cohen, L.D., 2005. Single quantum dot tracking based on perceptual grouping using minimal paths in a spatiotemporal volume. IEEE Trans. Image Process. 14, 1384–1395.
Carmosino, M., Giménez, I., Caplan, M., Forbush, B., 2008. Exon loss accounts for differential sorting of Na-K-Cl cotransporters in polarized epithelial cells. Mol. Biol. Cell 19, 4341–4351. https://doi.org/10.1091/mbc.e08-05-0478.
Casula, S., Shmukler, B.E., Wilhelm, S., Stuart-Tilley, A.K., Su, W., Chernova, M.N., Brugnara, C., Alper, S.L., 2001. A dominant negative mutant of the KCC1 K-Cl co-transporter: both N- and C-terminal cytoplasmic domains are required for K-Cl co-transport activity. J. Biol. Chem. 276, 41870–41878. https://doi.org/10.1074/jbc.M107155200.
Casula, S., Zolotarev, A.S., Stuart-Tilley, A.K., Wilhelm, S., Shmukler, B.E., Brugnara, C., Alper, S.L., 2009. Chemical crosslinking studies with the mouse Kcc1 K-Cl co-transporter. Blood Cells. Mol. Dis. 42, 233–240. https://doi.org/10.1016/j.bcmd.2009.01.021.
Chamma, I., Chevy, Q., Poncer, J.C., Lévi, S., 2012. Role of the neuronal K-Cl co-transporter KCC2 in inhibitory and excitatory neurotransmission. Front. Cell. Neurosci. 6, 5. https://doi.org/10.3389/fncel.2012.00005.
Chamma, I., Heubl, M., Chevy, Q., Renner, M., Moutkine, I., Eugène, E., Poncer, J.C., Lévi, S., 2013. Activity-dependent regulation of the K/Cl transporter KCC2 membrane diffusion, clustering, and function in hippocampal neurons. J. Neurosci. 33, 15488–15503. https://doi.org/10.1523/JNEUROSCI.5889-12.2013.
Chang, J.C., Tomlinson, I.D., Warnement, M.R., Ustione, A., Carneiro, A.M.D., Piston, D.W., Blakely, R.D., Rosenthal, S.J., 2012. Single molecule analysis of serotonin transporter regulation using antagonist-conjugated quantum dots reveals restricted, p38 MAPK-dependent mobilization underlying uptake activation. J. Neurosci. 32, 8919–8929. https://doi.org/10.1523/JNEUROSCI.0048-12.2012.
Chevy, Q., Heubl, M., Goutierre, M., Backer, S., Moutkine, I., Eugene, E., Bloch-Gallego, E., Levi, S., Poncer, J.C., 2015. KCC2 gates activity-driven AMPA receptor traffic through cofilin phosphorylation. J. Neurosci. 35, 15772–15786. https://doi.org/10.1523/JNEUROSCI.1735-15.2015.
Choquet, D., Triller, A., 2013. The dynamic synapse. Neuron 80, 691–703. https://doi.org/10.1016/j.neuron.2013.10.013.
Dahan, M., Lévi, S., Luccardini, C., Rostaing, P., Riveau, B., Triller, A., 2003. Diffusion dynamics of glycine receptors revealed by single-quantum dot tracking. Science 302, 442–445. https://doi.org/10.1126/science.1088525.
de Los Heros, P., Alessi, D.R., Gourlay, R., Campbell, D.G., Deak, M., Macartney, T.J., Kahle, K.T., Zhang, J., 2014. The WNK-regulated SPAK/OSR1 kinases directly phosphorylate and inhibit the K+-Cl- co-transporters. Biochem. J. 458, 559–573. https://doi.org/10.1042/BJ20131478.
Di Cristo, G., Awad, P.N., Hamidi, S., Avoli, M., 2017. KCC2, epileptiform synchronization, and epileptic disorders. Prog. Neurobiol. 162, 1–16. https://doi.org/10.1016/j.pneurobio.2017.11.002.
Doyon, N., Prescott, S. a, Castonguay, A., Godin, A.G., Kröger, H., De Koninck, Y., 2011. Efficacy of synaptic inhibition depends on multiple, dynamically interacting mechanisms implicated in chloride homeostasis. PLoS Comput. Biol. 7 e1002149. https://doi.org/10.1371/journal.pcbi.1002149.
Fiumelli, H., Cancedda, L., Poo, M., 2005. Modulation of GABAergic transmission by activity via postsynaptic Ca2+-dependent regulation of KCC2 function. Neuron 48, 773–786. https://doi.org/10.1016/j.neuron.2005.10.025.
Gamba, G., 2005. Molecular physiology and pathophysiology of electroneutral cation-chloride cotransporters. Physiol. Rev. 85, 423–493. https://doi.org/10.1152/physrev.00011.2004.
Gauvain, G., Chamma, I., Chevy, Q., Cabezas, C., Irinopoulou, T., Bodrug, N., Carnaud, M., Levi, S., Poncer, J.C., 2011. The neuronal K-Cl cotransporter KCC2 influences postsynaptic AMPA receptor content and lateral diffusion in dendritic spines. Proc. Natl. Acad. Sci. Unit. States Am. 108, 15474–15479. https://doi.org/10.1073/pnas.1107893108.
Gerrow, K., Triller, A., 2010. Synaptic stability and plasticity in a floating world. Curr. Opin. Neurobiol. 20, 631–639. https://doi.org/10.1016/j.conb.2010.06.010.
Glykys, J., Dzhala, V., Egawa, K., Balena, T., Saponjian, Y., Kuchibhotla, K.V., Bacskai, B.J., Kahle, K.T., Zeuthen, T., Staley, K.J., 2014. Local impermeant anions establish the neuronal chloride concentration. Science 343, 670–675. https://doi.org/10.1126/science.1245423.
Goldman, J., Andrews, S., Bray, D., 2004. Size and composition of membrane protein clusters predicted by Monte Carlo analysis. Eur. Biophys. J. 33, 506–512. https://doi.org/10.1007/s00249-004-0391-6.
Groban, E.S., Narayanan, A., Jacobson, M.P., 2006. Conformational changes in protein loops and helices induced by post-translational phosphorylation. PLoS Comput. Biol. 2, 238–250. https://doi.org/10.1371/journal.pcbi.0020032.
Gulyás, A.I., Sík, A., Payne, J.A., Kaila, K., Freund, T.F., 2001. The KCl cotransporter, KCC2, is highly expressed in the vicinity of excitatory synapses in the rat hippocampus. Eur. J. Neurosci. 13, 2205–2217. https://doi.org/10.1046/j.0953-816X.2001.01600.x.
Hartmann, A.-M., Blaesse, P., Kranz, T., Wenz, M., Schindler, J., Kaila, K., Friauf, E., Nothwang, H.G., AM, H., Blaesse, P.K.T., M, W., J, S., K, K., E, F., HG, N., 2009. Opposite effect of membrane raft perturbation on transport activity of KCC2 and NKCC1. J. Neurochem. 111, 321–331. https://doi.org/10.1111/j.1471-4159.2009.06343.x.
Hartmann, A.-M., Nothwang, H.G., 2015. Molecular and evolutionary insights into the structural organization of cation chloride cotransporters. Front. Cell. Neurosci. 8, 1–14. https://doi.org/10.3389/fncel.2014.00470.
Heubl, M., Zhang, J., Pressey, J.C., Al Awabdh, S., Renner, M., Gomez-Castro, F., Moutkine, I., Eugène, E., Russeau, M., Kahle, K.T., Poncer, J.C., Lévi, S., 2017. GABAAreceptor dependent synaptic inhibition rapidly tunes KCC2 activity via the Cl–sensitive WNK1 kinase. Nat. Commun. 8. https://doi.org/10.1038/s41467-017-01749-0.
Hou, Q., Huang, Y., Amato, S., Snyder, S.H., Huganir, R.L., Man, H.Y., 2008. Regulation of AMPA receptor localization in lipid rafts. Mol. Cell. Neurosci. 38, 213–223. https://doi.org/10.1016/j.mcn.2008.02.010.
Hübner, C.A., Stein, V., Hermans-Borgmeyer, I., Meyer, T., Ballanyi, K., Jentsch, T.J., 2001. Disruption of KCC2 reveals an essential role of K-Cl cotransport already in early synaptic inhibition. Neuron 30, 515–524. https://doi.org/10.1016/S0896-6273(01)00297-5.
Inoue, K., Furukawa, T., Kumada, T., Yamada, J., Wang, T., Inoue, R., Fukuda, A., 2012. Taurine inhibits K+Cl- cotransporter KCC2 to regulate embryonic Cl- homeostasis via with-no-lysine (WNK) protein kinase signaling pathway. J. Biol. Chem. 287, 20839–20850. Epub 2012 Apr 27. https://doi.org/10.1074/jbc.M111.319418.
Ivakine, E.A., Acton, B.A., Mahadevan, V., Ormond, J., Tang, M., Pressey, J.C., Huang, M.Y., Ng, D., Delpire, E., Salter, M.W., Woodin, M.A., McInnes, R.R., 2013. Neto2 is a KCC2 interacting protein required for neuronal Cl − regulation in hippocampal neurons. Proc. Natl. Acad. Sci. Unit. States Am. 110, 3561–3566. https://doi.org/10.1073/pnas.1212907110.
Jedlicka, P., Deller, T., Schwarzacher, S.W., 2010. Computational modeling of GABAA receptor-mediated Paired-pulse inhibition in the dentate gyrus. J. Comput. Neurosci. 29, 509–519. https://doi.org/10.1007/s10827-010-0214-y.
Kahle, K.T., Rinehart, J., Lifton, R.P., 2010. Phosphoregulation of the Na-K-2Cl and K-Cl cotransporters by the WNK kinases. Biochim. Biophys. Acta (BBA) - Mol. Basis Dis. 1150–1158. 1802. https://doi.org/10.1016/j.bbadis.2010.07.009.
Kaila, K., Price, T.J., Payne, J.A., Puskarjov, M., Voipio, J., 2014. Cation-chloride co-transporters in neuronal development, plasticity and disease. Nat. Rev. Neurosci. 15, 637–654. (submitted for publication). https://doi.org/10.1038/nrn3819.
Khirug, S., Yamada, J., Afzalov, R., Voipio, J., Khiroug, L., Kaila, K., 2008. GABAergic depolarization of the axon initial segment in cortical principal neurons is caused by the Na-K-2Cl cotransporter NKCC1. J. Neurosci. 28, 4635–4639. https://doi.org/10.1523/JNEUROSCI.0908-08.2008.
Kitamura, A., Ishibashi, H., Watanabe, M., Takatsuru, Y., Brodwick, M., Nabekura, J., 2008. Sustained depolarizing shift of the GABA reversal potential by glutamate receptor activation in hippocampal neurons. Neurosci. Res. 62, 270–277. https://doi.org/10.1016/j.neures.2008.09.002.
Korobova, F., Svitkina, T.M., 2010. Molecular architecture of synaptic actin cytoskeleton in hippocampal neurons reveals a mechanism of dendritic spine morphogenesis. Mol. Biol. Cell 21, 4042–4056. https://doi.org/10.1091/mbc.E09.
Kourdougli, N., Pellegrino, C., Renko, J.M., Khirug, S., Chazal, G., Kukko-Lukjanov, T.K., Lauri, S.E., Gaiarsa, J.L., Zhou, L., Peret, A., Castrén, E., Tuominen, R.K., Crépel, V., Rivera, C., 2017. Depolarizing γ-aminobutyric acid contributes to glutamatergic network rewiring in epilepsy. Ann. Neurol. 81, 251–265. https://doi.org/10.1002/ana.24870.
Kusumi, A., Nakada, C., Ritchie, K., Murase, K., Suzuki, K., Murakoshi, H., Kasai, R.S., Kondo, J., Fujiwara, T., 2005. Paradigm shift of the plasma membrane concept from the two-dimensional continuum fluid to the partitioned fluid: high-speed single-molecule tracking of membrane molecules. Annu. Rev. Biophys. Biomol. Struct. 34, 351–378. https://doi.org/10.1146/annurev.biophys.34.040204.144637.
Lee, H.H.C., Deeb, T.Z., Walker, J.A., Davies, P.A., Moss, S.J., 2011. NMDA receptor activity downregulates KCC2 resulting in depolarizing GABAA receptor-mediated currents. Nat. Neurosci. 14, 736–743. https://doi.org/10.1038/nn.2806.
Lee, H.H.C., Jurd, R., Moss, S.J., 2010. Tyrosine phosphorylation regulates the membrane trafficking of the potassium chloride co-transporter KCC2. Mol. Cell. Neurosci. 45, 171–179. https://doi.org/10.1016/j.mcn.2010.06.008.
Lee, H.H.C., Walker, J.A., Williams, J.R., Goodier, R.J., Payne, J.A., Moss, S.J., 2007. Direct protein kinase C-dependent phosphorylation regulates the cell surface stability and activity of the potassium chloride cotransporter KCC2. J. Biol. Chem. 282, 29777–29784. https://doi.org/10.1074/jbc.M705053200.
Li, H., Khirug, S., Cai, C., Ludwig, A., Blaesse, P., Kolikova, J., Afzalov, R., Coleman, S.K., Lauri, S., Airaksinen, M.S., Keinänen, K., Khiroug, L., Saarma, M., Kaila, K., Rivera, C., 2007a. KCC2 interacts with the dendritic cytoskeleton to promote spine development. Neuron 56, 1019–1033. https://doi.org/10.1016/j.neuron.2007.10.039.
Li, X., Serwanski, D.R., Miralles, C.P., Bahr, B. a, De Blas, A.L., 2007b. Two pools of Triton X-100-insoluble GABA(A) receptors are present in the brain, one associated to lipid rafts and another one to the post-synaptic GABAergic complex. J. Neurochem. 102, 1329–1345. https://doi.org/10.1111/j.1471-4159.2007.04635.x.
Li, X., Zhou, J., Chen, Z., Chen, S., Zhu, F., Zhou, L., 2008. Long-term expressional changes of Na+-K+-Cl- co-transporter 1 (NKCC1) and K+-Cl- co-transporter 2 (KCC2) in CA1 region of hippocampus following lithium-pilocarpine induced status epilepticus (PISE). Brain Res. 1221, 141–146. https://doi.org/10.1016/j.brainres.2008.04.047.
Lippincott-Schwartz, J., Snapp, E., Kenworthy, A., 2001. Studying protein dynamics in

living cells. Nat. Rev. Mol. Cell Biol. 2, 444–456. https://doi.org/10.1038/35073068.
Llano, O., Smirnov, S., Soni, S., Golubtsov, A., Guillemin, I., Hotulainen, P., Medina, I., Nothwang, H.G., Rivera, C., Ludwig, A., 2015. KCC2 regulates actin dynamics in dendritic spines via interaction with β-PIX. J. Cell Biol. 209, 671–686. https://doi.org/10.1083/jcb.201411008.
Lévi, S., Le Roux, N., Eugène, E., Poncer, J.C., 2015. Benzodiazepine ligands rapidly influence GABAA receptor diffusion and clustering at hippocampal inhibitory synapses. Neuropharmacology 88, 199–208. https://doi.org/10.1016/j.neuropharm.2014.06.002.
Mahadevan, V., Khademullah, C.S., Dargaei, Z., Chevrier, J., Uvarov, P., Kwan, J., Bagshaw, R.D., Pawson, T., Emili, A., De Koninck, Y., Anggono, V., Airaksinen, M., Woodin, M.A., 2017. Native KCC2 interactome reveals PACSIN1 as a critical regulator of synaptic inhibition. Elife 6, 1–34. https://doi.org/10.7554/eLife.28270.001.
Mahadevan, V., Pressey, J.C., Acton, B.A., Uvarov, P., Huang, M.Y., Chevrier, J., Puchalski, A., Li, C.M., Ivakine, E.A., Airaksinen, M.S., Delpire, E., McInnes, R.R., Woodin, M.A., 2014. Kainate receptors coexist in a functional complex with KCC2 and regulate chloride homeostasis in hippocampal neurons. Cell Rep. 7, 1762–1770. https://doi.org/10.1016/j.celrep.2014.05.022.
Marguet, D., Lenne, P.-F., Rigneault, H., He, H.-T., 2006. Dynamics in the plasma membrane: how to combine fluidity and order. EMBO J. 25, 3446–3457. https://doi.org/10.1038/sj.emboj.7601204.
Mercado, A., Broumand, V., Zandi-Nejad, K., Enck, A.H., Mount, D.B., 2006. A C-terminal domain in KCC2 confers constitutive K+-Cl - cotransport. J. Biol. Chem. 281, 1016–1026. https://doi.org/10.1074/jbc.M509972200.
Mohapatra, N., Tønnesen, J., Vlachos, A., Kuner, T., Deller, T., Nägerl, U.V., Santamaria, F., Jedlicka, P., 2016. Spines slow down dendritic chloride diffusion and affect short-term ionic plasticity of GABAergic inhibition. Sci. Rep. 6, 23196. https://doi.org/10.1038/srep23196.
Parvin, M.N., Gerelsaikhan, T., Turner, R.J., 2007. Regions in the cytosolic C-terminus of the secretory Na+-K +-2Cl- cotransporter NKCC1 are required for its homodimerization. Biochemistry 46, 9630–9637. https://doi.org/10.1021/bi700881a.
Pathak, H.R., Weissinger, F., Terunuma, M., Carlson, G.C., Hsu, F.-C., Moss, S.J., et al., 2007. Disrupted dentate granule cell chloride regulation enhances synaptic excitability during development of temporal lobe epilepsy. J. Neurosci. 27, 14012–14022. https://doi.org/10.1523/JNEUROSCI.4390-07.2007.
Payne, J.A., Xu, J.-C., Haas, M., Lytle, C., Ward, D., Forbush, B., 1995. Primary structure, functional expression and chromosomal localization of the bumetanide-sensitive Na-K-Cl cotransporter in human colon. J. Biol. Chem. 270, 17977–17985. https://doi.org/10.1074/jbc.270.30.17977.
Payne, J. a, Stevenson, J., Donaldson, L., 1996. Molecular characterization of putative K - Cl cotransporter in rat brain. J. Biol. Chem. 271, 16245–16252. https://doi.org/10.1074/jbc.271.27.16245.
Pike, L.J., 2009. The challenge of lipid rafts. J. Lipid Res. 50 (Suppl. l), S323–S328. https://doi.org/10.1194/jlr.R800040-JLR200.
Pinaud, F., Clarke, S., Sittner, A., Dahan, M., 2010. Probing cellular events, one quantum dot at a time. Nat. Methods 7, 275–285. 1444. Epub 2010 Mar 30. https://doi.org/10.1038/nmeth.
Plotkin, M.D., Kaplan, M.R., Peterson, L.N., Gullans, S.R., Hebert, S.C., Delpire, E., 1997. Expression of the Na(+)-K(+)-2Cl- cotransporter BSC2 in the nervous system. Am. J. Physiol. 272, C173–C183.
Pressey, J.C., Mahadevan, V., Khademullah, C.S., Dargaei, Z., Chevrier, J., Ye, W., Huang, M., Chauhan, A.K., Meas, S.J., Uvarov, P., Airaksinen, M.S., Woodin, M.A., 2017. A kainate receptor subunit promotes the recycling of the neuron-specific K-Cl co-Transporter KCC2 in hippocampal neurons. J. Biol. Chem. 292, 6190–6201. https://doi.org/10.1074/jbc.M116.767236.
Price, G.D., Trussell, L.O., 2006. Estimate of the chloride concentration in a central glutamatergic terminal: a gramicidin perforated-patch study on the calyx of held. J. Neurosci. 26, 11432–11436. https://doi.org/10.1523/JNEUROSCI.1660-06.2006.
Puskarjov, M., Ahmad, F., Kaila, K., Blaesse, P., 2012. Activity-dependent cleavage of the K-Cl cotransporter KCC2 mediated by calcium-activated protease calpain. J. Neurosci. 32, 11356–11364. https://doi.org/10.1523/JNEUROSCI.6265-11.2012.
Ramadurai, S., Holt, A., Krasnikov, V., Bogaart, G. Van Den, Antoinette, J., van den Bogaart, G., Killian, J.A., Poolman, B., 2009. Lateral diffusion of membrane proteins. J. Am. Chem. Soc. 131, 12650–12656. https://doi.org/10.1021/ja902853g.
Reid, K.H., Li, G.Y., Payne, R.S., Schurr, A., Cooper, N.G.F., 2001. The mRNA level of the potassium-chloride cotransporter KCC2 covaries with seizure susceptibility in inferior colliculus of the post-ischemic audiogenic seizure-prone rat. Neurosci. Lett. 308, 29–32. https://doi.org/10.1016/S0304-3940(01)01973-5.
Renner, M., Choquet, D., Triller, A., 2009a. Control of the postsynaptic membrane viscosity. J. Neurosci. 29, 2926–2937. https://doi.org/10.1523/JNEUROSCI.4445-08.2009.
Renner, M., Schweizer, C., Bannai, H., Triller, A., Lévi, S., 2012. Diffusion barriers constrain receptors at synapses. PLoS One 7, e43032. https://doi.org/10.1371/journal.pone.0043032.
Renner, M.L., Cognet, L., Lounis, B., Triller, A., Choquet, D., 2009b. The excitatory postsynaptic density is a size exclusion diffusion environment. Neuropharmacology 56, 30–36. https://doi.org/10.1016/j.neuropharm.2008.07.022.
Rinehart, J., Maksimova, Y.D., Tanis, J.E., Stone, K.L., Hodson, C. a., Zhang, J., et al., 2009. Sites of regulated phosphorylation that control K-Cl cotransporter activity. Cell 138, 525–536. https://doi.org/10.1016/j.cell.2009.05.031.
Rivera, C., Voipio, J., Payne, J. a, Ruusuvuori, E., Lahtinen, H., Lamsa, K., Pirvola, U., Saarma, M., Kaila, K., 1999. The K+/Cl- co-transporter KCC2 renders GABA hyperpolarizing during neuronal maturation. Nature 397, 251–255. https://doi.org/10.1038/16697.
Rivera, C., Voipio, J., Thomas-Crusells, J., Li, H., Emri, Z., Sipilä, S., et al., 2004. Mechanism of activity-dependent downregulation of the neuron-specific K-Cl cotransporter KCC2. J. Neurosci. 24, 4683–4691. https://doi.org/10.1523/JNEUROSCI.5265-03.2004.
Rønn, L.C., Hartz, B.P., Bock, E., 1998. The neural cell adhesion molecule (NCAM) in development and plasticity of the nervous system. Exp. Gerontol. 33, 853–864.
Russell, J.M., 2000. Sodium-potassium-chloride cotransport. Physiol. Rev. 80, 211–276.
Saxton, M.J., Jacobson, K., 1997. Single-particle tracking: applications to membrane dynamics. Annu. Rev. Biophys. Biomol. Struct. 26, 373–399. https://doi.org/10.1146/annurev.biophys.26.1.373.
Shimizu-Okabe, C., Tanaka, M., Matsuda, K., Mihara, T., Okabe, A., Sato, K., et al., 2011. KCC2 was downregulated in small neurons localized in epileptogenic human focal cortical dysplasia. Epilepsy Res. 93, 177–184. https://doi.org/10.1016/j.eplepsyres.2010.12.008.
Simard, C.F., Bergeron, M.J., Frenette-Cotton, R., Carpentier, G. a, Pelchat, M.-E., Caron, L., Isenring, P., 2007. Homooligomeric and heterooligomeric associations between K+-Cl- cotransporter isoforms and between K+-Cl- and Na+-K+-Cl- cotransporters. J. Biol. Chem. 282, 18083–18093. https://doi.org/10.1074/jbc.M607811200.
Simard, C.F., Brunet, G.M., Daigle, N.D., Montminy, V., Caron, L., Isenring, P., 2004. Self-interacting domains in the C terminus of a cation-Cl- cotransporter described for the first time. J. Biol. Chem. 279, 40769–40777. https://doi.org/10.1074/jbc.M406458200.
Somasekharan, S., Monette, M.Y., Forbush, B., 2013. Functional expression of human NKCC1 from a synthetic cassette-based cDNA: introduction of extracellular epitope tags and removal of cysteines. PLoS One 8. https://doi.org/10.1371/journal.pone.0082060.
Somasekharan, S., Tanis, J., Forbush, B., 2012. Loop diuretic and ion-binding residues revealed by scanning mutagenesis of transmembrane helix 3 (TM3) of Na-K-Cl cotransporter (NKCC1). J. Biol. Chem. 287, 17308–17317. https://doi.org/10.1074/jbc.M112.356014.
Strange, K., Singer, T.D., Morrison, R., Delpire, E., 2000. Dependence of KCC2 K-Cl cotransporter activity on a conserved carboxy terminus tyrosine residue. Am. J. Physiol. Cell Physiol. 279, C860–C867.
Tillman, T.S., Cascio, M., 2003. Effects of membrane lipids on ion channel structure and function. Cell Biochem. Biophys. 38, 161–190. https://doi.org/10.1385/CBB:38:2:161.
Triller, A., Choquet, D., 2008. New concepts in synaptic biology derived from single-molecule imaging. Neuron 59, 359–374. https://doi.org/10.1016/j.neuron.2008.06.022.
Uvarov, P., Ludwig, A., Markkanen, M., Soni, S., Hübner, C.A., Rivera, C., Airaksinen, M.S., 2009. Coexpression and heteromerization of two neuronal K-Cl cotransporter isoforms in neonatal brain. J. Biol. Chem. 284, 13696–13704. https://doi.org/10.1074/jbc.M807366200.
Wang, F., Wang, X., Shapiro, L.A., Cotrina, M.L., Liu, W., Wang, E.W., Gu, S., Wang, W., He, X., Nedergaard, M., Huang, J.H., 2017. NKCC1 up-regulation contributes to early post-traumatic seizures and increased post-traumatic seizure susceptibility. Brain Struct. Funct. 222, 1543–1556. https://doi.org/10.1007/s00429-016-1292-z.
Wang, W., Gong, N., Xu, T. Le, 2006. Downregulation of KCC2 following LTP contributes to EPSP-spike potentiation in rat hippocampus. Biochem. Biophys. Res. Commun. 343, 1209–1215. https://doi.org/10.1016/j.bbrc.2006.03.038.
Warmuth, S., Zimmermann, I., Dutzler, R., 2009. X-ray structure of the C-terminal domain of a prokaryotic cation-chloride cotransporter. Structure 17, 538–546. https://doi.org/10.1016/j.str.2009.02.009.
Waseem, T., Mukhtarov, M., Buldakova, S., Medina, I., Bregestovski, P., 2010. Genetically encoded Cl-Sensor as a tool for monitoring of Cl-dependent processes in small neuronal compartments. J. Neurosci. Methods 193, 14–23. https://doi.org/10.1016/j.jneumeth.2010.08.002.
Watanabe, M., Fukuda, A., 2015. Development and regulation of chloride homeostasis in the central nervous system. Front. Cell. Neurosci. 9, 1–14. https://doi.org/10.3389/fncel.2015.00371.
Watanabe, M., Wake, H., Moorhouse, A.J., Nabekura, J., 2009. Clustering of neuronal K+-Cl- cotransporters in lipid rafts by tyrosine phosphorylation. J. Biol. Chem. 284, 27980–27988. https://doi.org/10.1074/jbc.M109.043620.
Williams, J.R., Sharp, J.W., Kumari, V.G., Wilson, M., Payne, J.A., 1999. The neuron-specific K-Cl cotransporter, KCC2: antibody development and initial characterization of the protein. J. Biol. Chem. 274, 12656–12664. https://doi.org/10.1074/jbc.274.18.12656.
Woodin, M. a., Ganguly, K., Poo, M.M., 2003. Coincident pre- and postsynaptic activity modifies GABAergic synapses by postsynaptic changes in Cl- transporter activity. Neuron 39, 807–820. https://doi.org/10.1016/S0896-6273(03)00507-5.
Yamada, J., Okabe, A., Toyoda, H., Kilb, W., Luhmann, H.J., Fukuda, A., 2004. Cl- uptake promoting depolarizing GABA actions in immature rat neocortical neurones is mediated by NKCC1. J. Physiol. 557, 829–841. Epub 2004 Apr 16. https://doi.org/10.1113/jphysiol.2004.062471.
Zhao, B., Wong, A.Y.C., Murshid, A., Bowie, D., Presley, J.F., Bedford, F.K., 2008. Identification of a novel di-leucine motif mediating K+/Cl- cotransporter KCC2 constitutive endocytosis. Cell. Signal. 20, 1769–1779. https://doi.org/10.1016/j.cellsig.2008.06.011.
Zhou, H.Y., Chen, S.R., Byun, H.S., Chen, H., Li, L., Han, H.D., Lopez-Berestein, G., Sood, A.K., Pan, H.L., 2012. N-methyl-D-aspartate receptor- and calpain-mediated proteolytic cleavage of K+-Cl- cotransporter-2 impairs spinal chloride homeostasis in neuropathic pain. J. Biol. Chem. 287, 33853–33864. https://doi.org/10.1074/jbc.M112.395830.